STRUCTURAL AND SPECTROSCOPIC INVESTIGATIONS OF RACEMISATION IN C_3-SYMMETRIC COMPLEXES

Chiara McCormack B.Sc.

A Thesis Submitted for the Degree of

Doctor of Philosophy

The University of Edinburgh

2005

ACKNOWLEDGEMENTS

I would like to sincerely thank my supervisor Dr. Philip J. Bailey for his ideas, encouragement and optimism throughout my time at The University of Edinburgh. I am grateful to have been given the opportunity to spend an important part of my life in a prestigious university and a vibrant city. I consider myself lucky to have been a member of the AC3S Research and Training Network which has provided the opportunity to present my work to a variety of talented research groups throughout Europe. I also wish to express my thanks to Dr. Lesley Yellowlees for her ideas and input, Drs. Pedro Pinho and Robert Pfeiffer for their much appreciated organic knowledge and Dr. Sarah Resouly for her good humour and spirit during my initial years in the lab. My time in the lab would not have been the same had it not been for all of the members of the Bailey, Tasker and Robertson groups, past and present.

I would like to acknowledge Dr. Simon Parsons and the crystallography service for their invaluable assistance in solving my crystal structures. Special thanks must go to Stephen Moggach for his generosity and patience with my unending list of questions. I also wish to thank Dr. Andy Turner for his time and patience while carrying out the *ab initio* calculations which complemented my work. I am grateful for the assistance of the technical staff at Edinburgh University, in particular John Millar, Alan Taylor and Robert Smith.

Finally, I would like to thank my parents for their support throughout my education, Fraser who I could not have done this without, and I wish to mention all of my family and friends without whom this part of my life would be incomplete.

ABSTRACT

The study of ligands of the general formula $[E(L_2D)_3]$ (E = bridgehead atom, L = linking atom, D = donor atom) was undertaken. Complexation of such ligands is of interest as it provides intrinsically chiral C_3-symmetric complexes with both octahedral and tetrahedral metal centers (Fig. I).

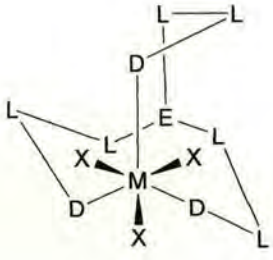

E = Central (bridgehead) atom
L = Linking atom
D = Donor atom

M = Metal
X = Non-tripod ligand

Figure I Complex of the type $[E(L_2D)_3MX_3]$ showing resultant C_3-symmetry

The possible exploitation of the chirality of C_3-symmetric complexes of such ligands would be crucially dependant upon the energy barriers to their racemisation. To this end, complexes of the novel ligand hydrotris(2-mercapto-1-ethylimidazolyl)borate ($NaTm^{Et}$) and the previously synthesised hydrotris(2-mercapto-1-benzylimidazolyl)borate ($NaTm^{Bn}$) were synthesised and Variable Temperature (VT) NMR was employed to investigate the energy barrier to racemisation in a range of tetrahedral and octahedral

complexes. The results from *ab initio* calculations on a number of structures were compared to the findings of the VT NMR calculations.

The novel complexes $[MnTm(CO)_3]$, [RuTm(*p*-cym)]Cl, $[RuTm\{C_6H_5(CO)OEt\}]Cl$ and $[SnTmCl_3]$ were synthesised. $[MnTm(CO)_3]$ (Tm = hydrotris(methimazolyl)borate) is the first example of a manganese complex of the Tm ligand. The isoelectronic but structurally different complexes $[Ru\{\kappa^3\text{-}HB(mt)_3\}Cp]$ and $[Ru\{\kappa^2\text{-}(\mu\text{-}H)B(mt)_3\}Cp]$ (mt = methimazole) were also synthesised. Although a crystal structure of $[Ru\{\kappa^2\text{-}(\mu\text{-}H)B(mt)_3\}Cp]$ has not been obtained we suggest that the complex is coordinated in a *bis*-chelate fashion by two thione sulphur atoms of the tripodal Tm ligand, and the coordination sphere is completed by a Cp ring and one hydrogen atom which is involved in an agostic B-H···Ru interaction.

The syntheses of new ligands of the type $[E(L_2D)_3]$ were attempted. The syntheses of the potential oxygen donor hydrotris(1-alkyl-4-imidazolin-2-one)borate from the reaction of 1-alkyl-4-imidazolin-2-ones and borohydride salts proved unsuccessful. Attempts to synthesise the potential carbon donor hydrotris(3-methyl-2-methyleneimidazolinyl)borate were hindered by problems in the isolation of the precursor hydrotris(2-methylimidazolyl)borate. An alternative route to the ligand was proposed and is currently being explored. The reaction of 2-mercapto-1-[(L)-(-)-α-methylbenzyl]imidazole and borohydride reagents proved an unsuccessful route to the synthesis of the chirally substituted ligand hydrotris(1-α-methylbenzyl-2-mercaptoimidazolyl)borate.

CONTENTS

ABBREVIATIONS

Ar, ar	aromatic
Bn	benzyl
BNA	benzylnicotinamide
br	broad
Bu	butyl
COD	cyclooctadiene
cp	cyclopentadiene
Cum	cumenyl
Cy	cyclohexyl
Cys	cysteine
d	doublet
DCM	dichloromethane
DFT	Density Functional Theory
DMF	dimethylformamide
DMSO	dimethylsulphoxide
DPPE	1,2-bis(diphenylphosphino)ethane
DPPF	1,1'-bis(diphenylphosphino)ferrocene
equiv	equivalent(s)
ES-MS	Electrospray Mass Spectrometry
et	ethyl
FAB-MS	Fast Atom Bombardment Mass Spectrometry
Hz	hertz
IR	infrared
J	spin-spin coupling constant
K	Kelvin
kJ	kilojoule
LADH	liver alcohol dehydrogenase
m	multiplet
M	Molar (mol l^{-1})
m	*meta*
M.p.	melting point
Me	methyl
Mes	mesityl

Methimazole, mt	2-mercapto-1-methylimidazole, 3-methyl-1-imidazolyl-2-thione
mmol	millimoles
NMR	Nuclear Magnetic Resonance
o	*ortho*
p	*para*
p-cym	*para*-cymene
Ph	phenyl
py	pyridine
q	quartet
RTt	tetrakis[(methylthio)methyl]borate
s	singlet
SERRS	Surface-Enhanced Resonance Ramen Spectroscopy
t	triplet
tacn	1,4,7-triazacyclononane
THF	tetrahydrofuran
Tm	hydrotris(2-mercapto-1-methylimidazolyl)borate
Tm^R	hydrotris(2-mercapto-1-R-imidazolyl)borate
Tol	tolyl
Tp	hydrotris(pyrazolyl)borate
Tt	hydrotris(thioxotriazolyl)borate
ttcn	1,4,7-trithiacyclononane
UV-Vis	Ultraviolet-visible
VT	Variable Temperature
δ	chemical shift (relative to tetramethylsilane)

1 Boron Centered, Non-classical Scorpionate Ligands

1.1 C_3-Symmetric Tripodal Ligands

Tripodal Ligands

The ligands considered in this project are of the type $[E(L_nD)_3]$ (E = central bridgehead atom, L = linking atom, D = donor atom) in which the donors are linked to the central tripod atom by monatomic links (L) (Fig. 1-1). By varying E, L and D a wide range of tripodal ligands can be synthesised.

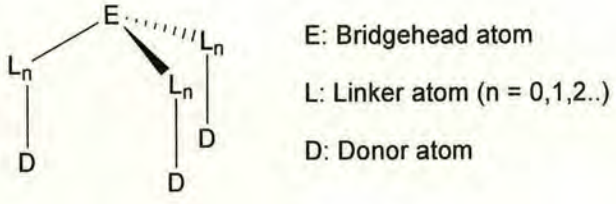

Figure 1-1

It is possible to introduce chirality into ligands of this type by the incorporation of chiral groups into the framework of the ligand. This can include substitution at E or L as long as the C_3-symmetry of the ligand is maintained. Another possibility is the attachment of chiral substituents to the donor groups of the ligand. A comprehensive review of such chemistry has been published by Christina Moberg.[1]

C_3-Symmetry Inducing Ligands

The hydrotris(pyrazolyl)borate ligand (Tp) (Fig. 1-2) can be thought of as a ligand of the form $[E(L_nD)_3]$, where n = 1. Upon coordination of the Tp ligand, three stable

six-membered rings are formed and the resulting metal ligand unit has C_{3v}-symmetry [Scheme 1-1(a)].

In 1996 the ligand hydrotris(2-mercapto-1-methylimidazolyl)borate (Tm, Fig. 1-2) was introduced by Reglinski *et al.*[2] This ligand conforms to the model for tripod ligands described above, however in this case there are two linking atoms between the bridgehead atom and the donor atoms.

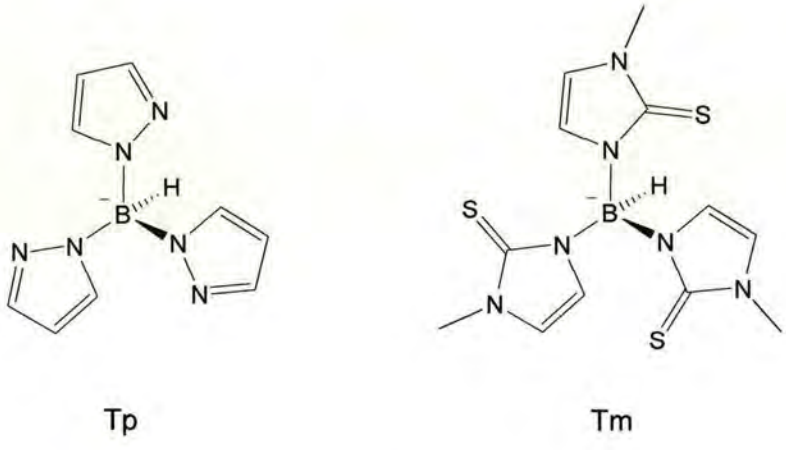

Figure 1-2

This relatively unexplored type of ligand is of interest because when such a ligand coordinates to a metal, three eight-membered rings are formed. Due to the associated angle strain, the tripod twists adopting a helical geometry. The metal-ligand unit formed on complexation of such ligands is therefore C_3-symmetric, which is a chiral point group [Scheme 1-1(b)].

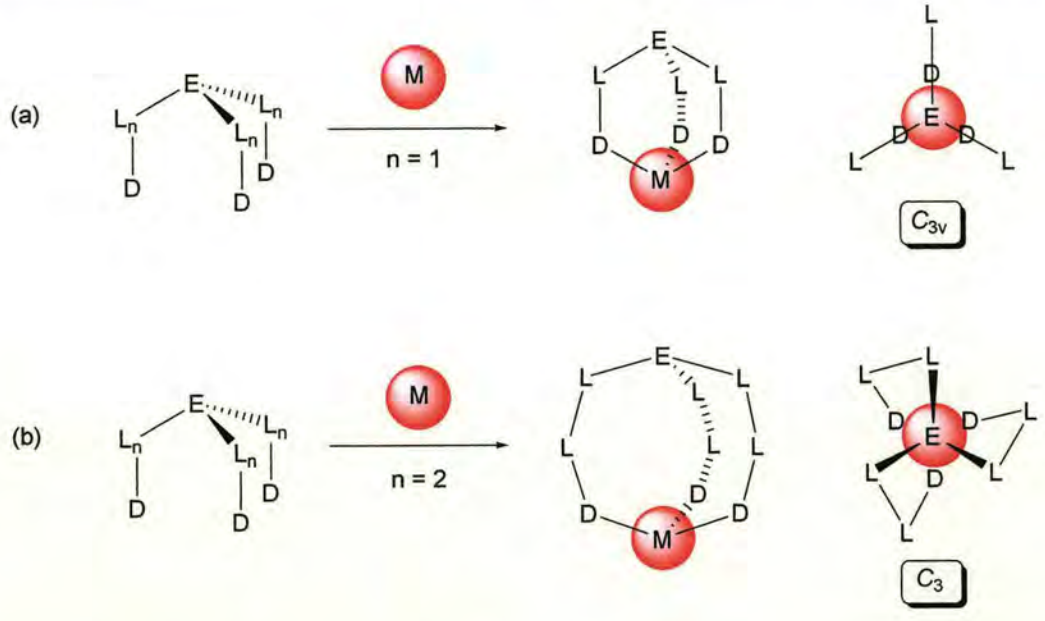

Scheme 1-1 (a) Coordination of $[E(L_1D)_3]$ to a metal (M) centre: (b) Coordination of $[E(L_2D)_3]$ to a metal (M) centre

Such complexes are academically very interesting and, in the future, could have potentially valuable applications, for example, in asymmetric catalysis. However, before this becomes a reality there is a need to expand the range of ligands of this type, investigate the chemistry of their complexes and understand the mechanisms by which such complexes may racemise.

1.2 Boron Centred Non-Classical Scorpionates

Trofimenko's synthesis of polypyrazolylborate ligands, introduced in 1970,[3] has opened up a wide area of chemistry; to date there have been over 2000 papers published on these ligands and their complexes alone. Trofimenko coined the phrase 'Scorpionates' for the family of polypyrazolylborate ligands to reflect the coordinative behavior of the ligand.[4] Over time derivatives of these ligands have been developed including ligands in which the central boron atom is substituted by a different central (bridgehead) atom and ligands in which the pyrazole group is replaced by alternative groups. This section comprises of a review of the latter: boron centered, non-classical scorpionate ligands.

1.2.1 Hydrotris(2-mercapto-1-methylimidazolyl)borate and its derivatives

1.2.1.1 Hydrotris(2-mercapto-1-methylimidazolyl)borate (Tm)*

Ligand Design and Preparation

Introduced by Reglinski *et al.* in 1996[2] as a soft analogue of the well established hydrotris(pyrazolyl)borate ligand (Tp), hydrotris(2-mercapto-1-methylimidazolyl)borate (Tm) has established itself as a very useful and versatile ligand. The design of the ligand centred around the fact that although the steric requirements of the Tp ligand can be controlled and varied, it is more difficult to alter its donor properties.[2] The idea of replacing the pyrazole groups with an alternative heterocycle seemed appropriate since

* Although the IUPAC name for the heterocycle is 3-methyl-1-imidazolyl-2-thione, the name 2-mercapto-1-methylimidazole (methimazole) is most often used in the literature. For clarity and ease of comparison to previous publications the latter nomenclature will be employed for the heterocycle and its derivates throughout this work.

the conjugated system could be retained allowing the distribution of electron density within the ligand. Furthermore, the motif of a protected pocket around the metal centre by incorporation of bulky groups adjacent to the donor atom could be fulfilled.[5] It is known that the heterocycle 2-mercapto-1-methylimidazole (methimazole) is more accurately represented as its thione tautomer rather than the thiol form[6, 7] (Fig. 1-3) and therefore could be employed in a similar condensation reaction to that used in the synthesis of Tp, thus replacing the hard nitrogen donors of Tp by soft sulphur donors.

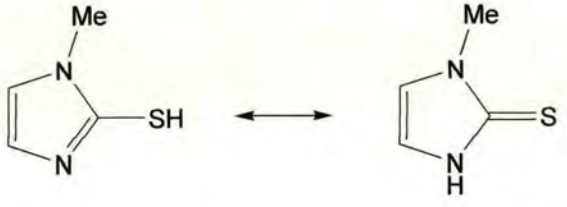

Figure 1-3 Tautomerisation in 2-mercapto-1-methylimidazole

The Tm ligand is formed from the reaction of 2-mercapto-1-methylimidazole with the borohydride anion[5] (Scheme 1-2). The synthesis is rather unusual as it does not involve the use of a solvent. Instead the reactants are heated together until melting begins. The side product of the reaction is hydrogen gas and this is used as an effective means to monitor the progress of the reaction.

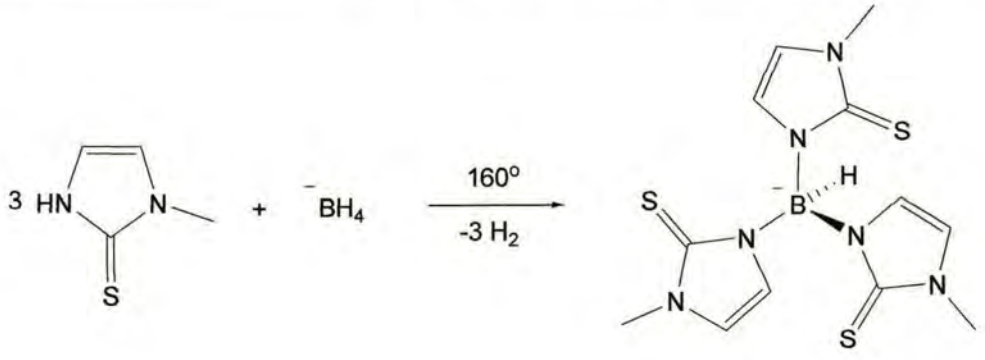

Scheme 1-2

Having synthesised this novel ligand, Reglinski was interested in investigating its properties. Its crystal structure[5] reveals an approximately C_3-symmetric structure in which the arms of the tripod are twisted into a propeller-like arrangement. It was also noted that the ligand is not prearranged for complexation; in fact, the arms are positioned in an inverted configuration with the three arms on the same side as the B-H bond. Much of the literature published by Reglinski *et al.* focuses on the complexation of the ligand and the development and understanding of its coordination chemistry.

Comparisons with Tp and Cyclopentadienyl (Cp) Ligands

Through a series of complexation studies Reglinski has illustrated that Tm is a facially capping, six-electron-donor ligand with synthetic utility comparable to Tp and Cp. It was proposed that the three ligands could be arranged in order of increasing hardness as follows: Tm→Cp→Tp.[8] The differences between the ligands have been exemplified through a number of complexation studies including the inability of TmCu(I) to coordinate carbon monoxide[2] unlike its Tp analogue which readily forms [CuTp(CO)],[9, 10] the formation of $[Bi(Tm)_2][Na(Tp)_2]$ and $[BiTmCl(\mu\text{-}Cl)]_2$,[11] neither of

which have Tp analogues and the ability of the Tm ligand to stabilise thallium(III).[12] Further comparisons were made by studying the influence of the facially capping ligands on the carbonyl and allyl fragments in the complexes $[(L)W(CO)_3I]$ and $[(L)Mo(CO)_2(\eta^3\text{-}C_3H_5)]$ (L = Tm, Cp, Tp).[13] The evolution in donor properties in the series Cp→Tp→Tm is mirrored in the change in $\nu_{C\text{-}O}$ value for the complexes. Similarly the series displays progressively tighter binding of the allyl fragment of the molybdenum complex.

Tm in the Spectrochemical Series

The synthesis of $[Fe(Tm)_2]$ and $[Ni(Tm)_2]$ led to the conclusion that Tm is a weak field ligand lying between H_2O and Cl in the spectrochemical series.[14] The bond lengths in the iron(II) complex are longer than most Fe(II)-S distances and are consistent with high-spin Fe(II). The magnetic moment of the complex is also consistent with a high-spin d^6 metal ion. Results from magnetic measurements and UV-Vis spectra of $[Ni(Tm)_2]$ indicate the position of the ligand in the spectrochemical series.

Further Observations

The first complex of the Tm ligand, [ZnTmBr],[2] was shown by X-ray crystallography to be a tetrahedral molecule with C_3-symmetry. Some time later, in 2002, the complete series of Group 12 complexes [MTmX] (M = Zn, Cd, Hg; X = Cl, Br, I) were reported.[15] The ligand was shown to be κ^3-coordinated in all of the complexes. The chemistry of the Tm ligand has been extended to Group 16 with the synthesis of $[Te(\kappa^2\text{-}Tm)_2]$[16] in which the Tm ligands coordinate in the κ^2-mode and each displays a different conformation. Group 14 and 15 complexes of the ligand were also synthesised in the form of

$[Sn(Tm)_2]^{2+}$ and $[As(Tm)_2]^{+}$.[17] The use of the Tm anion as a surface modifier for colloidal silver particles to produce a novel soft coating for use in Surface-Enhanced Resonance Raman Spectroscopy (SERRS) technology was also investigated.[18]

Continued Research

Due to the continued success of Tm as a ligand, there has been increased interest by several research groups and a summary of this work is of value. Lobbia *et al.* have synthesised a range of silver(I) complexes including $[Ag(Tm)]_n$,[19] $[Ag(Tm)]_2$,[20] $[AgTmPR_3]$,[19, 21] (R = Ph, *p*-Tol, *m*-Tol, Bn, Mes, Cy) and [AgTm(L)] (L = DPPE, DPPF).[21] Copper(I) complexes have also been characterised[22] including $[Cu(Tm)]_n$, $[CuTmPR_3]$, (R = Ph, *p*-Tol, *m*-Tol, Cy) and [CuTm(py)] (py = pyridine). A number of organotin complexes, illustrating the varying coordination modes of the Tm ligand have also been characterised.[23] Hill and co-workers have published details of the complexes $[WTm(\equiv CR)(CO)_2]$,[24] $[RuTmH(CO)PPh_3]$[25] in which the Tm is coordinated in a κ^3-H,S,S' configuration, $[MoTm(\eta^2\text{-}SCNMe_2)(CO)_2]$,[26] and the interesting $[M\{B(mt)_3\}(CO)PPh_3]$ (M = Ru,[27] Os,[28] mt = methimazole) both of which exhibit metal-boron bonds and are the first structurally characterised metallaboratranes of their type. In their investigations into rhenium(I) organometallic complexes Santos *et al.* have reported the synthesis of $[ReTm(CO)_3]$.[29] The isostructural manganese complex $[MnTm(CO)_3]$ has been synthesised within our group as well as the complexes $[RuTmCl(DMSO)_2]$, [RuTm(*p*-cym)] and [RuTmCp].[30]

1.2.1.2 Substituted Derivatives of Tm

1-Substituted Derivatives of Tm

A number of research groups have adopted the Tm ligand and introduced derivatives for use in their particular field of chemistry. The 1-substituted derivatives of Tm, abbreviated to Tm^R are the largest subset and are detailed below.

Parkin *et al.* have synthesised hydrotris(2-mercapto-1-mesityl-imidazolyl)borate (Tm^{Mes}) and hydrotris(2-mercapto-1-phenyl-imidazolyl)borate (Tm^{Ph})[31] (Fig. 1-4).

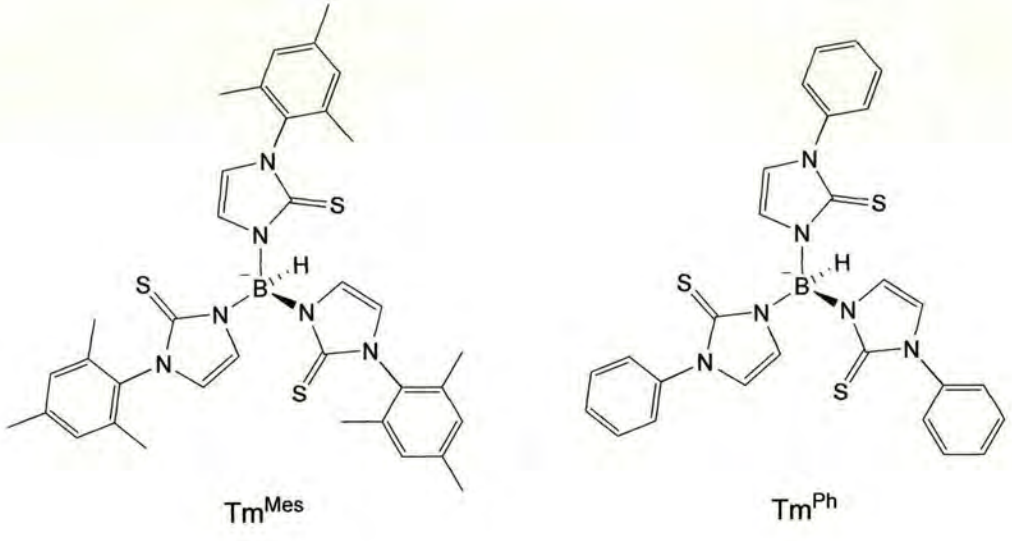

Figure 1-4

The group's interests lie in modeling zinc enzymes to gain an insight into the reasons various zinc enzymes use different amino acid residues at the active site. To this end, the complexes $[ZnTm^{Mes}(HOMe)][ClO_4]$,[31] $[ZnTm^{Ph}SPh]$[32] and $[ZnTm^{Ph}OH]$[33] were

synthesised. $[ZnTm^{Mes}(HOMe)]^+$ was identified as a model for the active site of liver alcohol dehydrogenase (LADH) and it has been concluded from the reactivity of the complex that the sulphur-rich environment in LADH may promote the binding of alcohol to zinc at the active site. $[ZnTm^{Ph}SPh]$ can be considered a good structural model for zinc enzymes that contain $[Zn(Cys)_4]$ fragments (Cys = cysteine). The reactivity of the thiolate linkage towards MeI and H^+ was investigated and results show that the reactivity mimics the chemistry of the Ada DNA repair protein (MeI) and the activation mechanism of matrix metalloproteins (H^+). $[ZnTm^{Ph}OH]$ represents the first structurally characterised terminal zinc hydroxide complex of a tridentate $[S_3]^-$donor ligand and was used as a model for the active site of 5-aminolevulinate dehydratase (ALAD). The modeling of Ada DNA repair protein involved the use of Tm^{Ph} and the ligand hydrotris(2-mercapto-1-(*p*-tolyl-imidazolyl)borate[34] ($Tm^{p\text{-}Tol}$) (Fig. 1-5) in the synthesis of $[ZnTm^{Ar}(mt^{Ar})][ClO_4]$ (mt = methimazole, Ar = Ph, *p*-Tol).[35]

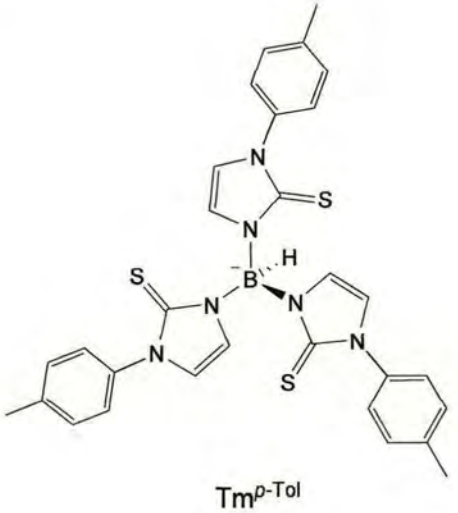

$Tm^{p\text{-}Tol}$

Figure 1-5

Lead complexes have an important role to play in investigations into the active site of ALAD as lead is known to interact with ALAD in the event of lead poisoning.[36] Replacement of zinc with lead in $ZnTm^{Ph}$ complexes allows the formation of the $[PbTm^{Ph}]^+$ cation[37] which is of particular interest as it is structurally very similar to the active site of Pb(II)-ALAD. The structure of $[Pb(Tm^{Ph})_2]$[38] was not used in enzyme modeling experiments however its crystal structure is noteworthy. One of the Tm^{Ph} ligands maintains a unique geometry whereby its tridentate coordination to the lead atom is supplemented by a Pb···B-H interaction. In other words, while one of the Tm^{Ph} ligands is κ^3-coordinated the other is, unusually, κ^4-coordinated (Fig. 1-6).

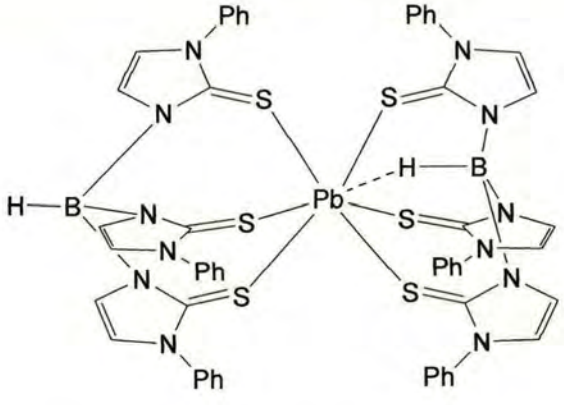

Figure 1-6 Structure of $[Pb(Tm^{Ph})_2]$

Parkin *et al.* have reported a number of other complexes of Tm^{Ph} including the thallium complexes $[Tl(Tm^{Ph})_2]_2$ and $[Tl(Tm^{Ph})_2][ClO_4]$, the latter Tl(III) complex being of particular interest because of the absence of a poly(pyrazolyl)borate analogue in the literature.[39] The comparison of $[M(Tm^{Ph})_2]$ (M = Co, Fe)[40] with their Tp analogues and

complexes of other sulphur-donor ligands show that the Tm^{Ph} ligand favors lower coordination numbers in divalent metal complexes.

Vahrenkamp *et al.* have developed the range of Tm derivatives further, synthesising hydrotris(2-mercapto-1-*t*-butyl-imidazolyl)borate ($Tm^{t\text{-}Bu}$) and hydrotris(2-mercapto-1-cumenyl-imidazolyl)borate (Tm^{Cum})[41] (Fig. 1-7).

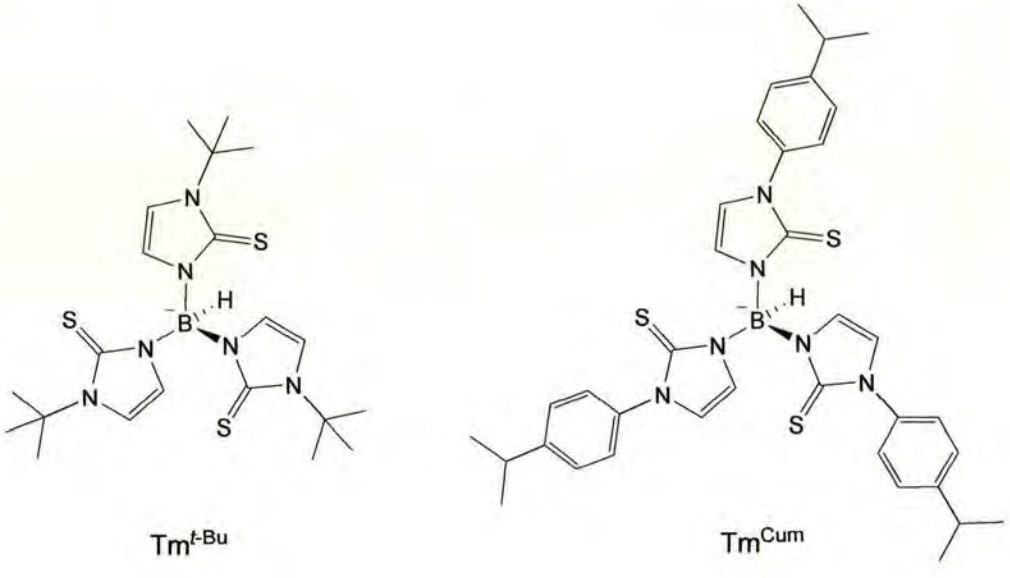

Figure 1-7

The complexes [$ZnTm^{R}X$] (R = *t*-Bu, Cum; X = F, Cl, ONO_2), [$Zn(Tm^{t\text{-}Bu})_2$] and [$ZnTm^{R}(OClO_3)$] (R = ^{t}Bu, Cum) were synthesised and used as models for the zinc enzyme horse liver alcohol dehydrogenase.[41] The reactivity of [$ZnTm^{R}(OClO_3)$] (R = ^{t}Bu, Cum) gives important insights into the structural and functional chemistry of LADH. Comparisons with the catalytic activity of the enzyme were also made by using

the complexes as catalysts in the oxidation of 2-propanol to acetone by BNA^+ and in the reduction of electron poor aldehydes to the corresponding alkoxide by BNAH (BNA = benzylnicotinamide). Vahrenkamp has also reported the formation of $[ZnTm^{t\text{-}Bu}]_4[ClO_4]_4$ crystals from the recrystallisation of $[ZnTm^{t\text{-}Bu}(OClO_3)]$ from methanol in the presence of 2-butylmercaptan.[42]

Inspired by the effect that the addition of bulky substituents at the 3-position of Tp had in the development of its bioinorganic and organometallic chemistry[34] Rheingold, Rabinovich and co-workers wished to develop the range of Tm ligands available by addition of bulky groups at the 1-position. The syntheses of hydrotris(2-mercapto-1-benzyl-imidazolyl)borate (Tm^{Bn}) (Fig. 1-8) and hydrotris(2-mercapto-1-*p*-tolyl-imidazolyl)borate ($Tm^{p\text{-}Tol}$) (Fig. 1-5) and their Group 12 complexes $[MTm^{R}Br]$ (M = Zn, Cd) were reported.[34, 43]

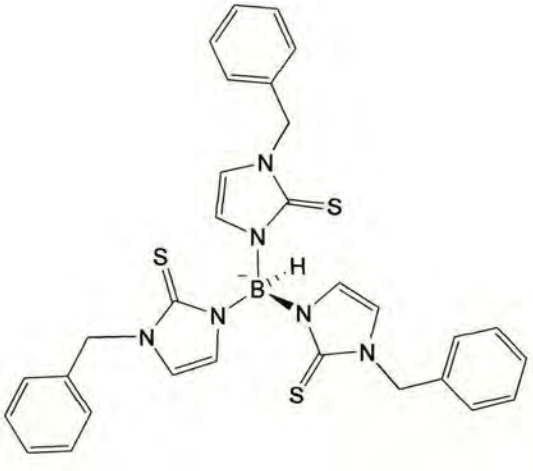

Tm^{Bn}

Figure 1-8

Using [CdTm$^{p\text{-Tol}}$Br] as a starting material, a route into the first series of neutral monothiolate complexes of cadmium, [CdTm$^{p\text{-Tol}}$SR] (R = Bn, Ph, *p*-Tol, C_6F_5), was established. The group is currently investigating the reactivity of the complexes in an attempt to model the scission of cysteine thiolate residues and associated formation of thioethers or thiols in a number of zinc enzymes. Rabinovich *et al.* have used Tm$^{t\text{-Bu}}$ (Fig. 1-7) to synthesise [MTm$^{t\text{-Bu}}$Br] (M = Zn, Cd, Hg) which was the first complete series of Tm metal complexes to be structurally characterised for any group of the periodic table.[44] In order to investigate whether cobalt could be reliably substituted for zinc in biological systems the paramagnetic complexes [CoTm$^{t\text{-Bu}}$X] (X = Cl, Br) and their derivatives including [CoTm$^{t\text{-Bu}}$PPh$_3$]X and [Co$_2$(Tm$^{t\text{-Bu}}$)$_2$X]Y (X = Cl, Br, I; Y = BF_4, BPh_4, PF_6) were synthesised.[45] While attempting the crystallisation of [CoTm$^{t\text{-Bu}}$PPh$_3$]BPh$_4$ the structure of [Co{B(mt$^{t\text{-Bu}}$)$_3$}PPh$_3$]BPh$_4$ (mt = methimazole) was obtained. Interestingly, this complex has a cobalt to boron dative bond, the second of three reported metallaboratranes[27, 28] containing the Tm ligand. The synthesis of the paramagnetic complexes [NiTm^{R}(DPPE)]X (R = ^{t}Bu, *p*-Tol; X = Cl, Br) led to a crystal structure of [NiTm$^{p\text{-Tol}}$(DPPE)]Cl being obtained.[46] The complex exhibits square pyramidal geometry and a Ni···H-B interaction can be identified. This complex is one of the first structurally characterised species having a [NiP$_2$S$_2$H] core (the other being its bis(mercaptoimidazolyl)borate counterpart, see Section 1.2.1.3) and interestingly, shows similarities to a number of transient species of importance in the catalytic cycle of [NiFe] hydrogenases.

Boron Functionalised Derivatives of Tm

Santos *et al.* have reported the only published examples of tris(2-mercapto-1-methylimidazolyl)borates with alkyl or aryl groups directly attached to the boron atom. The synthesis of $Li[RB(mt)_3]$ (Fig. 1-9) is reported and the relevance of their rhenium complexes $[Re\{RB(mt)_3\}(CO)_3]$ (R = Me, Ph; mt = methimazole) as models for the development of radiopharmaceuticals explored.[47]

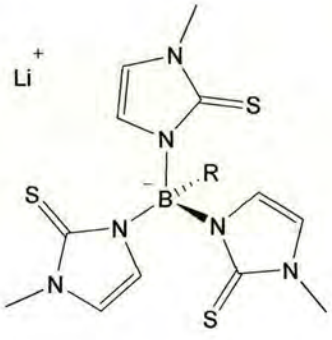

R = Me, Ph

Figure 1-9

*1.2.1.3 Dihydrobis(2-mercapto-1-methylimidazolyl)borate and its Derivatives**

Dihydrobis(2-mercapto-1-methylimidazolyl)borate $[H_2B(mt^{Me})_2]$ and its mesityl derivative $[H_2B(mt^{Mes})_2]$ (Fig. 1-10) were first synthesised by Parkin *et al.* as soft sulphur analogues of the acetylacetonato and bis(pyrazolyl)borato monoanionic bidentate ligands already in the literature.[48]

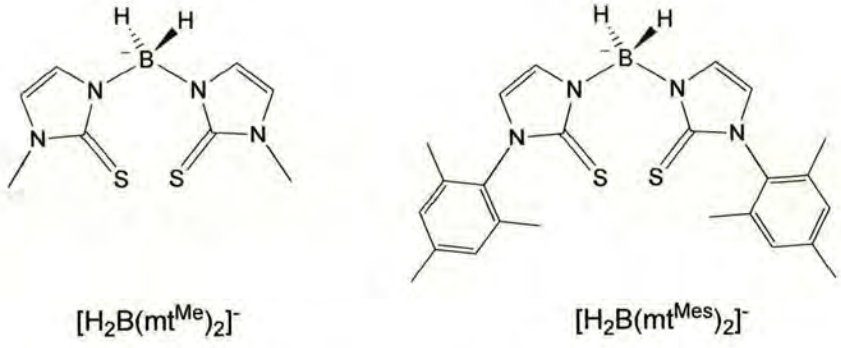

$[H_2B(mt^{Me})_2]^-$ $[H_2B(mt^{Mes})_2]^-$

Figure 1-10

The crystal structures of the complexes $[Zn\{H_2B(mt^{Me})_2\}Me]$, $[Zn\{H_2B(mt^{Me})_2\}I]$ and $[Zn\{H_2B(mt^{Mes})_2\}NO_3]$, published in the same article, revealed a $[HS_2]$ coordination whereby the coordination of the two sulphur donors was supplemented by an agostic Zn···H-B interaction. The tetrahedral complex $[Zn\{H_2B(mt^{Me})_2\}_2]$ was also isolated and an agostic interaction is not observed.

* As nomenclature for the dihydrobis(mercaptoimidazolyl)borates varies in the literature the most simple type was chosen for our purposes. The substituents attached to the boron atom will be explicitly identified as H, R or mt^R where H is a hydrogen atom, and R any alkyl of aryl group and mt^R the 1-substituted methimazole fragment.

Santos *et al.* developed an interest in the dihydrobis(mercaptoimidazolyl)borate ligands because of their solubility in water and stability towards hydrolysis and aerobic oxidation. These properties, plus the fact that they can be attached at a targeting molecule with relative ease, made them promising ligands for use in the development of novel radiopharmaceuticals. To extend the range of radiopharmaceuticals labeled with *fac*-$[M(CO)_3]^+$ the complexes $[M\{\kappa^3\text{-}H(\mu\text{-}H)B(mt^{Me})_2\}(CO)_3]$ (M = Re, ^{99}Tc, ^{99m}Tc) were synthesised.[49] The complexes are prepared with high radiochemical yield and with high specific activity and, in each case, show that the ligand coordinates in a tridentate fashion by two sulphur donors and an agostic M···H-B interaction. Investigations into the chemistry of Re and Tc carbonyl complexes and the influence of boron-substituents on the coordination chemistry of the ligands $Li[HRB(mt^{Me})_2]$ (R = Me, Ph)[29] (Fig. 1-11).

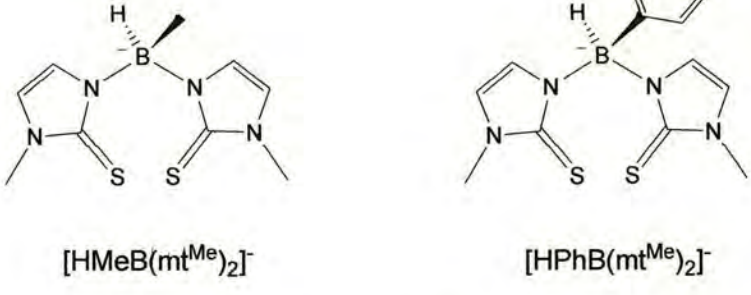

$[HMeB(mt^{Me})_2]^-$ $[HPhB(mt^{Me})_2]^-$

Figure 1-11

In view of the group's interest in the production of radiochemicals the complexes $[Re\{\kappa^3\text{-}R(\mu\text{-}H)B(mt^{Me})_2\}(CO)_3]$ (R = Me, Ph) were synthesised. Its similarities to the previously described $[H_2B(mt^{Me})_2]$ analogue led to the conclusion that the presence of substituents on the boron atom does not affect the coordination chemistry of the ligands and the robust nature of the agostic Re···H-B interaction is maintained. Interest in the coordination chemistry of uranium with a soft donor set led to the formation of $[U\{\kappa^3\text{-}R(\mu\text{-}H)B(mt^{Me})_2\}_2(THF)_3][BPh_4]$ (R = H, Ph).[50] The coordination in both complexes has been identified as tridentate with the ligand coordinating through its two sulphur donors and one agostic U···H-B interaction. Not only were $[Re\{\kappa^3\text{-}H(\mu\text{-}H)B(mt^{Me})_2\}(CO)_3]$ and its derivatives[51] found to be useful models for the labeling of biomolecules and the development of radiopharmaceuticals but the versatility of the ligand was also illustrated. Through variation of the nature of the co-ligands in complexes of the general formula $[Re\{H_2B(mt^{Me})_2\}(CO)_3(L)]$ [L = imidazole, 4-(dimethylamino)pyridine, *tert*-butylisonitrile, triphenylphosphine, ethylenediamine, DPPE], $H_2B(mt^{Me})_2$ was shown to coordinate in a tridentate, bidentate or monodentate fashion.

Continuing their investigations into the effects on the coordination chemistry of the substituted ligand, $H_2B(mt^{Me})_2$ was functionalised with piperazine fragments[52] (Fig. 1-12). Rhenium complexes of four novel ligands were synthesised and crystal structures show the ligands coordinated in a tridentate [S_2H] fashion.

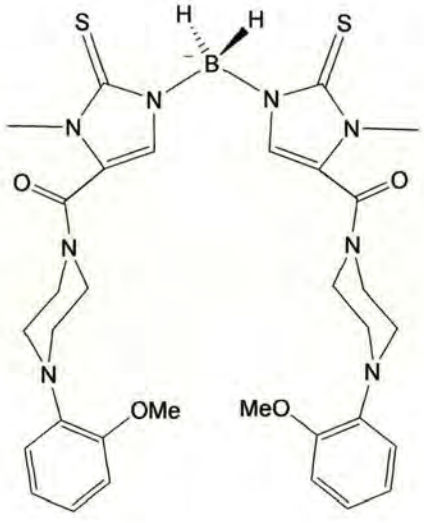

Figure 1-12 Example of a piperizine-functionalised $H_2B(mt^{Me})_2$ ligand

Rabinovich *et al.* have reported the synthesis of the paramagnetic complex $[Ni\{H_2B(mt^{Me})_2\}_2]$.[53] The presence of two *cis* Ni···H-B interactions in this complex highlights its relevance in the modeling of nickel hydrogenases. The group have expanded the range of dihydrobis(mercaptoimidazolyl)borates already synthesised by the formation of the novel ligands $H_2B(mt^R)_2$ (R = Bn, ^{t}Bu, *p*-Tol)[54] (Fig 1-13). The complexes $[M\{H_2B(mt^R)_2\}_2]$ (M = Zn, Cd, Hg) were synthesised and the crystal structures of $[Cd\{H_2B(mt^{Me})_2\}_2]$ and $[M\{H_2B(mt^{tBu})_2\}_2]$ (M = Zn, Cd, Hg) obtained.

These complexes all show the M···H-B agostic interactions now considered characteristic of the dihydrobis(mercaptoimidazolyl)borates.

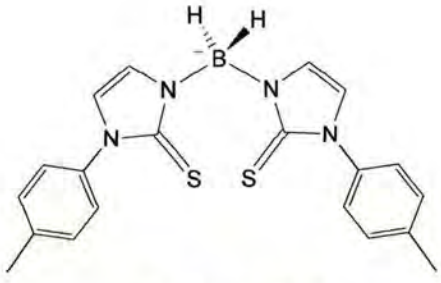

$[H_2B(mt^{p\text{-}Tol})_2]^-$

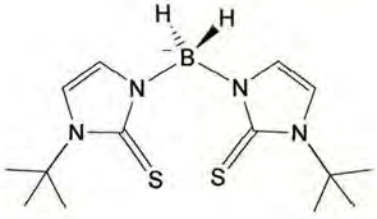

$[H_2B(mt^{t\text{-}Bu})_2]^-$

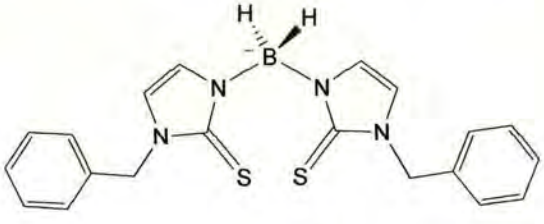

$[H_2B(mt^{Bn})_2]^-$

Figure 1-13

The cadmium thiolate complexes $[Cd\{H_2B(mt^{Me})_2\}SR]$ (R = Ph, *p*-Tol, C_6H_5) were synthesised from the novel $[Cd\{H_2B(mt^{Me})_2\}Br]$ and were fully charcterised.[55] The X-ray structure of $[Cd\{H_2B(mt^{Me})_2\}SC_6H_4Me]$ exhibits a dimeric structure in which the cadmium atoms display trigonal bipyramidal geometry being coordinated by the $H_2B(mt^{Me})_2$ ligand in $[S_2H]$ fashion and bridged by two thiolate groups. Recently Rabinovich *et al.* have synthesised the thallium(I) complexes $[Tl\{H_2B(mt^{R})_2\}]$ (R = Bn, ^{t}Bu, *p*-Tol)[56] as well as the previously reported $[Tl\{H_2B(mt^{Me})_2\}]$. Their clean

reaction with [Ni(DPPE)X_2] (X = Cl, Br)[46] demonstrates their potential as useful starting materials for the preparation of transition metal dihydrobis(mercaptoimidazolyl)borate complexes. The paramagnetic complexes [Ni{$H_2B(mt^R)_2$}(DPPE)]X (R = Me, ^{t}Bu; X = Cl, Br) have been synthesised and the crystal structure of [Ni{$H_2B(mt^{Me})_2$}(DPPE)]Cl obtained.[46] The structure exhibits square pyramidal geometry and a weak Ni···H-B interaction is observed. As with their Tm analogues (Section 1.2.1.2), the complex exhibits a [NiP_2S_2H] core similar to that observed in transient species which appear in the catalytic cycle of [NiFe] hydrogenases.

1.2.1.4 Related Ligands

A number of boron centred, non-classical scorpionate ligands exist whereby the methimazole group is replaced by an alternative heterocycle. These ligands do not have such an expansive range of derivatives as the Tm ligand and will therefore be dealt with together.

In their investigations into the restrictions on the synthesis of ligands produced using the melt reaction, Reglinski *et al.* reported the synthesis of sodium hydrotris(2-mercaptothiazolyl)borate (NaTz) and hydrotris(2-mercaptobenzothiazolyl)borate (NaTbz)[8] [Fig. 1-14(a), (b)]. Recently the ligand tetrakis(2-mercaptothiazolyl)borate (Mte) [Fig. 1-14(c)] was prepared by Silva *et al.* by reacting potassium borohydride and 2-mercaptothiazole in a melt reaction and its crystal structure was obtained.[57] It was noted from its X-ray structure that the diameter of the cavities created by the packing of

the rings is comparable to that found for zeolite-type compounds. No complexes of the ligand have yet been reported.

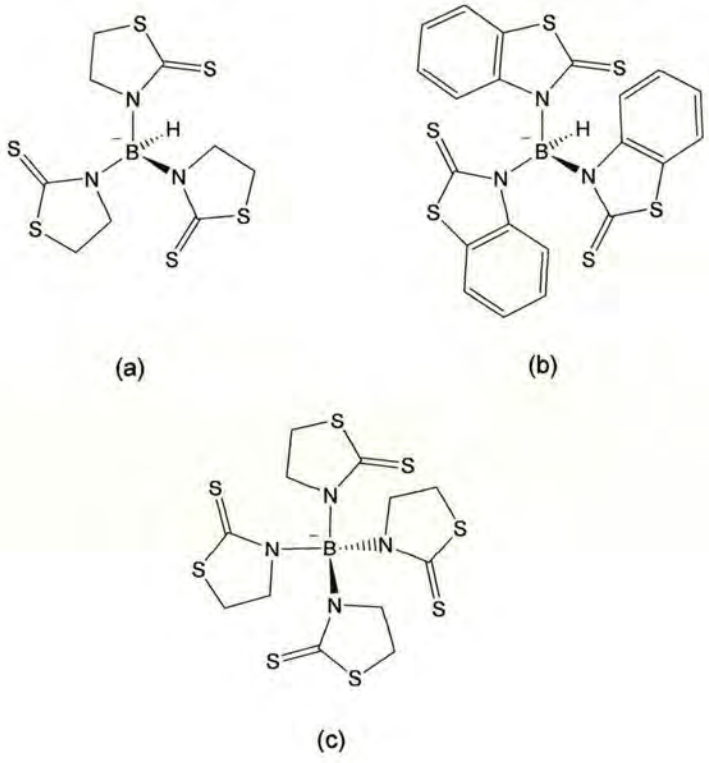

Figure 1-14 (a) Tz Ligand (b) Tbz Ligand (c) Mte Ligand

Around the same time as Reglinski was developing the above-mentioned ligands, work in our group was focusing on the synthesis of the $[N_3/S_3]$ ambidentate tripod ligand hydrotris(thioxotriazolyl)borate (Tt) [Fig. 1-15]. The ambidentate flexibility of the ligand was shown with the synthesis of the complexes $[Na(H_2O)_6][Na(Tt)_2]$, $[NaTt(DMF)_3]$ and $[MnTt(CO)_3]$ in which the ligand is coordinated by the harder

nitrogen atoms, and the complexes $[Bi(Tt)_2]Cl$ and $[SnTt(CO)_3]$ in which it is through the three sulphur donors that the ligand coordinates.[58]

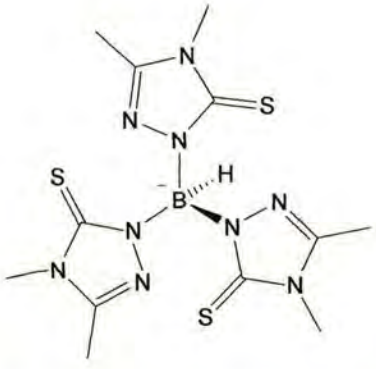

hydrotris(thioxotriazolyl)borate (Tt)

Figure 1-15

Subsequently, Marchiò *et al.* have taken an interest in investigating the effect of steric hindrance near the potential sulphur and nitrogen donors on the coordination chemistry of the ligand. The first sterically hindered ligand synthesised was hydrotris(4-ethyl-3-methylthioxotriazolinyl)borate ($Tr^{Et, Me}$)* [59] (Fig. 1-16). To favour a monomeric species, a molar ratio of 1:1 was used in the synthesis of its copper(I) complex however the product was shown to be $[Cu(Tr^{Et, Me})]_2$. The flexibility of the ligand is confirmed by the molecular structure in which each copper atom is coordinated by two sulphur donors from one ligand and one sulphur donor from the second ligand. One of the copper atoms

* As before, nomenclature for the ligands has been taken directly from the authors. Marchiò *et al.* have used the abbreviation Tr for this type of ligand (as opposed to Tt used by Bailey *et al.*). The superscript describes the substituents on the 5-thioxo-1,2,4-triazolinyl rings, the first referring to the substituent on the N(4) nitrogen and the second to the substituent in the C(3) carbon.

is also observed supporting a Cu···H-B interaction. The structure of $[Cu(Tr^{Et, Me})]_2$ is similar to that of its methyl, methyl-substituted analogue[58] and it is postulated that the ethyl groups do not cause steric hindrance due to the propeller-like conformation adopted by the complex. The ligand hydrotris(4-phenyl-3-methylthioxotriazolinyl)borate ($Tr^{Ph, Me}$) (Fig. 1-16) was synthesised and the complexes $[M(Tr^{Ph, Me})_2]$ (M = Zn, Co, Ni) and $[Bi(Tr^{Ph, Me})_2]$ reported.[60] Interestingly, both $[Zn(Tr^{Ph, Me})_2].7.5H_2O.1.5CH_3CN$ and $[Zn(Tr^{Ph, Me})_2].8DMF$ display different coordination modes and geometries, the former being tetrahedral with each of the ligands coordinated in an κ^2, $[S_2]$ fashion whereas the latter displays octahedral geometry with both ligands coordinated in an κ^3, $[N_3]$ fashion. The cobalt and nickel complexes are coordinated by three nitrogen donors of each of the ligands and the softer bismuth atom is coordinated by the three sulphur donors of the ligands.

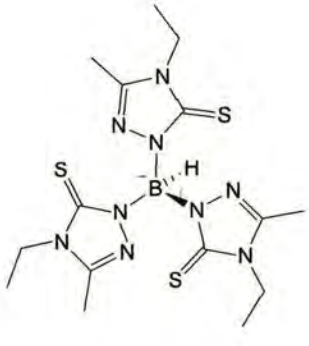

hydrotris(4-ethyl-3-ethylthioxotriazolinyl)borate
($Tr^{Et, Me}$)

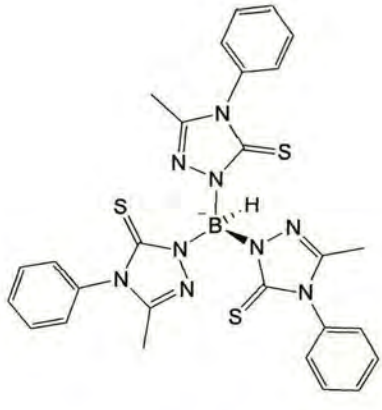

hydrotris(4-phenyl-3-methylthioxotriazolinyl)borate
($Tr^{Ph, Me}$)

Figure 1-16

Recently the ligand hydrotris(1,4-dihydro-4-methyl-3-(2-pyridyl)-5-triazolinyl)borate ($Tr^{Me,\ o\text{-}Py}$) (Fig. 1-17) was synthesised and the complex $[Ni(Tr^{Me,\ o\text{-}Py})_2]$ isolated.[61] The complex displays octahedral geometry and $[N_4S_2]$ coordination. Once again the flexibility of the ligand is confirmed. The two ligands are coordinated in an [SNN'] fashion whereby one arm of each tripod is coordinated to the nickel by the sulphur donor, the second arm chelates the metal with the triazoline and pyridine nitrogen atoms and the third arm remains uncoordinated.

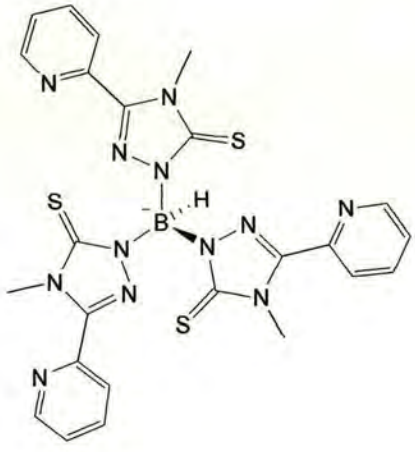

hydrotris(1,4-dihydro-4-methyl-3-(2-pyridyl)-5-triazolinyl)borate
($Tr^{Me,\ o\text{-}Py}$)

Figure 1-17

Marchiò *et al.* have reported the synthesis of dihydrobis(thioxotrazolyl)borate ($Bt^{Et,Me}$)[62] (thioxotriazoline = 5-thioxo-1,4-dihydro-4-ethyl-3-methyl-1,2,4-triazole) (Fig. 1-18). The complexes $[Zn(Bt^{Et,Me})_2]$, $[Bi(Bt^{Et,Me})_3]$ and $[Ni(Bt^{Et,Me})_2]$ were synthesised and interestingly, although the ligand is a potential ambidentate $[N_2/S_2]$

donor, all of the metal atoms are coordinated in the [S_2] mode with the presence of agostic M···H-B interactions.

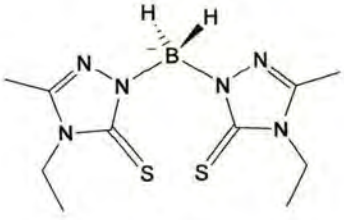

dihydrobis(thioxotriazolyl)borate ($Bt^{Et,Me}$)

Figure 1-18

The final ligand to be mentioned is that developed by Riordan *et al.* in an attempt to investigate κ^1 coordination of thiophene and its derivatives with the aim of elucidating the mechanism of catalytic hydrodesulfurisation (HDS). Potassium tetrakis(2-thienyl)borate (Fig. 1-19) was synthesised by reaction of the lithiated heterocycle with boron trifluoride etherate and treatment of the product with potassium chloride however no complexes have been isolated to date.[63] Theoretical calculations were carried out contrasting the ligand to RTt (Section 1.2.2) which is known to be more reactive.

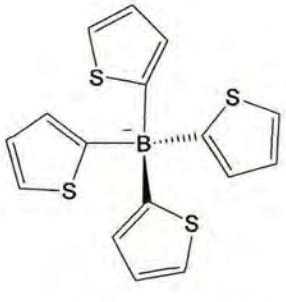

tetrakis(2-thienyl)borate

Figure 1-19

1.2.2 Tetrakis[(methylthio)methyl]borate and its derivatives*

The poly(methylthiomethyl)borates were first introduced by Riordan *et al.* in 1994 as a face capping, acyclic, sulphur analogue of the Tp ligand. The ligand tetrakis[(methylthio)methyl]borate, $[B(CH_2SCH_3)_4]^-$ (RTt) (Fig. 1-20) was prepared by reaction of $LiCH_2SCH_3$ and boron trifluoride etherate and the complexes *fac*-$[Mo(RTt)(CO)_3][Bu_4N]$ and $[Fe(RTt)_2]$ synthesised.[64] The ligand was shown to coordinate in a face capping, tridentate fashion in both cases. This research was continued by the synthesis of $[M(RTt)_2]$ (M = Co, Ni)[65] and the previously reported[64] $[Fe(RTt)_2]$. The octahedral geometry observed in $[Fe(RTt)_2]$ was confirmed in both the cobalt and nickel complexes. In the same publication the ligand $[PhB(CH_2SCH_3)_3]$ (PhTt) (Fig. 1-20) was reported and complexes of iron, cobalt and nickel synthesised. All of the complexes display spectroscopic and structural properties consistent with a moderately strong ligand field and comparisons to the tridentate ligands 1,4,7-trithiacyclononane (ttcn), 1,4,7-triazacyclononane (tacn) and Tp were made.

* Nomenclature used for these ligands has been taken directly from the authors of the relevant papers. In this work, ligands mentioned for the first time will be identified by their molecular formula, in square brackets, followed by the abbreviated name in round brackets e.g. $[PhB(CH_2SCH_3)_3]$ (PhTt). From then on the ligand will be referred to by its abbreviated name.

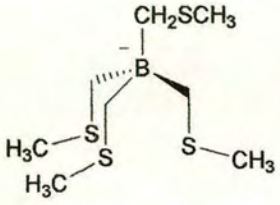

tetrakis[(methylthio)methyl]borate (RTt)

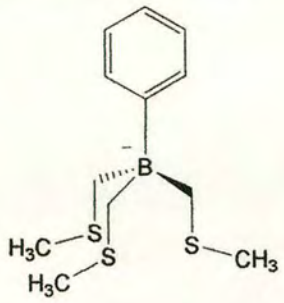

phenyltris[(methylthio)methyl]borate (PhTt)

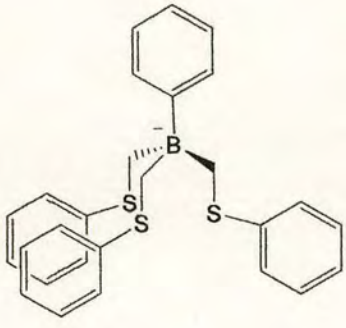

phenyltris[(phenylthio)methyl]borate ($PhTt^{Ph}$)

Figure 1-20

The synthesis of the copper(I) complex $[Cu(PhTt)]_4$ has been reported[66] and the X-ray crystal structure shows the copper ions in an almost coplanar array with approximately tetrahedral geometries. A monomeric copper(I) complex has been synthesised by employing the substituted ligand phenyltris[(phenylthio)methyl]borate, $[PhB(CH_2SPh)_3]$ ($PhTt^{Ph}$) (Fig. 1-20).[67]

The fact that the bridging of copper ions, observed in the structure of $[Cu(PhTt)]_4$, is hindered by phenyl-substituted sulphur donors when the $PhTt^{Ph}$ ligand is employed suggests that control of the structural chemistry of complexes of thioether ligands can be achieved. To confirm this, the complexation of the tridentate ligands PhTt, $PhTt^{Ph}$, (Fig. 1-20) $[PhB(CH_2S^tBu)_3]$ ($PhTt^{tBu}$) and $[PhB(CH_2Sp\text{-}Tol)_3]$ ($PhTt^{p\text{-}Tol}$) [68] (Fig. 1-21) and the bidentate ligands $[Ph_2B(CH_2SCH_3)_2]$ (Ph_2Bt),[69] $[Et_2B(CH_2SCH_3)_2]$ (Et_2Bt) and $[Ph_2B(CH_2SPh)_2]$ (Ph_2Bt^{Ph})[68] (Fig. 1-22) were investigated.

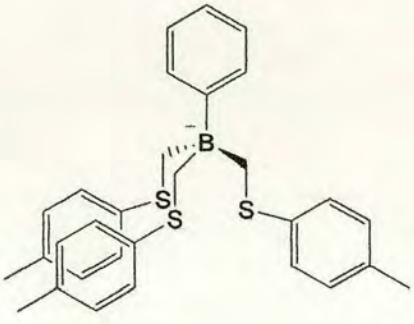

phenyltris[(*p*-tolylthio)methyl]borate ($PhTt^{p\text{-}Tol}$)

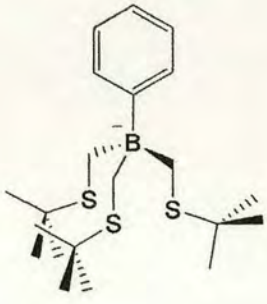

phenyltris[(*tert*-butylthio)methyl]borate ($PhTt^{t\text{-}Bu}$)

Figure 1-21

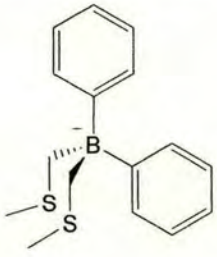

diphenylbis[(methylthio)methyl]borate (Ph_2Bt)

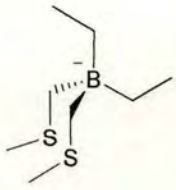

diethylylbis[(methylthio)methyl]borate (Et_2Bt)

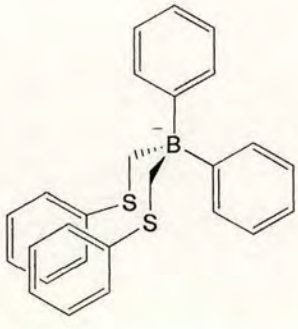

diphenylbis[(phenylthio)methyl]borate (Ph_2Bt^{Ph})

Figure 1-22

A series of copper(I) complexes was formed in which the empirical stoichiometry of 1:1 was maintained. It was concluded that control of the structural chemistry in the complexes could be achieved by variation of the boron substituents and/or the thioether sulphur and by modifying the number of chelate arms the ligand possesses.

The complex $[Ni(Ph_2Bt)_2]$ was synthesised from the bidentate ligand PhBt and used as a model for the investigation of the redox chemistry in enzymes such as [NiFe] hydrogenases and carbon monoxide dehydrogenase.[69] Expanding the range of bidentate

thioether ligands available, the ligand $[Ph_2B(CH_2S^tBu)_2]$ (Ph_2Bt^{tBu}) (Fig. 1-23) was reported[70] and the nickel complexes of both Ph_2Bt^{tBu} and the previously synthesised Ph_2Bt[69] were isolated. The results confirmed that the substitution of the sulphur donors is an important factor in the structure of the product. While the unsubstituted Ph_2Bt forms the complex $[Ni(Ph_2Bt)_2]$, the ligand Ph_2Bt^{tBu} forms $[(Ph_2Bt^{tBu})Ni(\eta^2\text{-}CH_2S^tBu)]$ *via* borato ligand B-C bond cleavage which reduces the steric congestion at the nickel centre.

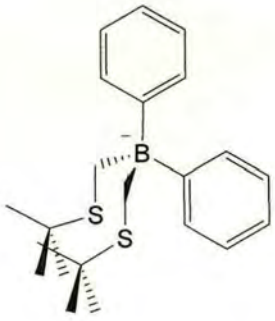

diphenylbis[(*tert*-butylthio)methyl]borate ($Ph_2Bt^{t\text{-}Bu}$)

Figure 1-23

As previously mentioned, thioether ligands of the type $PhTt^R$ (R = Ph, *p*-Tol, ^{t}Bu) have aided the synthesis of complexes of reduced nuclearity.[68] This point has been further illustrated by the fact that, unlike PhTt, the ligand $PhTt^{tBu}$ is bulky enough to prevent 2:1 complexation with cobalt(II) and Nickel(II); the tetrahedral complexes

[M(PhTt^{tBu})Cl] (M = Co, Ni) were synthesised and the molecular structure of [Ni(PhTt^{tBu})Cl] obtained.[71]

The ligand PhTt^{tBu} has been used extensively by Riordan *et al.* in enzyme modeling. The tetrahedral complex [Zn(PhTt^{tBu})Cl] and its derivative [Zn(PhTt^{tBu})SPh] have been reported[72] and the latter appears to be a good model for the active site in methionine synthases. The synthesis of the chloride-bridged dimer [Cd(PhTt^{tBu})Cl]$_2$ is reported in the same article and comparisons between the zinc and cadmium complexes are made in relation to cadmium-substituted zinc proteins. The lack of suitable complexes supported by thioether donors which would give valuable insight into the active site of many enzymes, for example acetyl CoA synthase (ACS), led Riordan *et al.* to synthesise the organometallic cobalt(II) and nickel(II) complexes [Co(PhTt^{tBu})(CH$_3$)] and [(κ^2-PhTt^{tBu})Ni(η^2-CH$_2$S^{tBu})].[73] The latter was the unexpected product during the attempted synthesis of [Ni(PhTt^{tBu})(CH$_3$)] and was proven to be a result of borato ligand alkylation. The nickel complex [Ni(PhTt^{tBu})CO] has also been reported[74] and was used as a model for important Ni-CO reaction intermediates in the catalytic cycle of ACS. Spectroscopic analysis and DFT calculations were used to investigate the Ni-CO bond and comparisons to the postulated Ni$^+$-CO intermediate in ACS were made. To further the understanding of this enzyme, the group undertook the synthesis of thiolate-bridged Ni-Cu complexes.[75] One such complex has been structurally characterised and comparisons between the complexes and the active site of ACS are made.

The group have also reported the synthesis and characterisation of the Ni(III)$_2$(μ-O)$_2$ species [Ni$_2$(PhTt^{tBu})$_2$(μ-O)$_2$] from [Ni(PhTt^{tBu})(CO)].[76, 77] The ability of the ligand to

support both Ni(I) and Ni(II) species is noted, as well as the potential for further exploration and understanding of the chemistry of dioxygen activation. To this end, a 1:1 complex was sought and the need for a larger substituent on the sulphur was identified.

The ligand $PhTt^{Ad}$ (Ad = 1-adamantyl) (Fig. 1-24) was chosen and its synthesis reported.[78] The preparation of nickel(I) complexes was successful and $[Ni(PhTt^{Ad})Cl]$ and $[Ni(PhTt^{Ad})L]$ (L = CO, PMe_3) are reported. It was concluded that the new ligand imparts identical electronic properties to those of $PhTt^{tBu}$ but with greater steric requirements and the preparation of a ligand that only allows the formation of 1:1 complexes was therefore successful.

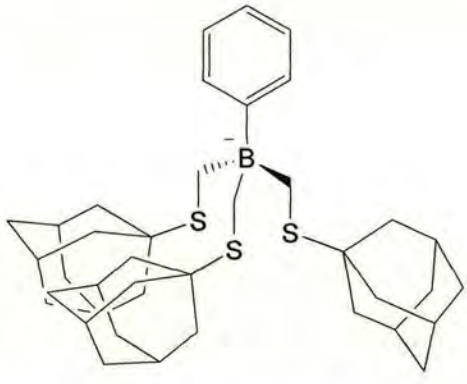

phenyltris[(1-adamantyl(thiomethyl)]borate ($PhTt^{Ad}$)

Figure 1-24

As well as investigating the use of ligands in enzyme modeling, Riordan *et al.* are interested in the formation of metal-ion complexes featuring [S_3] donor sets that have the potential for use in coordination polymers and supramolecular arrays. For this reason the synthesis of a suitable derivative of PhTt was appealing. Consequently, the ligand ferrocenyltris[(methylthio)methyl]borate (FcTt) (Fig. 1-25) and its complexes [M(FcTt)$_2$] (M = Fe, Co, Ni) and [Cu(FcTt)]$_4$ have been reported.[79] The ligand is synthesised from the reaction of $LiCH_2SCH_3$ and dibromoferrocenylborane. It has been concluded that this novel ligand has similar electronic properties to those of PhTt.

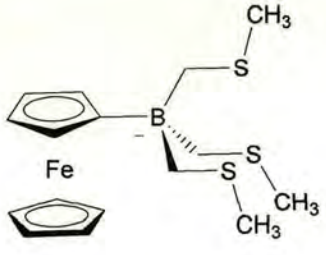

ferrocenyltris[(methylthio)methyl]borate (FcTt)

Figure 1-25

1.2.3 Tris(phosphino)borate Ligands

The ligand $PhB(CH_2PPh_2)_3$ abbreviated to $PhBP_3$ (Fig. 1-26) was first reported by Tilley *et al.* in 1999.[80] The ligand synthesis involves the addition of three equivalents of $[Li(TMED)][CH_2PPh_2]$ to dichlorophenylborane in an analogous procedure to that used by Riordan in the synthesis of the RTt ligands reviewed in Section 1.2.2.

$PhBP_3$ $PhBP_3'$

Figure 1-26

The complex $[Ir(PhBP_3)(H)(\eta^3\text{-}C_8H_{13})]$ was reported and used in mechanistic studies of the activation of silanes.[80, 81] This complex exhibits a previously unidentified reaction type in the extrusion of dimesitylsilylene from dimesitylsilane to give $[(PhBP_3)(H)_2Ir{=}SiMes_2]$. The mechanism of the silane activation was probed by the formation and investigation of the complex $[(PMe)_3(H)_2Ir = SiMes_2][MeB(C_6F_5)_3]$.[80] Furthermore the complexes $[Ir(PhBP_3)(H)(\eta^3\text{-}C_8H_{13})]$, $[Ir(PhBP_3)(H)(\eta^3\text{-}C_3H_5)]$ and derivatives were synthesised and their reactivity explored.[82] It was found that $PhBP_3$ is sterically quite demanding as well as being strongly electron-donating towards Ir compared to Cp*Ir and $Tm^{Me_2}Ir$ complexes.

The affinity of this novel ligand for soft metals was confirmed by Nocera *et al.* with the formation of the complex [Sn(PhBP$_3$)Cl].[83] It was noted that this complex is one of a small number of tin(II) centers coordinated by phosphorus. The chemistry of the ligand was developed further with the synthesis of Tl(PhBP$_3$)[84] and its clean reaction with CoI_2 to afford [Co(PhBP$_3$)I] illustrates its usefulness as a precursor for transition metal complexes of PhBP$_3$. The cobalt complex also provided a route into the Co(III) imido complex [(PhBP$_3$)Co≡ N-*p*-tolyl] *via* [Co(PhBP$_3$)(PMe$_3$)].[85] Following on from their preliminary work with cobalt, Peters *et al.* synthesised the complexes [Co(PhBP$_3$)(μ-Br)]$_2$, and [Co(PhBP$_3$)(μ-Cl)]$_2$.[86] These complexes, and the previously synthesised [Co(PhBP$_3$)I], proved to be very reactive towards oxygen and the complex [PhB{$CH_2P(O)Ph_2$}$_2$(CH_2PPh_2)]CoI was synthesised by the reaction of [Co(PhBP$_3$)I] with O_2.

The ability of PhBP$_3$Ir complexes to activate C-H bonds has also been explored. The ligand PhBP$_3$ has been used to develop the understanding of the chemical reactivity of Fe(I) in relation to the redox chemistry of iron in biological systems. The complex [Fe(PhBP$_3$)(PPh_3)] was synthesised and its crystal structure reveals the iron atom has a four-coordinate pseudotetrahedral geometry.[87] The reactivity of the complex was investigated and the oxidation of [Fe(PhBP$_3$)(PPh_3)] to [Fe(PhBP$_3$)(N-*p*-tolyl)] is reported as well as the reaction of [Fe(PhBP$_3$)(N-*p*-tolyl)] with CO to give [Fe(PhBP$_3$)$(CO)_2$]. The platinum chemistry of PhBP$_3$ in relation to C-H activation has been explored with the synthesis of the octahedral complex [Pt(PhBP$_3$)Me_3] and the square planar complex [Pt(κ^2-PhBP$_3$)Me_2][$^nBu_4N$].[88] Although [Pt(PhBP$_3$)Me_3] exhibits

stability in air and moisture and in the presence of acids and reductants, derivatives of $[Pt(\kappa^2\text{-}PhBP_3)Me_2][^nBu_4N]$ were easily obtained with the complex showing particular reactivity at the pendant phosphine arm.

In an attempt to synthesise a more strongly donating ligand, $PhBP_3$ was modified by replacing the soft aryl phosphine donors with harder, more electron-releasing alkyl phosphine donors. To this end, the ligand $PhB(CH_2P^iPr_2)_3$ (abbreviated to $PhBP_3'$) (Fig. 1-26) was synthesised.[89] The complexes $[Fe(PhBP_3')Cl]$, $[Co(PhBP_3')X]$ (X = Cl, I), $[Ru(PhBP_3')(\mu\text{-}Cl)]_2$ and derivatives, including CO and PMe_3 species, were formed and comparisons to their $PhBP_3$ analogues made. Continuing their research into the chemistry of complexes containing metal-silicon bonds, Tilley *et al.* employed the ligand $PhBP_3'$ to synthesise electron-deficient, coordinatively unsaturated complexes. The paramagnetic, monomeric, four-coordinate species $[Fe(PhBP_3')Br]$ was formed and its crystal structure obtained.[90] The complex $[Fe(PhBP_3')Si(SiMe_3)_3]$ and other derivatives were synthesised and the chemistry of all of these complexes is currently being investigated.

2 Design of Novel Tripodal Ligands

2.1 INTRODUCTION

One of the objectives within our group is the design, synthesis and application of new ligand systems for homogeneous catalysis. Inspired by the C_3-symmetry-inducing ligands introduced by Reglinski *et al.*, it was proposed that novel ligands with varied donor properties would significantly broaden the range of metal centers available for complexation and eventually lead to complexes suitable for catalytic testing. The attempted design and syntheses of such ligands will be dealt with in Sections 2.3.1 and 2.3.2. In an attempt to add a second facet of chirality to the ligands synthesised by Reglinski, thereby controlling the configuration of the complexed ligand and thus leading to enantiomerically pure complexes, an effort was made to synthesise a derivative of the Tm ligand, substituted with a chiral group at the 2-position, the results of which are detailed in Section 2.3.3.

2.2 Ligand Design

Tripodal ligands provide a useful way to control the stereochemistry of the coordination environment at an octahedral metal centre. The bicyclic structure formed on coordination of a metal ion by a tripodal ligand provides a stable and relatively rigid framework into which chiral elements may be introduced in order to achieve the desired stereochemical properties. This is of obvious significance in the application of octahedral metal complexes in asymmetric catalysis.

We are particularly interested in tripod ligands with diatomic links between the central and donor atoms, $[E(L_2D)_3]$ (Fig. 1-1) as they represent a relatively unexplored type of tripod ligand. The conformation of the 8-membered chelate rings formed on metal complexation of such a ligand provides intrinsically chiral C_3-symmetric complexes with both octahedral and tetrahedral metal centres (Scheme 1-1). Such complexes could have potentially valuable applications in asymmetric catalysis since the chirality may be efficiently transmitted to the remaining co-ordination site(s) by the use of planar aromatic groups which are known to function effectively in this role in the C_2-symmetric diphosphine complexes.[91]

Here follows a brief description of our target ligands, the reasons for our choices and the chemistry of related ligands previously synthesised.

2.2.1 Oxygen Donor Ligands

2.2.1.1 Background

Previously Explored Oxygen Donor Ligands

Oxygen chelate ligands such as alkoxides, crown ethers, β-diketones and tropolonates are commonly found in the literature however there are few examples of tridentate oxygen donor ligands available. Work by Kläui has opened up this area of chemistry significantly. In 1979[92] the first example of a monoanionic tridentate oxygen donor ligand providing complexes with local C_{3v} symmetry at the complexed metal was synthesised (L_{OR}^-, Fig. 2-1). The ligands are highly soluble, organometallic half-sandwich compounds that are stable in air and dissolve without decomposition. Notably these ligands form complexes with a wide variety of metal ions ranging across the periodic table.[93]

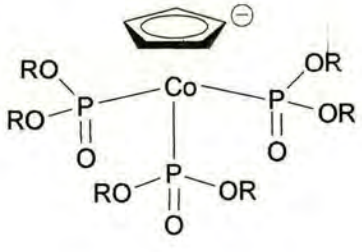

Figure 2-1 Kläui's L_{OR}^- ligand

More recently Leung *et al.* have synthesised a chiral version of Kläui's ligand from optically active phosphites. The chiral C_3-symmetric anionic tris(phosphinite) ligand (Fig. 2-2) is shown to complex to both hard and soft metal ions and studies into the catalytic activity of its sodium complex in Cu-catalysed aziridination of styrene, the Ti-catalysed ring opening of cyclohexene oxide and the allylation of benzaldehyde have been carried out.[94]

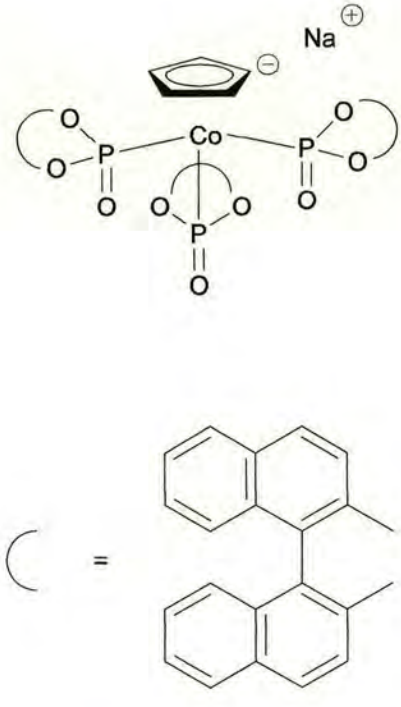

Figure 2-2 Leung's tris(phosphinite) ligand

Nugent *et al.* have developed the use of chiral trialkanolamine ligands (Fig. 2-3) that have been used in the enantioselective ring opening of epoxides[95, 96] and oxidation of sulfides.[97, 98] The homochiral trialkanolamines are easily prepared in enantiopure form from the reaction of ammonia and the appropriate epoxide. They have been shown to form thermally robust tetradentate complexes with early transition metals and a highly asymmetric environment is created around the metal centre. Zirconium complexes of these ligands have been tested and proved to be highly selective catalysts for epoxide desymmetrisation. Peroxo-titanium complexes of such ligands were shown to be capable of oxidizing sulfides to sulfoxides and the reactivity and enantioselectivity of the complexes were investigated.

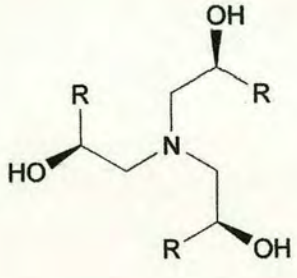

R = H, Me, Ph, ^{t}Bu

Figure 2-3 Trialkanolamine ligand

2.2.1.2 Synthetic Strategy

A simple strategy was undertaken whereby, upon synthesis of the appropriate heterocycle, namely 1-alkyl-4-imidazolin-2-one, the conventional melt reaction between the heterocycle and sodium borohydride would be carried out (Scheme. 2-1).

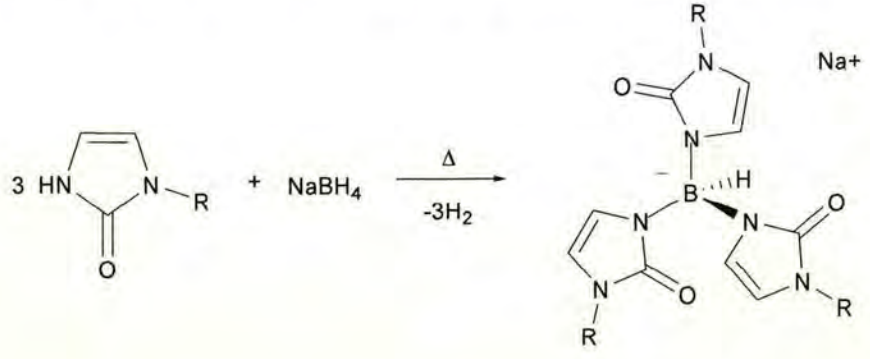

Scheme 2-1 Synthetic strategy for the preparation of sodium hydrotris(1-alkyl-4-imidazolin-2-one)borate

Our confidence in this synthetic route was supported by studies by Reglinski *et al.* into the limitations of the melt procedure.[8] Their investigations into the synthesis of thiazolylborates led to the conclusion that it is not the pK_a of the imine but the melting point of the heterocycle that determines the success of the reaction. It was found that as the melting point of the thione increases the amount of hydrogen produced as a side product decreases. The reaction of both 2-mercaptothiazoline (M.p. 105-107 °C) and methimazole (M.p.144-147 °C) with borohydride produce the desired ligands. The heterocycle 2-mercaptobenzothiazoline (M.p. 177-181 °C) does produce the desired ligand however the yield is low, there are large amounts of impurities and isolation of the product proves difficult. Furthermore, imidazolidinethione (M.p. 197-200 °C) does

not couple with the borohydride anion. As the melting points of 1-phenyl-4-imidazolin-2-one and 1-ethyl-4-imidazolin-2-one are 134-136 °C and 124-126 °C respectively we were confident that the chosen strategy would prove successful (Table. 2-1).

Table 2-1 Comparison of pK_a and melting points of thiones[8] and imidazolinones

Heterocycle	Structure	pK_a	M.p. (°C)
2-Mercaptothiazoline	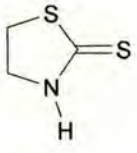	4.7	105-107
1-Ethyl-4-imidazolin-2-one	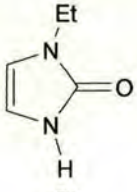	-	124-126
1-Phenyl-4-imidazolin-2-one	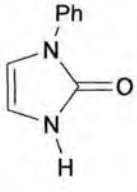	-	134-136
Methimazole	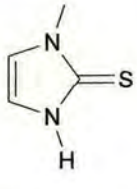	4.7	144-147
2-Mercaptobenzothiazoline	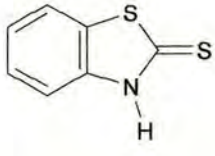	4.2	177-181
Imidazolidinethione	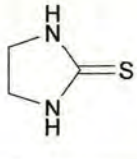	4.6	197-200

2.2.2 Carbon Donor Ligands

2.2.2.1 Background

Inspired by the recent explosion of interest in imidazolium derived N-heterocyclic carbenes as ligands and their applications in catalysis,[99] we were interested in the synthesis of a tripodal carbon donor ligand.

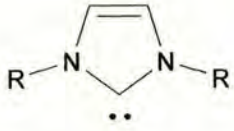

A

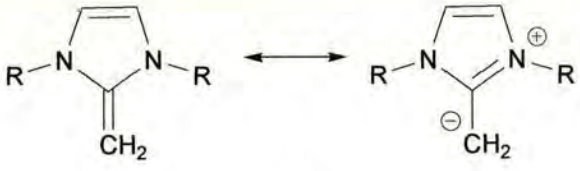

B

Figure 2-4 Example of an N-hetrocyclic carbene ligand (A) and the 2-methyleneimidazoline ligand (B)

The N-heterocyclic carbene ligand (**A**) shown in Fig 2-4 is simply derived by C-H deprotonation of N,N-dialkylimidazolium cations and the 2-methyleneimidazoline ligand (**B**) [Fig. 2-4] is similarly prepared by treatment of the dimethylimidazolium cation with ^{t}BuLi.[100] The tris-carbene donor tripod ligand hydrotris(3-methylimidazolin-2-ylidene)borate ($TRIS^{Me}$) incorporating three NHC donors into a ligand analogous to the ubiquitous hydrotris(pyrazolyl)borate has been

prepared in high yield by the route shown in Scheme 2-2.[101] Its precursor, hydrotris(imidazolyl)borate (**C**), can be prepared in high yield *via* the conventional melt reaction of imidazole with KBH_4. Methylation with $[Me_3O]BF_4$ followed by deprotonation provides the monoanionic tripodal ligand $TRIS^{Me}$ which has been successfully coordinated to a variety of metal ions.

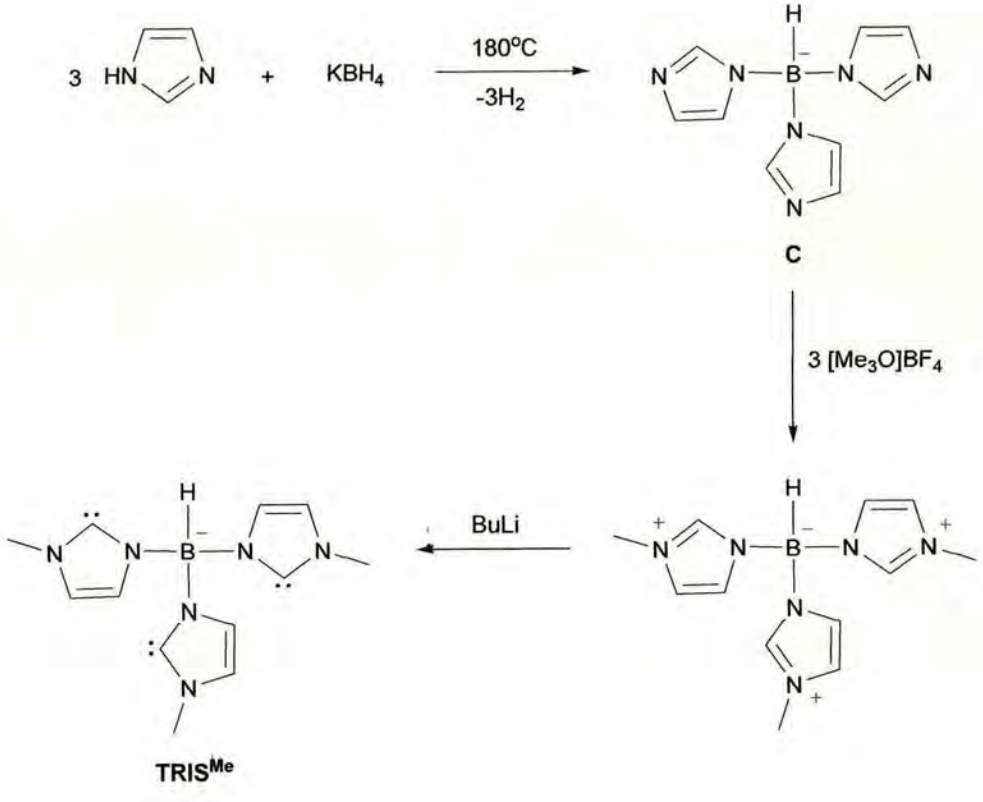

Scheme 2-2 Preparation of $TRIS^{Me}$

Synthesised in 1993,[100] the 1,3,4,5-tetramethyl-2-methyleneimidazoline system [MI, Fig. 2-5(a)] is an interesting ligand as it coordinates to metals in its zwitterionic form rather than in the enamine form. This can be deduced from the geometry around

the coordinated carbon atom in its complexes.[100, 102-104] In the $Mo(CO)_5$ complex, for example, the C-C-Mo bond angle is 110.4° indicating sp^3 hybridisation, and the C-C bond length is 143 pm consistent with a single bond [Fig 2-5(b)]. The system may therefore be viewed as a *neutral* alkyl ligand. This remains the only reported example of a transition metal complex of this ligand, however a number of lanthanide complexes have been characterised which show similar structural features.[103] Even in the uncomplexed state considerable electron density is located at this carbon atom as indicated by its low frequency signal in the ^{13}C NMR spectrum (40 ppm) and by AM1 calculations.[100]

(a) 1,3,4,5-tetramethyl-2-methyleneimidazolene (MI)

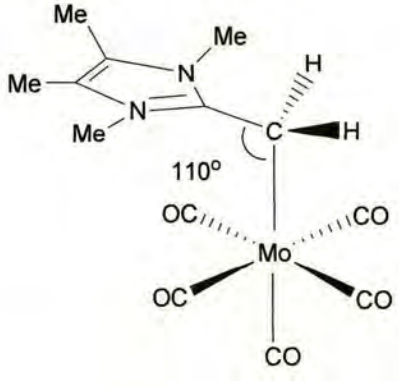

(b) [$Mo(CO)_5$(MI)]: coordination of MI in zwitterionic form

Figure 2-5

Thus, this heterocyclic system seems like a very interesting candidate for incorporation into a tripodal ligand (Fig 2-6). A range of studies have shown N-heterocyclic carbenes to be very powerful σ-donors which, in contrast to Fischer carbenes, display very little π-acceptor character.[99] Their applications in catalysis are aided by the powerful trans-effect which these electronic properties confer, thus labilising *trans* ligands.

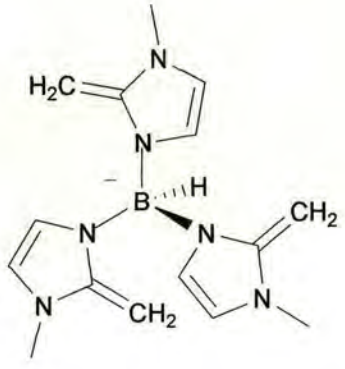

Figure 2-6 Target Ligand: hydrotris(3-methyl-2-methyleneimidazolinyl)borate (TMI)

Similar donor characteristics may be anticipated for the 2-methyleneimidazoline (MI) ligands. This may be inferred from the trans-influence evident from the structural data available for the complex [(MI)Mo(CO)$_5$] [Fig. 2-5(b)][102] in which the Mo-CO bond *trans* to the MI ligand is significantly shorter (196.9 pm compared with an average of 205.1 for the *cis* CO ligands), while the C-O bond for the *trans* ligand is the longest (115.6 pm compared with a mean of 114.0 for the *cis* ligands). These data indicate

significantly greater Mo→CO π-donation to the CO ligand *trans* to the MI ligand with consequent shortening of the Mo-CO and lengthening of the C-O bonds for this ligand in comparison to those *cis* to the MI ligand. The three coordination sites *trans* to a coordinated hydrotris(3-methyl-2-methyleneimidazolinyl)borate TMI ligand will therefore be strongly labilised and this should provide for rapid exchange processes at these sites and thus efficient catalytic processes. As will be explained in detail in Section 5.1.1, the racemisation of complexes containing ligands of this type with octahedral metal ions may proceed through dissociative and non-dissociative mechanisms. The activation energy of the dissociative process corresponds to the energy of the metal-donor bond cleaved in the first step of this process. The powerful σ-donor characteristics of the donor carbon atoms in the target ligand should provide strong coordination and correspondingly high energies to racemisation *via* the dissociative mechanism, particularly in complexes with inert metal ions [e.g. Ru(II), Rh(III)].

2.2.2.2 Synthetic Strategy

It was decided that the best route to the synthesis of hydrotris(3-methyl-2-methyleneimidazolinyl)borate was an analogous procedure to that of $TRIS^{Me}$ (Scheme 2-2). The synthesis of the precursor hydrotris(2-methylimidazolyl)borate (Scheme 2-3, **A**) has previously been reported.[105] It was hoped that methylation of hydrotris(2-methylimidazolyl)borate followed by deprotonation of the methyl group should provide the target hydrotris(3-methyl-2-methyleneimidazolinyl)borate ligand (TMI, Scheme 2-3).

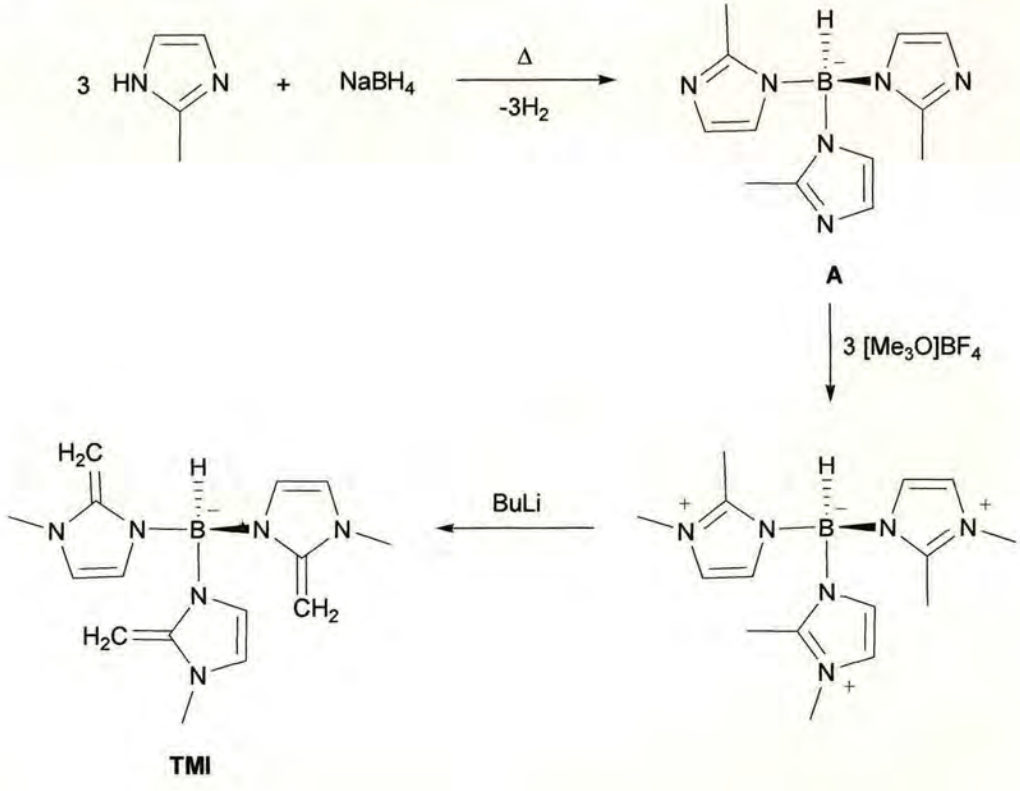

Scheme 2-3 Synthetic strategy for preparation of hydrotris(3-methyl-2-methyleneimidazolinyl)borate ligand

2.2.3 Addition of Chiral Groups to the Backbone of the Tm Ligand

2.2.3.1 Background

A detailed description of the Tm ligand has been given in Chapter 1. It only remains to discuss briefly the effect of placing a chiral group on the backbone of the ligand. We have seen in Section 1.1 that tripodal ligands of the type $[E(L_2D)_3]$, and hence the Tm ligand, form complexes of C_3-symmetry. However, although the complexes are chiral, a racemic mixture will always form since coordination, leading to a helically twisted unit, is equally likely to provide the λ or the δ configuration* (Fig. 2-7).

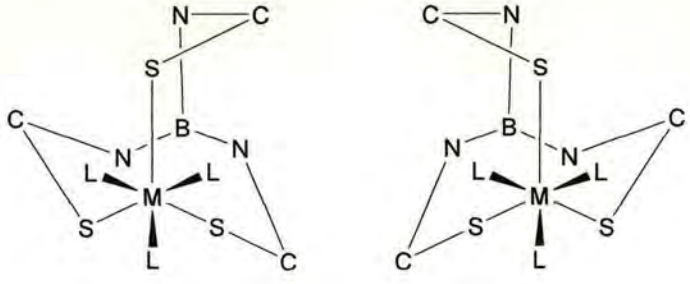

Figure 2-7 Schematic showing possible conformations in complexes of the Tm ligand (only directly involved atoms included)

Our aim was to synthesise a heterocycle with a chirally pure group at the 1-position. By using this heterocycle in the synthesis of a Tm-derived ligand the configuration of the complexed ligand could be directed and an enantiomerically pure complex would be obtained.

* See Appendix 3 for parameters describing configuration of complexes of the Tm ligand

2.2.3.2 Synthetic Strategy

By choosing (L)-(-)-α-methylbenzylamine, a cheap, commercially available chiral amine, the synthesis of (L)-(-)-α-methylbenzylaminoacetaldehyde diethyl acetal was possible. It was hoped that this would cyclise according to the adapted literature procedure[106] to produce 2-mercapto-1-[(L)-(-)-α-methylbenzyl]imidazole. Our goal was to use this heterocycle in the conventional melt reaction to form the desired ligand (Scheme 2-4). The fact that there is precedent in the literature for the synthesis of Tm derivatives with bulky groups in the 1-position, such as Tm^{Bz}, Tm^{tBu} and $Tm^{p\text{-}Tol}$ (See Chapter 1 for a comprehensive review), provided confidence that this would be a straightforward synthesis.

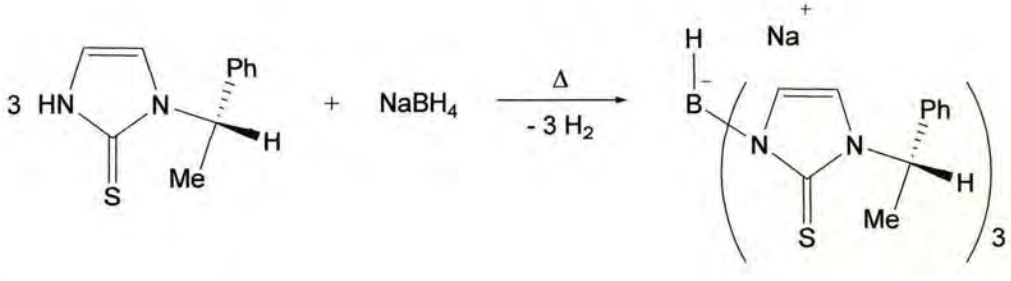

Scheme 2-4 Synthetic strategy for the synthesis of hydrotris(1-α-methylbenzyl-2-mercaptoimidazolyl)borate

2.3 Ligand Synthesis

2.3.1 Oxygen Donor Ligands

2.3.1.1 Attempted Synthesis of Hydrotris(1-alkyl-4-imidazolin-2-one)borate

N-(2,2-dimethoxyethyl)-N-phenylurea (1)

N-(2,2-dimethoxyethyl)-N-phenylurea was synthesised by an adaptation of the method described by Forrest *et al.*[107] as described in Section 6.3 (Scheme 2-5).

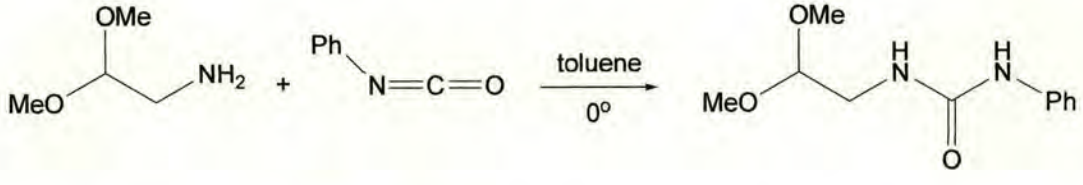

Scheme 2-5 Preparation of 1 N-(2,2-dimethoxyethyl)-N-phenylurea

1-Phenyl-4-imidazolin-2-one (2)

The cyclisation of **1** to give 1-phenyl-4-imidazolin-2-one (Scheme 2-6) was carried out according to the procedure published by Wong *et al.*[108] and is described in Section 6.3.

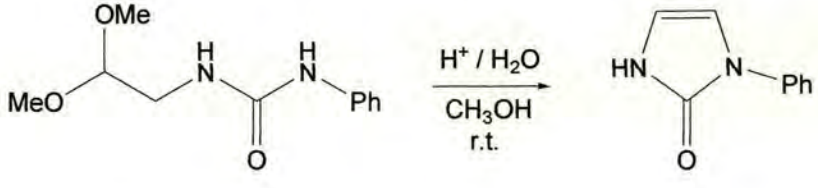

Scheme 2-6 Preparation of 1-phenyl-4-imidazolin-2-one

General Procedure for the Reaction of 2 with Sodium borohydride (For specific conditions refer to Table 2-2)

In various attempts to synthesise sodium hydrotris(1-phenyl-4-imidazolin-2-one)borate a finely ground mixture of **2** and sodium borohydride was added to a round bottomed Schlenk flask which was fitted with a volumetric device for the measurement of hydrogen evolution.* Following a similar procedure to that of Reglinski *et al.* for the preparation of NaTm[5] the starting materials were stirred and heated slowly in the absence of solvent until they began to melt. When the first signs of melting were observed the temperature was raised slowly keeping the evolution of gas at a steady pace. The reaction was stopped when the apparent evolution of gas ceased or the reaction solidified or became discoloured. NMR and mass spectroscopy confirmed only the presence of unreacted starting material, **2**.

Table 2-2 Reaction conditions for experiments involving 2 and sodium borohydride

Equiv.	Solvent	Temp. (°C)	Product
3	-	160	1-Phenyl-4-imidazolin-2-one
4	-	160	1-Phenyl-4-imidazolin-2-one
3.2	-	200	Decomposition
3.2	-	220	Decomposition
3.2	-	290	Decomposition

* Appendix 2

N-Ethyl-N-(2,2-dimethoxyethyl)urea (3)

The compound **3** was synthesised by an adaptation of the method described by Forrest *et al.*[107] as described in Section 6.3 (Scheme 2-7).

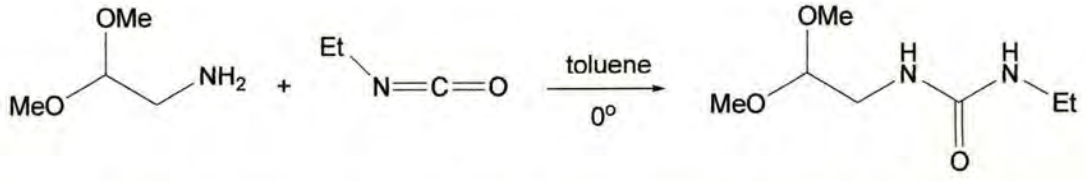

Scheme 2-7 Preparation of N'-Ethyl-N-(2,2-dimethoxyethyl)urea

1-Ethyl-4-imidazolin-2-one (4)

The cyclisation of **3** to give 1-ethyl-4-imidazolin-2-one (Scheme 2-8) was carried out according to the procedure published by Wong *et al.*[108] and is described in Section 6.3.

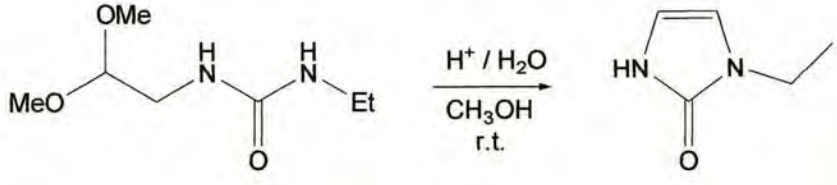

Scheme 2-8 Preparation of 1-Ethyl-4-imidazolin-2-one

Reaction of 4 with Sodium Borohydride

A finely ground mixture of **4** and sodium borohydride was added to a round bottomed Schlenk flask which was fitted with a volumetric device for the measurement of hydrogen evolution.* Following a similar procedure to that of Reglinski *et al.* for the

* Appendix 2

preparation of NaTm[5] the starting materials were stirred and heated slowly in the absence of solvent until they began to melt. When the first signs of melting were observed the temperature was raised slowly keeping the evolution of gas at a steady pace. The reaction was heated to 130 °C and allowed to cool. NMR and mass spectroscopy confirmed only the presence of unreacted starting material, **4**.

General Procedure for the Reaction of 4 with Sodium Borohydride in Solution (For specific conditions refer to Table 2-3)

In various attempts to synthesise sodium hydrotris(1-ethyl-4-imidazolin-2-one)borate a finely ground mixture of **4** and sodium borohydride was added to a round bottomed Schlenk flask which was fitted with a reflux condenser connected to a volumetric device for the measurement of hydrogen evolution.* Dry solvent was added and the solution refluxed until the apparent evolution of gas had ceased. The reaction mixture was allowed to cool and the solvent was stripped under vacuum. NMR and mass spectroscopy confirmed only the presence of the starting material **4**.

Table 2-3 Reaction conditions for experiments involving 4 and sodium borohydride

Equiv.	Solvent	Temp. (°C)	Reaction Time	Product
3	Toluene	111	3 d	1-Ethyl-4-imidazolin-2-one.
3	Toluene	111	5 d	
3	Dimethylacetamide	160	1 ½ h	
3	Dimethylacetamide	160	3 h	

* Appendix 2

Reaction of Sodium 1-Ethyl-4-imidazolin-2-one (5) with Dichlorophenylborane

It was hoped that by using a more reactive boron source the formation of the ligand would become more favourable and phenyltris(1-ethyl-4-imidazolin-2-one)borate could be isolated. The sodium salt of 1-ethyl-4-imidazolin-2-one was synthesised according to the procedure detailed in Section 6.3 (Scheme 2-9). The salt was easily isolated in good yield.

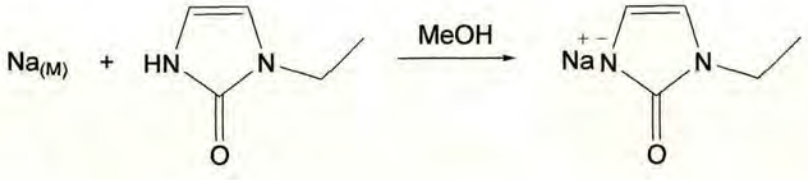

Scheme 2-9 Preparation of Sodium 1-Ethyl-4-imidazolin-2-one

The reaction between **5** and dichlorophenylborane was carried out as described in Section 6.3 (Scheme 2-10) however NMR and mass spectroscopy confirmed only the presence of the starting materials.

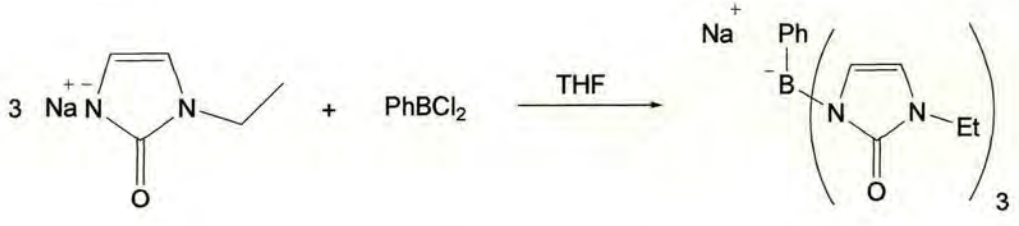

Scheme 2-10 Attempted reaction of 5 with dichlorophenylborane

Tris(1-ethyl-4-imidazolin-2-one)(dimethylamine)borate (6)

The ligand **6** was synthesised *via* the route described in Section 6.3 and shown in Scheme 2-11. The product, a cream coloured, hygroscopic solid, was isolated in high yield.

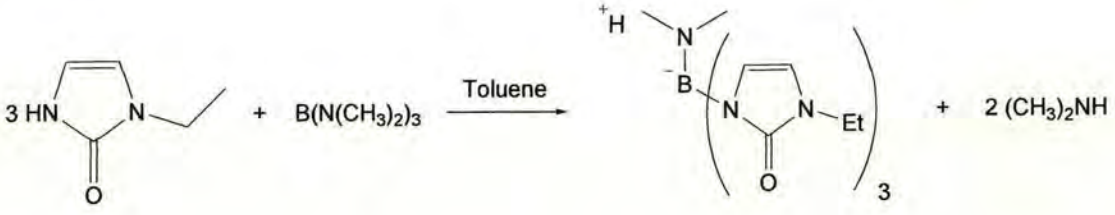

Scheme 2-11 Preparation of tris(1-ethyl-4-imidazolin-2- one)-(dimethylamine)borate

Spectroscopic Analysis

The ^{1}H NMR spectrum of the product shows clean signals for all of the expected protons. A triplet is observed for the methyl protons (1.20 ppm), a singlet for the methyl protons of the amine (2.66 ppm), a quartet for the methylene protons (3.58 ppm) and two doublets for the imidazole protons (6.01, 6.12 ppm). The ES-MS exhibits a peak representing the molecular ion (M^{+} = 390). It was noted that there is the possibility for the oxygen atoms, rather than the nitrogen atoms, to coordinate to the boron. For this reason we investigated the liquid IR of **4** and **6**. We would expect a substantial shift to lower frequency of the C-O stretch with oxygen coordination[109] however the bands remain relatively unchanged between **4** (1678 cm^{-1}) and **6** (1666 cm^{-1}). The ^{13}C NMR spectrum supports these results with the signals for the urea carbons of **4** and **6** found at 154.54 and 155.95 ppm respectively.

Attempted Synthesis of Potassium Hydrotris(1-ethyl-4-imidazolin-2-one)borate

To synthesise hydrotris(1-ethyl-4-imidazolin-2-one)borate salts the dimethylamino-group needed to be removed from **6** and replaced by a hydrogen. It was envisioned that this could be carried out by the deprotonation of **6** followed by acetylation of the amino-group and subsequent treatment with base (Scheme 2-12).

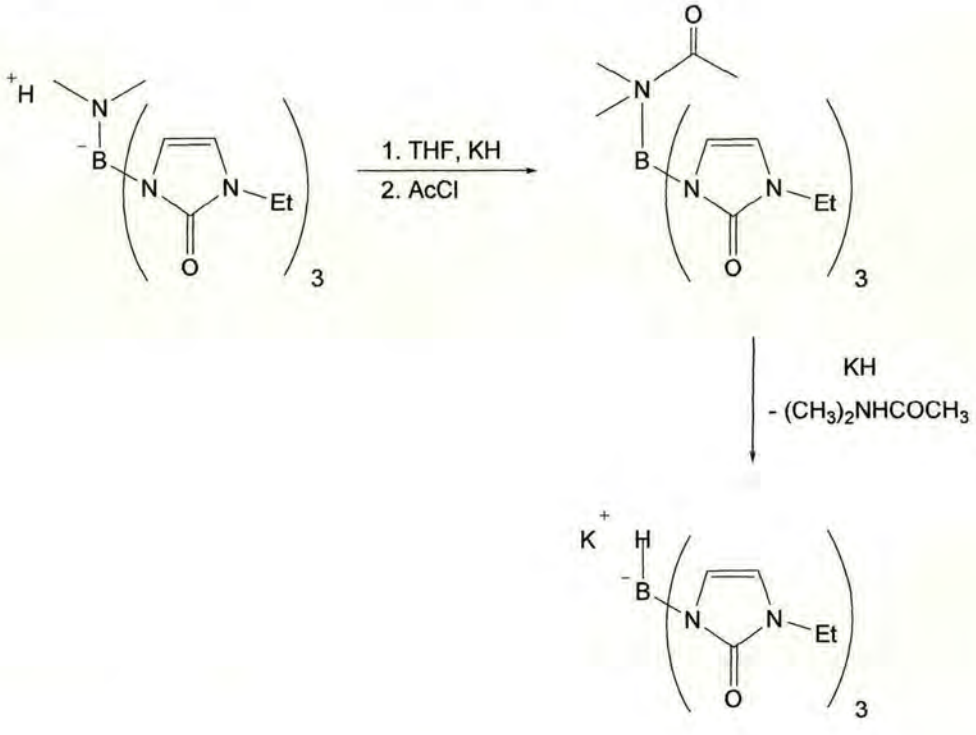

Scheme 2-12 Attempted synthesis of hydrotris(1-ethyl-4-imidazolin-2-one)borate

The product isolated from this reaction, however, was characterised as 1-ethyl-4-acetyl-4-imidazolin-2-one (**7**). We postulate that the product of the deprotonation is in fact quite unstable and decomposes to 1-ethyl-4-imidazolin-2-one. When acetyl chloride

is added in the presence of base it reacts with the decomposition product 1-ethyl-4-imidazolin-2-one producing 1-ethyl-4-acetyl-4-imidazolin-2-one (Scheme 2-13).

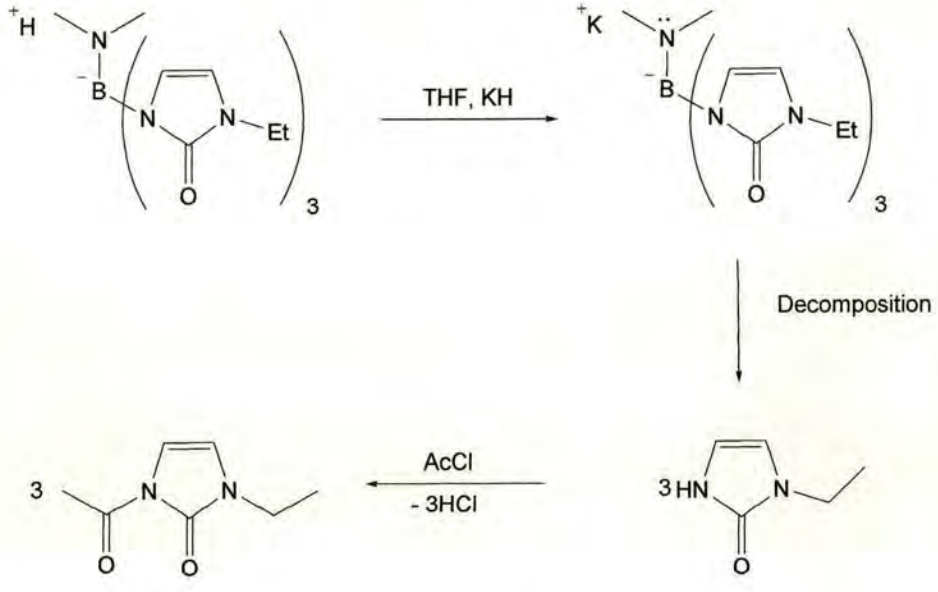

Scheme 2-13 Proposed reaction pathway upon treatment of tris(1-ethyl-4-imidazolin-2-one)(dimethylamine)borate with KH and AcCl

1-Ethyl-4-acetyl-4-imidazolin-2-one (7)

In an attempt to verify the above result **4** was treated with base followed by acetyl chloride (Scheme 2-14). The product was fully characterised and is identical to the product obtained following the decomposition.

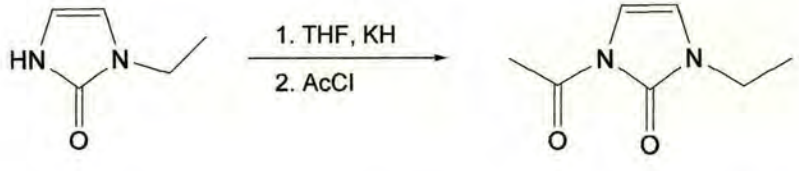

Scheme 2-14 Preparation of 1-Ethyl-4-acetyl-4-imidazolin-2-one

2.3.1.2 Conclusions

The attempted synthesis of hydrotris(1-alkyl-4-imidazolin-2-one)borate using 1-phenyl-4-imidazolin-2-one (**2**) or 1-ethyl-4-imidazolin-2-one (**4**) and the conventional melt procedure proved unsuccessful. This was a surprising result as it has been reported[8] that the success of the melt reaction depends, not on the pK_a of the imine proton, but on the melting point of the heterocycle and in the case of **2** and **4** the melting points are within the range known to give successful reactions. We must therefore conclude that there is another reason for the failure of this reaction. It is notable that the heterocycles compared by Reglinski are, in fact, all thiones (2-mercaptothiazoline, methimazole, 2-mercaptobenzothiazoline and imidazolidinethione) with a range of pK_a values between 4.2 and 4.7. The pK_a values of **2** and **4** could not be found in the literature however it is likely that they are higher than the thiones due to resonance stabilisation of the anion.[110] It is possible that a significant difference in pK_a such as this could adversely affect the reaction. The hygroscopic nature of the 1-alkyl-4-imidazolin-2-ones should also be noted. Although the imidazolinones can be handled in air, over time the compounds take up water. All of the detailed reactions were carried out in dry glassware under an atmosphere of nitrogen, however there is the possibility that water introduced by the addition of sodium borohydride could hinder the reaction. For this reason the reaction was carried out using dry potassium borohydride however this reaction was also unsuccessful.

In an attempt to find another route to the ligand, tris(dimethylamino)borane was employed as an alternative boron source. Its reaction with the hetrocycle **4** proved

successful and tris(1-ethyl-4-imidazolin-2-one)(dimethylamine)borate (**6**) was isolated in high yield. Problems arose, however, with the replacement of the dimethylamino group. Treatment of **6** with potassium hydride brings about decomposition and ultimately confirming this route as ineffective.

2.3.2 Carbon Donor Ligands

2.3.2.1 Attempted Synthesis of Hydrotris(3-methyl-2-methyleneimidazolinyl)borate

Reaction of 2-Methylimidazole with Sodium Borohydride in DMF

In an adaptation of the reported synthesis of sodium hydrotris(2-methylimidazolyl)borate[105] by Zaidi *et al.* three equivalents of 2-methylimidazole and finely ground sodium borohydride were added to a dry Schlenk tube fitted with a reflux condenser and a volumetric device for the measurement of hydrogen evolution.* The reaction was refluxed for 24 h (Scheme 2-15). As the literature reports, a white solid precipitated from of solution however only two molar equivalents of hydrogen were produced. Analysis of the white solid indicated the production of hydrogen dihydrobis(2-methylimidazolyl)borate (**8**).

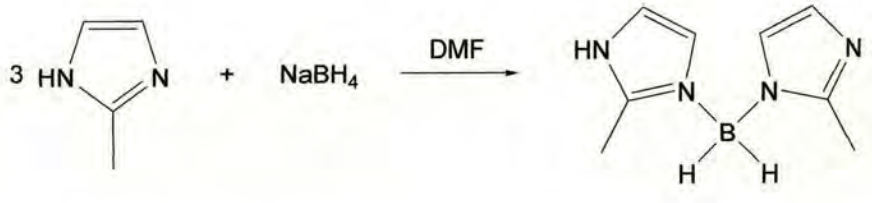

Scheme 2-15 Reaction of 2-methylimidazole and sodium borohydride in DMF

Reaction of 2-Methylimidazole with Sodium Borohydride (Melt)

In an attempt to find an alternative route to sodium hydrotris(2-methylimidazolyl)borate Reglinski's melt reaction[5] was employed. 2-methylimidazole,

* Appendix 2

however, has a tendency for sublimation, and a large amount of the starting material was observed condensing on the sides of the Schlenk tube leaving a substantial amount of starting material unavailable for reaction. For this reason it was decided that the melt reaction was unsuitable and subsequent attempts to synthesise the ligand were limited to reactions in solution.

General Procedure for the Reaction of 2-Methylimidazole with Sodium Borohydride in Solution. (For specific conditions refer to Table 2-4)

In various attempts to synthesise sodium hydrotris(2-methylimidazolyl)borate a finely ground mixture of 2-methylimidazole and sodium borohydride was added to a Schlenk tube which was fitted with a reflux condenser connected to a volumetric device for the measurement of hydrogen evolution.* Dry solvent was added and the solution was heated.

Table 2-4 Reaction conditions for experiments involving 2-methylimidazole and sodium borohydride in solution

Equiv.	Solvent	Temp. (°C)	Reaction Time (h)	Product
3.2	Toluene	111	24	Hydrogen dihydrobis(2-methylimidazolyl)borate
3.2	Toluene	111	96	
3.2	Xylene	115	4	
3.2	Diglyme	90	5	
3.2	Diglyme	100	5	
3.2	Diglyme	125	5	

* Appendix 2

In the case of the reactions in toluene and diglyme a white solid precipitated out of solution. This solid was isolated and shown by NMR, mass spectrometry, elemental analysis and X-ray diffraction to be hydrogen dihydrobis(2-methylimidazolyl)borate (**8**) in which one of the two 2-methylimidazole groups is protonated at the imine nitrogen making the two rings inequivalent. In the case of the reaction in xylene all reactants and products remained in solution during the reaction. Upon cooling the volume of solvent was reduced and ether was added. The white solid that was recovered was shown by NMR, mass spectrometry, elemental analysis and X-ray diffraction to be **8**. It seems that because of the production of **8**, a neutral species, which in most cases precipitates out of solution, it was impossible to obtain the tris-substituted ligand by this route. The mechanism for this reaction is unknown but from the structural evidence (Fig. 2-8) we postulate the following route (Scheme 2-16).

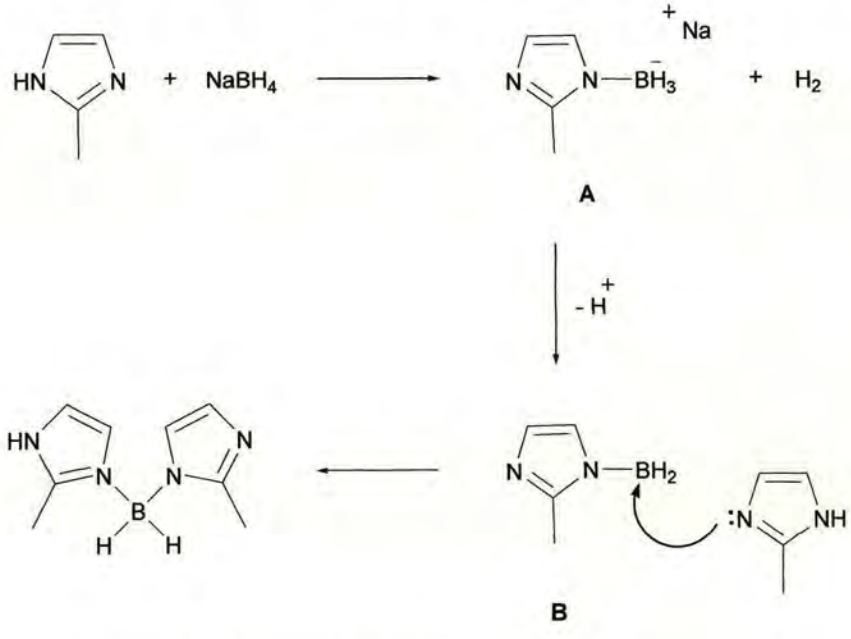

Scheme 2-16 Proposed mechanism for the synthesis of 8

It is possible that the first equivalent of 2-methylimidazole undergoes a condensation reaction with sodium borohydride in the usual manner producing the negatively charged species (**A**) and one equivalent of hydrogen. At this stage loss of a proton provides the neutral species (**B**) upon which nucleophilic attack by a second equivalent of 2-methylimidazole may occur producing **8**.

Hydrogen Dihydrobis(2-methylimidazolyl)borate (8)

8 was synthesised as described in Section 6.3 (Scheme 2-17). The white solid was isolated in high yield.

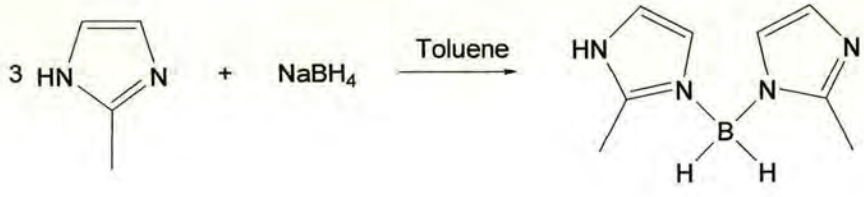

Scheme 2-17 Preparation of hydrogen dihydrobis(2-methylimidazolyl)borate

Spectroscopic Analysis and Molecular Structure

Analysis of the solid reveals that the boron is substituted by two heterocycles and only one set of signals is observed for the protons in the ^{1}H NMR spectrum. The molecular ion peak is observed in the ES-MS (M^{+}– H = 335). The crystal structure of **8** is shown in Figure 2-8 with selected bond lengths and bond angles listed in Table A-1. The B-N distances are 1.549(3) and 1.578(3) Å which are similar to the B-N bond lengths in complexes of the TRIS ligand [1.544(6)-1.557(6) Å].[101] The crystal structure of the

ligand reveals that one of the two 2-methylimidazole groups is protonated at the imine nitrogen making the two rings inequivalent.

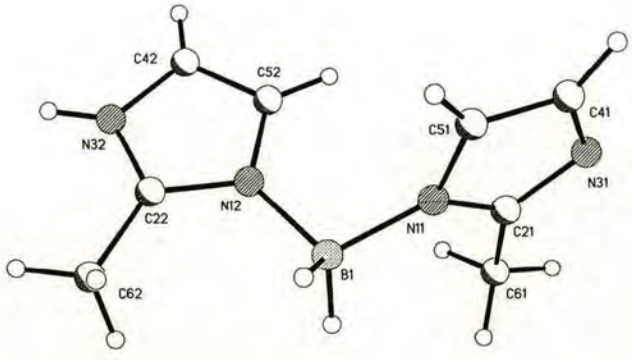

Figure 2-8. Molecular structure of hydrogen dihydrobis(2-methylimidazolyl)borate

Attempted Synthesis of Sodium Hydrotris(2-methylimidazolyl)borate from 8

In an attempt to synthesise sodium hydrotris(2-methylimidazolyl)borate from **8** the latter was treated with one equivalent of potassium hydride as described in Section 6.3. It was hoped that by addition of one equivalent of 2-methylimidazole to a toluene solution of the deprotonated ligand the tris-substituted ligand would be formed (Scheme 2-18).

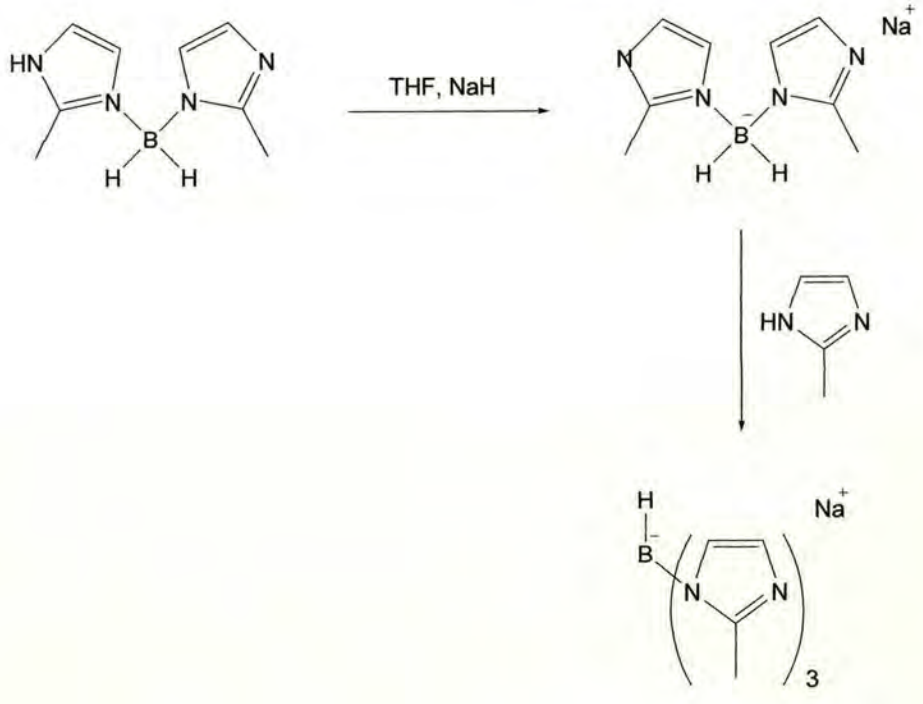

Scheme 2-18 Attempted synthesis of sodium hydrotris(2-methylimidazole)borate from 8

The deprotonation of **8** seemed to be successful and the product was characterised by NMR and mass spectrometry. The signals for the methyl protons (2.19 ppm) and the imidazole protons (6.67, 6.73 ppm) were observed in the ^{1}H NMR spectrum however this technique cannot confirm whether or not the deprotonation took place. For this reason the mass spectrum of the product was important. Although it is difficult to confirm, without doubt, the presence of the deprotonated ligand, the mass spectra indicate it has been formed. The molecular ion peak in the ES-MS of hydrogen dihydrobis(2-methylimidazolyl)borate (**8**) is observed at 176.8 whereas the spectrum of the deprotonated ligand displays the molecular ion peak at 174.9. The fact that this result

has been confirmed in a number of separate experiments leads us to the conclusion that the reaction is successful. Furthermore, the differences in solubility, which ultimately led to the abandonment of this reaction, confirm the disparity of starting material and product. This compound is insoluble in toluene and failed to react with 2-methylimidazole when refluxed overnight. Upon investigation of the solubility of the deprotonated ligand it was found that it was insoluble in common solvents and only slightly soluble in DMF. The reaction of the deprotonated ligand with 2-methylimidazole was therefore attempted in DMF however analysis of the product revealed only unreacted starting materials.

General Procedure for the Reaction of 2-Methylimidazole with Tris(dimethylamino)borane in Solution (For specific conditions refer to Table 2-5)

Three equivalents of 2-methylimidazole were added to a solution of tris(dimethylamino)borane in solution.

Table 2-5 Reaction conditions for experiments involving 2-methylimidazole and tris(dimethylamino)borane

Equiv.	Solvent	Temp. (°C)	Reaction Time (h)	Product
3	Benzene	69	20	Hydrogen tetrakis(2-methylimidazolyl)borate
3	Toluene	111	20	Hydrogen tetrakis(2-methylimidazolyl)borate
3	THF	20	20	2-Methylimidazole
1	Benzene	69	2	Hydrogen tetrakis(2-methylimidazolyl)borate

In the case of reaction in toluene and benzene, the reaction was refluxed overnight and the solvent removed under vacuum yielding a white powder. Analysis of the solid revealed only the presence of hydrogen tetrakis(2-methylimidazolyl)borate **(9)** [Scheme 2-19(a)].

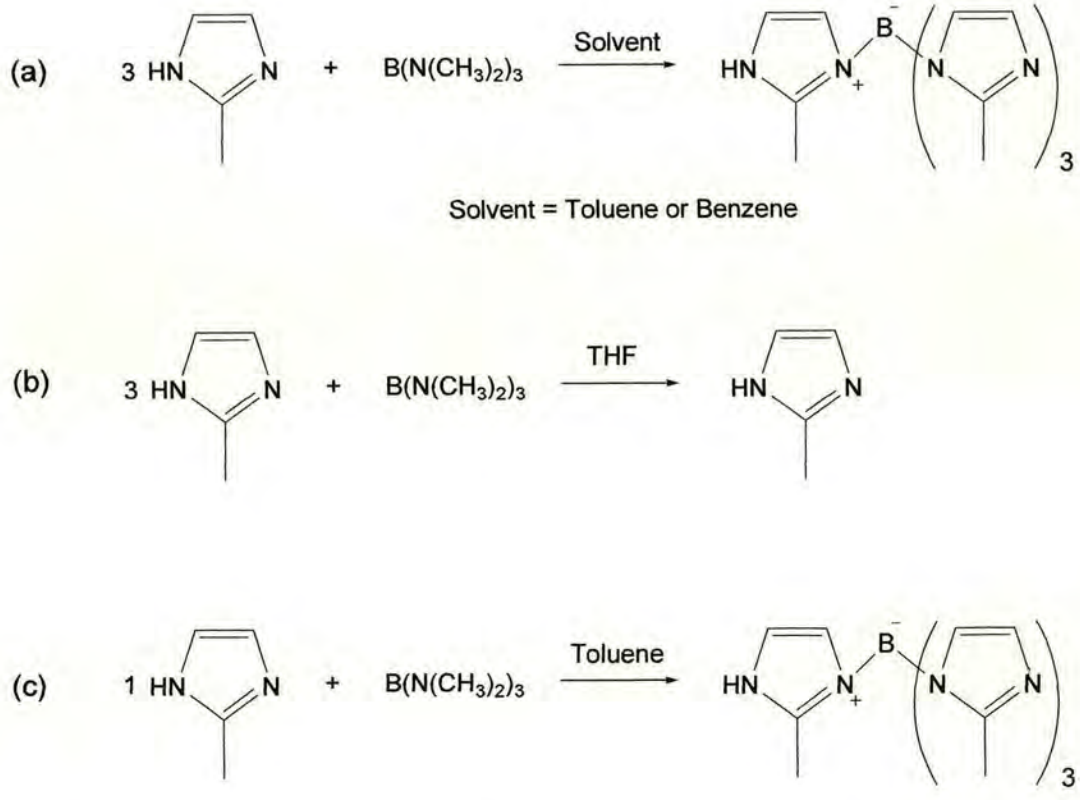

Scheme 2-19 Reactions of 2-methylimidazole and tris(dimethylamino)borane in solution

It was thought that by lowering the reaction temperature the tris-substituted ligand would form. THF was chosen as the solvent because of its ability to dissolve

2-methylimidazole. This reaction failed to produce the desired product; in fact analysis indicated only the presence of starting materials [Scheme 2-19(b)]. An attempt to form the mono-substituted ligand by control of the stoichiometry was also made. It was thought that the heterocycle would react with tris(dimethylamino)borane to yield bis(dimethylamine)(2-methylimidazole) borate, which could then be reacted with subsequent equivalents of 2-methylimidazole eventually leading to the synthesis of tris(2-methylimidazole)(dimethylamine)borate. Surprisingly, the use of equimolar amounts of 2-methylimidazole and tris(dimethylamino)borane in toluene produced **9**, the tetra-substituted ligand [Scheme 2-19(c)]. The mechanism in this case must differ from that of the 'conventional' reaction mechanism between methimazole, for example, and tris(dimethylamino)borane (Scheme 2-20).

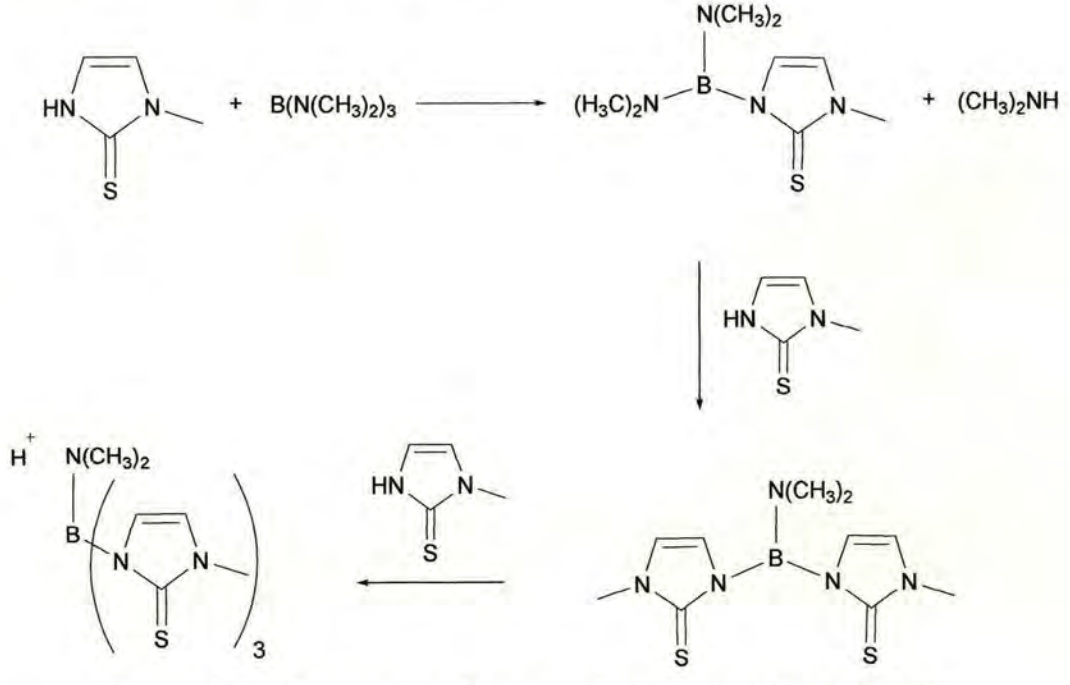

Scheme 2-20 'Conventional' reaction between methimazole and tris(dimethylamino)borane

We postulate that instead of elimination of dimethylamine in an acid-base reaction as seen in Scheme 2-20, the first step in the reaction between 2-methylimidazole and tris(dimethylamino)borane involves the coordination of the lone pair of the nitrogen to the boron of the $B(NMe_2)_3$. This would result in a significant increase in the basicity of the NMe_2 groups as the formation of the tetrahedral species would preclude the B-N π-bonding which is present in $B(NMe_2)_3$. This would therefore provide a strongly basic intermediate, **A,** which quickly reacts with three equivalents of 2-methylimidazole forming **8** (Scheme 2-21).

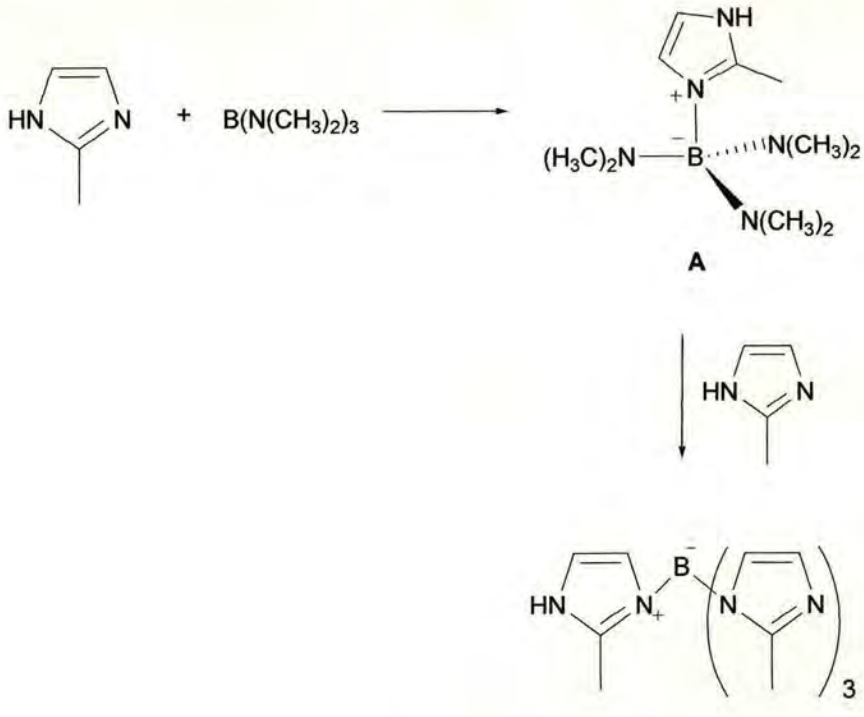

Scheme 2-21 Proposed pathway for reaction of 2-methylimidazole with tris(dimethylamino)borane

The formation of **9** even when the stoichiometry of the reactants is 1:1 indicates that the acid-base reaction of the initially formed intermediate **A** with 2-methylimidazole is faster than the initial coordination of 2-methylimidazole to $B(NMe_2)_3$. If this is the case, there seems to be a subtle balance between N-H acidity and imine nitrogen basicity, which determines the outcome of these reactions. The strong B-N π-bonding present in $B(NMe_2)_3$ significantly reduces its Lewis acidity and a strongly basic donor is therefore required to form a species such as **A**. If a comparison is made with pyrazolyl and methimazole, which are known to react in the 'conventional' way to produce the $[(azolyl)_3B(NHMe_2)]$ species (Scheme. 2-20), it is apparent that the lower acidity and higher basicity of 2-methylimidazole result in the alternative reaction pathway.

Hydrogen Tetrakis(2-methylimidazolyl)borate (9)

To fully characterise the compound which had been the product of all reactions between 2-methylimidazole and tris(dimethylamino)borane, **9** was synthesised as described in Section 6.3 (Scheme 2-22). The white solid, which was obtained in high yield, was characterised by NMR, mass spectrometry and elemental analysis.

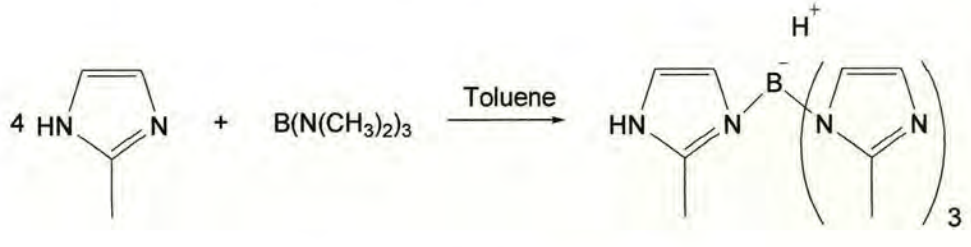

Scheme 2-22 Preparation of 9

Spectroscopic Analysis

The ^{1}H NMR spectrum of **9** displays the expected signals for the product. A singlet is observed at 1.99 ppm for the methyl protons and two doublets are observed at 6.92 and 7.23 ppm for the imidazole protons. The fact that the signal for the methyl protons is shifted upfield from those of free 2-methylimidazole (2.59 ppm) is a good indication that complexation has occurred. Moreover, the imidazole protons in 2-methylimidazole appear as a singlet integrating for two protons at 7.11 ppm whereas in **9** the protons appear as a pair of doublets, indicating that in the coordinated state they experience different environments. Although ^{1}H NMR is a valuable tool in the characterisation of the product we are unable to gain insight into the number of boron-coordinated heterocycles as in any case the integration will be identical. For this reason mass spectrometry is an important technique in the characterisation of **9** and a peak for the ionization of the product ($M^+ - H = 335$) is observed in the ES-MS.

2.3.2.2 Conclusions

The synthetic strategy for the preparation of the hydrotris(3-methyl-2-methyleneimidazolinyl)borate ligand was dependant on the previously reported[105] synthesis of the hydrotris(2-methylimidazolyl)borate ligand. This step was, however, more difficult than anticipated and after numerous and varied attempts it was concluded that the reported synthesis is unreliable. We have concluded that reaction between 2-methylimidazole and borohydride reagents can only produce the neutral ligand hydrogen dihydrobis(2-methylimidazolyl)borate, **8**. The mechanism we propose will always lead to this neutral species which is then inert to further substitution.

The use of tris(dimethylamino)borane as a boron source also gives an unexpected result. All attempts to synthesise tris(2-methylimidazole)(dimethylamine)borate led, in fact, to the production of hydrogen tetrakis(2-methylimidazolyl)borate, **9**. A mechanism for this reaction had been postulated.

A final attempt to synthesise hydrotris(2-methylimidazolyl)borate was undertaken however the deprotonation of **8** leads to a highly insoluble material which remained unreacted when further equivalents of 2-methylimidazole were added.

As numerous routes to the synthesis of hydrotris(2-methylimidazolyl)borate proved unsuccessful, a different approach to the synthesis of hydrotris(3-methyl-2-methyleneimidazolinyl)borate is needed. A possible route would be *via* the previously synthesised hydrotris(imidazolyl)borate (Scheme 2-23).

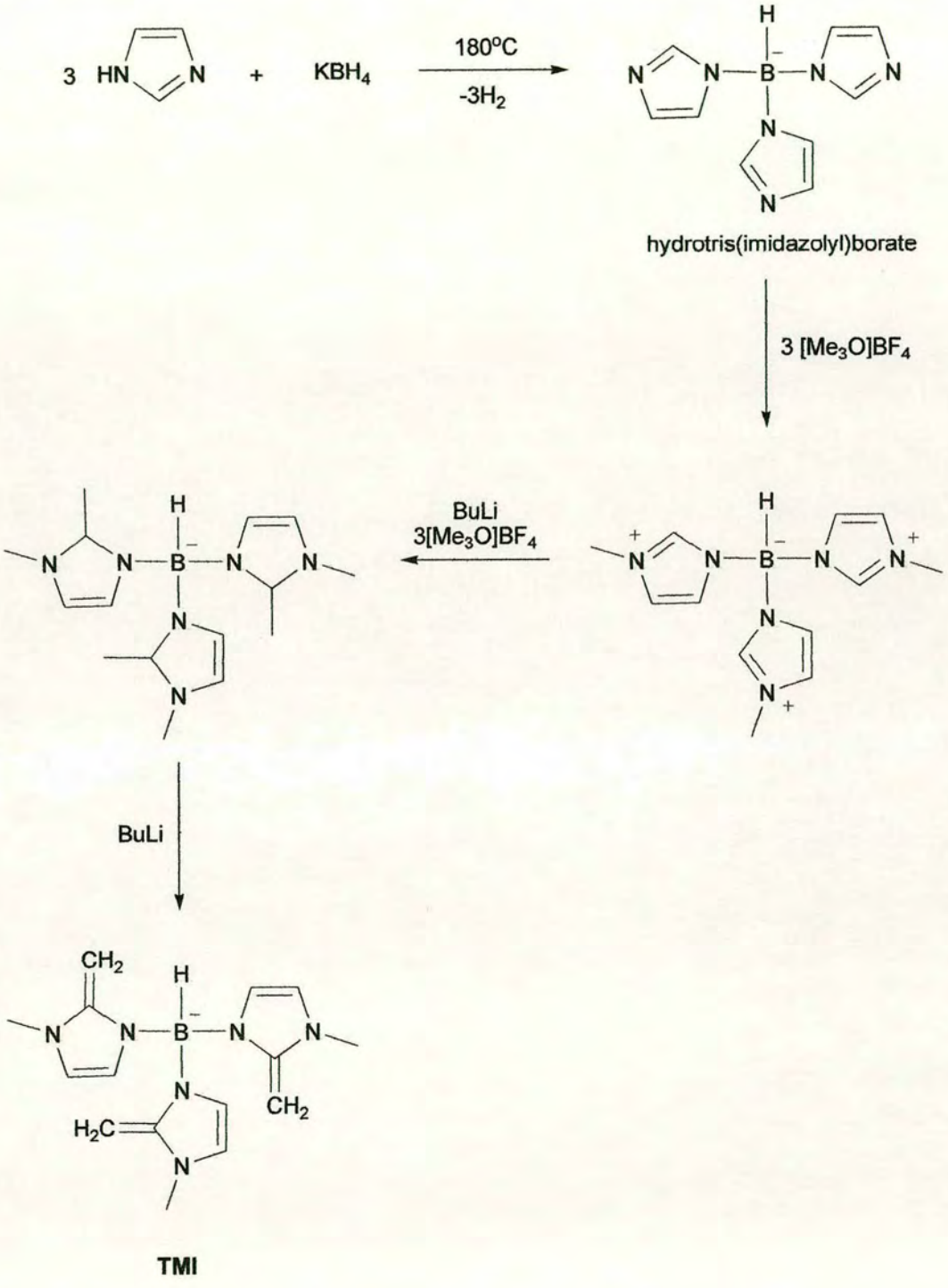

Scheme 2-23 Alternative synthetic strategy for the formation of TMI

2.3.3 Addition of Chiral Groups to the backbone of the Tm Ligand

2.3.3.1 Attempted Synthesis of Hydrotris(1-α-methylbenzyl-2-mercaptoimidazolyl)borate

(L)-(-)-α-Methylbenzylaminoacetaldehyde Diethyl Acetal (10)

In an adaptation of the method described by Beaumont *et al.* for the preparation of *tert*-butylaminoacetaldehyde diethyl acetal,[111] (L)-(-)-α-methylbenzylaminoacetaldehyde diethyl acetal was formed from bromoacetaldehyde diethylacetal and (L)-(-)-α-methylbenzylamine as described in Section 6.3 (Scheme 2-24).

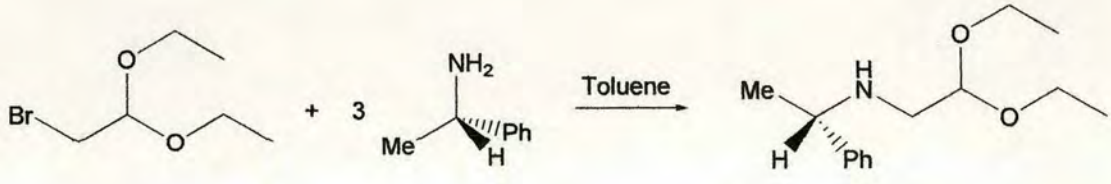

Scheme 2-24 Preparation of (L)-(-)-α-methylbenzylaminoacetaldehyde diethyl acetal

2-Mercapto-1-[(L)-(-)-α-methylbenzyl]imidazole (11)

An adaptation of the literature method for the preparation of 1-substituted-2-mercaptoimidazoles[106] reported by Jones *et al.* was employed for the synthesis of **11** (Scheme 2-25). The product was isolated in low yield as described in Section 6.3. The low yield is probably due to the harsh conditions needed for the cyclisation.

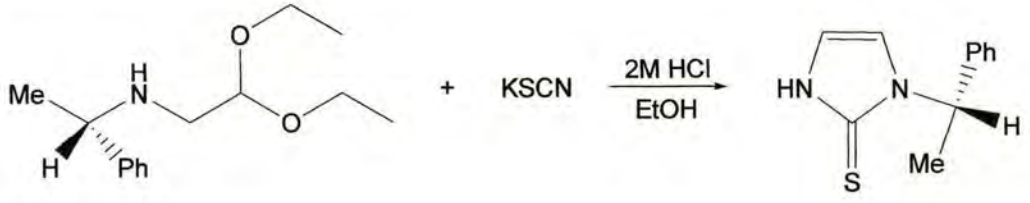

Scheme 2-25 Preparation of 2-mercapto-1-[(L)-(-)-α-methylbenzyl]imidazole

Reaction of 11 with Sodium Borohydride

In an initial attempt to synthesise sodium hydrotris[2-mercapto-1-{(L)-(-)-α-methylbenzyl}imidazolyl]borate an adaptation of Reglinski's melt reaction[5] was used. The reaction was stopped after 3 hours as the mixture had darkened considerably. Analysis of the solid revealed only the presence of starting materials.

Reaction of 11 with Potassium Borohydride

It was thought that by using a more reactive borohydride reagent the imidazole would react to form the desired product. A melt reaction was set up as before and potassium borohydride used instead of sodium borohydride. The reaction was heated slowly to 160 °C over 5 hours. Analysis of the solid revealed only the presence of starting materials.

General Procedure for the Reaction of 11 with Borohydride Salts in Solution (For specific conditions refer to Table 2-6)

In various attempts to synthesise hydrotris[2-mercapto-1-{(L)-(-)-α-methylbenzyl}imidazolyl]borate a finely ground mixture of **11** and sodium or potassium borohydride was added to a Schlenk tube which was fitted with a reflux condenser connected to a volumetric device for the measurement of hydrogen evolution.* Dry solvent was added and the solution refluxed until evolution of gas ceased or the reaction became highly discoloured. NMR and mass spectrometry of the isolated products confirmed only the presence of the unreacted starting material, **11**.

Table 2-6 Reaction conditions for experiments involving 11 and borohydride salts

Equiv.	Solvent	Temp. (°C)	Reaction Time (h)	Product
3	Toluene	111	120	2-Mercapto-1-((L)-(-)-α-methylbenzyl)imidazole
3	Xylene	140	15	
3	DMF	150	15	

* Appendix 2

2.3.3.2 Conclusions

The reaction of 2-mercapto-1-[(L)-(-)-α-methylbenzyl]imidazole (**11**) and borohydride reagents proved unsuccessful. This was very unexpected as there is precedent in the literature for the synthesis of Tm derivatives with bulky groups in the 1-position. The reasons for this failure are as yet unclear as the melting point of the heterocycle is in the appropriate range for a successful reaction.

3 Complexes of the Tm Ligand

3.1 INTRODUCTION

Since its synthesis in 1996, the Tm ligand has been shown to complex to a wide variety of metals (See Chapter 1 for a comprehensive review). Because the ligands we have chosen to study are so closely related to Tm, in many instances the Tm ligand was utilised in order to investigate whether or not certain reactions were likely to work. This Chapter summarises the novel complexes of the Tm ligand that have been synthesised over the course of this project.

3.2 Preparation of Starting Materials

A number a commonly used, well-described precursors were employed throughout the course of these studies. In this section, a brief description of the adapted procedures for their syntheses and, where relevant, a short overview of the chemistry involved is undertaken.

[MnBr(CO)$_5$]

Pentacarbonylmanganese halides are useful precursors for the synthesis of many complexes. The literature procedure[112] describes the use of CS_2 as the reaction solvent. To avoid the use of such a toxic solvent, an adaptation of the literature method was developed. A stoichiometric equivalent of bromine was added to $[Mn_2(CO)_{10}]$ in dichloromethane as described in Section 6.2 (Scheme 3-1). $[MnBr(CO)_5]$ was isolated in high yield and purity.

$$[Mn_2(CO)_{10}] + Br_2 \xrightarrow{CH_2Cl_2} 2\,[Mn(CO)_5Br]$$

Scheme 3-1 Preparation of [MnBr(CO)$_3$]

fac-*[Mn(CO)$_3$ (MeCN)$_3$]PF$_6$*[113]

$[Mn(CO)_3(MeCN)_3][PF_6]$ was synthesised as described in Section 6.2 (Scheme 3-2). The product was isolated as yellow crystals in high yield. The solution IR spectrum of this complex exhibits two strong ν_{C-O} bands, which suggests a C_{3v} symmetric product and, therefore, *fac*-coordination.

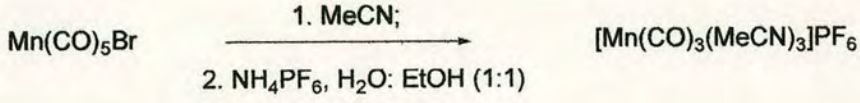

Scheme 3-2 Preparation of $[Mn(CO)_3(MeCN)_3]PF_6$

***[RuCl$_2$(p-cym)]$_2$*[114]**

$[RuCl_2(p\text{-cym})]_2$ is a useful starting material for the preparation of ruthenium complexes. It is soluble in a range of solvents and gives air stable solutions. Hydrated ruthenium trichloride was reacted with α-terpinine as described in Section 6.2 to produce the dimer in high yield (Scheme 3-3).

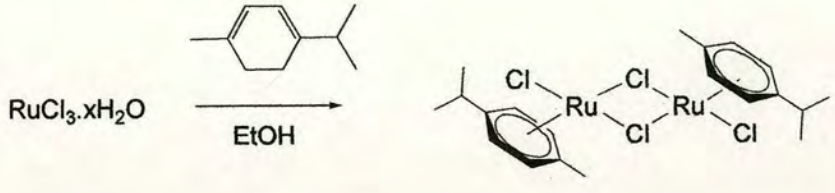

Scheme 3-3 Preparation of $[RuCl_2(p\text{-cym})]_2$

Three Step Synthesis of [Ru(Cp)(MeCN)$_3$]PF$_6$[115]

[Ru(C$_6$H$_6$)Cl$_2$]$_2$[116]

Hydrated ruthenium trichloride reacts with 1,4-cyclohexadiene as described in Section 6.2 to produce the complex [Ru(C$_6$H$_6$)Cl$_2$]$_2$ in high yield (Scheme 3-4). This complex was used as the precursor for the synthesis of [Ru(C$_6$H$_6$)Cp]PF$_6$.

Scheme 3-4 Preparation of [Ru(C$_6$H$_6$)Cl$_2$]$_2$

[Ru(C$_6$H$_6$)Cp]PF$_6$[115]

A mixture of [Ru(C$_6$H$_6$)Cl$_2$]$_2$, potassium carbonate and freshly cracked cyclopentadiene was reacted as described in Section 6.2 to provide [Ru(C$_6$H$_6$)Cp]PF$_6$ in good yield (Scheme 3-5). This complex was synthesised as the starting material for the preparation of [Ru(Cp)(MeCN)$_3$]PF$_6$.

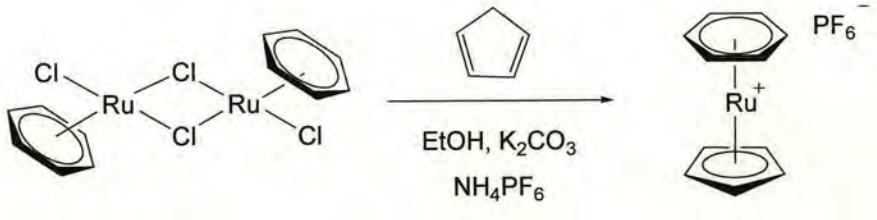

Scheme 3-5 Preparation of [Ru(C$_6$H$_6$)Cp]PF$_6$

$[Ru(Cp)(MeCN)_3]PF_6$[115]

An acetonitrile solution of $[Ru(C_6H_6)Cp]PF_6$ was degassed and photolysed using a 150 W medium pressure Hg lamp as described in Section 6.2 (Scheme 3-6). $[Ru(Cp)(MeCN)_3]PF_6$ was isolated in high yield.

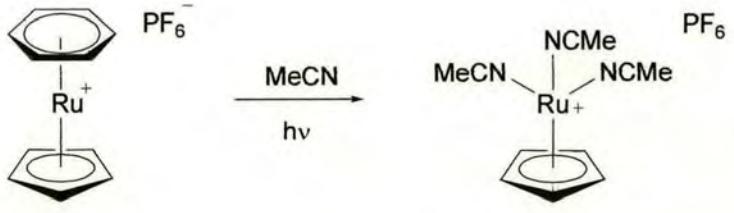

Scheme 3-6 Preparation of $[RuCp(MeCN)_3]PF_6$

$[RuCl_2Cp]_2$

From the reaction between hydrated ruthenium trichloride and freshly cracked cyclopentadiene, $[RuCl_2Cp]_2$ was formed in moderate yield as described in Section 6.2 (Scheme 3-7).

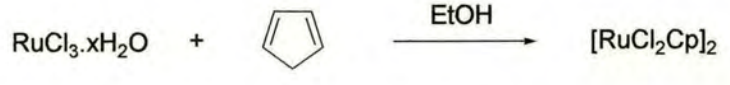

Scheme 3-7 Preparation of $[RuCl_2Cp]_2$

3.3 Ligand Synthesis

3.3.1 Sodium Hydrotris(methimazolyl)borate (12)

Sodium hydrotris(methimazolyl)borate was synthesised according to the literature procedure[5] published by Reglinski *et al.* and is described in Section 6.3 (Scheme 3-8). This procedure involves the use of a melt reaction whereby the reactants are added to a dry round-bottomed flask fitted with a volumetric device for the measurement of hydrogen evolution.* The system is flushed with nitrogen and subsequently heating is initiated. The reaction is carried out in the absence of solvent. As the reactants begin to melt the evolution of hydrogen begins and frothing of the mixture is observed. The temperature is raised slowly, keeping the evolution of hydrogen at an even rate. Once the calculated amount of hydrogen has been evolved the reaction is halted. A maximum temperature of 160 °C is reached. Soxhlet extraction of the product into chloroform yields the ligand in high purity and moderate yield.

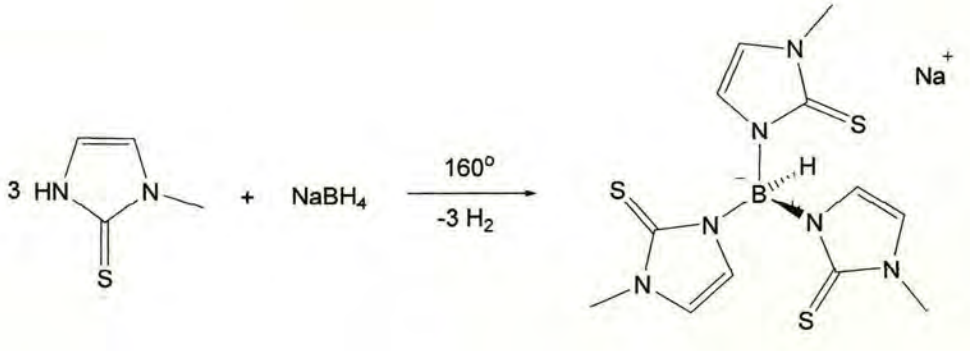

Scheme 3-8 Preparation of NaTm

* Appendix 2

3.4 Complex Synthesis

3.4.1 Synthesis and Characterisation of Manganese Complexes of the Tm Ligand

[MnTm(CO)$_3$] (13)

The manganese(I) complex **13** was synthesised *via* two routes. The product of each reaction was characterised spectroscopically and comparisons prove the compounds to be the same.

[MnTm(CO)$_3$] from NaTm and [Mn(MeCN)$_3$(CO)$_3$]PF$_6$

A stoichiometric equivalent of **12** in ethanol was added to [Mn(MeCN)$_3$(CO)$_3$]PF$_6$ as described in Section 6.3 (Scheme 3-9) which resulted in the formation of **13** in good yield and high purity.

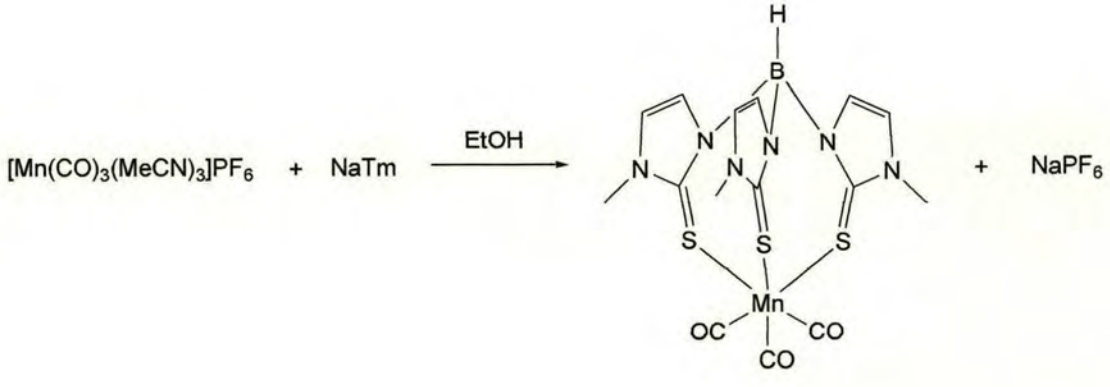

Scheme 3-9 Preparation of [MnTm(CO)$_3$]

[MnTm(CO)$_3$] from NaTm and [Mn(CO)$_5$Br]

The reaction of **12** and [Mn(CO)$_5$Br] was carried out as described in Section 6.3 (Scheme 3-10). The solid was isolated in good yield and purity.

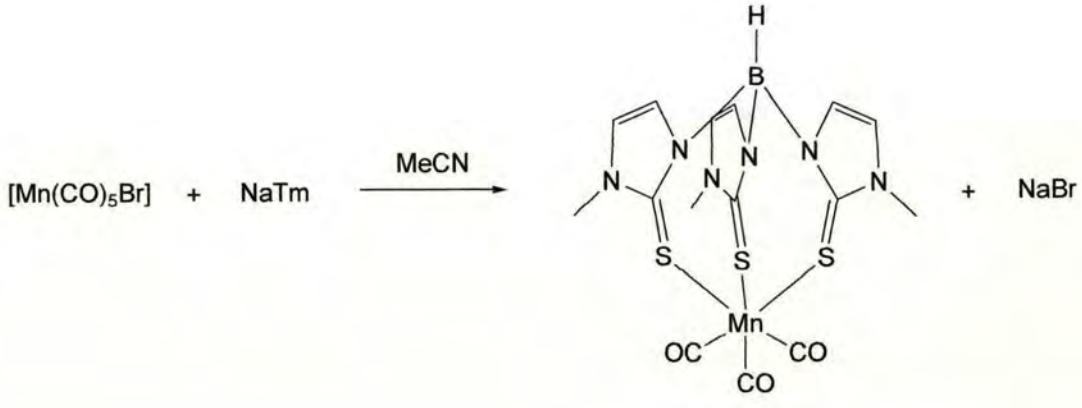

Scheme 3-10 Preparation of [MnTm(CO)$_3$]

Spectroscopic Analysis

The solid state IR of the complex is not unusual; the complex displays a ν_{B-H} absorption at 2470cm^{-1}. There are however, some noteworthy observations in the solution IR spectrum of **13**. Two ν_{C-O} signals are observed; these consist of two medium intensity bands at 2003 and 1905cm^{-1}. This result is consistent with the carbonyl stretches found in the IR of the analogous [ReTm(CO)$_3$] although the ν_{C-O} bands in the latter appear at lower energy (1987 and 1863cm^{-1}).[29] This is, however, inconsistent with the known structure; given the C_3 symmetry conferred on the complex by the twisted conformation of the [MnTm] unit, three bands are predicted for the C-O stretching

modes. This is particularly strange in view of the observation of three bands due to C-O stretching in [HB(thioxotriazolyl)$_3$Mn(CO)$_3$] in which the ligand is N-coordinated, thus providing a complex of C_{3v} symmetry.[58] The probable reason is the near coincidence of two of the three bands expected for a C_3-symmetric tricarbonyl complex. In the solid state KBr disc spectrum of **13** four absorptions of approximately equal intensity due to C-O stretching are observed at 1994, 1984, 1896 and 1884 cm^{-1} which are attributable to the presence of two independent molecules in the unit cell of the complex. The ^{1}H and ^{13}C NMR spectra are, however, consistent with the X-ray crystal structure of **13**. The protons of the three mercaptoimidazole groups are equivalent which suggests a symmetrical mononuclear structure in solution. The molecular ion peak (M^+ = 518) is observed in the FAB-MS.

Molecular Structure

Single crystals suitable for X-ray diffraction studies were obtained by slow diffusion of hexane into a dichloromethane solution. This is the first example of a manganese complex of the Tm ligand, although it is isostructural with the previously described [ReTm(CO)$_3$][29]. The S-coordination by the tripodal Tm and three CO ligands provide C_3 molecular symmetry. There are two independent molecules in the unit cell and, although minor differences are observed in their metrical parameters, discussion will be restricted to that containing Mn(1) (Fig. 3-1). The manganese atom adopts a slightly distorted octahedral geometry. There are only minor deviations from 90° in the angles around Mn, with the S-Mn-S angles being 94.329(18)°, C-Mn-C 91.86(8)° and S-Mn-C 85.81(6)°.

The Mn-S distances are 2.4015(5) Å, significantly longer than the literature values for Mn-S distances in other manganese carbonyls of the type $[MnL(CO)_3]$ where L represents sulphur donors such as tetrathiacyclododecanes[117, 118] and trithiacyclononane.[119] The Mn-C distances [1.8020(18) Å] compare favourably to the Mn-CO distances of the above-mentioned literature. Selected bond distances and angles are provided in Table A-2.

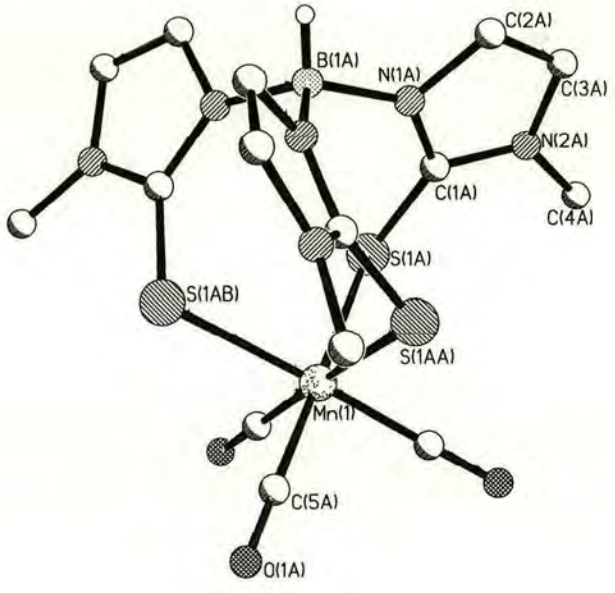

Figure 3-1 Molecular structure of $[MnTm(CO)_3]$ (Hydrogen atoms omitted for clarity)

3.4.2 Synthesis and Characterisation of Ruthenium Complexes of the Tm Ligand

[RuTm(p-cym)]Cl (14)

The ruthenium complex was synthesised *via* the route shown in Scheme 3-11. Treatment of the dimer $[RuCl_2(p\text{-cym})]_2$[114] with **12** as described in Section 6.3 results in the formation of **14** as a dark red solid in high yield.

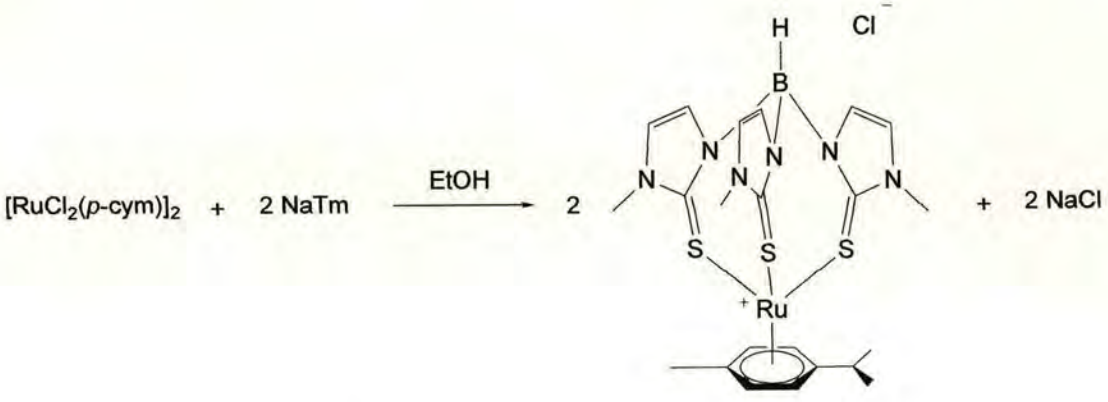

Scheme 3-11 Preparation of [RuTm(*p*-cym)]Cl

Spectroscopic Analysis

The ^1H and ^{13}C NMR spectra obtained for **14** are consistent with the structure found in the solid state; the protons of the mercaptoimidazole groups are equivalent. An interesting feature of this spectrum is the appearance of the signal due to the arene CH protons of the *p*-cymene ligand. The Ru(II)(*p*-cymene) fragment is found in many complexes and these protons usually appear as a clear $(AB)_2$ system in their NMR spectra.[120-122] However, in the spectrum of **14** a complex multiplet appears between 5.48

and 5.61 ppm. This can be attributed to the diastereotopic nature of these protons in the chiral environment provided by the coordination of the Tm ligand. The complex shows a single ν_{B-H} absorption at 2405 cm^{-1}. This value shows a shift to lower frequency relative to that of the free ligand (2480 cm^{-1}). **14** was also characterised by FAB-MS. The molecular ion peak (M^+ = 552) was observed as well as a peak representing the ionisation of the complex (M^+– Cl = 517).

Molecular Structure

Single crystals suitable for X-ray diffraction studies were obtained by slow diffusion of pentane into a dichloromethane solution. An X-ray crystal determination shows **14** to crystallise with one molecule of water in the unit cell. This is most likely due to the fact that the solvents used for crystallisation were not previously dried and the procedure was carried out in the presence of air and moisture. The Tm ligand adopts a facially capping arrangement with the *p*-cymene ligand completing the coordination sphere (Fig. 3-2). The average Ru-C distance is 2.210(26) Å while those for Ru-S differ significantly: 2.3930(7), 2.4174(8) and 2.4222(7) Å. These distances are similar in length to the Ru-S bonds in the complex [RuTm(CO)(PPh_3)] synthesised by Hill *et al.*[27] The three S-Ru-S angles are all close to 90° [90.40(3)-93.38(3)]. Selected bond distances and angles are provided in Table A-3.

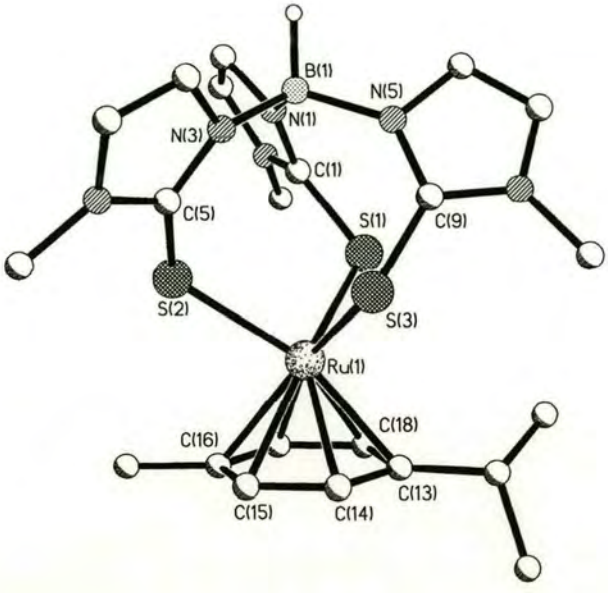

Figure 3-2 Molecular structure of [RuTm(*p*-cym)]Cl (Hydrogen atoms, counterion and solvents of crystallisation omitted for clarity)

[RuTmCp] (15a, 15b)

[Ru{κ^2-(μ-H)B(mt)$_3$}Cp] (15a)

[Ru(Cp)(MeCN)$_3$]PF$_6$[115] and **12** were reacted to produce the stable, dark red product in high yield (Scheme 3-12).

$$2\ \text{NaTm} + [\text{Ru(Cp)(MeCN)}_3]\text{PF}_6 \xrightarrow{\text{MeCN}} 2\ [\text{RuTmCp}] + \text{NaPF}_6$$

Scheme 3-12 Preparation of [Ru{κ^2-(μ-H)B(mt)$_3$}Cp]

Spectroscopic Analysis

The ^{1}H NMR spectrum of **15a** shows a splitting of the mercaptoimidazole signals. The methyl protons are split into two signals which integrate for three and six protons. Similarly, both sets of CH protons are split into two signals which integrate for two and one proton(s). In the absence of a crystal structure it is postulated that the splitting of the signals in the ^{1}H NMR spectrum is due to bidentate coordination of the Tm ligand to the ruthenium center and that the third arm of the tripod remains uncoordinated. However no evidence could be found for the presence of a coordinated acetonitrile molecule which such a coordination would imply if an 18-electron configuration were to be maintained. The molecular ion peak (M^+=518) is observed for the complex which is consistent with the formulation as [RuTmCp]. A number of coordinatively unsaturated 16-electron half-sandwich Ru(II) complexes containing Cp*[123-126] and arenes[120, 127] are known. These are stabilised either by π-donation from ligands such as halides or alkoxides or by hard donors such as TMEDA amidinates or amides. One example containing a chelating phosphine ligand is also known.[128] Given the evidence that the Tm ligand is a strong electron donor[13] it is conceivable that its S donors could be capable of stabilising a 16-electron Ru complex. However, there is precedent in the literature for the presence of agostic B-H···M interactions in dihydrobis(2-mercapto-1-methylimidazolyl)borate complexes[29, 49, 51, 54] as well as in complexes of the Tm ligand.[21, 26] In the case of Tm, this interaction is accommodated by the chelation of two methimazole donors with the third arm of the tripod remaining as a pendant group. The integration in the ^{1}H NMR spectrum of **15a** fits such a structure and the IR spectrum of

the complex further supports this theory. A strong absorption is observed at 2113 cm^{-1} which is comparable with the $\nu_{B\text{-}H\cdots Re}$ absorption of 2140 cm^{-1} found in the rhenium complex of dihydrobis(2-mercapto-1-methylimidazolyl)borate.[49] These values are significantly lower than the B-H absorption in the free ligand (2480 cm^{-1}) and in that of [Ru{κ^3-HB(mt)$_3$}Cp] (**15b**) (2348 cm^{-1}) in which an agostic interaction is absent (Fig. 3-4). As already mentioned, in the absence crystallographic data it is difficult to confirm the structure, however on the evidence of NMR and, importantly, IR data we suggest that the complex **15a** is coordinated in a *bis*-chelate fashion by two thione sulphur atoms of the tripodal Tm ligand, and the coordination sphere is completed by a Cp ring and one hydrogen atom which is involved in an agostic B-H···Ru interaction (Fig. 3-3).

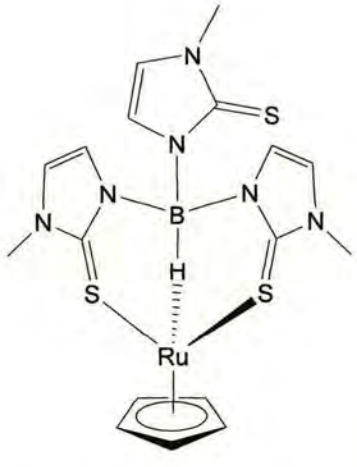

Figure 3-3 Postulated structure of [Ru{κ^2-(μ-H)B(mt)$_3$}Cp]

[Ru{κ^3-HB(mt)$_3$}Cp] (15b)

Treatment of the dimer $[RuCl_2Cp]_2$ with two equivalents of **12** affords the red solid in high yield and purity (Scheme 3-13).

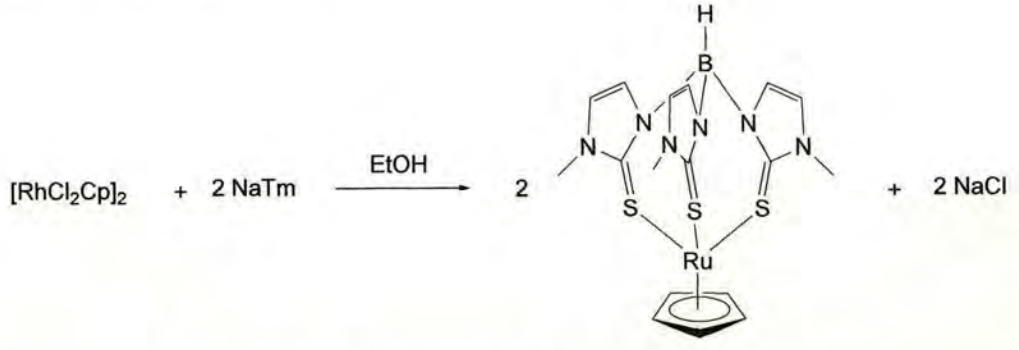

Scheme 3-13 Preparation of [Ru{κ^3-HB(mt)$_3$}Cp]

Spectroscopic Analysis

It is quite interesting that by changing the conditions of the reactions two complexes (**15a** and **15b**) that are isoelectronic yet structurally different have been synthesised. The NMR spectrum of **15b** shows only one environment for the protons of the ligand suggesting that all three sulphur donors are coordinated to the ruthenium ion. A singlet representing the methyl protons of the methimazole ring is observed at 1.56 ppm, the CH groups of the cyclopentadienyl ring are represented by a singlet at 5.45 ppm and the CH protons of the methimazole groups are observed as two doublets at 6.85 and 7.07 ppm. A single $\nu_{B\text{-}H}$ absorption is observed at 2348 cm^{-1} in the IR spectrum. This value differs significantly from the $\nu_{B\text{-}H\cdots Re}$ absorption observed at 2113 cm^{-1} for **15a** and is consistent with the B-H stretches in this work which are not involved in agostic

interactions. **15b** was also characterised by FAB-MS and the molecular ion peak (M^+=518) was observed.

Molecular Structure

Single crystals suitable for X-ray diffraction studies were obtained by slow diffusion of pentane into a dichloromethane solution. An X-ray crystal determination of **15b** shows there are two independent molecules in the unit cell, and although minor differences are observed in their metrical parameters, discussion will be restricted to that containing Ru(1) (Fig. 3-4) The Tm ligand adopts a facially capping arrangement with the Cp ligand completing the coordination sphere. The average Ru-S distance is 2.405(8) Å, similar to that of [RuTm(*p*-cym)]Cl (**14**). The Ru-C distances fall in the range 2.174(3)-2.264(3) Å. The three S-Ru-S angles are slightly greater than 90° falling in the range 93.8(2)-94.04(19). Selected bond distances and angles are provided in Table A-4.

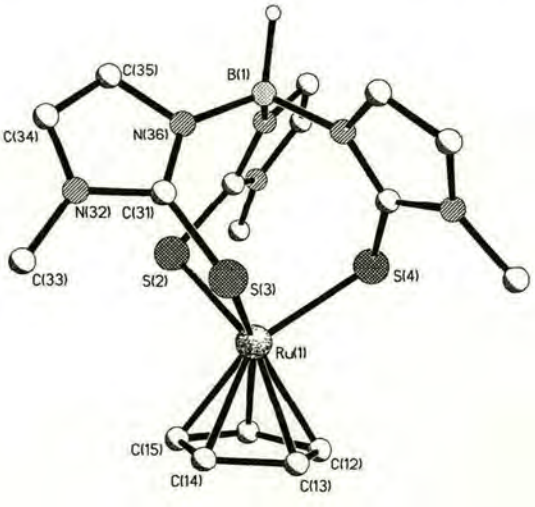

Figure 3-4 Molecular structure of [Ru{κ^3-HB(mt)$_3$}Cp] (Hydrogen atoms omitted for clarity)

[RuTm{C_6H_5(CO)OEt}]Cl (16)

From the reaction between $[RuCl_2(C_6H_5(CO)OEt)]_2$ and **12** as described in Section 6.3, **16** was isolated in high yield (Scheme 3-14).

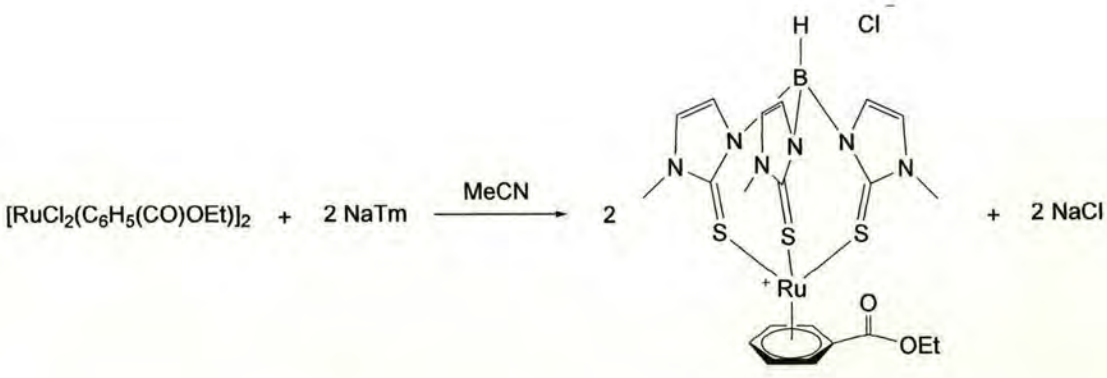

Scheme 3-14 Preparation of [RuTm(C_6H_5(CO)OEt]Cl

Spectroscopic Analysis

^1H and ^{13}C NMR data of **16** are consistent with a structure whereby the Tm ligand is coordinated to the ruthenium centre by all three of its sulphur donors. The ^1H NMR spectrum displays a single signal for both the 4- and 5-H indicating that all three arms of the tripod are equivalent. An absorption in the IR for the ν_{B-H} is seen at 2438 cm^{-1} and a peak representing the ionisation of the complex (M^+– Cl = 603) is observed in the FAB-MS.

3.4.3 Synthesis and Characterisation of a Cadmium Complex of the Tm Ligand

[CdTmBr] (17)

The cadmium complex [CdTmBr] was previously synthesised by Reglinski *et al.*[15] An alternative route to the complex is described below. This route could be considered attractive as it avoids the use of the thallium precursor TlTm. The complex is instead obtained from the reaction of an equimolar mixture of hydrated cadmium bromide and **12** as described in Section 6.3 (Scheme 3-15). The complex is obtained as a white solid of high purity in moderate yield.

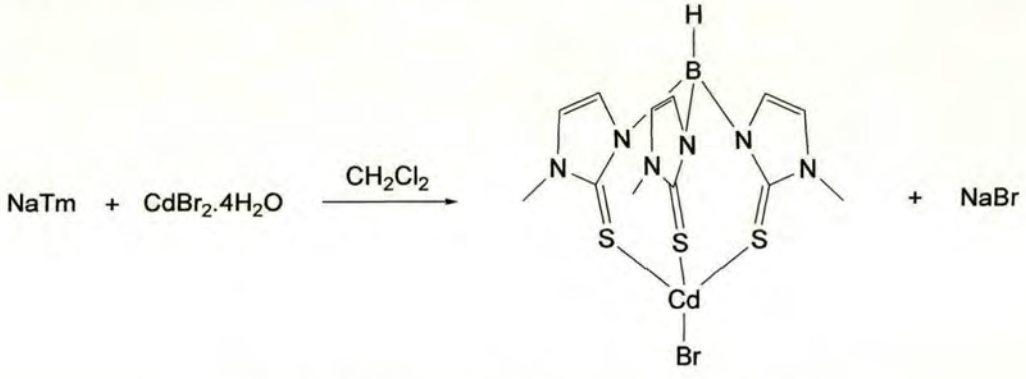

Scheme 3-15 Alternative route to [CdTmBr]

Spectroscopic Analysis

Analytical and spectroscopic data for the complex compare favourably to the previously described complex. The signals in the ^{1}H NMR spectrum are consistent with the three arms of the tripod being equivalent. An absorption in the IR spectrum for the $\nu_{B\text{-}H}$ is seen at 2382 cm^{-1} and peaks representing the molecular ion (M^+ = 543) and the ionisation of the complex (M^+– Br = 463) are observed in the FAB-MS.

Molecular Structure

For completeness, the crystal structure of **17** was obtained and is shown in Fig. 3-5. Unsurprisingly, the molecule was found to be isostructural with the same complex previously reported by Reglinski.[15] Selected bond lengths and bond angles are listed in Table A-5 and as can be seen from Table 3-1 below, almost all are similar to the previously published data.

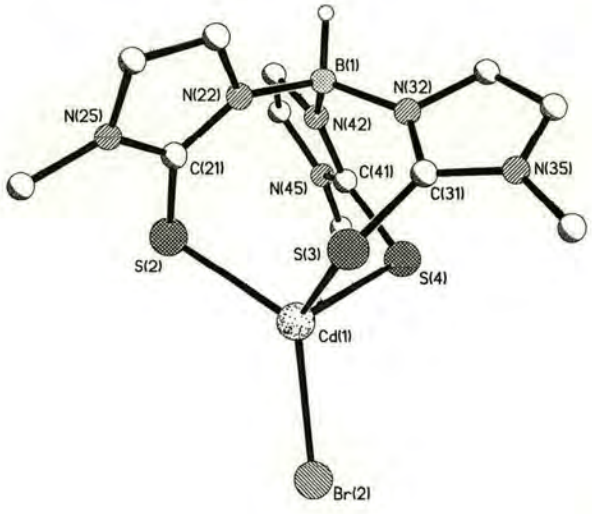

Figure 3-5 Molecular structure of [CdTmBr] (Hydrogen atoms omitted for clarity)

Table 3-1 Selected structural parameters of [CdTmBr]

	Literature Values[15]	Complex 17
Bond Lengths (Å)		
Cd-S(2)	2.5413(9)	2.5362(15)
Cd-S(3)	2.544(1)	2.5464(15)
Cd-S(4)	2.616(1)	2.6193(17)
Cd-Br	2.5674(4)	2.5647(9)
Bond Angles (°)		
S(2)-Cd-Br	124.99(3)	124.89(4)
S(3)-Cd-Br	121.62(3)	121.63(4)
S(4)-Cd-Br	101.94(2)	101.90(4)
S(2)-Cd-S(3)	102.30(3)	102.64(5)
S(3)-Cd-S(4)	100.30(3)	100.29(5)
S(4)-Cd-S(2)	100.78(3)	100.44(5)

3.4.4 Synthesis and Characterisation of a Tin Complex of the Tm Ligand

[SnTmCl$_3$] (18)

Upon addition of tin(IV) chloride to **12** as described in Section 6.3 (Scheme 3-16), the white suspension immediately turns yellow. **18** can be isolated by filtration giving a yellow powder in good yield.

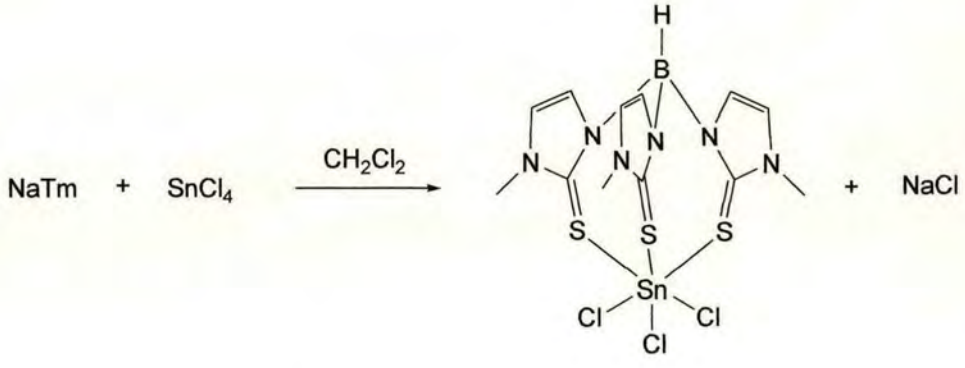

Scheme 3-16 Preparation of [SnTmCl$_3$]

Spectroscopic Analysis

^{1}H and ^{13}C NMR data of **18** are consistent with a structure whereby the Tm ligand is coordinated to the tin atom by all three of its sulphur donors. The ^{1}H NMR spectrum displays a single signal for both the 4- and 5-H indicating that all three arms of the tripod are equivalent. An absorption in the IR for the $\nu_{B\text{-}H}$ is seen at 2344 cm^{-1}.

4 Synthesis of Complexes Suitable for Variable Temperature NMR

4.1 INTRODUCTION

This chapter focuses on the design of ligands and complexes suitable for Variable Temperature (VT) NMR investigations detailed in Chapter 5. A number of possible approaches could be taken in order to provide a molecule which would be suitable for dynamic NMR studies. For example, introduction of a chiral centre (R*) on the 3-fold axis (**A**) or three equivalent chiral centres on each of the donor arms (so as not to disrupt the C_3 symmetry) (**B**) would provide a suitable complex (Fig. 4-1).

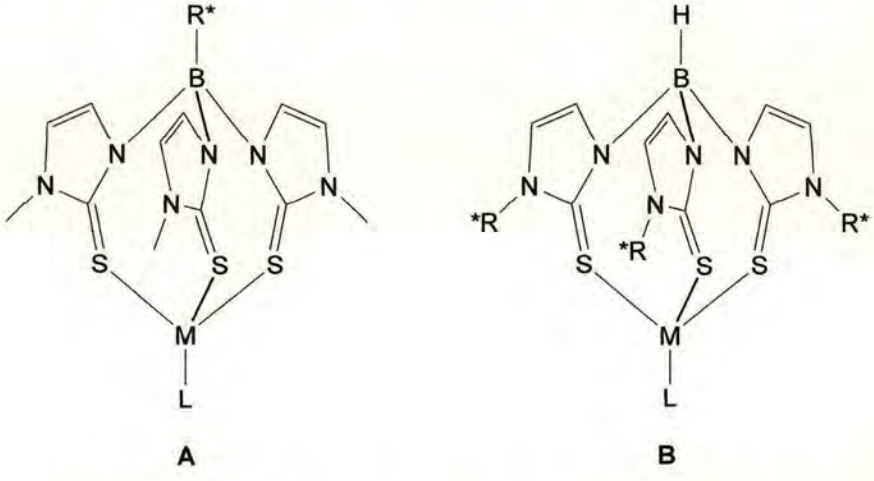

Figure 4-1 Possible target complexes for VT NMR studies

Racemisation of such a complex would result in interconversion between diastereoisomers for which, in principle, every NMR signal would be different. A much simpler method, which we devised, is the introduction of diastereotopic methylene groups on the N(1) position on the ligand. When coordinated to the metal centre the target ligands, hydrotris(2-mercapto-1-ethylimidazolyl)borate (Tm^{Et}) and hydrotris(2-mercapto-1-benzylimidazolyl)borate Tm^{Bn}, would contain diastereotopic protons,

i.e. protons which are inequivalent in the NMR. These protons can be used as a 'handle' to estimate the energy barrier to the racemisation of the complexes, a principle that is described in detail in Section 5.2.

4.2 Preparation of Starting Materials

All but one of the starting materials used in the syntheses detailed in this chapter have already been described in Section 3.1.

[PPh_3AuCl]

In an adaptation of the literature procedure[129] for the synthesis of [$AuClPPh_3$], a solution of hydrogen tetrachloroaurate was treated with triphenylphosphine as described in Section 6.2 (Scheme 4-1). The white solid was isolated in moderate yield.

$$HAuCl_4.3H_2O + 2\ PPh_3 \xrightarrow{THF} PPh_3AuCl + Ph_3P{=}O$$

Scheme 4-1 Preparation of [$AuClPPh_3$]

4.3 Ligand Synthesis

4.3.1 2-Mercapto-1-ethylimidazole (19)

Using a modification of the literature procedure for the preparation of N-substituted aminoacetaldehyde diethylacetal,[111, 130] a solution of bromoacetaldehyde diethylacetal and ethylamine in toluene was heated to 90 °C overnight. It was hoped that the product, N-ethylaminoacetaldehyde diethylacetal, could be treated with potassium isothiocyanate to produce the desired heterocycle (Scheme 4-2) in accordance with the published procedure for the preparation of 1-substituted-2-mercaptoimidazoles.[106] Unfortunately the first step proved unsuccessful and the tendency for dialkylation was confirmed (Scheme 4-3).

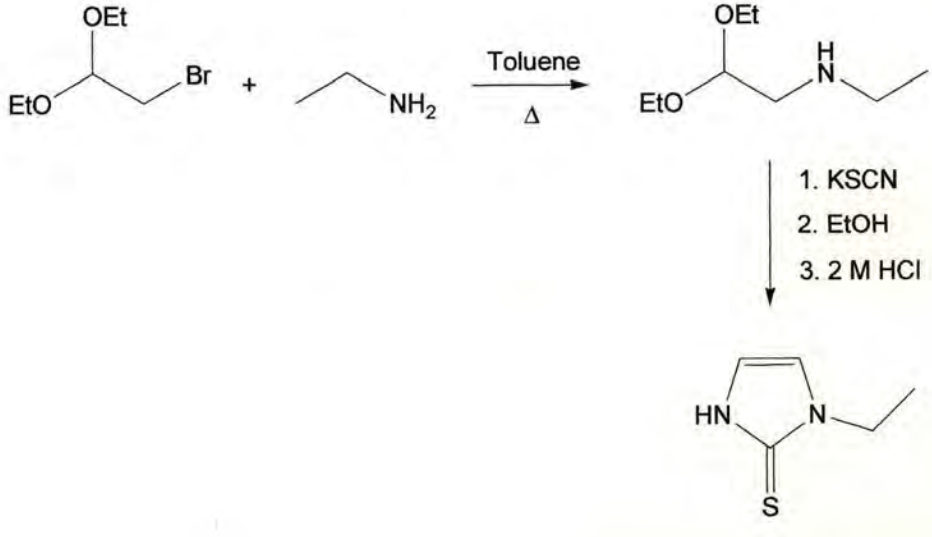

Scheme 4-2 Attempted synthesis of N-ethylaminoacetaldehyde diethylacetal and synthetic strategy for the preparation of 2-mercapto-1-ethylimidazole

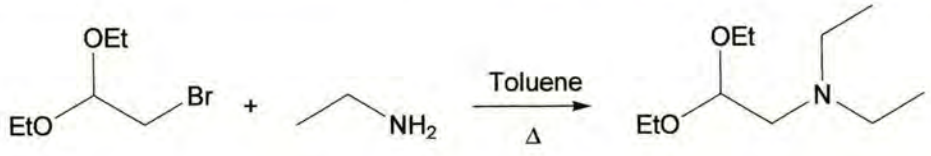

Scheme 4-3 Reaction of bromoacetaldehyde diethylacetal and ethylamine leading to dialkylation

The subsequent attempt to prepare 2-mercapto-1-ethylimidazole employed an adaptation of Kister's literature method for the preparation of 2-mercapto-1-phenylimidazole.[131] Aminoacetaldehyde diethylacetal was treated with ethyl isothiocyanate at 0 °C. Ethanol was added and the reaction refluxed for two hours [Scheme 4-4(a)]. This reaction was unsuccessful. The reaction was repeated using THF in the first step to dissipate the heat evolved [Scheme 4-4(b)]. Ethanol was added and the reaction was refluxed as before however this did not facilitate the production of the desired heterocycle.

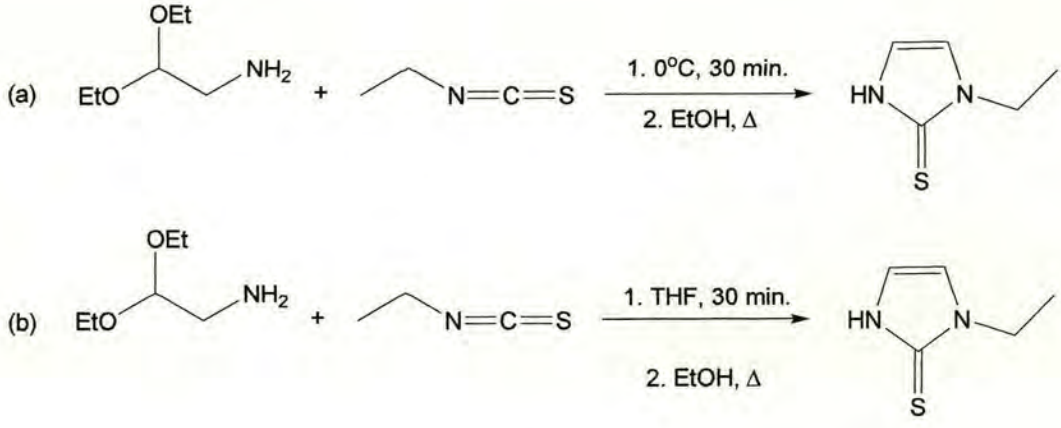

Scheme 4-4 Attempted syntheses of 2-mercapto-1-ethylimidazole

In studying the reaction of aminoacetaldehyde diethylacetal and ethyl isothiocyanate it was noted that acidic conditions would be needed for the cyclisation to be successful. The reaction was repeated and following the treatment of aminoacetaldehyde diethyl acetal with ethyl isothiocyanate HCl was added and the reaction refluxed for three hours. This approach appeared promising with analysis showing a mixture of product and starting materials. It seemed the reaction needed more severe conditions to go to completion.

Reaction of aminoacetaldehyde diethylacetal and ethyl isothiocyanate in THF followed by treatment with H_2SO_4 overnight as described in Section 6.3 produced the desired product (Scheme 4-5). The heterocycle **19** was isolated as a pale brown crystalline solid. The moderate yield of 56% can probably be attributed to the harsh reaction conditions needed to produce the compound. The proposed mechanism for this reaction is shown in Scheme 4-6.

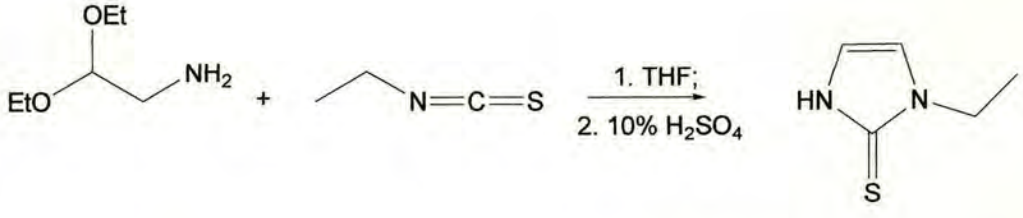

Scheme 4-5 Preparation of 2-mercapto-1-ethylimidazole

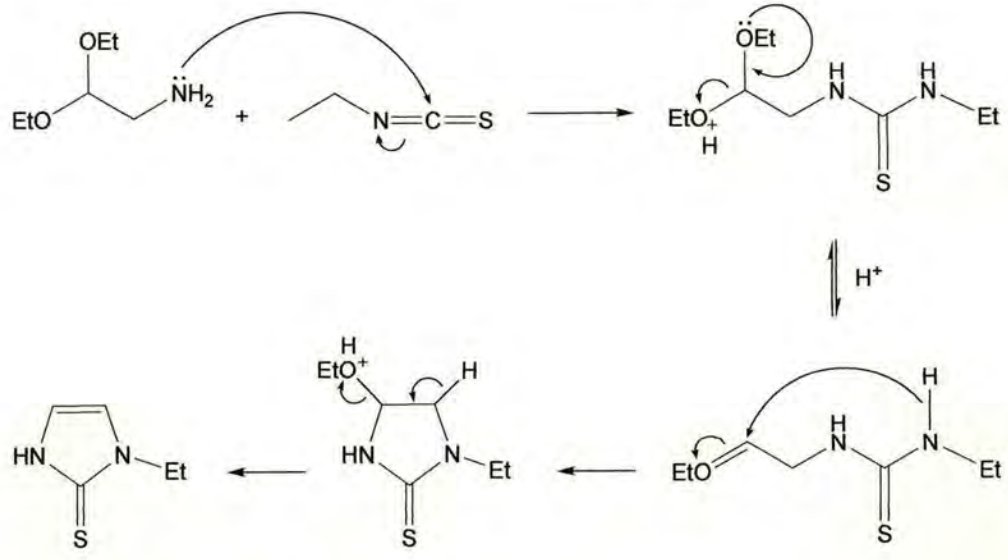

Scheme 4-6 Mechanism for the reaction of aminoacetaldehyde diethylacetal and ethyl isothiocyanate

4.3.2 Sodium Hydrotris(2-mercapto-1-ethylimidazolyl)borate ($NaTm^{Et}$) (20)

The synthesis of the desired ligand, sodium hydrotris(2-mercapto-1-ethylimidazolyl)borate ($NaTm^{Et}$), was based on the analogous preparation of the Tm ligand[5] as described in Section 6.3 (Scheme 4-7). The ligand was isolated as a white powder in moderate yield and high purity.

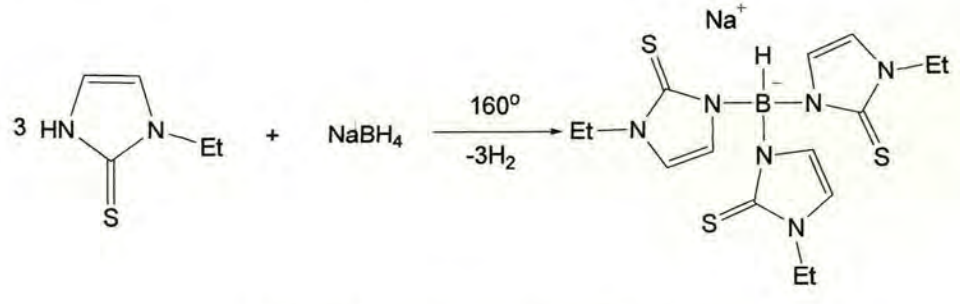

Scheme 4-7 Preparation of $NaTm^{Et}$

4.3.3 2-Mercapto-1-benzylimidazole (21)

The synthesis of 2-mercapto-1-benzylimidazole is based on analogy with that of **19** as described in Section 4.3.1 (Scheme 4-8). The product was isolated in high yield and purity.

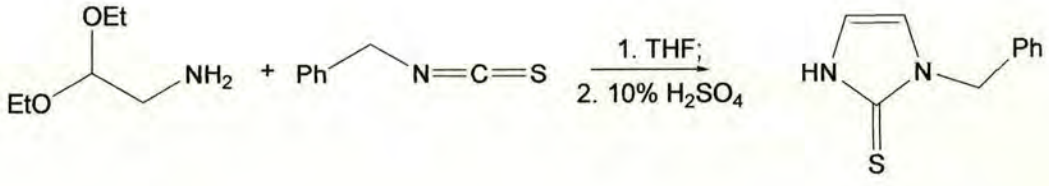

Scheme 4-8 Preparation of 2-mercapto-1-benzylimidazole

4.3.4 Sodium Hydrotris(2-mercapto-1-benzylimidazolyl)borate ($NaTm^{Bn}$) (22)

In an adaptation of the literature procedure,[34] a mixture of **21** and $NaBH_4$ was reacted to produce the desired ligand as described in Section 6-3 (Scheme 4-9). The ligand was isolated in good yield and high purity.

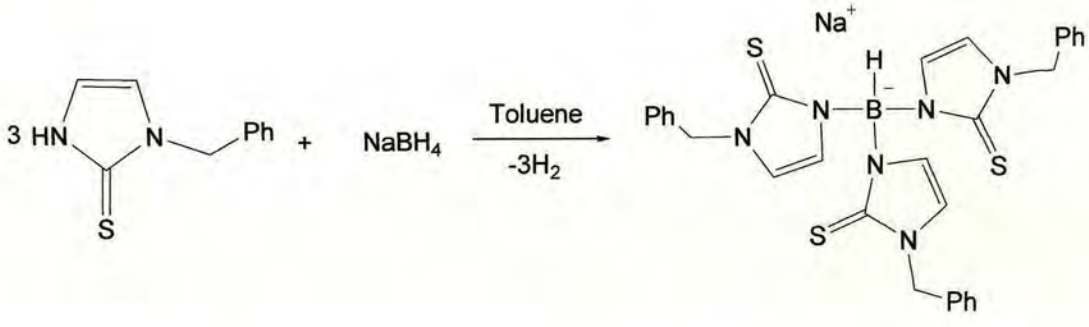

Scheme 4-9 Preparation of $NaTm^{Bn}$

4.4 Complex Synthesis

4.4.1 Tetrahedral Complexes

4.4.1.1 Group 12: Synthesis and Characterisation of Zinc, Cadmium and Mercury Complexes of Tm^{Et}

[$ZnTm^{Et}Cl$] (23)

The zinc(II) complex **23** was readily obtained by reaction of zinc chloride and ligand **20** as described in Section 6.3 (Scheme 4-10). The product was isolated as a white solid of high purity in moderate yield.

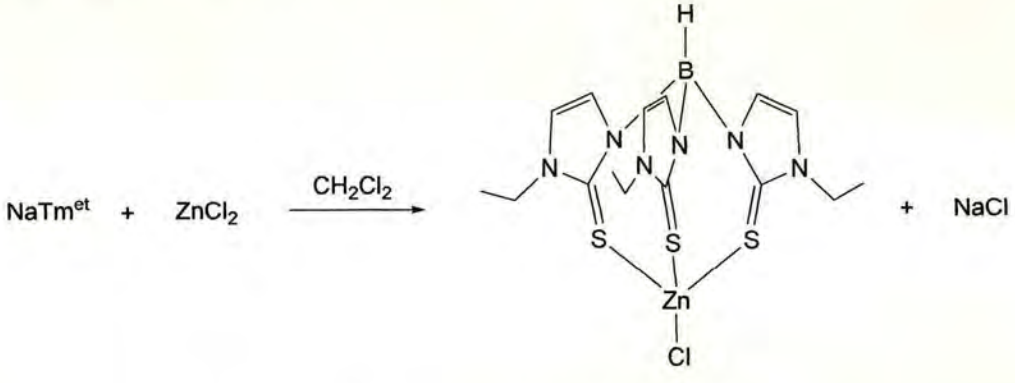

Scheme 4-10 Preparation of [$ZnTm^{Et}Cl$]

Spectroscopic Analysis

Analysis of **23** suggests a mononuclear, symmetrically coordinated structure in solution. The protons of the three methimazolyl groups are equivalent, confirming that the zinc centre is coordinated by all three sulphur donors. A ν_{B-H} absorption is observed at 2422 cm^{-1} in the IR spectrum and a peak corresponding to the [$ZnTm^{Et}$] fragment ($M^+ - Cl = 459$) is observed in the FAB-MS.

Molecular Structure

The crystal structure of **23** is shown in Fig. 4-2 with selected bond lengths and bond angles listed in Table A-6. The zinc atom is coordinated by Tm^{Et} which acts as a S_3^- face capping ligand. The S-Zn-S angles are 107.67(3), 102.64(2) and 105.57(2)° while the S-Zn-Cl angles are 108.24(3), 113.27(3) and 118.52(3)°. This distortion from normal tetrahedral angles is most likely due to the angle strain induced by the coordination and subsequent torsion of the tridentate ligand. The Zn-S distances fall in the narrow range 2.3560(7)-2.3660(7) Å. The Zn-Cl distance [2.2464(7) Å] is significantly longer than that of [ZnTmCl][15] [2.2409(7) Å] and [$ZnTm^{t\text{-}Bu}Cl$][41] [2.239(1) Å] and, as expected, is significantly shorter than the Zn-Br distances in [ZnTmBr] [2.364(2) Å][2] and [$ZnTm^{Bn}Br$] [2.3540(17) Å][34] and the Zn-I distances in [TmZnI] [2.5797(9) Å].[15]

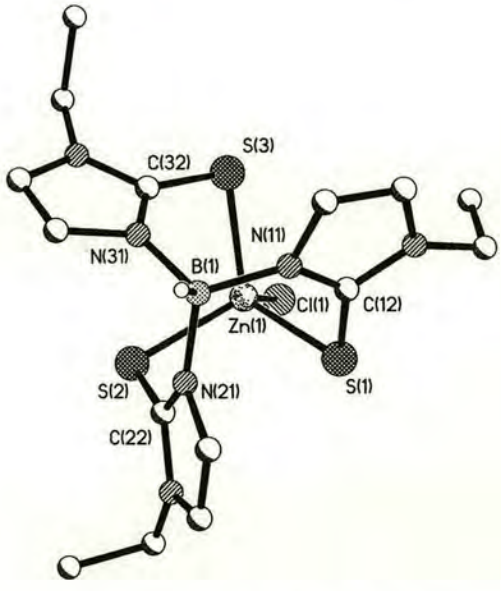

Figure 4-2 Molecular structure of [$ZnTm^{Et}Cl$] (Hydrogen atoms and solvent of crystallisation omitted for clarity)

[CdTm^{Et}Br] (24)

The synthesis of **24** was based on analogy with that of **17** and is described in Section 6.3 (Scheme 4-11). The complex was obtained in high yield as colourless crystals.

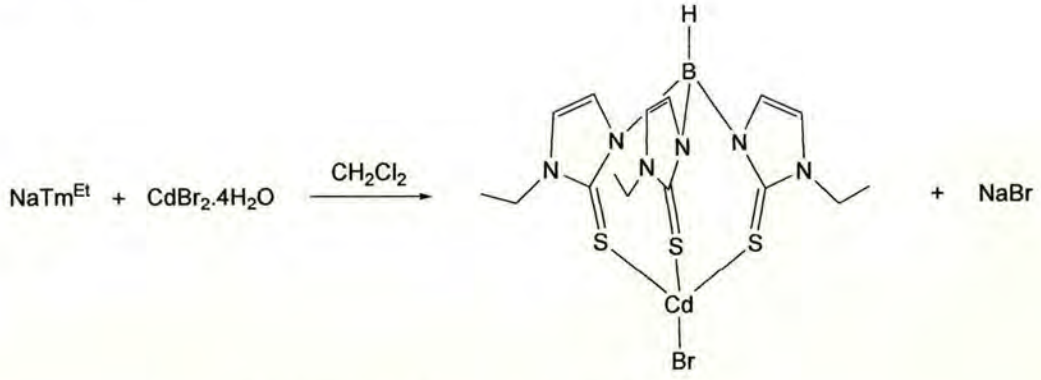

Scheme 4-11 Preparation of [CdTm^{Et}Br]

Spectroscopic Analysis

As with **23**, analysis of **24** reveals a mononuclear complex with tetrahedral geometry. The methimazolyl protons are equivalent suggesting coordination through all three sulphur donors and this is also suggested in the crystal structure (Fig. 4-3). A weak parent ion peak (M^+ = 585) and a stronger peak for the [CdTm^{Et}] fragment (M^+– Br = 506) are observed in the FAB-MS and a ν_{B-H} absorption is identified at 2406 cm^{-1} in the IR spectrum.

Molecular structure

Figure 4-3 shows the crystal structure of **24** and selected bond lengths and bond angles are listed in Table A-7. The cadmium atom is positioned in a slightly distorted tetrahedral environment. The S-Cd-S angles [101.478(17), 103.801(16) and

101.642(17)°] are significantly smaller than that of the analogous angles in **23**. It is postulated that, due to its larger atomic radius, the cadmium atom sits farther out of the plane of the sulphur donors thereby forming a more acute S-Cd-S angle. The effects of this can also be seen in the Cd-S distances [average 2.547(19) Å], which are significantly longer than the analogous Zn-S distances [average 2.321(65) Å]. The Cd-Br bond length [2.5517(2) Å] is shorter than the Cd-Br bond length in the reported structure of [CdTmBr] [2.5674(4) Å][15] and significantly longer than the Cd-Br bond length in the published structures [CdTm^{Bn}Br][34] [2.5336(4) Å] and [CdTm$^{t\text{-}Bu}$Br][44] [2.5364(4) Å]. This suggests that although the substituted groups on the nitrogen atom point away from the metal centre, they still have an effect on the geometry of the complex. A progressive increase in steric bulk causes a decrease in S-Cd-S angle; the angle range decreases from 113.57(3)-110.45(3)° in [CdTmCl] to 103.801(16)-101.478(17) in **24**. This may indirectly allow the relative shortening of the Cd-Br bond.

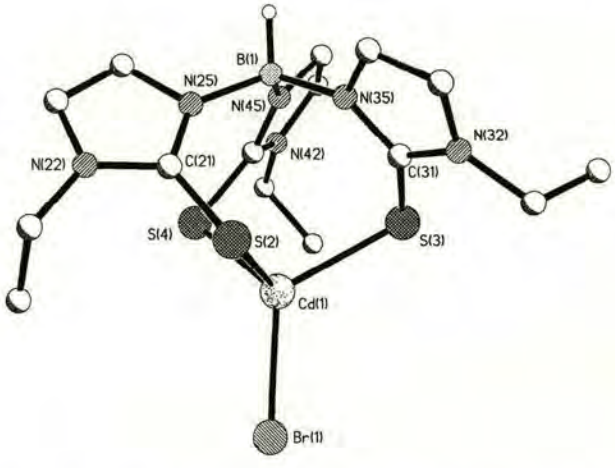

Figure 4-3 Molecular structure of [CdTm^{Et}Br] (Hydrogen atoms and solvent of crystallisation omitted for clarity)

[HgTm^{Et}Cl] (25)

To complete the series, the mercury(II) complex **25** was synthesised as described in Section 6.3 (Scheme 4-12). The pale yellow solid was obtained in high yield. Attempts to grow crystals suitable for X-ray diffraction were unsuccessful.

$$NaTm^{Et} + HgCl_2 \xrightarrow{CH_2Cl_2} [HgTm^{Et}Cl] + NaCl$$

Scheme 4-12 Synthesis of [HgTm^{Et}Cl]

Spectroscopic Analysis

Analysis of the spectroscopic data suggests that a mercury complex of the Tm^{Et} ligand has been synthesised; the ^{1}H NMR shows a single set of signals for the methimazolyl protons, the molecular ion peak ($M^+ = 629$) as well as a peak representing the [HgTm^{Et}] fragment ($M^+ - Cl = 594$) is observed in the FAB-MS and an absorption at 2430 cm^{-1} in the IR is identified as the B-H stretch. It is, however, difficult to assign a geometry to the complex as mercury is known to form two-coordinate, linear and four-coordinate, tetrahedral complexes.[132] The ^{1}H NMR spectrum displays broad signals for the methylene and imidazole protons suggesting some sort of dynamic process is occurring at room temperature. A crystal structure of the complex has not been obtained to date. The reason for synthesising this, and other complexes described in this section, was for the purpose of investigating the possible dynamic behaviour of such complexes. The results of dynamic NMR experiments on **25** and its postulated structure are detailed in Section 5.2.5.

4.4.1.2 Group 12: Synthesis and Characterisation of Zinc, Cadmium and Mercury Complexes of Tm^{Bn}

To investigate the differences in energy which could arise from variation of the substituent on the nitrogen atom of the ligand, $NaTm^{Bn}$ was synthesised (Scheme 4-9) and complexes of Group 12 were formed.

[$ZnTm^{Bn}Cl$] (26)

Addition of the ligand **22** to zinc chloride as described in Section 6.3 affords **26** in good yield and purity (Scheme 4-13).

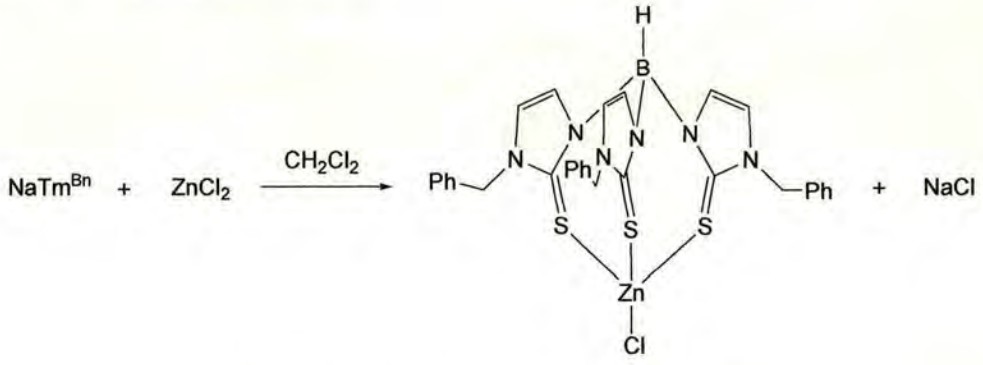

Scheme 4-13 Preparation of [$ZnTm^{Bn}Cl$]

Spectroscopic Analysis

Analysis of **26** confirms a similar coordination geometry to that of its Tm^{Et} analogue (**23**) with the zinc atom coordinated by the three sulphur donors, and the coordination sphere completed by the chlorine ligand. This is apparent from the ^1H NMR spectrum, in which the methimazolyl protons are equivalent. The parent ion is not visible in the FAB-MS, however a peak representing the [$ZnTn^{Bn}$] fragment ($M^+ - Cl = 645$) is observed. The ν_{B-H} absorption is seen at 2435 cm^{-1} in the IR spectrum.

[CdTm^{Bn}Br] (27)

In an analogous synthesis to that of **24** treatment of hydrated cadmium bromide with the ligand **22** as described in Section 6.3 results in the formation of **27** in very high yield and purity (Scheme 4-14).

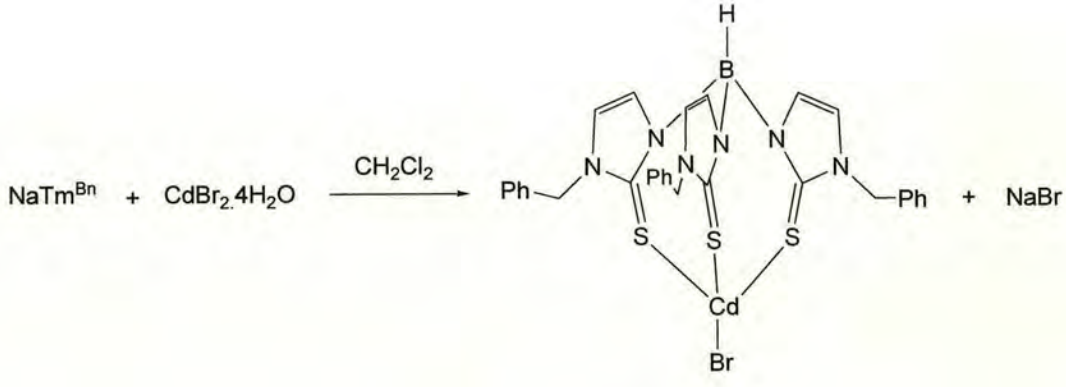

Scheme 4-14 Preparation of [CdTm^{Bn}Br]

Spectroscopic Analysis

As in the ^{1}H NMR spectrum of **24** the protons of the methimazolyl groups in **27** are equivalent, suggesting that the cadmium atom is coordinated by all three sulphur donors. This coordination can be seen in the crystal structure (Fig. 4-4). Although the peak for the parent ion is not apparent in the FAB-MS, a peak representing the [Tm^{Bn}Cd] fragment (M^+– Br = 693) is observed. The ν_{B-H} absorption is observed at 2422 cm^{-1} in the IR.

Molecular structure

Crystals suitable for X-ray diffraction studies were grown (Fig. 4-4) and, unsurprisingly, the molecule was found to be isostructural with the same complex previously reported by Bakbak *et al.*[34] Selected bond lengths and bond angles are listed in Table A-8 and as can be seen from Table 4-1 (below), none of these differ significantly from the previously published structure.

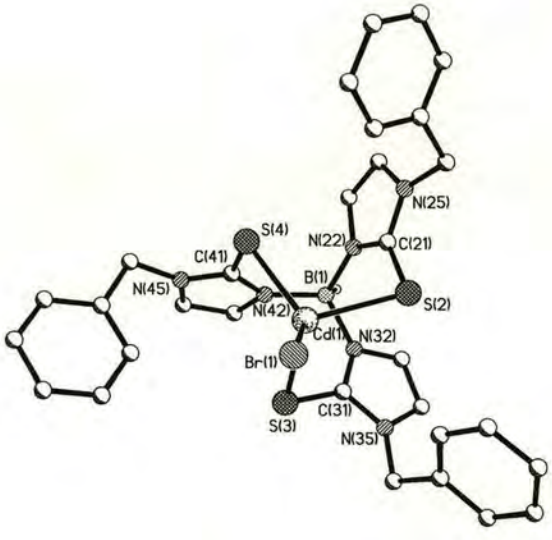

Figure 4-4 Molecular structure of [CdTm^{Bn}Br] (Hydrogen atoms omitted for clarity)

Table 4-1 Selected structural parameters of [CdTm^{Bn}Br]

	Literature Values[34]	Complex 27
Bond Lengths (Å)		
Cd-S(2)	2.5693(9)	2.5656(19)
Cd-S(3)	2.5448(9)	2.5406(17)
Cd-S(4)	2.5154(9)	2.5116(18)
Cd-Br	2.5336(4)	2.5352(9)
Bond Angles (°)		
S(2)-Cd-Br	114.60(2)	114.50(5)
S(3)-Cd-Br	108.85(2)	108.91(5)
S(4)-Cd-Br	121.97(2)	122.03(5)
S(2)-Cd-S(3)	102.02(3)	101.93(6)
S(3)-Cd-S(4)	104.23(3)	104.27(6)
S(4)-Cd-S(2)	102.99(3)	103.01(6)

[HgTm^{Bn}Cl] (28)

28 was synthesised *via* the route shown in Scheme 4-15. The mercury(II) complex was readily obtained from the reaction of the ligand **22** and mercury dichloride as described in Section 6.3. The pale yellow powder was obtained in good yield. Attempts to crystallise the complex proved unsuccessful.

$$NaTm^{Bn} + HgCl_2 \xrightarrow{CH_2Cl_2} [HgTm^{Bn}Cl] + NaCl$$

Scheme 4-15 Preparation of [HgTm^{Bn}Cl]

Spectroscopic Analysis

As with its Tm^{Et} analogue (**25**), analysis of the spectroscopic data of the mercury complex, **28**, does not lead to definitive conclusions. The ^{1}H NMR spectrum exhibits one set of signals for the methimazolyl protons, a peak is observed for the [HgTm^{Bn}] fragment (M^+– Cl = 780) in the FAB-MS and the $\nu_{B\text{-}H}$ absorption is identified at 2367 cm^{-1} in the IR. However, as before, it is difficult to comment on the geometry of the complex and, unlike in the case of **25,** the variable temperature NMR spectra detailed in Section 5.2.1 do not offer any conclusions. Without further evidence we can only make the assumption that the structure of **28** is analogous to its Tm^{Et} counterpart, the structure of which is discussed in Section 5.2.5.

4.4.1.3 Group 11: Synthesis and Characterisation of Copper, Silver and Gold Complexes of Tm^{Et}

[$CuTm^{Et}PPh_3$] (29)

The ligand **20** was added to copper(I) chloride and triphenylphosphine as described in Section 6.3 (Scheme 4-16). The white precipitate was collected to afford **29** in good yield.

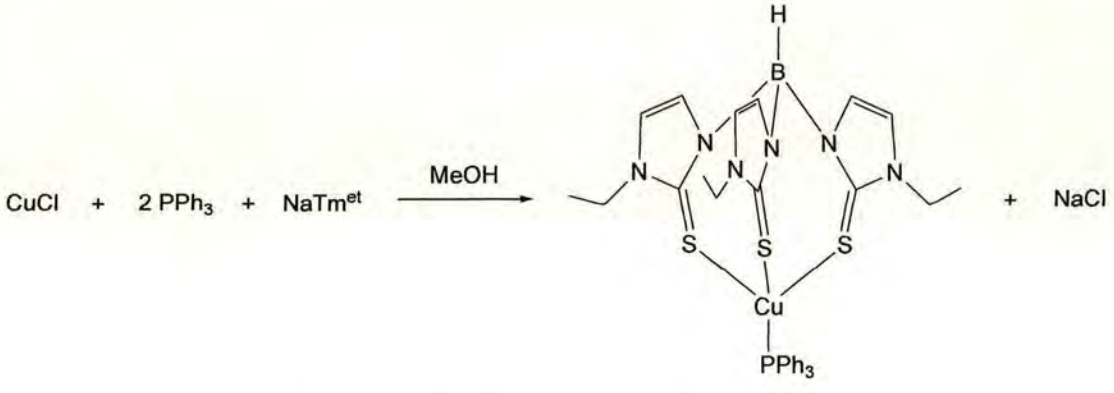

Scheme 4-16 Preparation of [$CuTm^{Et}PPh_3$]

Spectroscopic Analysis

The ^1H NMR spectrum of **29** suggests a mononuclear structure and this is confirmed by mass spectrometry and IR data. FAB-MS reveals the molecular ion peak ($M^+ = 719$) and a peak representing the ionization of the complex ($M^+ - PPh_3 = 457$). An absorption for the ν_{B-H} stretch is observed at 2375 cm^{-1} in the IR spectrum. Confirmation of the structure of **29** is obtained from the crystal data.

Molecular structure

The crystal structure of **29** is shown in Figure 4-5 with selected bond lengths and bond angles listed in Table A-9. The copper centre adopts a distorted tetrahedral geometry with S-Cu-S and S-Cu-P bond angles of 102.47(3)° and 115.80(2)° respectively. The S-Cu-S angles are significantly smaller than the previously reported[22] [CuTm (*m*-tolyl$_3$P)] [104.59(6)°] and [CuTm (*p*-tolyl$_3$P)] [107.10(4)°] while the S-Cu-P angles are significantly larger than those of the above mentioned complexes whose S-Cu-P angles are 114.00(4)° and 111.75(2)° respectively. This is most likely due to the increased steric interaction between the ethyl groups of the ligand and the phenyl groups of the phosphine ligand. This effect is further illustrated by the Cu-S [2.3868(8) and 2.3868(9) Å] and Cu-P distance(s) [2.2306(16) Å] which are significantly longer than their *m*-tolyl and *p*-tolyl analogues.

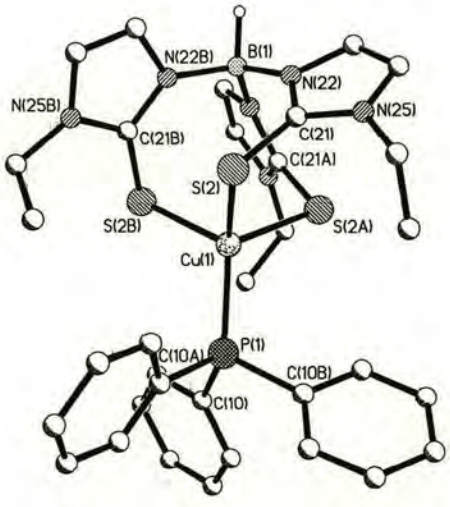

Figure 4-5 Molecular structure of [CuTm^{Et}PPh$_3$] (Hydrogen atoms for omitted for clarity)

[AgTm^{Et}PPh$_3$] (30)

In a modification of the procedure for the preparation of **29**, silver tetrafluoroborate and triphenylphosphine were treated with the ligand **20** as described in Section 6.3 (Scheme 4-17). The reaction produced the silver(I) complex **30** in good yield. Attempts to crystallise the complex proved unsuccessful.

$$NaTm^{Et} + AgBF_4 + 2\,PPh_3 \xrightarrow{THF} [AgTm^{Et}PPh_3] + NaBF_4$$

Scheme 4-17 Preparation of [AgTm^{Et}PPh$_3$]

Spectroscopic Analysis

^{1}H NMR reveals that the methimazolyl protons of **30** are equivalent at room temperature. The presence of molecular ion peak (M^+ = 764) and a peak representing the ionization of the complex (M^+– PPh_3 = 501) in the FAB-MS and the observation of a $\nu_{B\text{-}H}$ absorption at 2365 cm^{-1} in the IR spectrum suggest that a silver complex has been synthesised, however the signals for the methylene protons in the ^{1}H NMR spectrum suggest that fluxional processes are occurring at room temperature. These details of these processes and, consequently, a possible structure for the complex are outlined in Section 5.2.6.

[AuTm^{Et}PPh$_3$] (31)

To complete the series of Group 11 complexes, **31** was synthesised by addition of the ligand **20** to [AuClPPh$_3$] as described in Section 6.3 (Scheme 4-18). The pale brown

solid was isolated in high yield and purity. Attempts to crystallise the complex proved unsuccessful.

$$NaTm^{Et} + [AuClPPh_3] \xrightarrow{CH_2Cl_2} [AuTm^{Et}PPh_3] + NaCl$$

Scheme 4-18 Preparation of $[AuTm^{Et}PPh_3]$

Spectroscopic Analysis

It was expected that the Au(I) complex would be linear given the tendency of gold(I) to form linear complexes.[132] This was confirmed by the ^{1}H NMR spectrum of the complex. The spectrum of **31** differs from the other Group 11 complexes in that the methylene protons do not appear diastereotopic however the signals for the methyl and methimazolyl protons in the ^{1}H NMR spectrum appear at the expected values for complexes of the Tm^{Et} ligand. There is evidence in the FAB-MS that the Tm^{Et} ligand has coordinated to the gold atom; both the molecular ion peak (M^+ = 853) and the peak representing the ionization of the complex ($M^+ - PPh_3$ = 590) are observed. The ν_{B-H} absorption is observed at 2373 cm^{-1} in the IR. From these results we would suggest a linear geometry about the gold centre with a triphenylphosphine ligand and one of the methimazolyl arms coordinated (Fig. 4-6). The fact that the methimazolyl protons are equivalent in the ^{1}H NMR at room temperature suggests a rapid exchange of the pendant arms of the Tm^{Et} ligand between coordinated and uncoordinated states. Further NMR investigations of **31** are detailed in Section 5.2.6.

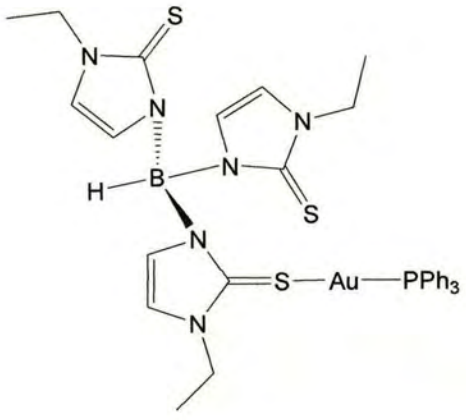

Figure 4-6 Postulated structure of [AuTm^{Et}PPh$_3$]

4.4.2 Octahedral Complexes

4.4.2.1 Group 7: Synthesis and Characterisation of a Manganese Complex of Tm^{Et}

$[MnTm^{Et}(CO)_3]$ (32)

The synthesis of **32** was based on analogy with that of its Tm counterpart, **13**. $[Mn(MeCN)_3(CO)_3]PF_6$ was chosen over $[MnBr(CO)_5]$ as the starting material as its reaction with NaTm provided a cleaner route to the desired product. **32** was isolated as a yellow powder in good yield as described in Section 6.3 (Scheme 4-19).

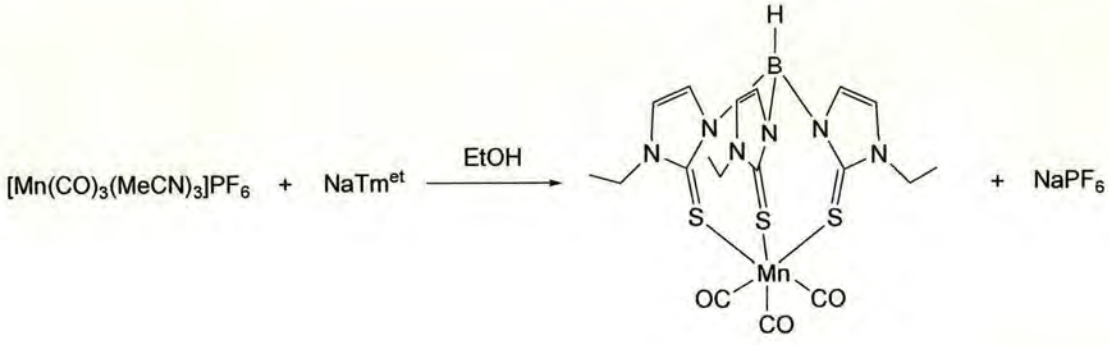

Scheme 4-19 Preparation of $[MnTm^{Et}(CO)_3]$

Spectroscopic Analysis

From analysis of **32** we propose a similar structure to that of its Tm analogue (**13**). The signals in its ^1H NMR spectrum suggest that the manganese centre is coordinated by all three sulphur donors and a peak representing the parent ion ($M^+ = 532$) is observed in the FAB-MS. The solid state IR spectrum of the complex is not unusual; the complex displays a ν_{B-H} absorption at $2437cm^{-1}$. The liquid IR spectrum of this complex exhibits

the unusual absorptions also observed in **13**. Two ν_{C-O} signals are observed, these consist of two medium intensity bands at 2007 and 1908cm^{-1}. These data are inconsistent with the postulated C_3-symmetric structure in which three bands are predicted and is most likely due to the near coincidence of two of the three bands expected for a C_3-symmetric tricarbonyl complex. In the solid state KBr disc spectrum of **32** two absorptions are observed at 1883 and 1987 cm^{-1} which suggests that, unlike its Tm^{Et} analogue there is just one molecule in the unit cell of the complex. Unfortunately this cannot be verified as a crystal structure of the complex has not been obtained to date.

4.4.2.2 Group 8: Synthesis and Characterisation of Ruthenium Complexes of Tm^{Et}

$[RuTm^{Et}$(p-cym)]Cl (33)

Treatment of $[Ru(p\text{-cym})Cl_2]_2$ with the ligand **20** affords **33** as described in Section 6.3 (Scheme 4-20). The solid was isolated as an orange solid in high yield and purity.

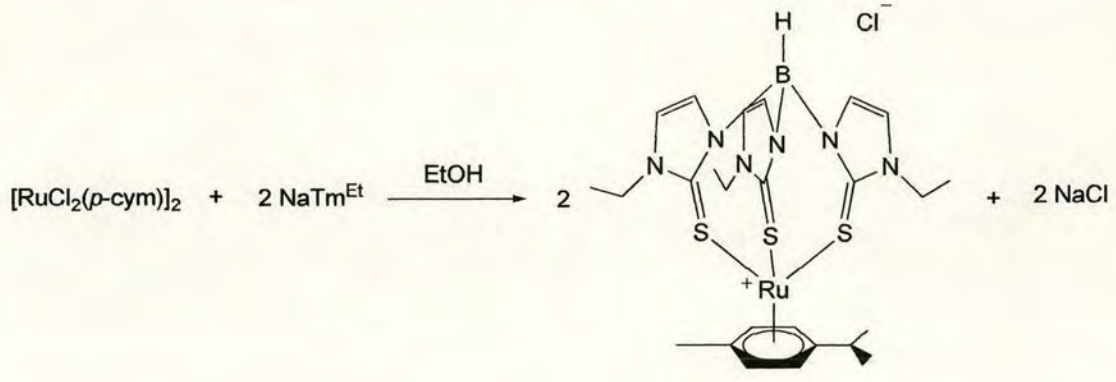

Scheme 4-20 Preparation of $[RuTm^{Et}(p\text{-cym})]Cl$

Spectroscopic Analysis

Analysis of **33** suggests that the ruthenium atom is coordinated by the sulphur donors of the ligand in an η^3 fashion. The ^1H NMR signals for the three sets of imidazole protons are equivalent confirming a symmetrical coordination of the arms of the tripod. As expected the signals for the methylene protons is a multiplet reflecting the diastereotopic nature of the protons. This phenomenon will be dealt with in more detail in Section 5.2.8. The molecular ion peak ($M^+ - Cl = 629$) is observed in the FAB-MS and a $\nu_{B\text{-}H}$ absorption is identified at 2428 cm^{-1} in the IR spectrum.

Molecular Structure

The crystal structure of **33** is shown in Fig. 4-7 with selected bond lengths and bond angles listed in Table A-10. The complex crystallised with one molecule of water in the unit cell. The ruthenium atom is coordinated by three sulphur donors with an average Ru-S distance of 2.419(8) Å, a similar value to the two Ru-S distances unaffected by the trans influence in [RuTm(CO)(PPh_3)] [2.4066(14) and 2.4112(14) Å].[27] The S-Ru-S angles [90.76(3), 88.97(3) and 93.12(3)°] deviate slightly from normal octahedral angles. The average Ru-C(*para*-cymene) distance for **33** is 2.206(24) Å which is similar to the average Ru-C(*para*-cymene) distances in [RuTm(*p*-cym)]Cl (**14**) [2.210(26) Å] and other Ru(para-cymene) fragments in complexes such as [RuTp(*p*-cym)] [2.206(27) Å][122] (Tp = hydrotris(pyrazolyl)borate) and [(Ru(*p*-cym){η^2-(^{i}PrN)$_2$PPh(NH^{i}Pr)}]$^+$ [2.185(23) Å].[120]

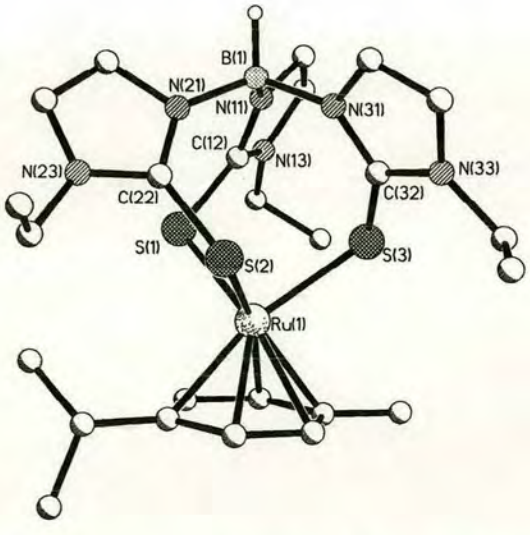

Figure 4-7 Molecular structure of [RuTm^{Et}(*p*-cym)]Cl (Hydrogen atoms, counterion and solvent of crystallisation omitted for clarity)

[RuTm^{Et}(p-cym)]PF$_6$ (34)

To prevent the chloride counter-ion being available as a ligand in event of dissociation of one of the sulphur donors and thereby produce a complex suitable for VT NMR experiments an ion exchange reaction was carried out on **33** as described in Section 6.3 (Scheme 4-21). **34** was obtained in high yield and purity.

$$[RuTm^{Et}(p\text{-cym})]Cl + NH_4PF_6 \xrightarrow{THF} [RuTm^{Et}(p\text{-cym})]PF_6 + NH_4Cl$$

Scheme 4-21 Counterion exchange of [RuTm^{Et}(*p*-cym)]Cl

Spectroscopic Analysis

The analysis of **34** is almost identical to that of **33** and is detailed in Section 6.3. It was difficult to conclusively prove the reaction was successful, however physical results indicate a new species had formed as changes during the reaction were noted and the colours of the products are different.

[RuTm^{Et}Cp](35)

A suspension of $[RuCl_2Cp]_2$ in ethanol reacted with the ligand **20** as described in Section 6.3 (Scheme 4-22). The red crystalline solid was obtained in high yield.

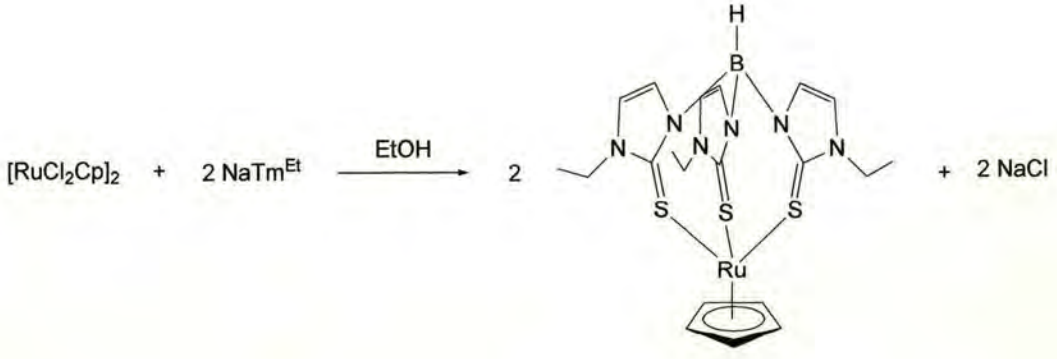

Scheme 4-22 Preparation of [RuTm^{Et}Cp]Cl

Spectroscopic Analysis

The NMR spectrum of **35** shows only one environment for the protons of the Tm ligand suggesting that all three sulphur donors are coordinated to the ruthenium ion. A triplet representing the methyl protons in the 1-position is observed at 1.28 ppm. The signal representing the methylene protons is a multiplet indicating their diastereotopic nature. The CH groups of the cyclopentadienyl ring are represented by a singlet at 5.26 ppm and the CH protons of the methimazolyl groups are observed as two doublets at 6.93 and 7.07 ppm. A single ν_{B-H} absorption is observed at 2346 cm^{-1} in the IR. **35** was also characterised by FAB-MS and the molecular ion peak ($M^+ = 560$) is observed.

4.4.2.3 Group 8: Synthesis and Characterisation of a Tin Complex of Tm^{Et}

$[SnTm^{Et}Cl_3]$ (36)

Tin(IV) chloride was added to the ligand **20** as described in Section 6.3 resulting in the formation of a yellow precipitate which was isolated in high yield and purity (Scheme 4-23).

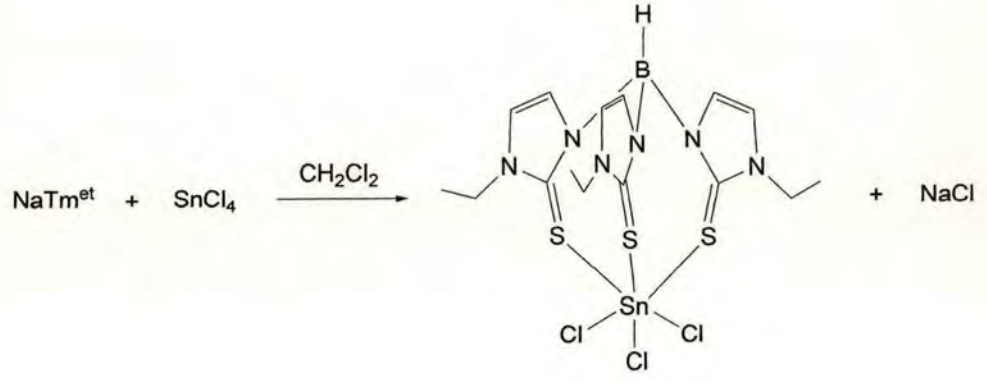

Scheme 4-23 Preparation of $[SnTm^{Et}Cl_3]$

Spectroscopic Analysis

Analysis of **36** suggests that the tin atom is coordinated by all three sulphur donors of the Tm^{Et} ligand and the coordination sphere is completed by three chlorine ligands. The ^1H and ^{13}C NMR spectra are consistent with this; a peak for the molecular ion is observed in the FAB-MS ($M^+ = 619$), and a ν_{B-H} absorption is identified at 2370 cm^{-1}. Due to the low solubility of the complex crystals suitable for X-ray diffraction were not obtained.

4.4.2.4 Attempted Synthesis of a Labile Octahedral Complex

Since all of the octahedral complexes synthesised thus far are of inert metal ions, it was likely that the information obtainable from their NMR spectra would be limited. For this reason, a complex of Tm^{Et} containing a labile metal centre was sought.

Reaction of $MoCl_2O_2$ with $NaTm^{Et}$ in THF

Molybdenum dichloride dioxide and **20** were reacted in THF as described in Section 6.3 (Scheme 4-24).

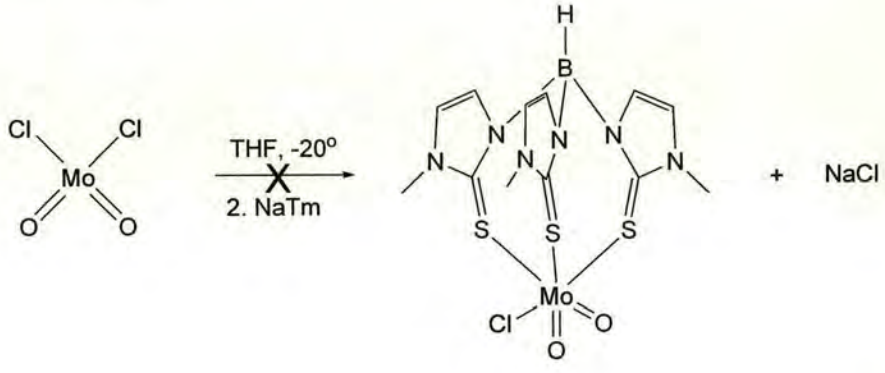

Scheme 4-24 Attempted reaction of molybdenum dichloride and $NaTm^{Et}$

This reaction was unsuccessful and the unreacted ligand was recovered. Diamagnetic complexes of labile octahedral metal ions with these ligands suitable for dynamic NMR studies have yet to be prepared.

5 VARIABLE TEMPERATURE NMR & *AB INITIO* CALCULATIONS

5.1 INTRODUCTION

The chirality of complexes containing tripod ligands $E(L_2D)_3$ relies upon the twisted conformation of the bicyclo[3.3.3] metal-ligand cage formed upon complexation and induced by the angle strain present in the system [Section 1.1, Scheme 1-1(b)]. The exploitation of the chirality of such complexes would be crucially dependant upon the energy barrier to their racemisation. In this chapter both Variable Temperature NMR and *ab initio* calculations are employed to investigate the energy barrier to racemisation in a range of tetrahedral and octahedral complexes.

5.1.1 Postulated mechanisms for racemisation

The inter-conversion of enantiomeric structures $[E(L_2D)_3ML_n]$ (n = 1, 3) described in Section 1.1 can be envisaged to take place through either dissociative or non-dissociative processes.[24]

Non-dissociative Mechanism

The two enantiomeric forms of such complexes represent mirror image conformations of the metal-ligand unit. Thus, a non-dissociative mechanism would involve a relative twisting of the boron and metal portions of the cage structure by ±120°, converting one enantiomer to the other *via* an achiral, C_{3v} symmetric transition state which occurs at an angle of ±60° (Fig. 5-1). This mechanism of interconversion could take place in both octahedral and tetrahedral complexes, however molecular models indicate that considerable angle strain is present in the C_{3v}-symmetric transition structure. This would suggest that the activation energy for such a conversion would be relatively high. It is

therefore postulated that, for a substitution-inert metal centre [e.g. Ru(II)], the energy barrier to racemisation will be high. Labile tetrahedral complexes, however, would be more likely to favour a dissociative mechanism as described in the next section.

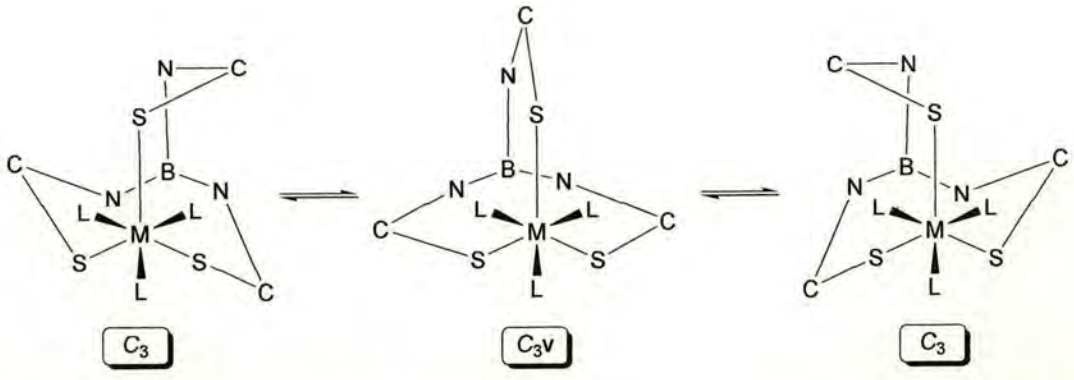

Figure 5-1 Non-dissociative interconversion between enantiomeric forms in an octahedral complex (a similar mechanism may be envisaged for complexes of tetrahedral metal ions)

The non-dissociative twist mechanism involves an increase in the S-M-S angles at the metal towards 120° at the transition state. It is therefore expected that the energy barrier to racemisation would be higher in octahedral than in tetrahedral complexes as, in octahedral complexes, a S-M-S angle of 90° means that the geometry of the complex is farther from the C_3v-symmetric transition state than in a tetrahedral complex where the angle is 109.5°.

Dissociative Mechanism

Dissociative mechanisms for the racemisation of this type of complex, in which the interconversion is facilitated by dissociation of one of the donors from the metal, may also be envisaged. A consideration of the factors involved indicates that the processes must be different for octahedral and tetrahedral complexes. In an octahedral complex, dissociation of one of the tripod donor arms provides a 5-coordinate species susceptible to Berry pseudo-rotation. The racemisation process is completed by recoordination of the dissociated donor to provide a 1:1 mixture of enantiomers (Fig. 5-2). Given the low energy of the pseudo-rotation process,[133] the activation energy for racemisation *via* this mechanism would be provided by the dissociation energy of the metal-donor bond, and thus be closely correlated with the lability of the metal centre, the nature of the tripod donor and the trans-effect/influence of the non-tripod ligands present.

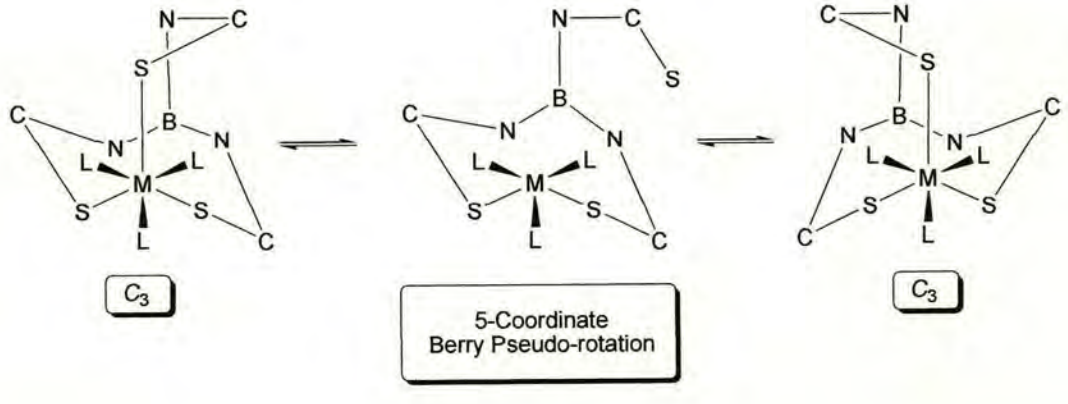

Figure 5-2 Dissociative mechanism for the interconversion between enantiomeric forms in an octahedral complex

In the case of a tetrahedral complex, such a mechanism is not available. One conceivable alternative would involve dissociation of one of the tripod donor arms followed by pyramidal inversion at the 3-coordinate metal centre and subsequent reassociation of the tripod arm. However, such a process does not provide the enantiomeric structure. Instead, an untenable structure of C_{3v} symmetry, in which the non-tripod ligand (L) is located within the bicyclic cage directed towards the boron atom, is envisaged (Fig. 5-3).

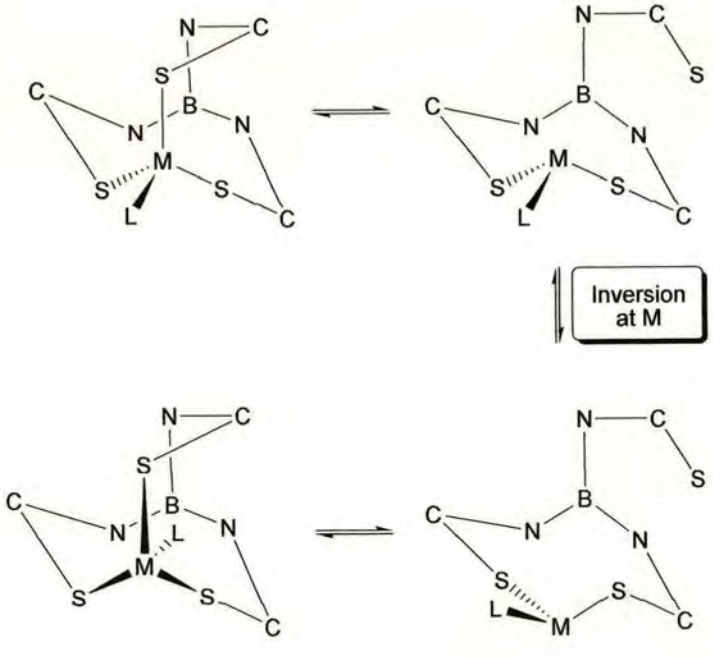

Figure 5-3 Postulated result of dissociative mechanism in tetrahedral complexes involving pyramidal inversion at the metal

A more likely scenario is that, upon dissociation, the 8-membered ring containing the metal inverts and recoordination of the tripod donor arm provides the enantiomeric system (Fig. 5-4).

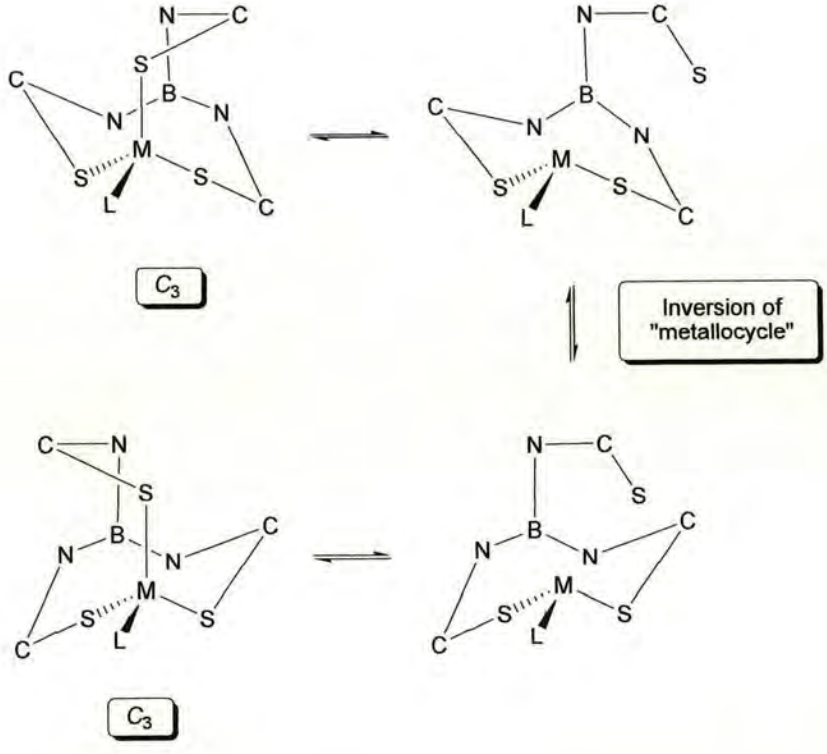

Figure 5-4 Postulated mechanism for the interconversion between enantiomeric forms of a tetrahedral complex

For the two remaining metal-coordinated donor arms, the motion of the atoms during this process may be envisaged as being similar to those occurring during the non-dissociative racemisation process. However, the overall energy of the process will be lower as the required motion is not hindered by the presence of a bicyclic cage

structure which imposes significant angle strain at the C_{3v} symmetric transition state [Fig. 5-5(a)]. Analysis of molecular models indicates that this is due to the higher conformational mobility of the metal and/or boron centre once one of the ligand tripod arms is dissociated [Fig. 5-5(b)].

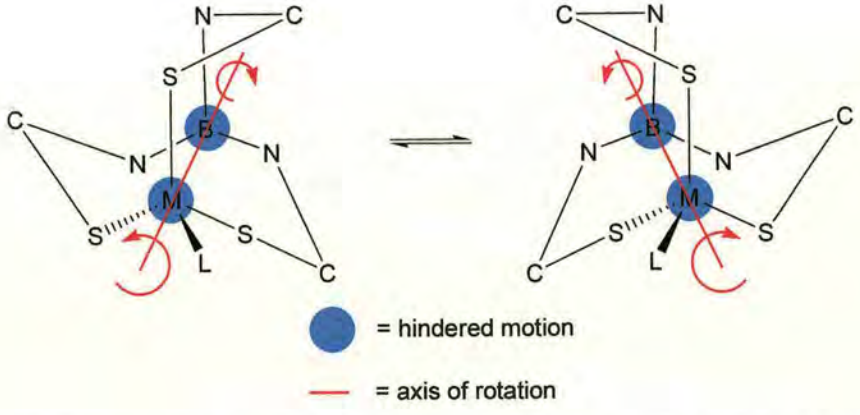

(a) Rotation involved in non dissociative racemisation showing hindered mobility of atoms due to presence of bicyclic cage

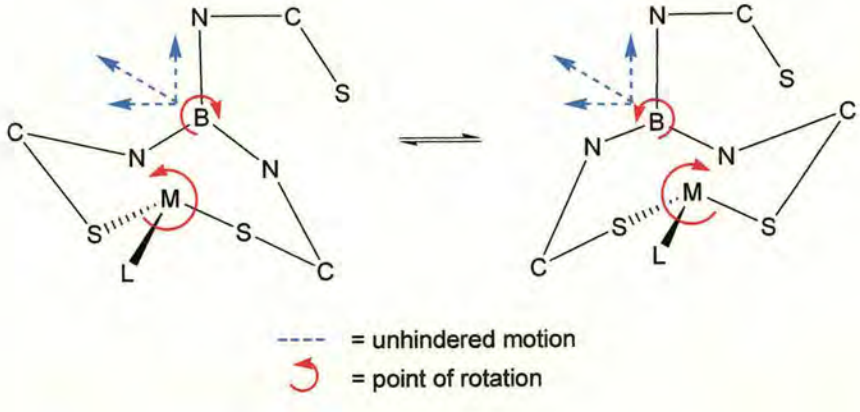

(b) Rotation involved in dissociative racemisation showing higher mobility of atoms due to absence of bicyclic cage

Figure 5-5

5.1.2 Aims

A significant part of this project has been the exploration of the mechanisms described above. By incorporating groups which contain diastereotopic protons into the ligand and recording ^{1}H NMR spectra at different temperatures, line shape analysis can be used to determine the activation energy of the racemisation process, thus providing insight into the mechanisms operating. For this purpose Tm ligands containing ethyl and benzyl nitrogen substituents in place of the usual methyl group (Tm^{Et} and Tm^{Bn}) were synthesised and complexed to a range of metals (Chapter 4). The complexes could then be used in NMR investigations. To explore the subject further we planned to carry out *ab initio* calculations on a number of systems and compare the energies obtained with our experimental values.

5.2 Variable Temperature NMR

Background

NMR spectra usually provide a time-averaged view of all possible conformations and orientations of the molecule brought about by fast molecular motion.[134] However, if the energy barrier between inequivalent forms of a molecule is sufficiently high to slow their interconversion to a rate comparable with the frequency of the absorbed radiation, the two forms may be distinguished by the spectrometer. In the intermediate regime progressive broadening and coalescence of signals will be observed until the interconversion rate is too rapid for the spectrometer to distinguish between the two forms and the time averaged signal is observed. The rate of interconversion processes may, of course, be varied by changing the temperature and thus, for processes occurring at suitable rates, Variable Temperature NMR (VT NMR) spectra can provide information on energy barriers to interconversion *via* Line Shape Analysis. If we consider a molecule interconverting between two chiral enantiomeric conformations of equal energy in which a pair of diastereotopic protons are present we can use VT NMR to gain information about the processes occurring. For simple two-site exchange with equal populations[135] we can use the example of the spectra shown in Fig. 5-6.

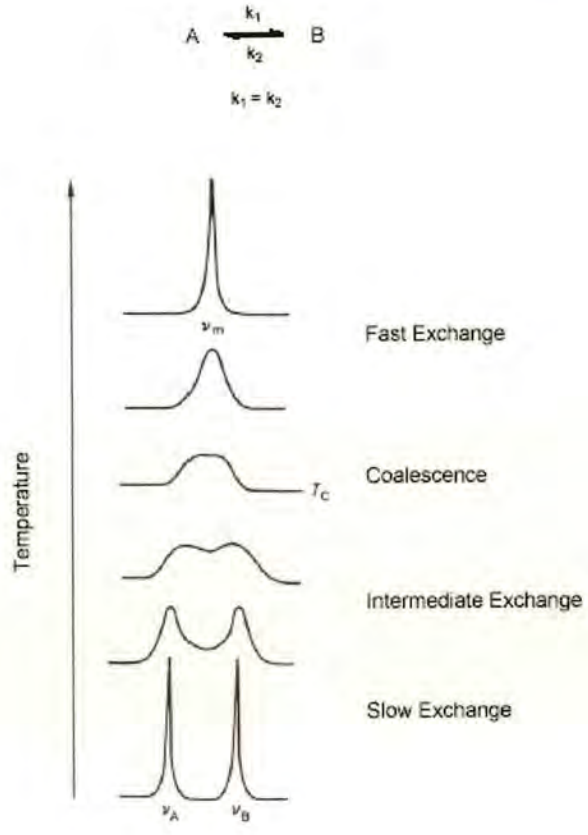

Figure 5-6 Two site exchange for nuclei with equal populations (adapted from NMR Spectroscopy by Michael K. Denk[136])

For **slow exchange** between A and B two equally intense, narrow peaks are observed for the protons and as the rate of exchange increases the lines begin to broaden. The phase which occurs as the rate of exchange increases further still is known as **intermediate exchange**. This is represented by the lines moving towards each other and broadening until they unite to form a single, wide, flat-topped peak. The point at which this is observed is known as the **coalescence point**. When the rate of exchange becomes

sufficiently fast that the nuclei are no longer distinguishable on the NMR timescale, a single, sharp line is observed. This phase is known as **fast exchange**. It is possible to observe these transformations by varying the temperature in the NMR experiment.

Applying this principal to the complexes that we are interested in, two ligands were synthesised (Tm^{Et}, Tm^{Bn}, Section 4.3) which, when coordinated to the metal centre, would contain diastereotopic protons i.e. protons which are inequivalent in the NMR spectra (Fig. 5-7). These protons can be used as a 'handle' to estimate the energy barrier to the racemisation of the complexes using the calculations described in Section 5.2.4.

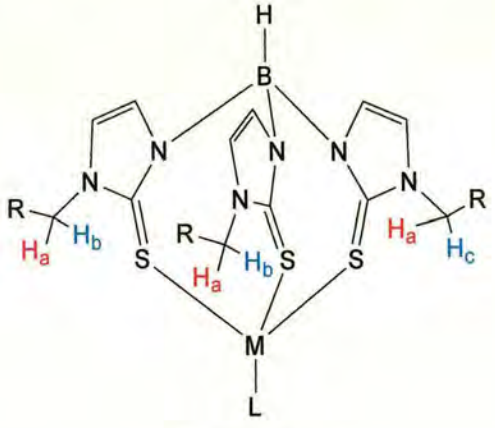

Figure 5-7 Tetrahedral complex of Tm^{Et} (R = Me) or Tm^{Bn} (R = Ph) with two sets of diastereotopic protons highlighted in red and blue (highlighted protons would also be diastereotopic in an octahedral complex)

Appearance of the Spectra

It is possible to predict the number of lines expected for the diastereotopic protons. For complexes of the Tm^{Et} ligand a doublet of quartets is expected for each of the two sets of protons, i.e. a 16-line signal. This can be explained by the fact that each proton (H_a or H_b, Fig. 5-7) is geminally coupled to the other diastereotopic proton providing a doublet which is in turn split by the protons of the methyl group (vicinal coupling) providing a doublet of quartets. For complexes of the Tm^{Bn} ligand a simpler spectrum is predicted. The diastereotopic protons (H_a, H_b) are coupled to each other giving rise to two geminally-coupled doublets, i.e. a four line signal.

Practical Considerations

The complexes were dissolved in approximately 0.5 mL of the appropriate solvent and added to a standard NMR tube. Room temperature data were collected for the sample and a series of high and/or low temperature studies then carried out as described in Section 6.4. This involved slowly increasing or decreasing the temperature in 10 °C increments. Once the variable temperature data had been collected, the sample was allowed to adjust to ambient temperature and a second room temperature spectrum was recorded to confirm the reversibility of the results.

The choice of solvent was important as the solubility of the complexes, coordinative nature of the solvent and its boiling point and freezing point had to be considered. When a non-coordinating solvent was required tetrachloroethane-d_2 or chloroform-*d* was used, the choice being dependant on the temperature range needed. Tetrachloroethane-d_2

(liquid range – 44 – +146°C) was used for complexes with a higher coalescence point while chloroform-*d* (liquid range – 64 – +62°C) could be used for complexes displaying a lower coalescence point. Both acetonitrile-d_3 (liquid range – 45 – +82°C) and DMSO-d_6 (liquid range +18 – +189°C) were used as coordinating solvents however in some cases the use of DMSO-d_6 was the only alternative due to solubility issues of the complexes (Section 5.2.9). A further limitation encountered was that of the NMR spectrometer itself. All of the VT NMR experiments were carried out using a 360 MHz spectrometer on which the highest and lowest safely accessible temperatures were approximately 373 K and 213 K respectively. In many instances the liquid range of the solvent in conjunction with the temperature constraints of the spectrometer meant that it was not possible to obtain all of the required data for the complex. For example the coalescence temperature was found to be beyond the highest accessible temperature of the instrument in a particular solvent whereas in an alternative solvent the spectrum recorded at the lowest accessible temperature did not display slow exchange. These issues resulted in approximations being used in some cases and are fully described in the appropriate sections.

Calculations

In order to estimate the energy barrier to racemisation of the complexes the following equations were used:

Equation 5-1 Eyring Equation

$$k = \frac{R\,T}{N\,h}\, e^{-\Delta G^{\ddagger} / R\,T}$$

R: Universal Gas Constant, 8.314 J K^{-1} mol^{-1}

T: Temperature (K)

N: Avogadro Constant, 6.022 x 10^{23} mol^{-1}

h: Planck Constant, 6.626 x 10^{-34} J s

$\Delta G^{\ddagger}$: Free Enthalpy of Activation (kJ mol^{-1})

$$k = 2.22\,\Delta v$$

$\therefore$ Equation 5-1 can be simplified to:

Equation 5-2

$$\Delta G = R\,T_c\,[\,22.96 + \ln (T_c / \Delta v)\,]$$

T_c = Coalescence Temperature (K)

Δv: Separation between signals in the absence of exchange (Hz)

5.2.1 Group 12: Zinc, Cadmium and Mercury

[ZnTm^{Et}Cl] (23)

The room temperature signals representing the methylene protons in the VT NMR of [ZnTm^{Et}Cl] in tetrachloroethane-d_2 are shown in Fig. 5-8. At this temperature a sharp set of signals representing slow exchange is observed for the protons. As discussed in Section 5.2.2, a 16-line signal is expected for the methylene protons, however from Fig. 5-8 it is clear that only 12 lines are observed. This is due to the fact that for each proton the quartets arising from vicinal coupling are superimposed giving what appear to be two 6-line signals. The coupling constants may be deduced as shown in Fig. 5-8. For [ZnTm^{Et}Cl], the geminal and vicinal couplings are 14.1and 7.1 Hz respectively.

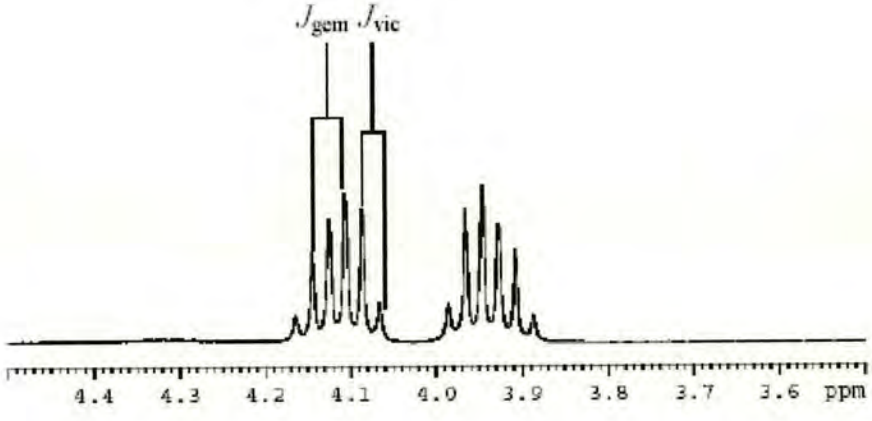

Figure 5-8 Coupling constants for in room temperature NMR of [ZnTm^{Et}Cl]

(gem = geminal, vic = vicinal)

As the temperature of the sample is increased (Fig. 5-9) a certain amount of broadening is observed, however coalescence is beyond the accessible temperature range of the instrument. The only conclusion we can draw, therefore, is that the coalescence point is higher than 373 K and, applying Equation 5-2, we can calculate that the energy barrier to racemisation is greater than 77 kJ mol^{-1} (Scheme 5-1).*

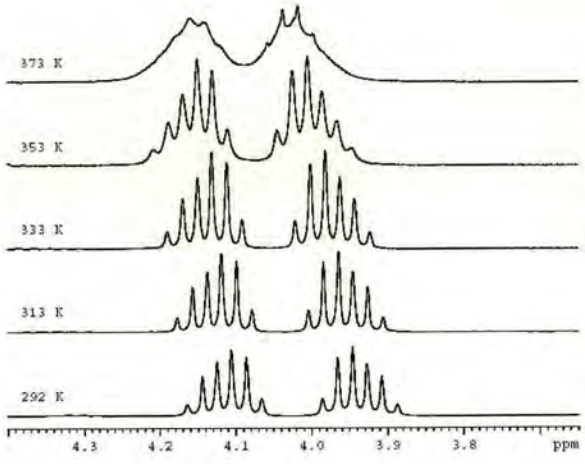

Figure 5-9 Methylene signals in VT NMR of [ZnTm^{Et}Cl] in tetrachloroethane-d_2 solution

* The application of Equation 5-2, as shown in Scheme 5-1, will only be explicitly detailed for one complex (**23**) as the calculation of ΔG was carried out in exactly the same manner for all complexes.

$$\Delta G = R\,T_c\,[\,22.96 + \ln(T_c / \Delta v)\,] \qquad \textbf{(Eqn. 5-2)}$$

$\Delta G^{\ddagger}$: Free Enthalpy of Activation (kJ mol^{-1})

R: Universal Gas Constant, 8.314 J K^{-1} mol^{-1}

T_c: Coalescence Temperature (K)

Δv: Separation between signals in the absence of exchange (Hz)

For [ZnTm^{Et}Cl] in tetrachloroethane-d_2:

$$T_c = >373\ K$$

$$\Delta v = 57.7\ Hz$$

$$\Delta G = R\,T_c\,[\,22.96 + \ln(T_c / \Delta v)\,]$$

$$\Delta G_{>373} = 8.314\,(373)\,[\,22.96 + \ln(373 / 57.7)\,]$$

$$\Delta G_{>373} = >76.99\ kJ\ mol^{-1}$$

Scheme 5-1 Calculation of energy barrier to racemisation (ΔG) of [ZnTm^{Et}Cl] in tetrachloroethane-d_2

To explore whether the mechanism of racemisation occurring is a dissociative one, the VT NMR experiments were repeated in coordinating solvents. It was expected that if the energy barrier to racemisation in a coordinating solvent was lower than that in a non-coordinating solvent a dissociative mechanism could be inferred. This is due to the stabilisation of the intermediate by coordination of the solvent (Fig. 5-10).

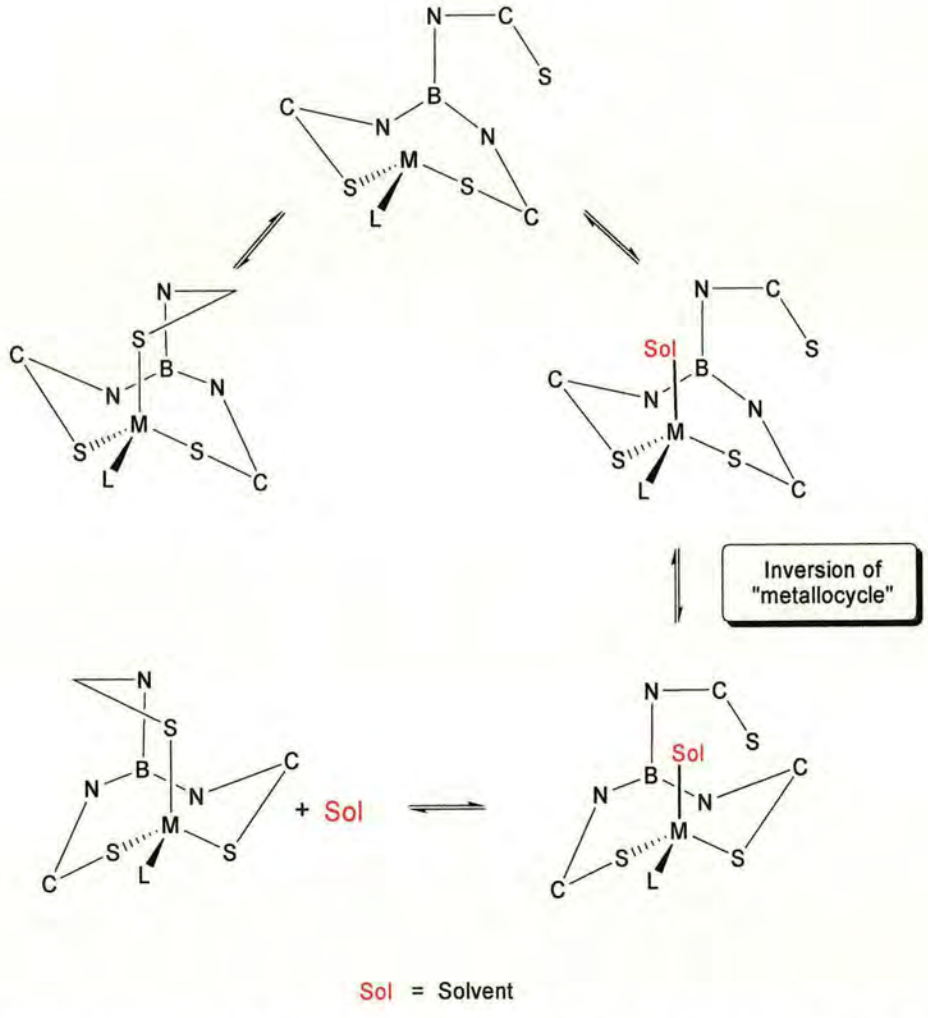

Figure 5-10 Stabilisation of intermediate in dissociative mechanism by coordinating solvent in tetrahedral complexes

Results from the VT NMR spectra of [ZnTm^{Et}Cl] (**23**) indicate that the energy barrier to racemisation in a coordinating solvent is lower than that in a non-coordinating solvent. The experiments were performed in acetonitrile-d_3 and DMSO-d_6. In acetonitrile-d_3 (Fig. 5-11), the signals display intermediate exchange at approximately 348 K; this is significantly different from experiments in tetrachloroethane-d_2 where, at this temperature, slow exchange still takes place. The activation energy can only be approximated (>72 kJ mol^{-1}) as the coalescence temperature is beyond the liquid range for acetonitrile. At 238 K the geminal and vicinal couplings are 14.0 and 7.0 Hz respectively.

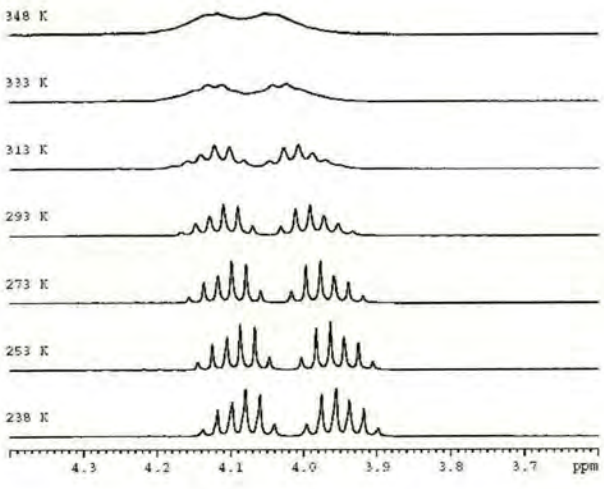

Figure 5-11 Methylene signals in VT NMR of [ZnTm^{Et}Cl] in acetonitrile-d_3 solution

In DMSO-d_6 (Fig. 5-12) the coalescence temperature is even lower than in acetonitrile. Coalescence is observed at approximately 293 K and as the sample is heated, fast exchange, represented by a quartet, is observed. Although slow exchange is not observed, and therefore a value for the separation between signals at slow exchange (Δv) cannot be obtained, an approximation for the activation energy can be made. By making a series of calculations using a broad range of values for Δv in Equation 5-2 it is noted that the resulting values obtained for ΔG are within a relatively narrow range, i.e. the value of Δv used in Equation 5-2 does not significantly alter the resulting value for ΔG. Thus, with a coalescence temperature of 293 K, the energy barrier for the racemisation is estimated as 56-60 kJ mol^{-1}.

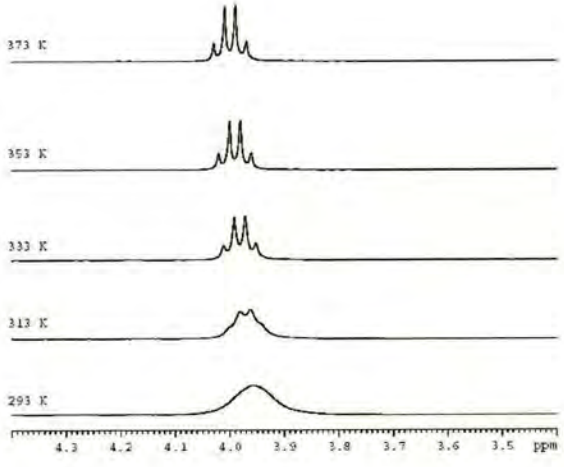

Figure 5-12 Methylene signals in VT NMR of [ZnTm^{Et}Cl] in DMSO-d_6 solution

It is clear from experiments in acetonitrile-d_3 and DMSO-d_6 that the use of a coordinating solvent lowers the barrier to racemisation relative to that in a non-coordinating solvent supporting the theory that the mechanism taking place in tetrahedral complexes is a dissociative one. The activation energy in DMSO-d_6 (56-60 kJ mol^{-1}) compared with acetonitrile-d_3 (>72 kJ mol^{-1}) suggests a greater stabilisation of the intermediate species due to stronger coordination of the softer solvent.

[ZnTm^{Bn}Cl] (26)

To investigate whether addition of a bulkier group in the N(1)-position would affect the energy barrier to racemisation of the complexes, VT NMR experiments for the zinc complex, **26** were carried out (Fig. 5-13). In this complex, benzyl groups replace the ethyl groups in [ZnTm^{Et}Cl] (**23**). At room temperature a set of sharp signals is observed consisting of two doublets as predicted in Section 5.2.2 and representing slow exchange (the spectrum also displays a sharp singlet at 5.27 ppm which is identified as an impurity of dichloromethane). At room temperature (293 K) the geminal coupling is 15.0 Hz. As the temperature is increased the signals begin to broaden. The separation of the signals at the highest accessible temperature (373 K) would suggest that the coalescence point is a good deal higher than 373 K and we can only estimate an energy barrier of greater than 77 kJ mol^{-1}. As the energy of the processes occurring in complexes **23** and **26** are not accessible, it is not possible, in this case, to comment on the effect of substitution in the N(1) position of the ligand.

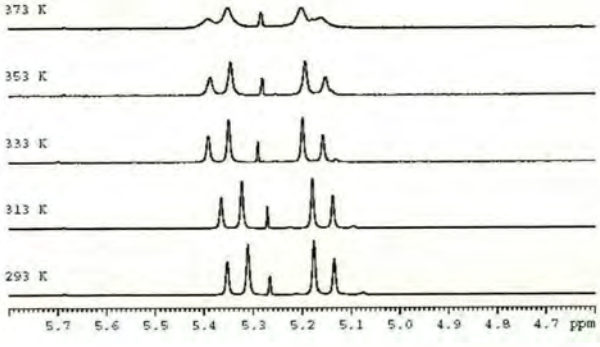

Figure 5-13 Methylene signals in VT NMR of [ZnTm^{Bn}Cl] in tetrachloroethane-d_2 solution

The results from experiments in DMSO-d_6 give slightly more insight into the effect of substitution in the N(1) position of the ligand on the activation energy. The coalescence point is observed at approximately 303 K, however slow exchange is not observed (Fig. 5-14). It is therefore necessary to take an approximate value for the separation between signals in the static structure (Δv), giving an estimated value of 58-63 kJ mol^{-1} for the activation energy.

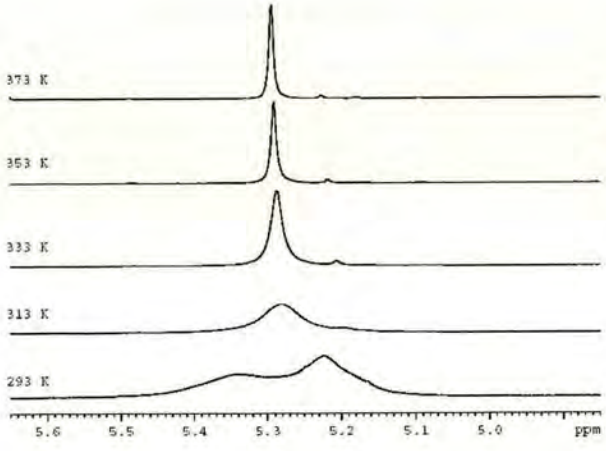

Figure 5-14 Methylene signals in VT NMR of [ZnTm^{Bn}Cl] in DMSO-d_6 solution

This value is comparable to the estimated value for the energy barrier to racemisation of the ethyl analogue, **23** in DMSO-d_6 (56-60 kJ mol^{-1}) suggesting that the addition of bulky groups to the backbone of the ligand does not significantly affect the activation energy. These results are not surprising when the crystal structure of [ZnTm^{Bn}Br][34] (Fig. 5-15) is studied.

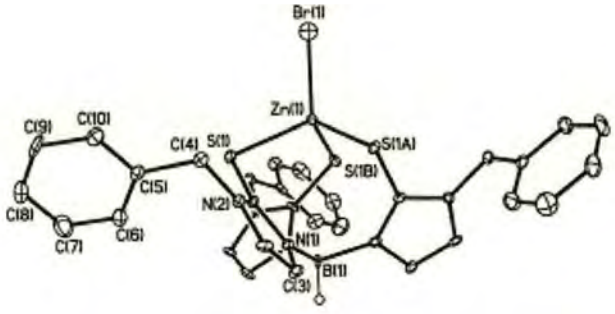

Figure 5-15 Crystal structure of [ZnTm^{Bn}Br][34]

It is clear that the benzyl groups point away from the helical backbone of the structure and a significant change in the energy barrier to racemisation would not be expected. This is confirmed by the similarity of the torsion angles* in the structures of [ZnTm^{Et}Cl] and [ZnTm^{Bn}Br] which are 46.3 and – 46.5° respectively. The results of experiments in DMSO-d_6 are also in agreement with the theory that the use of coordinating solvents significantly lowers the activation energy and thus suggest that tetrahedral complexes undergo dissociative racemisation.

[CdTm^{Et}Br] (24)

The cadmium complex **24** was subjected to VT NMR experiments in tetrachloroethane-d_2. The room temperature signals for the methylene protons (Fig. 5-16) display slow exchange (see Section 5.2.2 for explanation of appearance of spectrum) and the geminal and vicinal couplings are 14.1and 7.1 Hz respectively. The coalescence temperature is approximately 373 K. The energy barrier to racemisation of

* Appendix 3

the complex may therefore be approximated as 77 kJ mol^{-1}, a lower value than that for its zinc analogue (**23**) in the same solvent (>77 kJ mol^{-1}) for which coalescence occurs *above* 373 K. The fact that the Cd(II) complex has a lower activation energy suggests that the size and/or lability of the metal centre is a factor in the energy barrier to racemisation. Working under the assumption that a dissociative mechanism is occurring in tetrahedral complexes and, therefore, that the activation energy depends on the dissociation energy of the metal-sulphur bond, this result confirms that the energy barrier to racemisation decreases as the metal is changed from Zn(II) to the larger[132] Cd(II) ion.

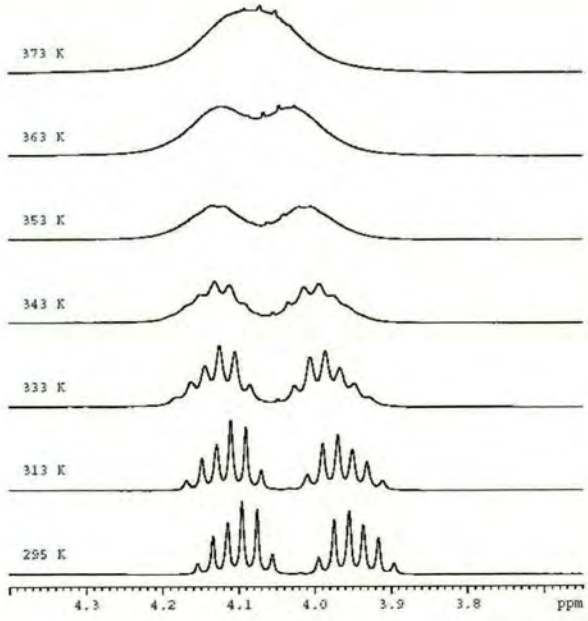

Figure 5-16 Methylene signals in VT NMR of [CdTm^{Et}Br] in tetrachloroethane-d_2 solution

The coalescence temperature for complex **24** in acetonitrile-d_3 is observed at 333 K (Fig. 5-17) and the energy barrier to racemisation is found to be approximately 69 kJ mol^{-1}. As expected, this is a lower value than in the non-coordinating solvent, tetrachloroethane-d_2 (77 kJ mol^{-1}).

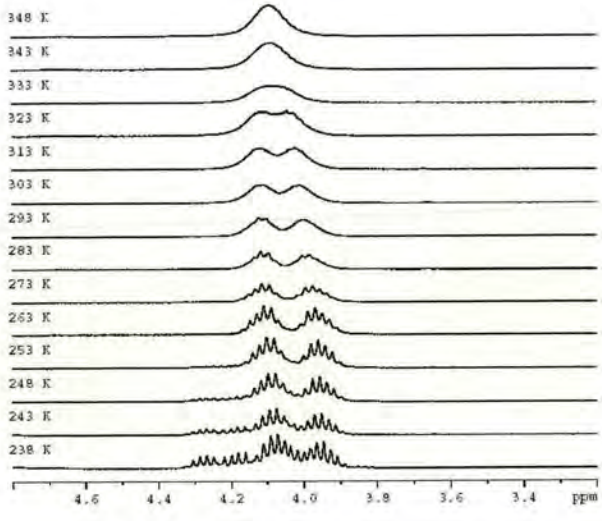

Figure 5-17 Methylene signals in VT NMR of [CdTm^{Et}Br] in acetonitrile-d_3 solution

There are, however, some unexpected signals observed at low temperature. At approximately 253 K the appearance of a second set of signals is observed in the spectrum (Fig. 5-17). This second set of signals is also observed in the methyl region of the spectrum (Fig. 5-18) which gives an indication that a second species may be present in solution, however since this anomaly is occurring at the lowest accessible temperature for the instrument it is difficult to determine what is happening and, to date, no further data have been obtained which would provide an explanation.

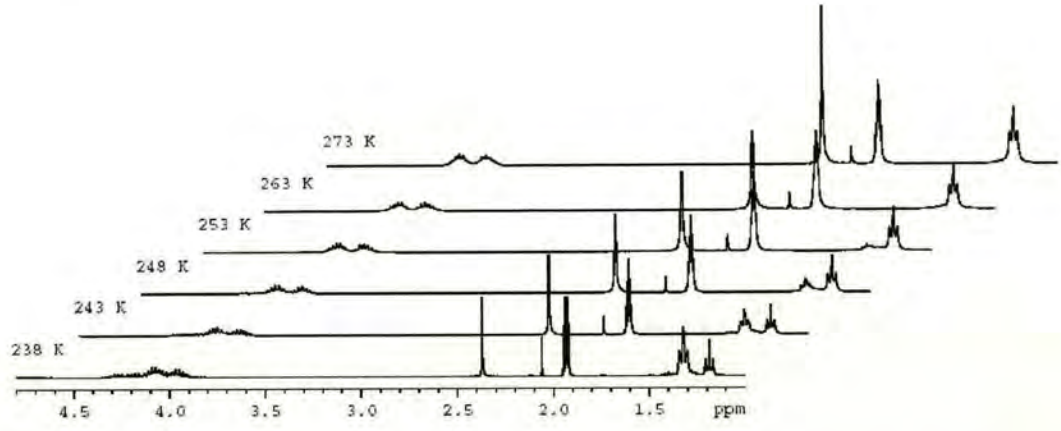

Figure 5-18 Methyl and Methylene signals in VT NMR of [CdTm^{Et}Br] in acetonitrile-d_3 solution

As with the zinc complex (**23**), the results from VT NMR experiments with [CdTm^{Et}Br] (**24**) in DMSO-d_6 do not reveal much information about the slow exchange processes but it is clear that the coordinating solvent lowers the activation energy relative to the non-coordinating solvent. Although slow exchange is not observed (Fig. 5-19), and therefore a value for Δv cannot be obtained, an approximation for the activation energy can be made as described for the NMR of **23** in DMSO-d_6. Thus, with a coalescence temperature of <293 K, the energy barrier for the racemisation of the complex is estimated as <61 kJ mol^{-1}. As in the case of the zinc centre in complex **23,** it seems that DMSO-d_6 has a greater affinity for the soft cadmium centre than acetonitrile-d_3 resulting in stabilisation of the intermediate species and thus lowering the energy barrier to racemisation.

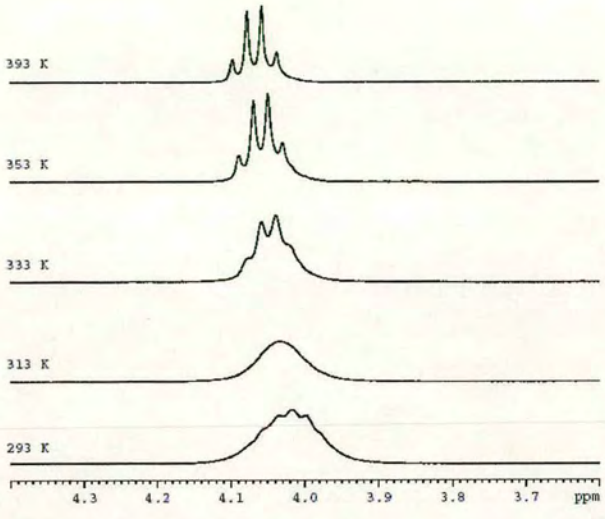

Figure 5-19 Methylene signals in VT NMR of [CdTm^{Et}Br] in DMSO-d_6 solution

[CdTm^{Bn}Br] (27)

Like the spectra of [ZnTm^{Bn}Cl] (**26**), the VT NMR spectra of **27** in tetrachloroethane-d_2 (Fig. 5-20) are not as informative as those for complexes of the Tm^{Et} ligand. This is due to the fact that, for slow exchange, the signals are well separated and therefore a higher temperature is needed for coalescence. At room temperature (293 K) the geminal coupling is 14.9 Hz. We would expect the energy barrier to racemisation in **27** to be similar to that for [CdTm^{Et}Br] (**24**) however from the spectra we can only approximate a value > 78 kJ mol^{-1}. The spectrum also displays a sharp singlet at 5.27 ppm which is identified as an impurity of dichloromethane.

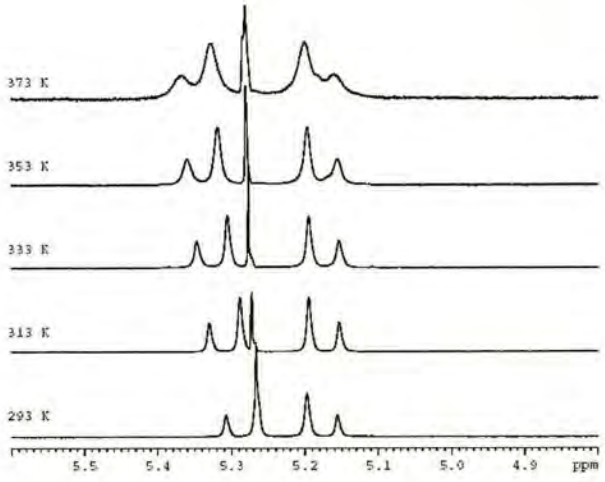

Figure 5-20 Methylene signals in VT NMR of [CdTm^{Bn}Br] in tetrachloroethane-d_2 solution

The NMR spectra in DMSO-d_6 (Fig. 5-21) show intermediate to fast exchange within the liquid range of the solvent. The coalescence point is at approximately 323 K and by taking an estimated value for the separation between signals at slow exchange ($\Delta\nu$) the activation energy is found to be in the range 63-68 kJ mol^{-1}.

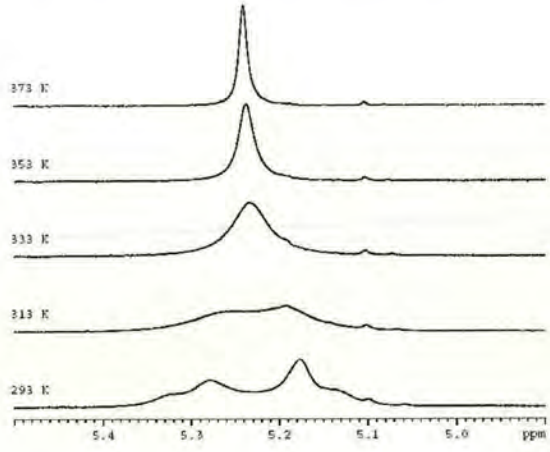

Figure 5-21 Methylene signals in VT NMR of [CdTm^{Bn}Br] in DMSO-d_6 solution

The value of 63-68 kJ mol^{-1} for the racemisation of **27** in DMSO-d_6 is only slightly higher than the value for the activation energy of its ethyl analogue, **24** in the same solvent (61-65 kJ mol^{-1}). This supports the conclusion drawn from the work on analogous zinc complexes that substitution at the N(1)-position does not significantly alter the energy barrier to racemisation. As in the case of the zinc complexes of Tm^{Et} and Tm^{Bn}, the crystal structures of [CdTm^{Et}Br] and [CdTm^{Bn}Br] may be compared (Figs. 4-3, 4-4). It is clear that the ethyl and benzyl groups point away from the helical

backbone of the structure. The torsion angles* in [$CdTm^{Et}Br$] and [$CdTm^{Bn}Br$] are – 46.9° and – 46.6° respectively and thus, a significant change in the energy barrier to racemisation would not be expected. It should also be noted that, as before, the use of a coordinating solvent leads to a substantial decrease in the energy barrier to racemisation of the complex suggesting the operation of a dissociative mechanism.

* Appendix 3

[HgTm^{Et}Cl] (25)

The room temperature signals for the methylene protons of **25** observed in tetrachloroethane-d_2 were sufficiently broadened so as to require low-temperature studies. The low-temperature signals show significant broadening and as the temperature is raised the broadening continues until coalescence is observed at approximately 323 K. As the temperature is increased further the signals begin to sharpen into a quartet (Fig. 5-22). The methylene signals undergoing slow exchange would be expected to have a ratio of 1:1 however the signals at the lowest accessible temperature seem to display an unusual ratio.

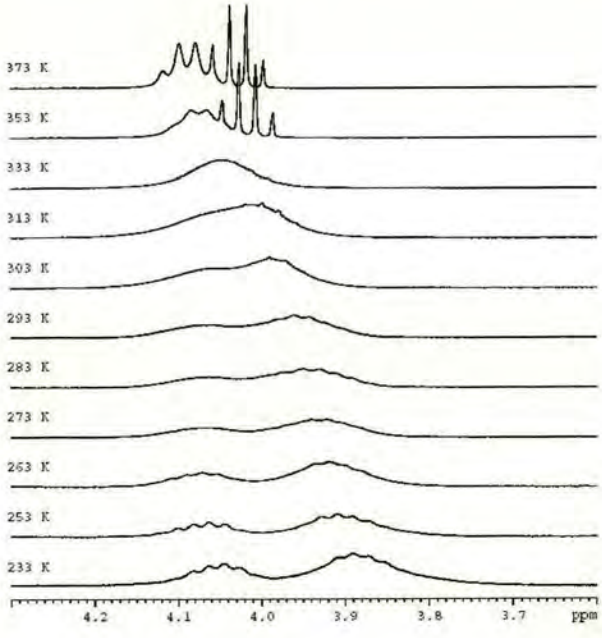

Figure 5-22 Methylene signals in VT NMR of [HgTm^{Et}Cl] in tetrachloroethane-d_2 solution

With the knowledge that Hg(II) complexes have a tendency to form two-coordinate, linear complexes as well as four-coordinate, tetrahedral complexes[132] the following theory was developed. If the mercury ion was coordinated by all three sulphur donors we would expect to see a change only in the diastereotopic protons with changes in temperature. This, however, is not the case as can be seen in Fig. 5-23. Dynamic behaviour is also observed for the methyl protons in the spectra of **25**. It seems that there are two different environments for the methyl *and* methylene protons at low temperature and that as the temperature is increased the signals become equivalent.

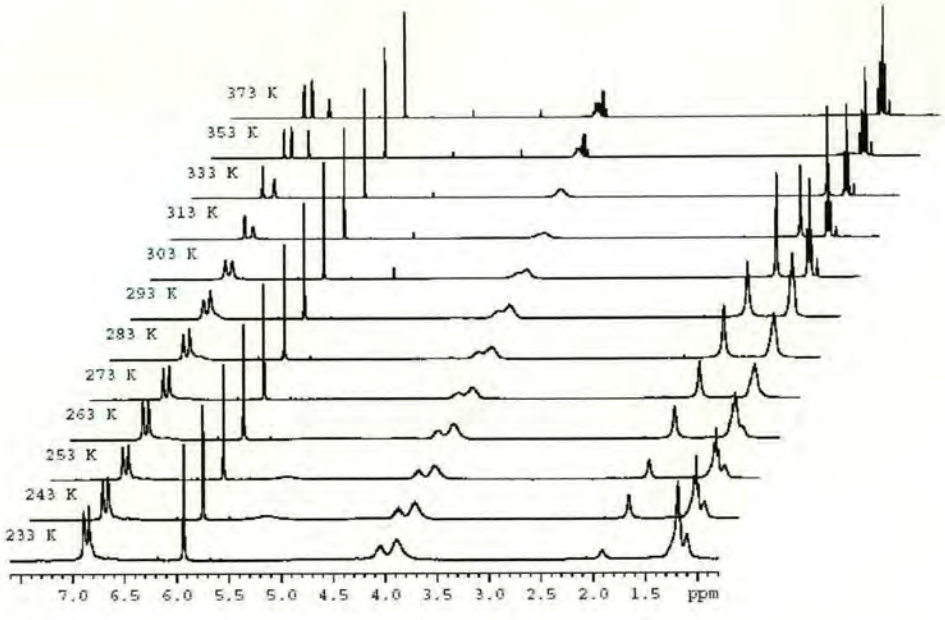

Figure 5-23 VT NMR of [HgTm^{Et}Cl] in tetrachloroethane-d_2 solution

It was postulated that the geometry of the Hg(II) complex is linear with the mercury atom in a two-coordinate environment, ligated by one sulphur donor from the tripod ligand and a chloride ligand (Fig. 5-24).

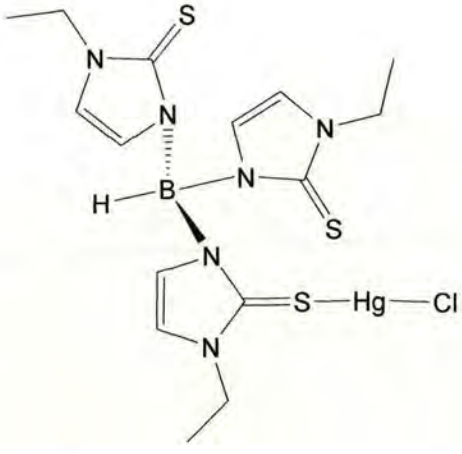

Figure 5-24 Postulated Structure of [HgTm^{Et}Cl]

The signals observed in the spectra could therefore be due to the two different environments of the ethyl groups, one set of signals arising from the coordinated arm of the tripod and the other from the two uncoordinated arms. It is possible that as the temperature of the sample is increased the exchange between coordinated and uncoordinated arms of the tripod becomes sufficiently fast that the protons become indistinguishable on the NMR timescale, (i.e. the mercury is "hopping" rapidly between the three sulphur donors of the tripod). The activation energy of this process, according to a coalescence temperature of 323 K and an estimated value for the separation between signals in the static structure ($\Delta\nu$), is in the range 63-66 kJ mol^{-1}. It is not surprising that

this value is similar to the values for the energy barrier to racemisation of [ZnTm^{Et}Cl] (**23**) and [CdTm^{Et}Br] (**24**) in tetrachloroethane-d_2 as it is the same feature of the complexes (the dissociation energy of the metal-sulphur bond) which controls the activation energy in both mechanisms. It was expected, therefore, that the activation energy in [HgTm^{Et}Cl] is not only similar to the other Group 12 complexes but completes the series of decreasing values with increasing ionic radii as we move down the periodic table.[137] This theory, however, does not account for the origin of the sharp quartet which appears in the spectrum at 353 K. The suggestion that the quartet arises from the methylene protons of a small amount of dissociated ligand is not viable as the signal is absent in the room temperature spectra recorded after VT NMR experiments were carried out i.e. the process is reversible. This led us to the conclusion that the second quartet seen in Fig. 5-22 must be involved in the dynamic process. In comparing the quartets it was noted that one is significantly sharper than the other suggesting the presence of two different species in solution. One possible explanation is that we are observing a metathesis reaction whereby an increase in temperature causes the formation of a certain amount of the *bis*-substituted product as shown in Scheme 5-2. Due to the achiral nature of the *bis*-substituted species* we would expect to observe a quartet representing the twelve methylene protons.

* For steric reasons the 'twist' of each tripod ligand will be in the opposite direction with respect to the other thereby introducing an inversion centre and forming a molecule which is achiral.

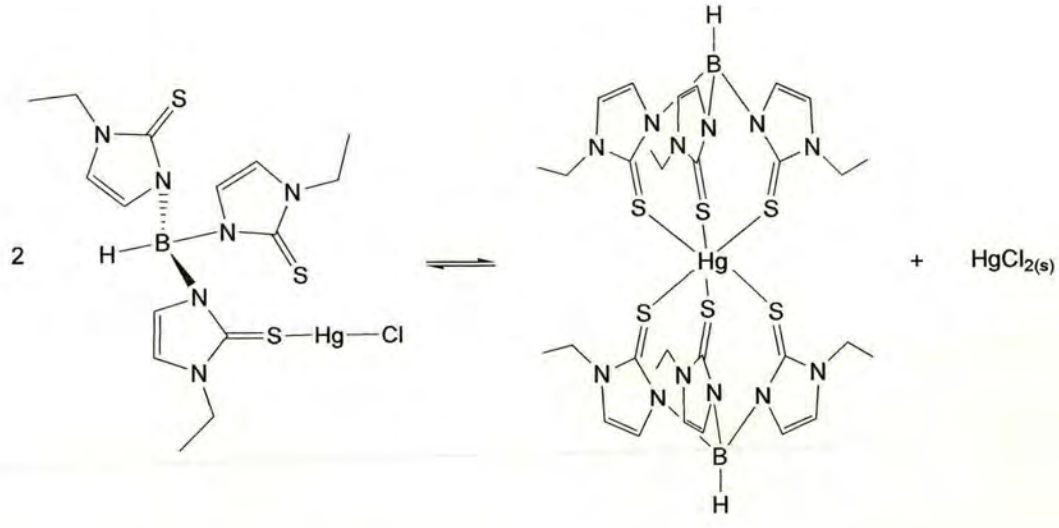

Scheme 5-2 Postulated disproportionation of [HgTm^{Et}Cl]

The theory outlined above is supported by the results of the VT NMR experiments of **25** in acetonitrile-d_3 (Fig. 5-25). A similar pattern is seen as the temperature changes whereby, at low temperature, two sets of signals with unequal ratios are observed and as the temperature is increased, coalescence followed by fast exchange is observed. A change to a more coordinating solvent such as this would be expected to stabilise the intermediates in the dynamic system, thereby lowering activation energy and this is found to be the case as the activation energy is in the range 52-57 kJ mol^{-1}.

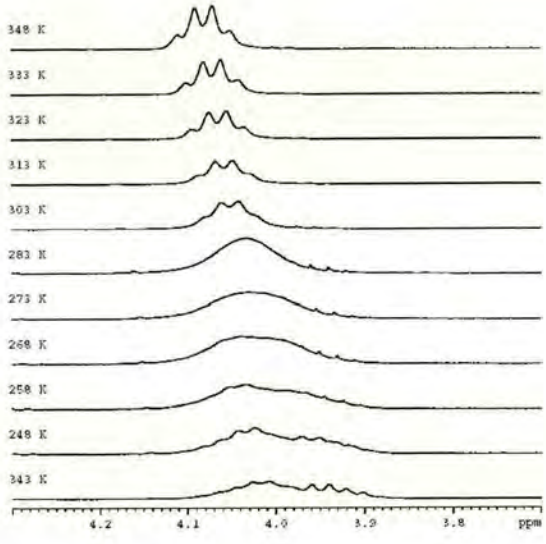

Figure 5-25 Methylene signals in VT NMR of [HgTm^{Et}Cl] in acetonitrile-d_3 solution

In DMSO-d_6 the range of signals between 293 and 373 K display intermediate to fast exchange (Fig. 5-26). The temperature at which coalescence is observed (293 K) and an estimate of the separation between signals in the static structure ($\Delta\nu$) gave a range of 57-61 kJ mol^{-1} for the activation energy of the process.

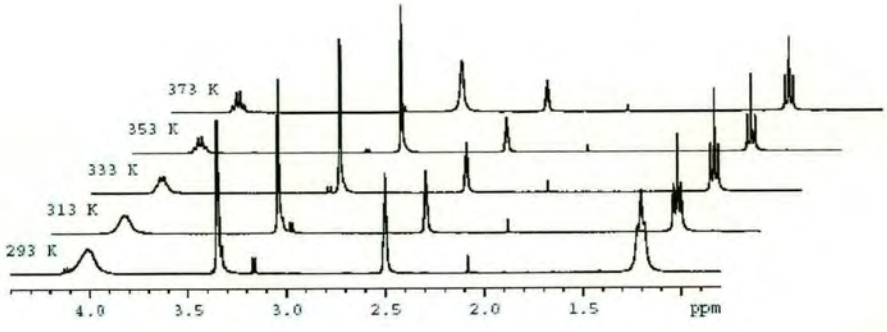

Figure 5-26 VT NMR of [HgTm^{Et}Cl] in DMSO-d_6 solution

[HgTm^{Bn}Cl] (28)

The VT NMR spectra of **28** in tetrachloroethane-d_2 (Fig. 5-27) and DMSO-d_6 (Fig. 5-28) do not aid in substantiating our theory concerning the processes occurring in Hg(II) complexes of Tm^{Et} and Tm^{Bn}. The methylene signals in both solvents are observed as a singlet representing fast exchange.

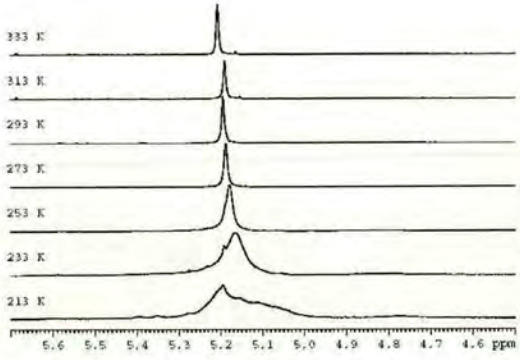

Figure 5-27 Methylene signals in VT NMR of [HgTm^{Bn}Cl] in tetrachloroethane-d_2 solution

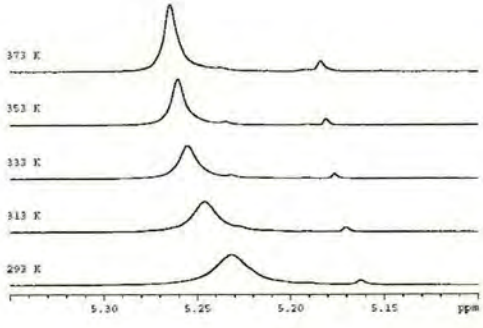

Figure 5-28 Methylene signals in VT NMR of [HgTm^{Bn}Cl] in DMSO-d_6 solution

5.2.2 Group 11: Copper, Silver and Gold

[CuTm^{Et}PPh$_3$] (29)

The signals representing the methylene protons in the VT NMR of **29** in chloroform-*d* are shown in Fig. 5-29. At low temperature (213 K) a sharp set of signals is observed for the protons, indicating slow interconversion between enantiomers. The geminal and vicinal couplings are 13.9 and 7.0 Hz respectively.

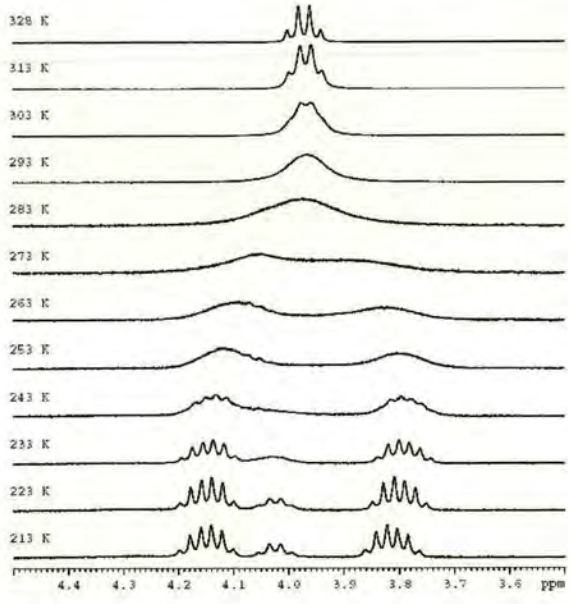

Figure 5-29 Methylene signals in VT NMR of [CuTm^{Et}PPh$_3$] in chloroform-*d* solution

As the sample is heated the signals begin to broaden until coalescence is observed at approximately 278 K. As the sample is heated further the signals sharpen and a quartet, characteristic of fast exchange, is observed. The energy barrier for the racemisation of

the complex is approximately 55 kJ mol^{-1}. This value is somewhat lower than the energies found for Group 12 complexes. If we assume that, as a tetrahedral complex, the copper is undergoing a dissociative mechanism, it is postulated that the lower energy barrier to racemisation in the Cu(I) complex compared to its Zn(II) and Cd(II) counterparts is due to a weaker Cu-S bond compared to Zn- or Cd-S bonds however this theory could not be substantiated as no data on metal-sulphur (thione) bond strengths could be found in the literature.

Unexpectedly, the results obtained from the NMR spectra in acetonitrile-d_3 (Fig. 5-30) suggest that the presence of a coordinating solvent does not significantly alter the activation energy in this complex. Coalescence is observed at 263 K, giving a value of 54 kJ mol^{-1} for the energy barrier to racemisation.

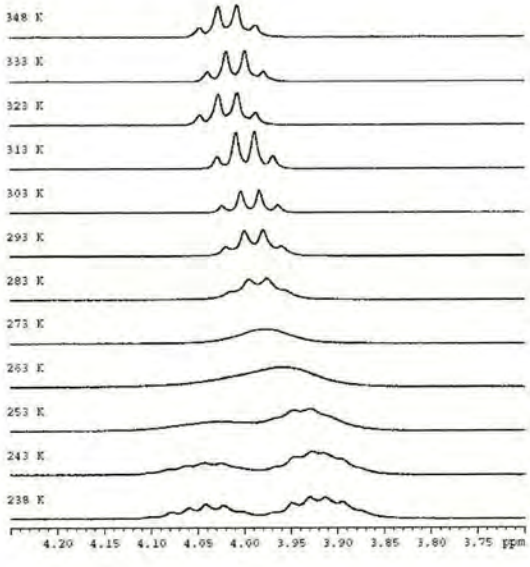

Figure 5-30 Methylene signals in VT NMR of [CuTm^{Et}PPh$_3$] in acetonitrile-d_2 solution

[AgTm^{Et}PPh$_3$] (30)

The VT NMR of **30** in chloroform-*d* is shown in Fig. 5-31. Initially the room temperature spectrum was taken and a broad signal was observed which was assumed to be the coalescence of the signals for the diastereotopic protons. When the sample was cooled down however, an unusual pattern emerged. In the slow exchange region two separate sets of signals are identified, one of which is similar to the expected pattern for the diastereotopic methylene protons while the other appears to be a broad quartet.

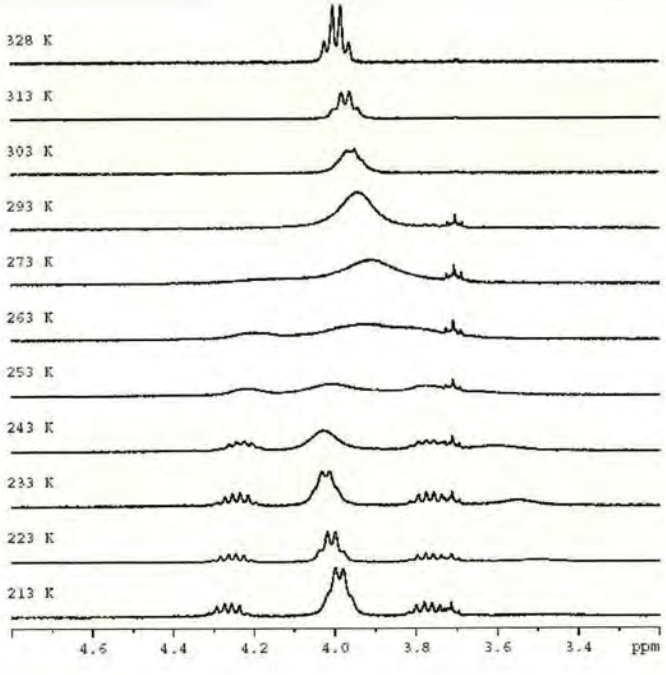

Figure 5-31 Methylene signals in VT NMR of [AgTm^{Et}PPh$_3$] in chloroform-*d* solution

Unexpected signals are also observed in the methyl region of the spectra (Fig. 5-32). It appears that there are two species present, giving rise to two sets of signals which broaden as the temperature is raised.

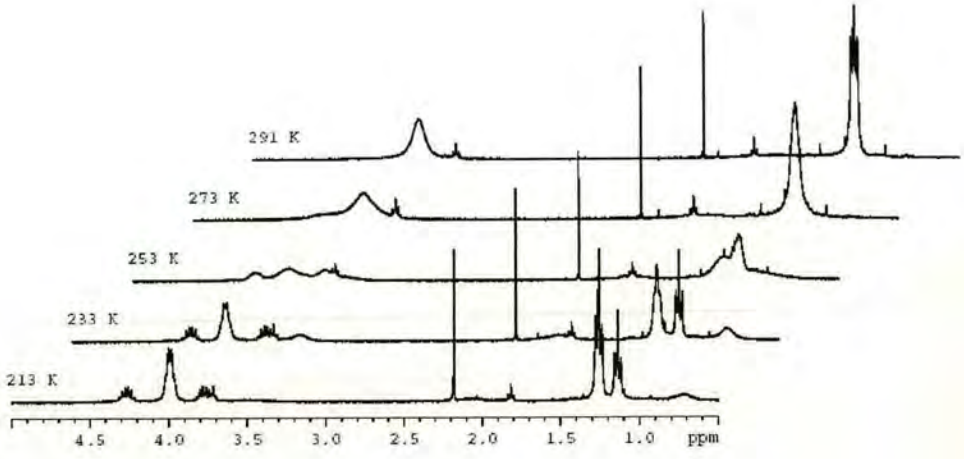

Figure 5-32 Selected signals from VT NMR of [AgTm^{Et}PPh$_3$] in chloroform-*d* solution

We postulate that, in solution, there are two geometries present; one, a two coordinate silver complex coordinated by triphenylphosphine and only one arm of the tripod, and the other, a four coordinate species with symmetrical coordination of the tripod arms (Scheme 5-3).

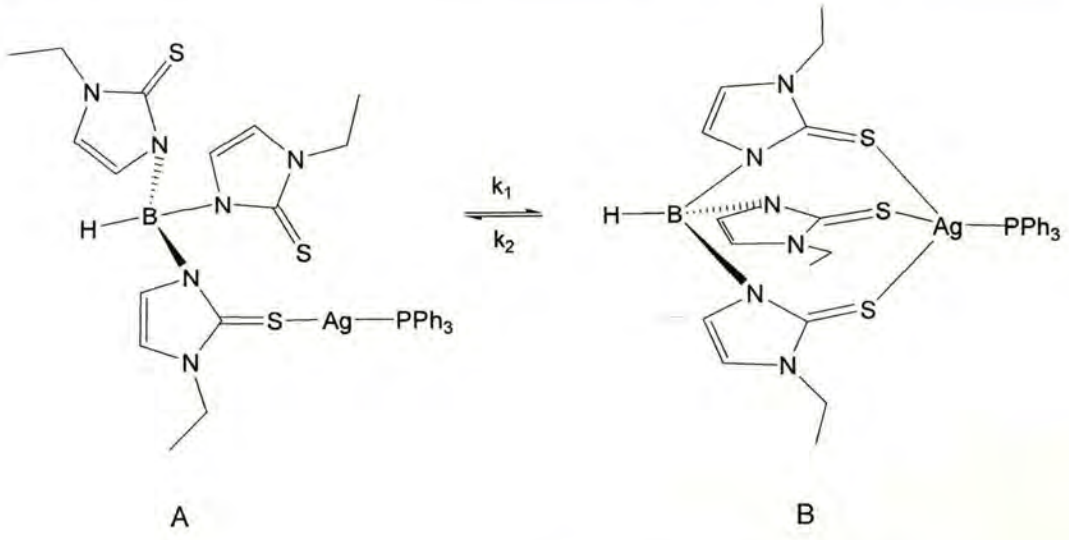

A B

Scheme 5-3 Postulated species of [AgTm^{Et}PPh$_3$] in solution

The spectra in Fig. 5-32 suggest that the two coordinate species (**A**) is undergoing rapid exchange of the coordinated and uncoordinated sulphur donors thereby displaying a triplet and quartet for the methyl and methylene protons respectively. The imidazole protons appear as a doublet and do not give any further insight into the geometry. At low temperature the four coordinate species (**B**) displays, as expected, a 6-line signal for each of the diastereotopic methylene protons and a triplet for the methyl protons. These signals are observed to coalesce as the temperature of the sample is increased. At 213 K the geminal and vicinal couplings are 13.9 and 7.0 Hz respectively. The integration of the signals (Fig. 5-33) confirms the relationship between the quartet at 3.99 ppm and the triplet at 1.26 ppm for **A**, and between the multiplets at 3.77 and 4.26 ppm and the triplet at 1.14 ppm for **B**.

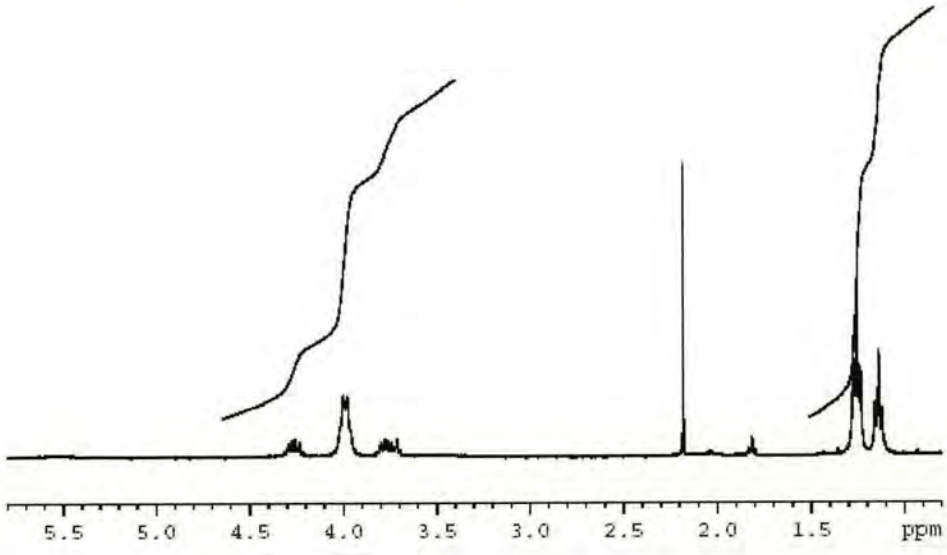

Figure 5-33 Methyl and methylene signals from VT NMR of [AgTm^{Et}PPh$_3$] in chloroform-*d* solution (213 K)

The activation energy of the racemisation of the four coordinate species (**A**) was determined as described previously (Section 5.2.4). Taking a coalescence temperature of 273 K the energy barrier to racemisation is approximately 53 kJ mol^{-1}. This is only slightly lower than the activation energy found for its copper analogue, **29**. The results from the VT NMR of **30** in acetonitrile do not provide any further insight into the processes as slow exchange is below the lowest accessible temperature for acetonitrile-d_3 (Fig. 5-34). At this temperature (238 K) coalescence is occurring and the energy barrier for the racemisation is approximately 45-50 kJ mol^{-1}. As in the case of **29** in acetonitrile-d_3 the presence of a coordinating solvent has a rather smaller effect on the energy barrier to racemisation of the complex compared to the Group 12 tetrahedral complexes investigated.

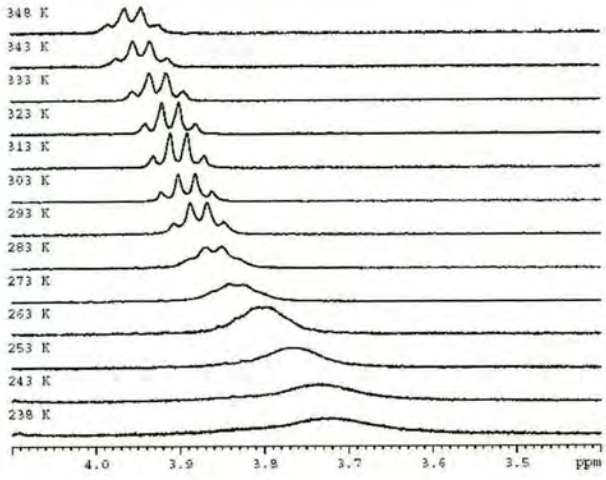

Figure 5-34 Methylene signals in VT NMR of [AgTm^{Et}PPh$_3$] in acetonitrile-d_3 solution

[AuTm^{Et}PPh$_3$] (31)

For completeness the gold complex, **31** was synthesised and VT NMR experiments were carried out in DCM-d_2. As discussed in Chapter 4, a 2-coordinate, linear geometry is expected for the Au(I) complex (Fig. 4-6) and this seems to be the case as the methylene protons are represented by a quartet which does not display any dynamic behaviour between 203 and 303 K (Fig. 5-35). The appearance of a single quartet, rather than two quartets suggests that hopping of the metal between the arms of the tripod is occurring quickly on the NMR timescale thereby revealing a single signal for the methylene protons.

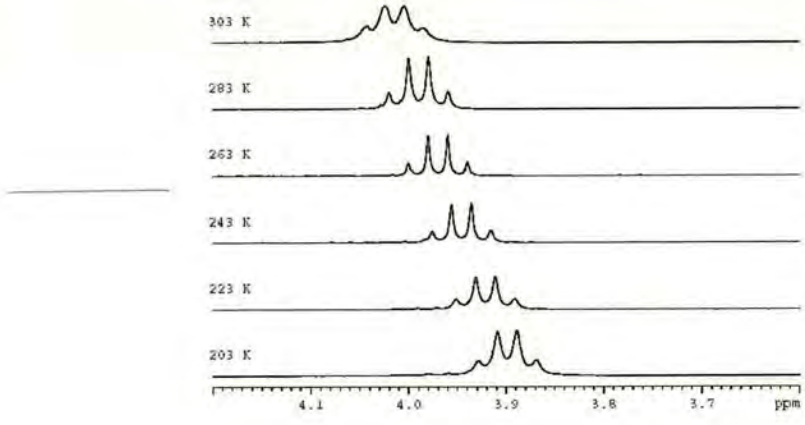

Figure 5-35 Methylene signals in VT NMR of [AuTm^{Et}PPh$_3$] in dichloromethane-d_2 solution

5.2.3 Group 7: Manganese

[MnTm^{Et}(CO)$_3$] (32)

The NMR spectrum of **32** (Fig 5-36) is quite weak due to the low solubility of the complex, however it is clear that no changes are observed in the signals up to the highest accessible temperature for the instrument (373 K). The geminal and vicinal couplings are 14.0 and 7.0 Hz respectively. The activation energy cannot be determined however it is shown to be substantially greater than 74 kJmol^{-1}.

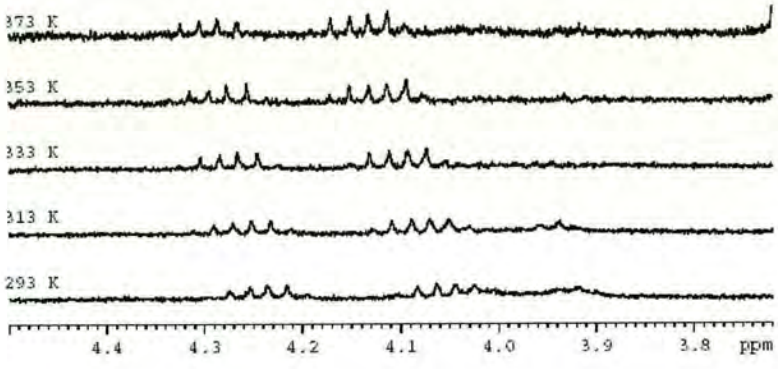

Figure 5-36 Methylene signals in VT NMR of [MnTm^{Et}(CO)$_3$] in tetrachloroethane-d_2 solution

To explore whether the presence of a coordinating solvent would affect the activation energy, the experiments were repeated in DMSO-d_6 (Fig. 5-37). As with tetrachloroethane-d_2 no broadening is observed up to 373 K suggesting the activation energy is significantly greater than 77 kJ mol^{-1} and the geminal and vicinal couplings are

13.7 and 7.0 Hz respectively. A quartet is observed in the spectrum which is due to the presence of a small amount of free ligand in the sample.

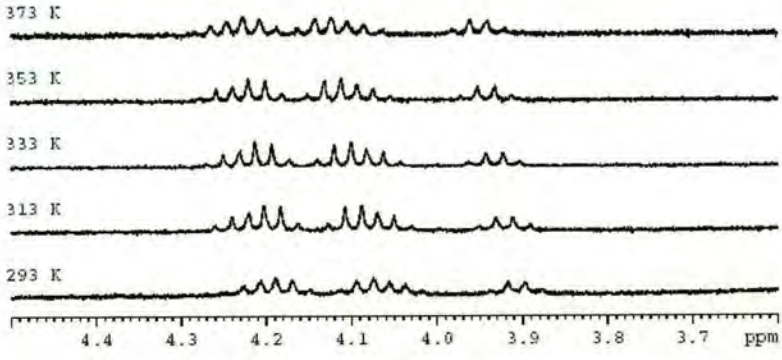

Figure 5-37 Methylene signals in VT NMR of [MnTm^{Et}(CO)$_3$] in DMSO-d_6 solution

The results of experiments in both tetrachloroethane-d_2 and DMSO-d_6 suggest that, if racemisation is occurring, the process is significantly higher in energy compared with that in tetrahedral complexes. The experimental results for complex **32** does not, however, reveal any information on the mechanism of racemisation.

5.2.4 Group 8: Ruthenium

[RuTm^{Et}(p-cym)]$^+$

The complexes [RuTm^{Et}(*p*-cym)]X (X = Cl (**33**), PF_6(**34**)) gave somewhat unexpected results when NMR spectra were recorded in a range of solvents. In tetrachloroethane-d_2, and DMSO-d_6 an apparent quartet is observed for the methylene protons of **33** (Fig. 5-38).

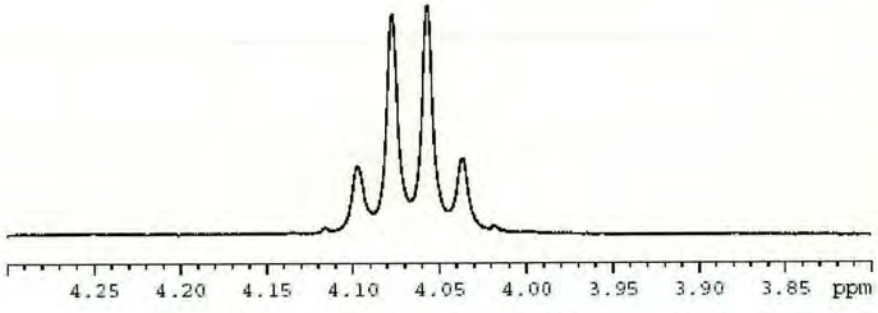

(a) Methylene signals of [RuTm^{Et}(*p*-cym)]Cl in tetrachloroethane-d_2 solution (293K)

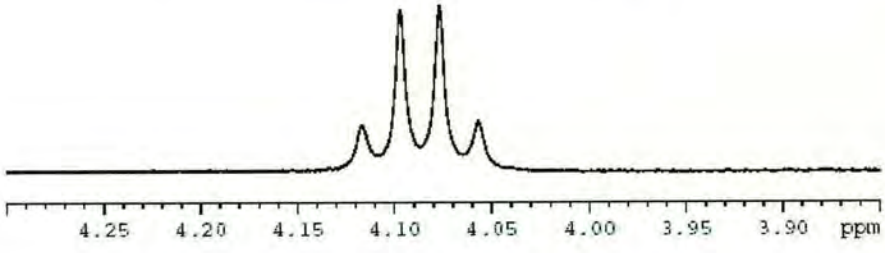

(b) Methylene signals of [RuTm^{Et}(*p*-cym)]Cl in DMSO-d_6 solution (293K)

Figure 5-38

Under normal circumstances this would suggest that the protons were not, in fact, diastereotopic however further NMR data and the crystal structure of the complex prove that the protons should be diastereotopic. In this complex both the methylene protons of the ligand *and* the arene CH protons of the *p*-cymene group are expected to be diastereotopic (Fig. 5-39).

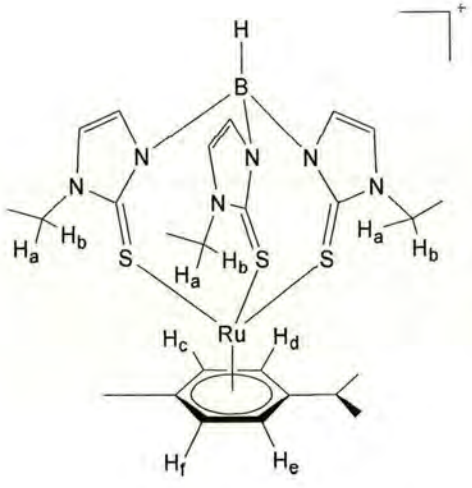

Figure 5-39 Structure of [RuTmEt(p-cym)]$^+$ with sets of diastereotopic protons labeled

The CH arene protons in a [Ru(II)(p-cym)] fragment usually appear as a clear $(AB)_2$ system in their NMR spectra[120-122] [Fig. 5-40(b)] however in all of the spectra recorded in this work these protons appear as four doublets, one representing each inequivalent proton [Fig. 5-40(a)].

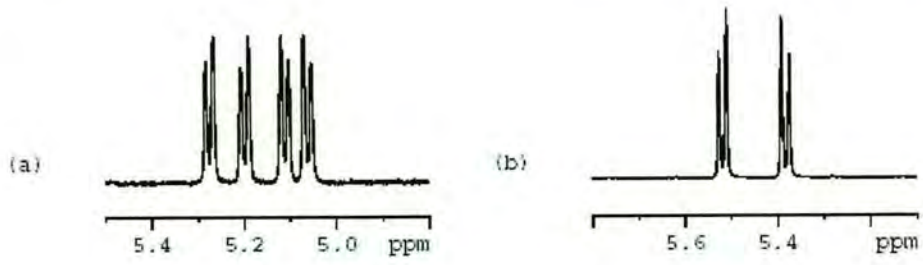

Figure 5-40 $CH_{p\text{-cym}}$ signals in (a) [RuTm^{Et}(*p*-cym)]Cl and (b) [RuCl$_2$(*p*-cym)]$_2$

Furthermore, the crystal structure clearly reveals that the ruthenium ion is coordinated by all three sulphur donors providing a complex of C_3-symmetry (Fig. 4-7). The spectra of the same complex recorded in chloroform-*d* and acetonitrile-d_3, however, displays more complicated signals for the methylene protons (Fig. 5-41).

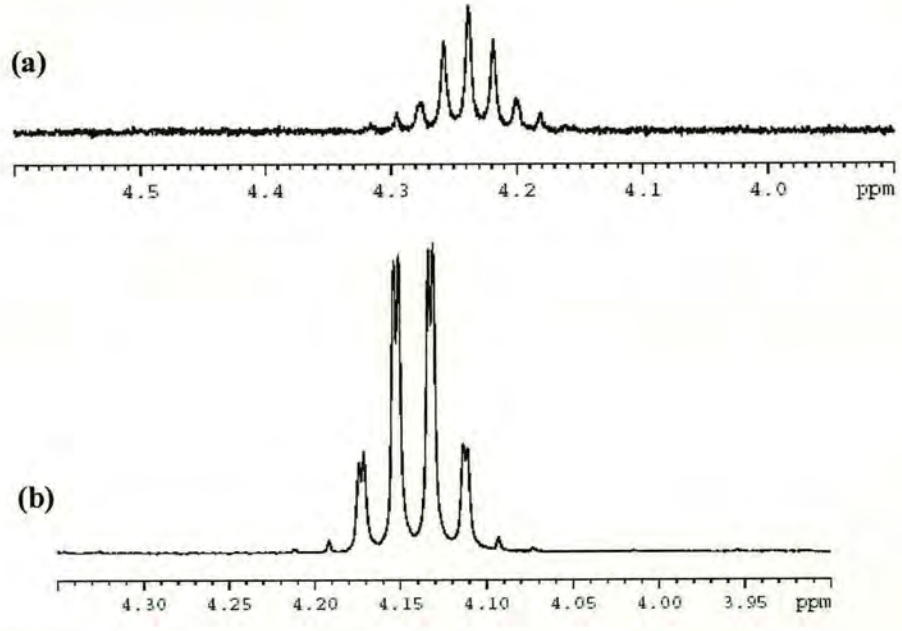

Figure 5-41 Methylene signals of [RuTm^{Et}(p-cym)]Cl at (293K) in (a) chloroform-*d* and (b) acetonitrile-d_3 solutions

It seems that, in chloroform-*d* solution, the difference in chemical shift between the diastereotopic protons is small enough to cause an overlap of the signals giving rise to what appears to be a 8-line signal representing *both* protons [Fig. 5-41(a)]. In acetonitrile-d_3 a quartet, in which there appears to be some additional splitting, is observed [Fig. 5-41(b)]. This suggests that the difference in chemical shift between the diastereotopic protons is less in acetonitrile-d_3 than in chloroform-*d*.

In summary, it seems that in chloroform-*d* and acetonitrile-d_3 the chemical shift of each of the methylene protons is slightly different whereas in tetrachloroethane-d_2, and DMSO-d_6 the chemical shift of the diastereotopic protons happens to coincide. This observation is especially surprising given the similarity of chloroform-*d* and tetrachloroethane-d_2 however the result is reproduced when the chloride counter ion is exchanged for PF_6^- and the spectra of **34** in chloroform-*d* and tetrachloroethane-d_2 display a similar set of results (Fig. 5-42).

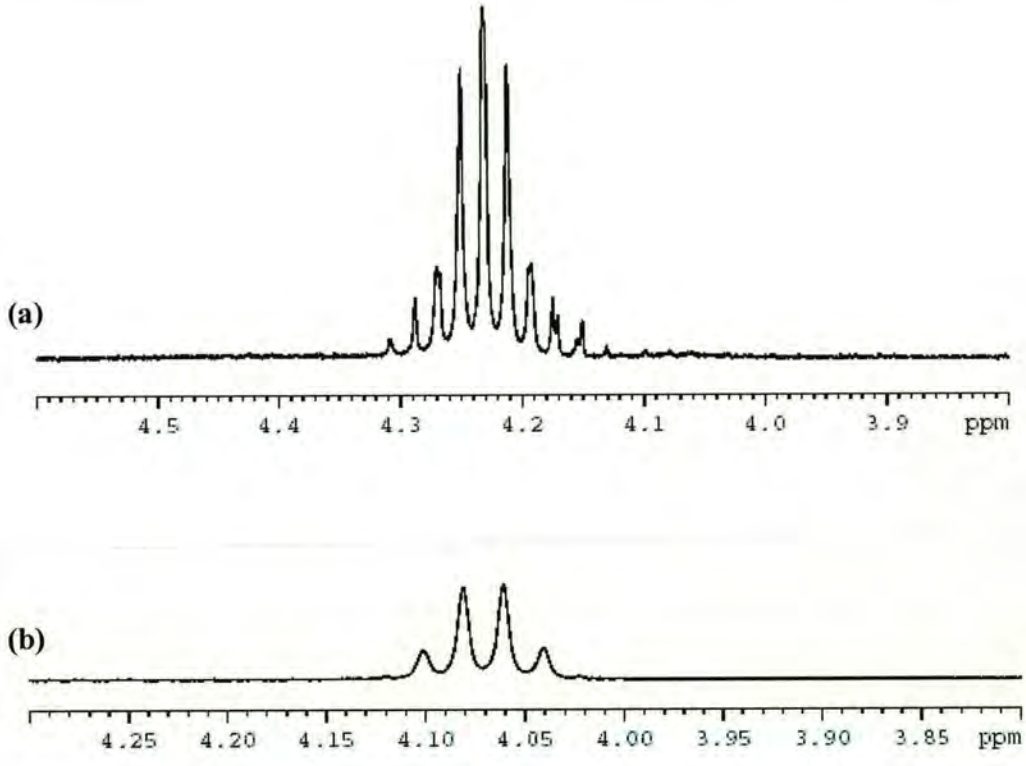

Figure 5-42 Methylene signals of [RuTm^{Et}(*p*-cym)]PF_6 in (a) chloroform-*d* and (b) tetrachloroethane-d_2 solutions

As the signals of **33** and **34** in chloroform-*d* would need a significant increase in temperature to cause coalescence the energy barriers to racemisation can only be said to be significantly greater than 76 and 79 kJ mol^{-1} respectively. However if we take the values in tetrachloroethane [Fig. 5-42(b)] and allow the value of Δv to approach zero we obtain an interesting result (Scheme 5-4).

$$\Delta G = R\,T_c\,[\,22.96 + \ln(T_c / \Delta v)\,] \qquad \textbf{(Eqn. 5-2)}$$

$\Delta G^{\ddagger}$: Free Enthalpy of Activation (kJ mol^{-1})

R: Universal Gas Constant, 8.314 J K^{-1} mol^{-1}

T_c: Coalescence Temperature (K)

Δv: Separation between signals in the absence of exchange (Hz)

For [RuTm^{Et}(*p*-cym)]PF_6 in tetrachloroethane-d_2:

$$T_c = >373 \text{ K}$$

$$\Delta v \rightarrow 0 \text{ Hz}$$

$$\Delta G = R\,T_c\,[\,22.96 + \ln(T_c / \Delta v)\,]$$

(a) $\Delta v = 0.5$ Hz

$$\Delta G_{>373} = 8.314\,(373)\,[\,22.96 + \ln(373 / 0.5)\,]$$

$$\Delta G_{>373} = >92 \text{ kJ mol}^{-1}$$

(b) $\Delta v = 0.1$ Hz

$$\Delta G_{>373} = 8.314\,(373)\,[\,22.96 + \ln(373 / 0.1)\,]$$

$$\Delta G_{>373} = >97 \text{ kJ mol}^{-1}$$

Scheme 5-4

It is clear that as the value of Δv approaches zero i.e. the diastereotopic signals coincide, the value for the activation energy of the ruthenium complex, **34** becomes significantly larger than for any other complex studied so far. In the examples taken in Scheme 5-4 a value of 0.5 Hz for Δv gives an activation energy of greater than 92 kJ mol^{-1} and a value of 0.1 Hz for Δv gives an activation energy of greater than 97 kJ mol^{-1}. This gives a good indication that, as previously mentioned, the energy barrier to racemisation in octahedral complexes with inert metal centers is considerably higher than for tetrahedral complexes and that the energy barrier to the non-dissociative "twist"mechanism of racemisation is high.

[RuTm^{Et}Cp] (35)

The NMR spectra of **35** are quite weak due to the low solubility of the complex (Fig. 5-43). The sample degraded at high temperatures over long periods and therefore a significant amount of change is observed in the spectra. The room temperature spectrum recorded after the series of VT spectra were obtained was significantly different from that obtained initially. It seems, however, that no significant broadening of the signals occurs up to the highest accessible temperature for the instrument (373 K). The geminal and vicinal couplings are 14.3 and 7.2 Hz respectively. The activation energy cannot be determined however it was noted that it is substantially greater than 77 kJmol^{-1}.

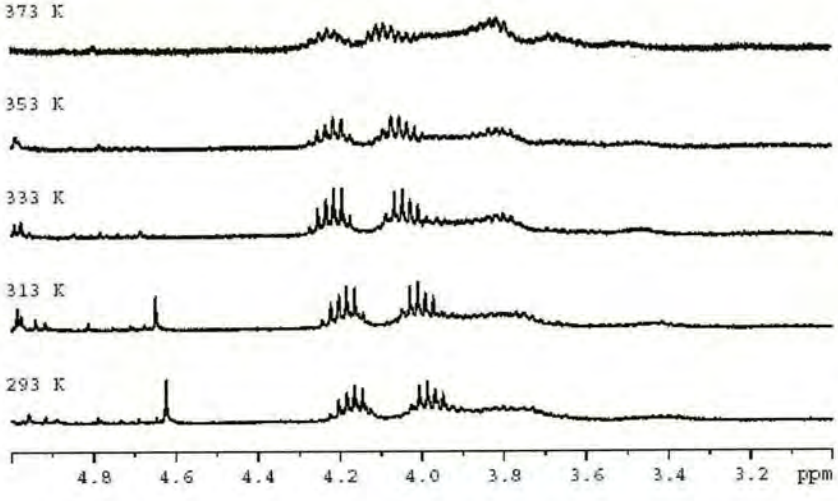

Figure 5-43 Methylene signals in VT NMR of [RuTm^{Et}Cp] in tetrachloroethane-d_2 solution

5.2.5 Group 14: Tin

[SnTm^{Et}Cl$_3$] (36)

The tin complex, **36** has low solubility and the VT NMR experiments were therefore carried out in DMSO-d_6. The spectrum obtained, which appears to be a 10-line signal representing *both* protons (Fig. 5-44), suggests that a combination of two factors, the difference in chemical shift of the diastereomeric protons and the values of geminal and vicinal coupling, lead to overlap of the lines in the predicted 16-line signal.

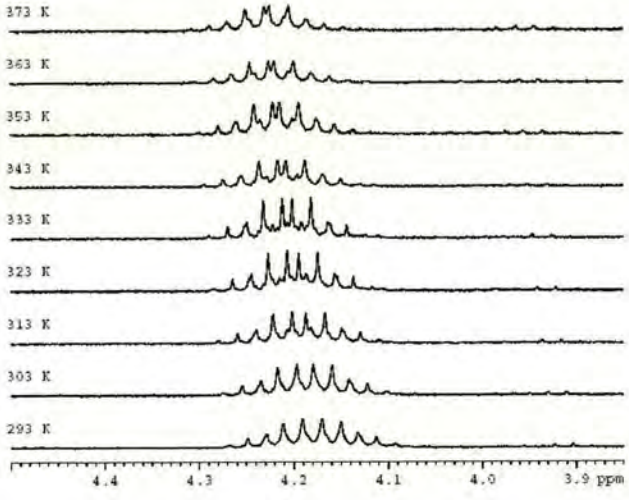

Figure 5-44 Methylene signals in VT NMR of [SnTm^{Et}Cl$_3$] in DMSO-d_6 solution

Although the signals seem to be converging slightly there is no sign that any significant broadening is occurring. Calculations for the activation energy provide a value of greater than 80 kJ mol^{-1} but the spectrum suggests that the energy barrier to racemisation is very significantly higher than this.

5.3 *Ab initio* Calculations

Ab initio calculations were conducted in collaboration with Dr. Andy Turner at The University of Edinburgh. *Ab initio* MO geometry optimisations [MP2[138] (method) / LanL2DZ[139, 140] (basis set)] using the Gaussian 98 suite of quantum chemistry programs[141] were carried out on the ground and transition state structures of tetrahedral zinc and octahedral manganese and rhenium centred C_3-symmetric complexes undergoing non-dissociative racemisation. The geometries were optimised at the MP2 level for the structures. The C_3-symmetric state was assigned as the ground state structure whilst the transition state was taken as the achiral, C_{3v} symmetric intermediate structure. From these calculations the energy difference between the ground state and transition state structures was established.

Zinc Centred Structure

Ab initio calculations were performed on the model system $[HB(C_3H_3N_2S)_3ZnCl]$ (Fig. 5-45), a simplified structure analogous to [ZnTmCl]. The theory that tetrahedral zinc complexes undergo dissociative racemisation is supported by the comparisons between the results of the calculated and experimental results. As discussed in Section 5.1.1 the non-dissociative mechanism would be expected to provide a higher energy barrier to racemisation than the dissociative mechanism in labile tetrahedral complexes. The calculated energy difference between the ground and transition state structures of the C_3-symmetric complex undergoing non-dissociative racemisation is 121 kJ mol^{-1}. This value is significantly higher than the experimental values for the energy barrier to

racemisation in [ZnTm^{Et}Cl] and [ZnTm^{Bn}Cl] (Section 5.2.5) in which a dissociative mechanism is thought to be taking place.

(a) Ground state structure of [HB($C_3H_3N_2S$)$_3$ZnCl] viewed perpendicular to and along the B-Zn axis

(b) Transition structure of [HB($C_3H_3N_2S$)$_3$ZnCl] viewed perpendicular to and along the B-Zn axis

Figure 5-45 *Ab initio* calculations of [HB($C_3H_3N_2S$)$_3$ZnCl]

Manganese Centred Structure

Ab initio calculations were performed on the model system $[HB(C_3H_3N_2S)_3Mn(CO)_3]$ (Fig. 5-46), a simplified structure analogous to $[MnTm(CO)_3]$. The calculated energy difference between the ground and transition state structures of the C_3-symmetric complex undergoing non-dissociative racemisation is 164 kJ mol^{-1}.

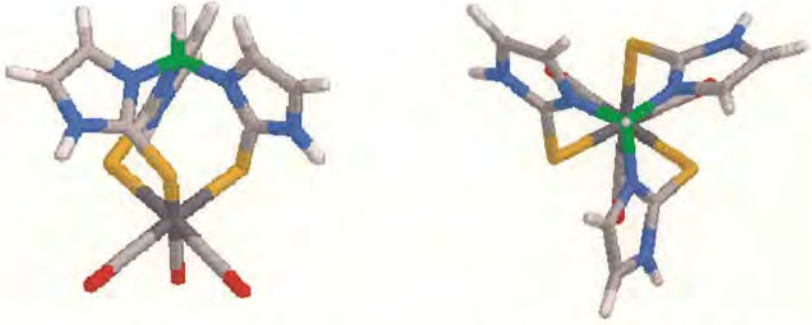

(a) Ground state structure of $[HB(C_3H_3N_2S)_3Mn(CO)_3]$ viewed perpendicular to and along the B-Mn axis

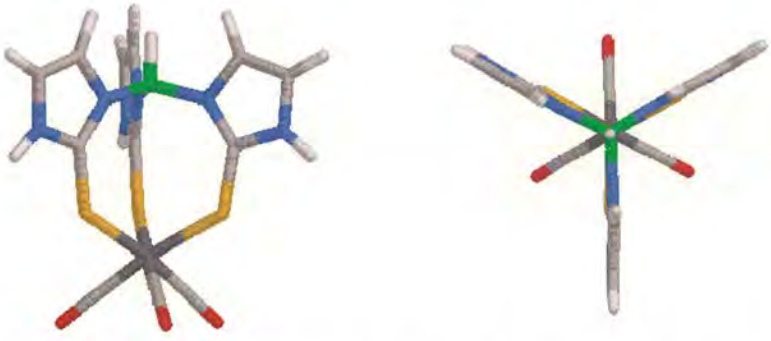

(b) Transition state structure of $[HB(C_3H_3N_2S)_3Mn(CO)_3]$ viewed perpendicular to and along the B-Mn axis

Figure 5-46 Ab initio calculations of $[HB(C_3H_3N_2S)_3Mn(CO)_3]$

As described in Section 5.1.1, for a non-dissociative mechanism it was expected that the energy barrier to racemisation would be higher in octahedral than in tetrahedral complexes due to the difference in angles around the metal ion. This is illustrated by comparison of the calculated energy values for $[HB(C_3H_3N_2S)_3ZnCl]$ and $[HB(C_3H_3N_2S)_3Mn(CO)_3]$, where the energy difference in the manganese centred structure is significantly larger than that in the zinc centred structure. Unfortunately it is not particularly useful to compare the results of *ab initio* calculations on the manganese centred structure with experimental values as the energy barrier to racemisation in $[MnTm^{Et}(CO)_3]$ can only been estimated to be greater than 77 kJ mol^{-1} although the experimental result is at least quantitively consistent with the calculated value.

Rhenium Centred Structure

Ab initio calculations were performed on the model system $[HB(C_3H_3N_2S)_3Re(CO)_3]$ (Fig. 5.47), a simplified structure analogous to $[ReTm(CO)_3]$. This system was examined to investigate the possible effect of metal size on the activation barrier. The calculated energy difference between the ground and transition state structures of the C_3-symmetric complex undergoing non-dissociative racemisation is 160 kJ mol^{-1}. As in the case of the manganese centred structure, comparison of the calculated energy values for $[HB(C_3H_3N_2S)_3ZnCl]$ and $[HB(C_3H_3N_2S)_3Re(CO)_3]$ reveal that the energy difference in the rhenium centred structure is significantly larger than that in the zinc centred structure. Comparison of the energy differences in $[HB(C_3H_3N_2S)_3Mn(CO)_3]$ and $[HB(C_3H_3N_2S)_3Re(CO)_3]$ is also useful as the it confirms the theory that the energy barrier to racemisation is lower for larger metals undergoing a non-dissociative

mechanism. This can be explained by the assumption that the larger rhenium ion has the effect of reducing the torsion in the molecule* thereby providing an equilibrium structure which is nearer to the C_{3v}-symmetric transition state than the corresponding manganese complex. In this case the effect is a relatively minor one.

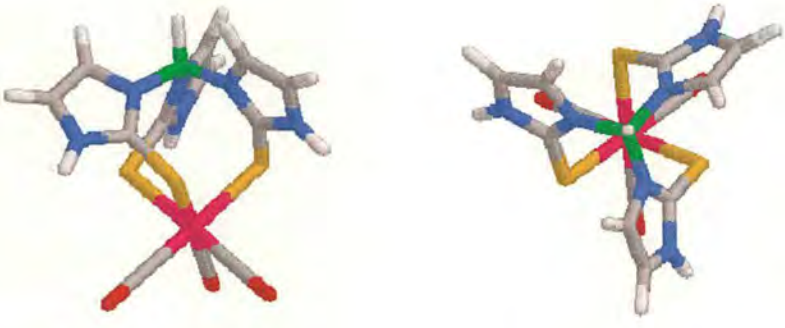

(a) Ground state structure of $[HB(C_3H_3N_2S)_3Re(CO)_3]$ viewed perpendicular to and along the B-Mn axis

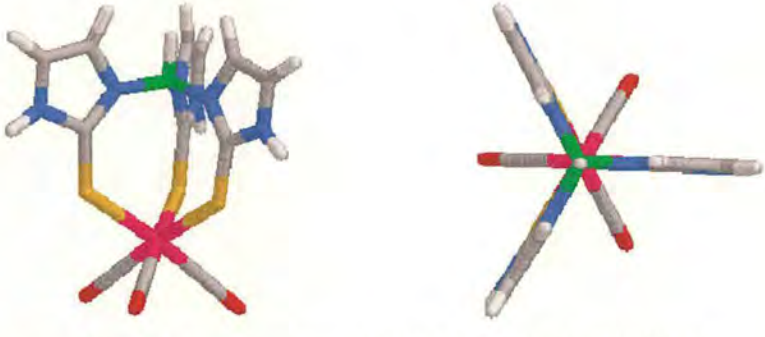

(b) Transition state structure of $[HB(C_3H_3N_2S)_3Re(CO)_3]$ viewed perpendicular to and along the B-Mn axis

Figure 5-47 Ab initio calculations of $[HB(C_3H_3N_2S)_3Re(CO)_3]$

* Appendix 3

5.4 Torsion Angles

It was postulated that in octahedral complexes of Tm^R (R = Et, Bn), a S-M-S angle of 90° would cause the geometry of the complex to be farther from the C_{3v}-symmetric transition state than in a tetrahedral complex where the angle is 109.5° and thus the energy barrier to racemisation *via* the non-dissociative twist mechanism would be higher in octahedral than in tetrahedral complexes. To investigate this theory the torsion angles of the molecular structures detailed in Chapter 4 were measured (Table 5-1). Both the previously described method introduced by Hill *et al.* and our own method, adapted from the work of Hill (Appendix 3) have been used in the measurements.

Table 5-1 Summary of torsion angles in experimental and calculated structures

Complex	θ^m (°)	ω'^m (°)	Model Structure	θ^m (°)	ω'^m (°)
[ZnTm^{Et}Cl]	46.31	-33.90			
[CdTm^{Et}Br]	-46.91	37.52			
[CdTm^{Bn}Br]	-46.59	40.34	Zn	48.27	-33.75
[CdTmBr]	46.84	39.95			
[CuTm^{Et}PPh$_3$]	47.23	-32.12			
[RuTm(*p*-cym)]Cl	45.14	-32.00			
[RuTm^{Et}(*p*-cym)]Cl	-45.51	28.90			
[MnTm(CO)$_3$] (1)	-41.40	29.16			
[MnTm(CO)$_3$] (2)	-46.89	29.19	Mn	-49.58	28.51
[RuTmCp] (1)	-48.40	32.61			
[RuTmCp] (2)	-45.99	28.42			
			Re	-49.73	30.97

θ^m: Mean N-B-M-S torsional angle

ω'^m: Mean C-N-B-M torsional angle

Numbers in brackets denote molecules in unit cell

The results in Table 5-1 are very surprising considering the difference in angle size between octahedral and tetrahedral complexes nevertheless, no trend in the torsion angles is apparent from these data. Not only do the angles vary from complex to complex regardless of metal geometry, but also may be significantly different in molecules occurring the in same unit cell as can be seen in both [$MnTm(CO)_3$] and [RuTmCp]. It seems, therefore, that the structure of the bicyclic cage contained in these complexes is quite flexible and that the geometry at the metal centre does not have a significant influence on the torsion as originally expected.

5.5 Conclusions

The results of variable temperature NMR experiments on complexes of the Tm^{Et} and Tm^{Bn} ligands are summarised in Table 5-2. The results of *ab initio* calculations on model complexes are given in Table 5-3.

Table 5-2 Summary of VT NMR results

Solvent / Complex	Non-Coordinating	Acetonitrile-d_3	DMSO-d_6
[ZnTm^{Et}Cl]	>77[a]	>72	56-60
[CdTm^{Et}Br]	77[a]	69	<61
[HgTm^{Et}Cl]	63-66[a]	52-57	57-61
[ZnTm^{Bn}Cl]	>77[a]		58-63
[CdTm^{Bn}Br]	>78[a]		63-68
[HgTm^{Bn}Cl]	Undetermined[a]		Undetermined
[CuTm^{Et}PPh$_3$]	55[b]	54	
[AgTm^{Et}PPh$_3$]	53[b]	45-50	
[AuTm^{Et}PPh$_3$]	n/a	n/a	
[MnTm^{Et}(CO)$_3$]	>>77[a]	Insoluble	>>78
[RuTm^{Et}(*p*-cym)]$^+$	>>97[a], (>>79[b])		
[RuTm^{Et}Cp]	>>77[a]		
[SnTm^{Et}Cl$_3$]	Insoluble	Insoluble	>>80

Superscripts denote non-coordinating solvent employed:
a: tetrachloroethane-d_2, b: chloroform-*d*;
n/a: not applicable;
Shaded areas represent unattempted experiments

Table 5-3 Summary of calculated results

Model Compound	Calculated Energy ($kJ\ mol^{-1}$)
$[HB(C_3H_3N_2S)_3ZnCl]$	121
$[HB(C_3H_3N_2S)_3Mn(CO)_3]$	164
$[HB(C_3H_3N_2S)_3Re(CO)_3]$	160

The Group 12 complexes display similar trends whereby in a non-coordinating solvent, the energy barrier to racemisation decreases with increasing size of the metal centre. A study of comparative bond dissociation energies of Zn-S, Cd-S and Hg-S would have proven extremely useful throughout the course of these investigations, allowing us to comment on the relative lability of the metal centres, however extensive searches of the literature proved unsuccessful. The presence of a coordinating solvent lowers the activation energy in all cases however the differences in activation energy of the complexes in different donating solvents were dependaent on the relationship between the donor properties of the coordinating solvent and the metal ion itself. It was concluded that the tetrahedral C_3-symmetric zinc and cadmium complexes were more than likely undergoing a dissociative mechanism of racemisation however a linear geometry was postulated for the mercury complex.

The effect of substitution of the N(1)-position on the ligand was investigated with the use of the Tm^{Bn} ligand. The results in non-coordinating solvents were inconclusive as the coalescence temperatures of the zinc and cadmium complexes were beyond the highest accessible temperature of the spectrometer. Results from experiments in a

coordinating solvent (DMSO-d_6), however, show that there is very little difference in the energy barrier to racemisation for the zinc and cadmium complexes compared with their ethyl substituted counterparts. This was unsurprising considering the comparison between the molecular structures of [ZnTm^{Et}Cl] (**23**) and [ZnTm^{Bn}Br] (**26**) and [CdTm^{Et}Br] (**24**) and [CdTm^{Bn}Br] (**27**). From the crystal structures it is clear that the N(1)-substituent points away from the helical backbone and the torsion angles in the complexes are found to be similar. Therefore, a significant change in the energy barrier to racemisation would not be expected.

The results from Group 11 complexes of Tm^{Et} were not as straightforward as their Group 12 counterparts. For the copper complex [CuTm^{Et}PPh$_3$] (**29**) the spectra appeared straightforward although the activation energy for racemisation of the complex was significantly lower than those for the Group 12 complexes investigated. It is postulated that the lower energy is due to a weaker Cu-S bond compared to Zn- and Cd-S bonds. As previously mentioned, however, a lack of literature data on relative metal-sulphur bond strengths prevented full understanding of the observed energy differences. The silver complex [AgTm^{Et}PPh$_3$] (**30**) displayed an unusual set of spectra and it was postulated that, in solution, two species are present giving rise to two separate sets of signals. The suggested species were a two-coordinate, linear complex and a four-coordinate, tetrahedral complex. The energy barrier to racemisation for the four-coordinate complex was found to be similar to that of the previously described copper complex. As expected the gold(I) complex [AuTm^{Et}PPh$_3$] (**31**) was shown to be linear and therefore the calculation of an activation energy was irrelevant.

The results of the experiments with tetrahedral complexes lead to the conclusion that a relatively low energy, dissociative mechanism occurs whereby dissociation of one of the tripod donor arms allows the inversion of the 8-membered ring containing the metal and recoordination of the tripod donor arm provides the enantiomeric system (Section 5.1.1). Given the postulated low energy of the conformational change occurring in the tetrahedral complexes following initial metal-sulphur bond cleavage the energy of the dissociative mechanism is likely to be closely correlated with the metal-sulphur bond energy, as metal-sulphur bond cleavage would be the rate determining step in the process. In the d^{10} metal ions of Group 12 which have zero ligand field stabilisation energy (LFSE) the activation energy has been shown to follow a correlation with metal ion size (the smaller Zn gives a higher energy process than the larger Cd and Hg) as would be predicted. *Ab initio* calculations on a tetrahedral complex undergoing non-dissociative racemisation give a significantly higher value for the energy barrier to racemisation than the values obtained form VT NMR thereby supporting the conclusion that a dissociative mechanism is taking place.

The investigation of octahedral complexes proved difficult as the temperatures needed for coalescence to occur seemed to be a great deal beyond the highest accessible temperature of the spectrometer. The spectra of $[MnTm^{Et}(CO)_3]$ (**32**) were recorded in tetrachloroethane-d_2 and DMSO-d_6 and no significant broadening was observed. A similar result was obtained for $[SnTm^{Et}Cl_3]$ (**36**) in DMSO-d_6. Both of these results suggest that the energy barrier to racemisation is significantly higher for octahedral than tetrahedral complexes. Although $[RuTm^{Et}(p\text{-cym})]^+$ (**33/34**) displayed unusual spectra

the activation energy found for the complex corroborated the theory that the energy barrier to racemisation for octahedral complexes is higher than for tetrahedral complexes.

In summary, no evidence of the occurrence of racemisation was found for the octahedral complexes studied so far. Even under the assumption that racemisation *is* occurring, it is not clear whether it is *via* a dissociative or a non-dissociative mechanism. If we consider octahedral metal complexes undergoing a dissociative mechanism, the low energy of Berry pseudorotation indicates that the energy barrier to racemisation will be dependant on the metal-sulphur bond energy. The energy of metal-sulphur bond cleavage will in turn be correlated with LFSE which determines the lability/inertness of the metal ion. If on the other hand a non-dissociative mechanism is occurring, the energy will be dependent upon factors which influence the angle strain in the transition state, principally metal size. For metals with a higher LFSE such as the metal centers employed in this study we had expected that the metal-sulphur bond energy would be sufficiently high that the non-dissociative mechanism would be more energetically favourable than the dissociative mechanism. It was also expected that the energy barrier to racemisation would, nonetheless, be relatively high compared to a similar mechanism in tetrahedral complexes due to the difference in angle size around the metal ion (Section 5.1.1). On the other hand, a*b initio* calculations on octahedral complexes undergoing a non-dissociative mechanism suggest that if the dissociation energy of the metal-sulphur bond is less than 160 kJ mol^{-1} the dissociative mechanism is more energetically favourable. Unfortunately, the absence of data associated with metal-

sulphur (thione) bond strengths in the literature prevents further postulation. For metals with a lower LFSE, the dissociative process may be competitive with the non-dissociative one, and the racemisation process may be of sufficiently low energy to be observed by VT NMR. Unfortunately the paramagnetism of such metal ions precludes their study using our NMR technique.

6 EXPERIMENTAL

6.1 General

All reactions were carried out under an atmosphere of dry, oxygen free dinitrogen, using standard Schlenk techniques. Solvents were freshly distilled over an appropriate drying agent* and further degassed before use where necessary. NMR spectra were recorded on a Bruker 250AC spectrometer operating at room temperature. ^{1}H and ^{13}C chemical shifts are reported in ppm relative to $SiMe_4$ ($\delta = 0$) and were referenced internally with respect to the protio solvent impurity and the ^{13}C resonances respectively. Multiplicities and peak types are abbreviated: singlet, s; doublet, d; triplet, t; multiplet, m; broad, br; aromatic, ar. Mass spectra were recorded on a Kratos MS50TC spectrometer (FAB-MS) and a Micromass Platform II (ES-MS). IR spectra were recorded from 4000 to 400 cm^{-1} with a Perkin-Elmer FT-IR instrument. Elemental analyses were performed using a Perkin Elmer 2400 CHN Elemental Analyser.

* Appendix 4

6.2 Synthesis of Starting Materials

Diphenylbenzylphosphine

To a solution of chlorodiphenylphosphine (15.96 g, 72.4 mmol) in THF (50 mL) was added benzyl magnesium chloride (36 mL of 2 M solution, 1 eq.) in THF (50 mL). The solution was stirred for 72 h. The volume of solution was reduced by ½ and H_2O (150 mL) added. The solid was extracted with ether and recrystallised from hot methanol yielding a white solid. Yield: 60%. ^{1}H NMR ($CDCl_3$, δ): 3.60 (d, 2H, CH_2), 7.03-7.66 (m, 15H, ar.). ^{13}C NMR ($CDCl_3$, δ): 50.92 (*C*H_2), 26.96-131.99 (*C*H, ar.). ^{31}P NMR ($CDCl_3$, δ): 31.55.

[MnBr(CO)$_5$]

An adaptation of the literature procedure[112] is described. To a solution of [$Mn_2(CO)_{10}$] (2.00 g, 5.13 mmol) in dichloromethane (50 mL) was added a solution of bromine (0.26 mL, 5.13 mmol) in dichloromethane (20 mL). This solution was added dropwise over 30 min. The solution was stirred for 1 h. and then filtered. Dichloromethane was added to the filtrate to redissolve any precipitated product. Hexane was added (100 mL) and the volume of solution reduced to approx. 30 mL on the rotary evaporator. The solid which precipitated was isolated by filtration, washed with cold pentane (20 mL) and dried under vacuum. Yield 2.13 g, 76%. Analytical data are in agreement with literature values.

$[Mn(CO)_3(MeCN)_3]PF_6$[113]

A solution of $[MnBr(CO)_5]$ (879 mg. 3.20 mmol) in acetonitrile (10 mL) was heated under reflux for 1 h. Upon cooling the solution was filtered and the volume of the filtrate reduced by half. A hot solution of ammonium hexafluorophosphate (527 mg, 3.23 mmol) in an equimolar mixture of water and ethanol (10 mL) was added and the solution left in the freezer overnight. A small amount of product was collected by filtration. The filtrate was treated with water and the resulting crystals collected by filtration. Yield 1.03 g, 79%. Analytical data are in agreement with literature values.

$[Ru(\eta^6\text{-}p\text{-cymene})Cl_2]_2$[114]

To a solution of ruthenium trichloride trihydrate (3.00 g, 14.5 mmol) in ethanol (200 mL) was added α-terpinine (25 mL, 85%). The solution was refluxed for 4 h. Upon cooling the crystals which settled were isolated by filtration, washed with cold methanol (30 mL) and dried under vacuum. The volume of the filtrate was reduced by half and the solution refrigerated at –20 °C overnight. The solid which had formed was isolated as with the first crop. Yield 3.20 g, 72%. Analytical data are in agreement with literature values.

$[Ru(C_6H_6)Cl_2]_2$

To a solution of ruthenium trichloride trihydrate (4.00 g, 19.3 mmol) in ethanol (200 mL) was added 1,4-cyclohexadiene (20 mL, 211.4 mmol). The solution was refluxed for 4 h. Upon cooling a solid settled out which was isolated by cannula

filtration. The solid was washed with methanol (3 x 30 mL) and dried under vacuum. Yield 4.30 g, 91%. Analytical data are in agreement with literature values.

$[Ru(C_6H_6)Cp]PF_6$ [115]

Potassium carbonate (3.90 g, 28.4 mmol) was added to a dry round bottomed flask and dried by heating under vacuum. Upon cooling $[Ru(C_6H_6)Cl_2]_2$ (2.36 g, 4.72 mmol) was added followed by ethanol (100 mL). Freshly cracked cyclopentadiene (7 mL, 84.8 mmol) was added and the mixture was heated to 60 °C for 7 hr. The reaction was cooled to room temperature and filtered through celite. The celite was rinsed with ethanol (50 mL) and the volume of the filtrate reduced to approx. 40 mL. An aqueous solution of ammonium hexafluorophosphate (3.2 g, 19.6 mmol in 32 mL H_2O) was added. The remaining ethanol was removed under vacuum and the suspension left in the refrigerator overnight. The suspension was filtered and the resulting solid dried under vacuum. The solid was dissolved in the minimum amount of acetone and ether added dropwise until the appearance of precipitate ceased. The mixture was left in the refrigerator overnight. The reaction was filtered yielding a cream coloured powder. Yield 2.69 g, 73%. Analytical data are in agreement with literature values.

$[RuCp(MeCN)_3]PF_6$ [115]

A solution of $[Ru(C_6H_6)Cp]PF_6$ (1.00 g, 2.57 mmol) in dry acetonitrile (120 mL) was prepared in a photolysis reactor Schlenk. The solution was degassed by bubbling with dry nitrogen for 30 min. The stirred solution was irradiated with the output of a 150 W

medium pressure Hg lamp for 36 h. The solvent was stripped under vacuum yielding the orange solid. Yield 1.07 g, 96%. Analytical data are in agreement with literature values.

$[RuCl_2Cp]_2$

A mixture of hydrated ruthenium trichloride (500 mg, 2.41 mmol) and freshly cracked cyclopentadiene (500 g, 7.93 mmol) in methanol (30 mL) was refluxed overnight. Upon cooling $[RuCl_2Cp]_2$ was collected by filtration and washed with methanol (3 x 10 mL) and ether (3 x 10 mL) and dried under vacuum. Yield 306 mg, 63%.

$[PPh_3AuCl]$

An adaptation of the literature procedure[129] is described. To a solution of hydrogen tetrachloroaurate (963 mg, 2.45 mmol) in THF (20 mL) was added triphenylphosphine (1.28 g, 4.88 mmol) in one portion. Almost immediately the solution became colourless and after a few seconds a white precipitate formed. The reaction was stirred at room temperature overnight. The solvent was stripped and the pale yellow powder dissolved in dichloromethane (30 mL). The solution was eluted through a silica dry-flash chromatography column with dichloromethane. The fractions were collected and the solvent stripped yielding a white powder. Yield 520 mg, 43 %. ^{1}H NMR ($CDCl_3$, δ): 7.40-7.74 (m, 15H, ar.). ^{13}C NMR ($CDCl_3$, δ): 128.09-134.15 (ar). ^{31}P NMR ($CDCl_3$, δ): 34.84. FAB-MS: 495 [M^+], 459 [M^+– Cl]. *Anal.* Found: C, 43.4; H, 3.1; N, 0.0. Calc. for $C_{18}H_{15}AuClP$: C, 43.7; H, 3.1; N, 0.0 %.

6.3 Ligand and Complex Synthesis

N-(2,2-dimethoxyethyl)-N-phenylurea (1)

An adaptation of the literature method[107] is described. To a solution of aminoacetaldehyde dimethylacetal (10.04 mL, 95.5 mmol) in toluene (25 mL) was added phenyl isocyanate (11.0 mL, 92.4 mmol) over 5 minutes with cooling to 0 °C. The solution was stirred at room temperature for 3 h. The solvent was stripped and the white solid washed with petroleum ether (60-80°). Yield 19.7 g, 95%. ^{1}H NMR ($CDCl_3$, δ): 3.40 (s, 6H, C*H*$_3$), 3.48 (d, 2H, C*H*$_2$), 4.41 (t, 1H, C*H*), 6.40 (s, 1H, N*H*), 6.56 (s, 1H, N*H*), 6.80-7.36 (m, 5H, ar.). ^{13}C NMR ($CDCl_3$, δ): 41.85 (*C*H$_2$), 54.54 (*C*H$_3$), 103.44 (*C*H), 120.52-138.51 (*C*H, ar.), 155.83 (C_{quat}). FAB-MS: 225 [M$^+$]. IR (KBr, cm^{-1}): ν_{C-O} 1650, ν_{N-H} 1560. *Anal.* Found: C, 59.9; H, 7.2; N, 13.6. Calc. for $C_{11}H_{16}N_2O_3$: C, 58.9; H, 7.2; N, 12.5%.

1-phenyl-4-imidazolin-2-one[108] (2)

1 (9.54 g, 42.5 mmol) was dissolved in a mixture of methanol (168 mL) and water (85 mL). A solution of 0.48M HCl (100 mL) was added dropwise over 1 h. After stirring for 72 h at room temperature the reaction was neutralised using 1M NaOH. The solvent was stripped during which the pH was maintained neutral. The solid was extracted with chloroform (4 x 20 mL) and the combined extracts dried over magnesium sulphate. The solvent was removed under vacuum yielding a pale yellow powder. Yield 6.36 g, 94%. ^{1}H NMR ($CDCl_3$, δ): 6.43 (t, 1H, 4- or 5-C*H*), 6.53 (t, 1H, 4- or 5-C*H*), 7.25-7.59 (m, 5H, ar) 10.97 (s, 1H, N*H*). ^{13}C NMR ($CDCl_3$, δ): 109.57 (4 or 5-*C*H), 110.95 (4- or

5-*C*H), 122.29-136.81 (*C*H, ar.), 153.79 (C_{quat}). FAB-MS: 159 [M^+]. IR (KBr, cm^{-1}): ν_{C-O} 1670, ν_{N-H} 1559. *Anal.* Found: C, 68.2; H, 4.6; N, 19.0. Calc. for $C_9H_8N_2O$: C, 67.9; H, 5.1; N, 17.6%.

General procedure for the Reaction of 2 with sodium borohydride (For specific conditions refer to Table 2-2)

In a typical experiment **2** (3-4 eq.) and sodium borohydride (1 eq.) were finely ground using a pestle and mortar and placed in a dry round-bottomed flask fitted with a volumetric device for the measurement of hydrogen evolution. The temperature was raised until gas evolution ceased or the reaction solidified and darkened considerably.

N'-ethyl-N-(2,2-dimethoxyethyl)urea (3)

An adaptation of the literature procedure for the preparation of N-(2,2-dimethoxyethyl)-N-phenylurea[107] is described. To a solution of aminoacetaldehyde dimethylacetal (14.5 g, 138 mmol) in toluene (25 mL) was added ethyl isocyanate (9.79 g, 138 mmol) over 5 minutes with cooling to 0 °C. The solution was stirred at room temperature for 1 h. The solvent was stripped yielding a yellow liquid. Yield: 21.4 g, 88% ^{1}H NMR ($CDCl_3$; δ): 1.34 (t, 3H, C*H*$_3$), 3.38 (q, 2H, C*H*$_2$), 3.45 (d, 2H, C*H*$_2$), 3.61 (s, 6H, C*H*$_3$), 4.59 (t, 1H, C*H*), 5.83 (m 2H, N*H*). ^{13}C NMR (DMSO, δ): 15.18 (*C*H$_3$), 34.72 (*C*H$_2$), 41.61 (*C*H$_2$), 54.07 (*C*H$_3$), 103.49 (*C*H), 158.69 (*C*O). ES-MS: 176.5 [M^+]. IR ($CHCl_3$, cm^{-1}): ν_{C-O} 1668. *Anal.* Found: C, 45.8; H, 9.2; N, 15.3. Calc. for $C_7H_{16}N_2O_3$: C, 47.7; H, 9.2; N, 15.9%.

1-ethyl-4-imidazolin-2-one[108] **(4)**

3 (10 g, 56.7 mmol) was dissolved in a mixture of methanol (240 mL) and water (115 mL). A solution of 0.48M HCl (135 mL) was added and the solution stirred at room temperature for 24 h. The reaction was neutralised using 1M NaOH. The solvent was stripped during which the pH was maintained neutral. The solid was extracted with chloroform (4 x 20 mL) and the combined extracts dried over magnesium sulphate. The solvent was removed under vacuum yielding a pale yellow powder. Yield 5.15 g, 81%. ^{1}H NMR ($CDCl_3$, δ): 1.43 (t, 3H, C*H*$_3$), 3.81 (q, 2H, C*H*$_2$), 6.33 (d, 1H, 3 or 5-C*H*), 6.44 (d, 1H, 3 or 5-C*H*). ^{13}C NMR ($CDCl_3$, δ): 14.63 (*C*H$_3$), 37.67 (*C*H$_2$), 108.26 (4- or 5-*C*H), 110.33 (4- or 5-*C*H), 154.54 (*C*O). ES-MS: 112.7 [M^+]. IR (KBr, cm^{-1}): ν_{B-H} 2443. IR ($CHCl_3$, cm^{-1}): ν_{C-O} 1678. *Anal.* Found: C, 52.9; H, 7.3; N, 24.2. Calc. for $C_5H_8N_2O$: C, 53.6; H, 7.2; N, 24.9%.

Reaction of 4 with sodium borohydride

A mixture of **4** (1.35 g, 9.95 mmol) and sodium borohydride (380 mg, 10.04 mmol) were finely ground using a pestle and mortar and placed in a dry round bottomed flask fitted with a volumetric device for the measurement of hydrogen evolution. The temperature was raised gradually to 130 °C. The reaction was allowed to cool. NMR and mass spectrometry confirmed only the presence of **4**.

General procedure for the Reaction of 4 with sodium borohydride (For specific conditions refer to Table 2-3)

In a typical experiment **4** (3 eq.) was added to a dry round-bottomed flask containing sodium borohydride (1 eq.). The flask was fitted with a condenser and a volumetric device for measurement of hydrogen evolution. Dry solvent was added and the reaction was refluxed until the evolution of gas had ceased. The reaction mixture was allowed to cool and the solvent was stripped under vacuum. NMR and mass spectrometry confirmed only the presence of the starting material **4**.

Sodium 1-ethyl-4-imidazolin-2-one (5)

A solution of **4** (1.09 g, 9.72 mmol) in methanol (10 mL) was added to a stirred solution of sodium metal (224 g, 9.74 mmol) in methanol (30 mL). After stirring for 2 h. the solution was filtered by cannula and the solvent stripped yielding a yellow solid. Yield 1.18 g, 90% ^{1}H NMR (DMSO, δ): 1.01 (t, 3H, C*H*$_3$), 3.42 (q, 2H, C*H*$_2$), 6.01 (d, 1H, 4- or 5-C*H*), 6.11 (d, 1H, 4- or 5-C*H*).

Reaction of 5 with dichlorophenylborane

To a stirred suspension of **5** (256 mg, 1.91 mmol) in THF (10 mL) was added dichlorophenylborane (1 mL of 0.6775 M solution in hexane). The reaction was stirred at room temperature overnight. The solution was filtered and the solvent stripped. NMR and mass spectrometry confirmed only the presence of sodium 1-ethyl-4-imidazolin-2-one

Tris(1-ethyl-4-imidazolin-2-one)(dimethylamino)borane (6)

To a solution of tris(dimethylamino)borane (0.500 mL, 2.86 mmol) in toluene (40 mL) was added **4** (961 mg, 8.57 mmol) in one portion. The reaction was refluxed overnight. The solvent was stripped under vacuum yielding a pale yellow solid. Yield 900 mg, 80 %. ^{1}H NMR ($CDCl_3$, δ): 1.20 (t, 9H, C*H*$_3$), 2.66 (s, 6H, C*H*$_3$), 3.58 (q, 6H, C*H*$_2$), 6.01 (d, 3H, 4- or 5-C*H*), 6.12 (d, 3H, 4- or 5-C*H*). ^{13}C NMR ($CDCl_3$, δ): 14.60 (*C*H$_3$), 37.54 (*C*H$_3$), 39.67 (*C*H$_2$), 110.46 (4- or 5-*C*H), 112.52 (4- or 5-*C*H), 155.95 (*C*O). ES-MS: 390 [M$^+$]. IR ($CHCl_3$, cm^{-1}): ν_{C-O} 1666. *Anal.* Found: C, 52.2; H, 7.5; N, 23.8. Calc. for $C_{17}H_{28}BN_7O_3$: C, 52.5; H, 7.3; N, 25.1 %.

Attempted synthesis of potassium hydrotris(1-ethyl-4-imidazolin-2-one)borate

To a suspension of **6** (206 mg, 0.529 mmol) in THF at 0 °C was added potassium hydride (21 mg, 0.524 mmol). The reaction was stirred at low temperature for 1 h. Acetyl chloride (0.04 mL, 0.563 mmol) was added and the reaction stirred at room temperature overnight. The solvent was stripped and the residue taken into DCM (30 mL) and washed with water (3 x 10 mL). The organic layer was dried over magnesium sulphate and the solvent stripped in a preweiged Schlenk. Toluene (10 mL) was added followed by potassium hydride (8 mg, 1 eq.) and the reaction was stirred overnight. The solvent was stripped yielding an orange powder. ^{1}H NMR ($CDCl_3$, δ): 1.26 (t, 9H, C*H*$_3$), 3.69 (q, 6H, C*H*$_2$), 5.97 (d, 3H, 4- or 5-C*H*), 6.25 (d, 3H, 4- or 5-C*H*). ^{13}C NMR (CD_3OD, δ): 13.22 (*C*H$_3$), 37.08 (*C*H$_2$), 107.74 (4- or 5-*C*H), 110.82 (4- or 5-*C*H),

153.49 (*C*O). FAB-MS: 367 [M^++Na]. IR ($CHCl_3$, cm^{-1}): ν_{C-O} 1678. *Anal.* Found: C, 45.7; H, 7.0; N, 17.4. Calc. for $C_{15}H_{22}BKN_6O_3$: C, 46.9; H, 5.8; N, 21.9 %.

1-ethyl-4-acetyl-4-imidazolin-2-one (7)

To a suspension of **4** (300 mg, 2.68 mmol) in THF (40 mL) at 0 °C was added potassium hydride (107 mg, 2.67 mmol) in one portion. The reaction was stirred at low temperature for 1 h. Acetyl chloride (0.19 mL, 1 eq.) was added and the reaction was stirred at room temperature overnight. The solvent was stripped and the residue taken into dichloromethane (20 mL) and washed with water (2 x 10 mL). The dichloromethane solution was dried over magnesium sulphate and the solvent stripped under vacuum. The colourless crystals, which sublimed on the sides of the Schlenk tube during drying under vacuum, were recovered and analysed and found to be 1-ethyl-4-acetyl-4-imidazolin-2-one. ^{1}H NMR ($CDCl_3$, δ): 1.53 (t, 3H, C*H*$_3$), 2.87 (s, 3H, C*H*$_3$), 3.87 (q, 2H, C*H*$_2$), 6.52 (d, 1H, 2-C*H*), 7.17 (d, 1H, 3-C*H*). ^{13}C NMR ($CDCl_3$, δ): 15.30 (*C*H$_3$), 24.92 (*C*H$_3$), 39.37 (*C*H$_2$), 107.31 (4-*C*H), 114.35 (5-*C*H), 152.15 (*C*O$_{imidazole}$), 169.62 (*C*O$_{acetyl}$). ES-MS: 154 [M^+], 177 [M^++Na]. *Anal.* Found: C, 54.5; H, 6.5; N, 17.9. Calc. for $C_7H_{10}N_2O_2$: C, 54.5; H, 6.5; N, 18.2 %.

Hydrogen dihydrobis(2-methylimidazolyl)borate (8)

A mixture of 2-methylimidazole (619 mg, 7.54 mmol) and sodium borohydride (95 mg, 2.51 mmol) in toluene (30 mL) was refluxed for 3 d. The solvent was decanted and the solid washed with toluene (2 x 10 mL) and dried under vacuum. Chloroform (30 mL)

was added and the mixture was refluxed for 2 h. The chloroform was decanted and the solid dried under vacuum yielding a white powder. Yield 437 mg, 99%. ^{1}H NMR (CD_3OD, δ): 2.17 (s, 6H, CH_3), 6.61 (d, 4H, 4- or 5-C*H*), 6.64 (d, 4H, 4- or 5-C*H*). ^{13}C NMR (DMSO, δ): 14.36 (CH_3), 123.00 (4- or 5-*C*H), 124.41 (4- or 5-*C*H), 146.31 (C_{quat}). ES-MS: 176 [M^+].

Reaction of 2-methylimidazole with sodium borohydride in DMF

An adaptation of the reported literature method[142] is described. 2-methylimidazole (1.00 g, 12.2 mmol) and finely ground sodium borohydride (149 mg, 3.94 mmol) were added to a dry Schlenk connected to a volumetric device for the measurement of hydrogen evolution. DMF (25 mL) was added and the reaction was heated to reflux. The reaction was refluxed for 24 h. The reaction was cooled and distilled to remove DMF. Analysis by NMR and mass spectrometry confirmed only the presence of **8**.

Reaction of 2-methylimidazole with sodium borohydride

2-methylimidazole (352 mg, 4.29 mmol) and finely ground sodium borohydride (52 mg, 1.37 mmol) were added to a dry Schlenk tube. The reaction was heated slowly to 160 °C. Upon cooling the crude product was transferred to a sublimation apparatus and heated to remove excess starting material. Analysis by ^{1}H NMR and mass spectrometry showed the product to be **8**.

General procedure for the Reaction of 2-methylimidazole with sodium borohydride in solution (For specific conditions refer to Table 2-4)

In a typical experiment 2-methylimidazole (3 eq.) and sodium borohydride were placed in a dry round-bottomed flask fitted with a volumetric device for the measurement of hydrogen evolution. Dry solvent was added and the reaction was refluxed. NMR and mass spectrometry confirmed only the presence of **8**.

Deprotonation of 8

To a suspension of hydrogen dihydrobis(2-methylimidazolyl)borate (231 mg, 1.31 mmol) in THF (10 mL) at 0°C was added NaH (33 mg, 1.32 mmol). A colour change of white to pale cream was noted and the evolution of gas observed. The reaction was stirred at reduced temperature for 30 min. and the solvent stripped yielding a cream coloured solid. Yield 229 mg, 99%. ^{1}H NMR (CD_3OD, δ): 2.19 (s, 6H, CH_3), 6.67 (d, 4H, 4- or 5-C*H*), 6.73 (d, 4H, 4- or 5-C*H*). ES-MS: 175 [M^+].

Attempted Synthesis of Sodium Hydrotris(2-methylimidazolyl)borate

To a suspension of **8** (231 mg, 1.31 mmol) in THF (10 mL) at 0 °C was added sodium hydride (33 mg, 1;32 mmol) in one portion. The reaction was stirred at low temperature for 30 min. The solvent was stripped and toluene (15 mL) was added followed by 2-methylimidazole (108 mg, 1.32 mmol) and the reaction was refluxed overnight. The resulting solid was filtered however NMR and mass spectrometry confirmed only the presence of starting material.

General procedure for the Reaction of 2-methylimidazole with tris(dimethylamino)borane in solution (For specific conditions refer to Table 2-5)

In a typical experiment 2-methylimidazole was added in one portion to a solution of tris(dimethylamino)borane. The solution was refluxed overnight. The reaction was allowed to cool and the solvent was stripped under vacuum. NMR and mass spectrometry confirmed only the presence of hydrogen tetrakis(2-methylimidazolyl)borate (**9**) in the case of benzene and toluene and 2-methylimidazole in the case of the room temperature reaction in THF.

Hydrogen tetrakis(2-methylimidazolyl)borate (9)

To a stirred suspension of 2-methylimidazole (403 mg, 4.91 mmol) in toluene (20 mL) was added tris(dimethylamino)borane (0.125 mL, 1.23 mmol). The reaction was refluxed overnight. The solvent was stripped under vacuum yielding a white solid. Yield 369 mg, 89%. ^{1}H NMR (CD_3OD, δ): 1.99 (s, 12H, C*H*$_3$), 6.92 (d, 4H, 4- or 5-C*H*), 7.23 (d, 4H, 4- or 5-C*H*). ^{13}C NMR (CD_3OD, δ): 12.45 (*C*H$_3$), 121.88 (4- or 5-*C*H), 124.25 (4- or 5-*C*H), 147.53 (C_{quat}). ES-MS: 335 [M^+– H]. *Anal.* Found: C, 55.1; H, 6.4; N, 31.9. Calc. for $C_{16}H_{21}BN_8$: C, 57.2; H, 6.0; N, 25.0%.

(L)-(-)-α-methylbenzylaminoacetaldehyde diethyl acetal (10)

An adaptation of the literature method for the preparation of *tert*-butylaminoacetaldehyde diethyl acetal[111] is described. To a solution of (L)-(-)-α-methylbenzylamine (25 mL, 193.9 mmol) in toluene (20 mL) was added

bromoacetaldehyde diethyl acetal (9.72 mL, 64.64 mmol) slowly to avoid heating. The solution was refluxed for 48 h. The solvent was stripped under vacuum and the excess amine removed by distillation yielding a brown oil. Yield 13.8 g, 90%. ^{1}H NMR ($CDCl_3$, δ): 1.46 (t, 6H, C*H*$_3$), 2.09 (d, 3H, C*H*$_3$), 3.10 (d, 2H, C*H*$_2$), 3.88 (q, 4H, C*H*$_2$), 4.77, (q, 1H, C*H*), 5.33 (t, 1H, C*H*), 7.11-7.86 (m, 5H, ar.). ^{13}C NMR ($CDCl_3$, δ): 15.13 (*C*H$_3$), 46.38 (*C*H$_3$), 52.04 (*C*H$_2$), 59.00 (*CH*), 63.18 (*C*H$_2$), 98.36 (*C*H), 127.09-137.25 (*C*H, ar.). EI-MS: 238 [M$^+$].

2-mercapto-1-((L)-(-)-α-methylbenzyl)imidazole (11)

An adaptation of the literature method for the preparation of 1-substituted-2-mercaptoimidazoles[106] is described. To a solution of **10** (31.19 g, 131.4 mmol) in ethanol (50 mL) was added potassium isocyanate (12.77 g, 131.4 mmol) and 2M HCl (65.70 mL, 131.4 mmol). The solution was heated to 100 °C overnight. The solvent was stripped under vacuum and the product extracted with hot acetone. The acetone was removed under vacuum and 2M NaOH (75 mL) added to the residue. After washing with ether (2 x 25 mL) the aqueous layer was separated and conc. HCl added slowly until a precipitate had formed. The solution was filtered yielding a cream coloured powder. Yield 4.30 g, 26%. ^{1}H NMR ($CDCl_3$, δ): 1.70 (d, 3H, C*H*$_3$), 6.16 (q, 1H, C*H*), 6.63 (d, 1H, 4- or 5-C*H*), 6.64 (d, 1H, 4- or 5-C*H*), 7.20-7.29 (m, 5H, ar.). ^{13}C NMR ($CDCl_3$, δ): 19.51 (*C*H$_3$), 53.09 (*C*H), 114.69 (4-*C*H), 115.28 (5-*C*H), 126.41-128.27 (*C*H, ar), 141.11 (C_{quat}), 160.40 (*C*S). FAB-MS: 204 [M$^+$]. *Anal.* Found: C, 64.7; H, 5.9; N, 13.2. Calc. for $C_{11}H_{12}N_2S$: C, 64.7; H, 5.9; N, 13.7 %.

Reaction of 11 with sodium borohydride.

Sodium borohydride (46 mg, 1.22 mmol) and **11** (750 mg, 3.67 mmol) were finely ground using a pestle and mortar and placed in a dry round-bottomed flask fitted with a volumetric device for the measurement of hydrogen evolution. The temperature was raised gradually to 155 °C. The reaction was allowed to cool yielding a dark intractable solid shown by NMR and mass spectrometry to contain only starting materials and decomposition products.

Reaction of 11 with potassium borohydride.

Finely ground **11** (200 mg, 0.979 mmol) was added to a round-bottomed Schlenk flask containing potassium borohydride (20 mg, 0.371 mmol). The flask was fitted with a volumetric device for the measurement of hydrogen evolution and the apparatus flushed with nitrogen. The temperature was raised gradually to 160 °C. The reaction was allowed to cool yielding a dark intractable solid shown by NMR and mass spectrometry to contain only starting materials and decomposition products.

General procedure for the Reaction of 11 with borohydride salts in solution (For specific conditions refer to Table 2-6)

In a typical experiment **11** (3 eq.) and the borohydride reagent were placed in a dry round-bottomed flask fitted with a volumetric device for the measurement of hydrogen evolution. Dry solvent was added and the reaction was refluxed. The reaction mixture

was allowed to cool and the solvent stripped under vacuum. NMR and mass spectroscopy confirmed only the presence of **11**.

Sodium hydrotris(methimazolyl)borate (12)

An adaptation of the literature procedure[5] is described. Finely ground 2-mercapto-1-methyl-imidazole (methimazole, 15.05 g, 132 mmol) and sodium borohydride (1.66 g, 44 mmol) were placed in a round-bottom flask with a stirring bar. The flask was fitted with a condenser and a volumetric device for the measurement of hydrogen evolution. The system was flushed with nitrogen. The mixture was heated slowly, began to melt at ~140 °C and vigorous gas evolution was observed. The temperature was raised slowly to 155 °C over 2 h. and the mixture began to darken. The mixture was allowed to cool and soxhlet extracted into chloroform yielding a white powder. Yield 10.9 g, 66%. ^{1}H NMR (CD_3OD, δ): 3.61 (s, 3H, C*H*$_3$), 6.70 (d, 1H, 3 or 5-C*H*), 6.90 (d, 1H, 3 or 5-C*H*). ^{13}C NMR (DMSO, δ): 34.57 (*C*H$_3$), 117.50 (4- or 5-*C*H), 121.61 (4- or 5-*C*H), 164.24 (*C*S). FAB-MS: 374 [M^+], 351 [M^+– Na]. EI-MS: 351 [M^+– Na]. IR (KBr, cm^{-1}): $\nu_{B\text{-}H}$ 2480. *Anal.* Found: C, 29.2; H, 5.3; N, 16.11. Calc. for $C_{12}H_{16}BN_6NaS_3$: C, 38.5; H, 4.3; N, 22.5%.

Synthesis of [MnTm(CO)$_3$] (13)

Reaction of NaTm with [Mn(MeCN)$_3$(CO)$_3$]PF$_6$

To a suspension of $[Mn(MeCN)_3(CO)_3]PF_6$ (600 mg, 1.47 mmol) in ethanol (30 mL) was added a solution of **12** (550 mg, 1.47 mmol) in ethanol (30 mL). The solution was

refluxed for 2 h. A yellow precipitate formed which was filtered off, washed with cold ethanol (3 x 10 mL) and dried under vacuum. Crystals suitable for X-ray diffraction were obtained by slow diffusion of hexane into dichloromethane. Yield 562 mg, 78%. ^{1}H NMR (DMSO; δ): 3.72 (s, 9H, C*H*$_3$), 7.10 (d, 3H, 4- or 5-C*H*), 7.43 (d, 3H, 4- or 5-C*H*). ^{13}C NMR (DMSO, δ): 33.94 (*C*H$_3$), 120.97 (4- or 5-*C*H), 122.95 (4- or 5-*C*H), 158.31 (*C*S). FAB-MS: 491 [M$^+$], 462 [M$^+$– CO], 406 [M$^+$– 3CO]. IR (toluene, cm^{-1}): $\nu_{C\text{-}O}$ 2003, 1905. IR (KBr, cm^{-1}) $\nu_{B\text{-}H}$ 2470. *Anal.* Found: C, 36.1; H, 3.1; N, 16.5. Calc. for $C_{15}H_{16}BMnN_6O_3S_3$: C, 36.8; H, 3.3; N, 17.1%.

Reaction of 12 with [Mn(CO)$_5$Br]

To a solution of [Mn(CO)$_5$Br] (0.200 g, 0.728 mmol) in acetonitrile (30 mL) was added **12** (0.270 g, 0.721 mmol) in one portion. The solution was refluxed for 1 ½ h. The solid which had formed was separated by cannula filtration, dissolved in dichloromethane (3 x 10 mL) and washed with water. The solvent was removed under vacuum yielding a yellow powder. Yield 247 mg, 70%. ^{1}H NMR (DMSO; δ): 3.65 (s, 9H, C*H*$_3$), 7.05 (d, 3H, 4- or 5-C*H*), 7.40 (d, 3H, 4- or 5-C*H*). ^{13}C NMR (DMSO, δ): 35.66 (*C*H$_3$), 122.68 (4- or 5-*C*H), 124.67 (4- or 5-*C*H), 160.01 (*C*S).FAB-MS: 491 [M$^+$]. IR (toluene, cm^{-1}): $\nu_{C\text{-}O}$ 2002, 1905. IR (KBr, cm^{-1}): $\nu_{B\text{-}H}$ 2470. *Anal.* Found: C, 35.2; H, 3.9; N, 14.0. Calc. for $C_{15}H_{16}BMnO_3S_3$: C, 36.8; H, 3.3; N, 17.1%.

[RuTm(*p*-cym)]Cl (14)

To a suspension of $[RuCl_2(p\text{-cym})]_2$ (1.03 g, 1.68 mmol) in ethanol (20 mL) was added a solution of **12** (1.26 g, 3.37 mmol) in ethanol (20 mL). The solution was refluxed for 4 h. Upon cooling the solution was filtered and the solvent removed under vacuum yielding a deep purple solid. Crystals suitable for X-ray diffraction were obtained by slow diffusion of pentane into dichloromethane. Yield 1.90 g, 91%. ^{1}H NMR (DMSO; δ): 1.19 (d, 6H, C*H*$_3$), 2.19 (s, 3H, C*H*$_3$), 2.96 (m, 1H, C*H*), 3.63 (s, 9H, C*H*$_3$), 5.48–5.61 (m, 4H, ar), 7.08 (d, 3H, 4 or 5-C*H*), 7.38 (d, 3H, 4 or 5-C*H*). ^{13}C NMR (DMSO, δ): 33.15 (*C*H$_3$), 44.10 (*C*H$_3$), 44.47 (*C*H$_3$), 95.50 (*C*H), 104.09 (*C*H), 113.16 (4-or 5-*C*H), 117.10 (4- or 5-*C*H), 129.53 (*C*H), 133.44 (C_{quat}), 144.41 (C_{quat}), 163.96 (C_{quat}). FAB-MS: 587 [M$^+$], 552 [M$^+$– Cl]. IR (KBr, cm^{-1}): $\nu_{B\text{-}H}$. 2405. *Anal.* Found: C, 40.0; H, 4.8; N, 12.6. Calc. for $C_{22}H_{30}BClN_6RuS_3.H_2O$: C, 41.3; H, 5.0; N, 13.1%.

[RuTmCp] (15)

[Ru{κ^2-(μ-H)B(mt)$_3$}Cp] (15a)

To a suspension of $[Ru(Cp)(MeCN)_3]PF_6$ (200 mg, 0.461 mmol) in acetonitrile (5 mL) was added a suspension of **12** (170 mg, 0.454 mmol) in acetonitrile (5 mL). The solution was refluxed for 2 h. The reaction was allowed to cool and the solvent was removed under vacuum. The remaining solid was taken into dichloromethane washed with water, and the solvent stripped under vacuum. Yield 211 mg, 90%. ^{1}H NMR (DMSO; δ): 3.53 (s, 3H, C*H*$_3$), 3.79 (s, 6H, C*H*$_3$), 4.85 (s, 5H, Cp), 6.31 (d, 2H, 4 or 5-C*H*), 6.44 (d, 1H, 4 or 5-C*H*), 7.05 (d, 2H, 4 or 5-C*H*) 7.37 (d, 1H, 4 or 5-C*H*). ^{13}C NMR (DMSO, δ): 33.60

(CH_3), 34.60 (CH Cp) 117.92 (CH imidazole), 119.04 (CH, Cp), 120.48 (CH imidazole) 122.59 (CH Cp) 163.76 (C_{quat}). FAB-MS: 518 [M^+]. IR (KBr, cm^{-1}): ν_{B-H} 2113.

[Ru{κ^3-HB(mt)$_3$}Cp] (15b)

To a suspension of $[RuCl_2Cp]_2$ (25 mg, 0.053 mmol) in ethanol (10 mL) was added **12** (39 mg, 0.104 mmol) in one portion. The solution was stirred overnight. The solvent was removed under vacuum, dichloromethane (15 mL) added and the solution filtered. The solvent was stripped yielding a red solid. Crystals suitable for X-ray diffraction were obtained by slow diffusion of pentane into dichloromethane. Yield 41 mg, 76%. ^1H NMR ($CDCl_3$, δ): 1.56 (s, 9H, CH_3), 5.45 (s, 5H, C*H*), 6.85 (d, 3H, 4- or 5-C*H*), 7.07 (d, 3H, 4- or 5-C*H*). ^{13}C NMR ($CDCl_3$, δ): 14.50 (CH_3), 35.21 (CH_2), 86.79 (*C*H), 120.50 (4- or 5-*C*H), 124.37 (4- or 5-*C*H). FAB-MS: 518 [M^+]. IR (KBr, cm^{-1}): ν_{B-H} 2348.

[RuTm(C_6H_5(CO)OEt)]Cl (16)

To a stirred and heating solution of $[RuCl_2(C_6H_5(CO)OEt)]_2$ (695 mg, 1.08 mmol) in acetonitrile (70 mL) was added a suspension of **12** (806 mg, 2.15 mmol) in acetonitrile (30 mL). The deep red solution was refluxed for 1 h. Upon cooling the solution was filtered and the solid taken into water (30 mL) and washed with ether (3 x 20 mL). The solvent was stripped yielding a dark red solid. Yield 1.14 g, 83 %. ^1H NMR ($CDCl_3$, δ): 1.30 (t, 3H, CH_3), 3.65 (s, 9H, CH_3), 4.31 (q, 2H, CH_2), 5.82 (m, 2H,*m*-C*H* ar), 6.03 (m, 1H, *p*-C*H* ar), 6.35 (m, 2H, *o*-C*H* ar), 6.79 (d, 3H, 4- or 5-C*H*), 7.01 (d, 3H, 4- or 5-C*H*).

^{13}C NMR ($CDCl_3$, δ): 14.33 (*C*H_3), 35.12 (*C*H_3), 62.23 (*C*H_2), 82.34-93.07 (*C*H, ar.), 121.36 (4- or 5-*C*H), 123.93 (4- or 5-*C*H), 154.75 (*C*O), 164.75 (*C*S). FAB-MS: 603 [M^+– Cl].]. IR (KBr, cm^{-1}): ν_{B-H} 2438. *Anal.* Found: C, 38.0; H, 4.1; N, 11.9. Calc. for $C_{21}H_{26}BClN_6O_2RuS_3$: C, 39.53; H, 4.1; N, 13.2%.

[CdTmBr] (17)

To a stirred suspension of $CdBr_2.4H_2O$ (50 mg, 0.145 mmol) in dichloromethane (10 mL) was added **12** (54 mg, 0.144 mmol) in one portion. After a few minutes the reactants had dissolved and a white precipitate had formed. The reaction was stirred for 2 h and filtered. Yield 53 mg, 68%. ^{1}H NMR ($CDCl_3$, δ): 3.54 (s, 9H, C*H*$_3$), 6.91 (d, 3H, 4- or 5-C*H*), 7.27 (d, 3H, 4- or 5-C*H*). .FAB-MS: 543 [M^+], 463 [M^+– Br]. IR (KBr, cm^{-1}): ν_{B-H} 2382. *Anal.* Found: C, 26.3; H, 3.0; N, 14.2. Calc. for $C_{12}H_{16}BBrCdN_6S_3$: C, 26.5; H, 3.0; N, 15.4%.

[SnTmCl$_3$] (18)

To a stirred suspension of **12** (0.40 g, 1.07 mmol) in dichloromethane (20 mL) was added $SnCl_4$ (0.125 mL, 1.07 mmol). A yellow precipitate formed immediately. The reaction was stirred for 2h. The solution was filtered yielding a yellow solid. Yield: 438 mg, 71%. ^{1}H NMR ($CDCl_3$, δ): 2.13 (s, 9H, C*H*$_3$), 7.50 (d, 3H, 4- or 5-C*H*), 7.70 (d, 3H, 4- or 5-C*H*). ^{13}C NMR ($CDCl_3$, δ): 36.41 (*C*H_3), 125.39 (4- or 5-*C*H), 127.45 (4- or 5-*C*H) 150.57 (*C*S). IR (KBr, cm^{-1}): ν_{B-H} 2344. *Anal.* Found: C, 23.7; H, 2.7; N, 13.3. Calc. for $C_{12}H_{16}BCl_3N_6S_3Sn$: C, 25.0; H, 2.8; N, 14.6%.

2-Mercapto-1-ethylimidazole (19)

To a stirred solution of aminoacetaldehyde diethylacetal (12 mL, 82.53 mmol) in THF (30 mL) was added ethylisothiocyanate (7.2 mL, 82.21 mmol) slowly to avoid excess heating. The solution was refluxed for 3½ h. The solvent was stripped under vacuum, 10% H_2SO_4 (195 mL) was added and the solution refluxed (100 °C) overnight. The pH was adjusted to neutral and the product was extracted with dichloromethane. The dichloromethane solution was dried over magnesium sulphate and the solvent stripped. The resulting solid was washed with hexane (4 x 20 mL) and recrystallised from hot toluene yielding a pale brown crystalline solid. Yield: 5.90 g, 56%. ^{1}H NMR ($CDCl_3$, δ): 1.55 (t, 3H, C*H*$_3$), 4.28 (q, 2H, C*H*$_2$), 6.90 (d, 1H, 4- or 5-C*H*), 6.92 (d, 1H, 4- or 5-C*H*). ^{13}C NMR ($CDCl_3$, δ): 14.06 (*C*H$_3$), 41.58 (*C*H$_2$), 114.23 (4- or 5-*C*H), 116.87 (4- or 5-*C*H), 158.95 (*C*S). FAB-MS: 129 [M$^+$]. EI-MS: 128.7 [M$^+$]. *Anal.* Found: C, 43.4; H, 6.5; N, 21.5. Calc. for $C_5H_8N_2S$: C, 46.8; H, 6.3; N, 21.9%.

Sodium hydrotris(2-mercapto-1-ethylimidazolyl)borate, NaTm^{Et} (20)

Finely ground $NaBH_4$ (0.44 g, 11.52 mmol) and **19** (5.17 g, 40.33 mmol) were added to a dry round-bottom flask fitted with a volumetric device for measurement of hydrogen evolution. The mixture was heated slowly to 160 °C and the reaction allowed to proceed until the required volume of gas had been produced. After soxhlet extraction into chloroform the volume of the solution was reduced and the product isolated by filtration. Yield: 3.17 g, 66%. ^{1}H NMR (DMSO, δ): 1.24 (t, 9H, C*H*$_3$), 3.99 (q, 6H, C*H*$_2$), 6.44 (d, 3H, 4- or 5-C*H*), 6.88 (d, 3H, 4- or 5-C*H*). ^{13}C NMR ($CDCl_3$, δ): 15.52 (*C*H$_3$), 43.16

(*C*H_2), 117.79 (4- or 5-*C*H), 120.20 (4- or 5-*C*H), 161.97 (*C*S). FAB-MS: 439 [M^++Na], 416 [M^+], 393 [M^+– Na]. EI-MS: 393 [M^+– Na]. IR (KBr, cm^{-1}): ν_{B-H} 2482. *Anal.* Found: C, 40.3; H, 6.9; N, 18.4. Calc. for $C_{15}H_{22}BN_6NaS_3$: C, 43.3; H, 5.3; N, 20.2%.

2-Mercapto-1-benzylimidazole (21)

To a stirred solution of aminoacetaldehyde diethylacetal (1.10 mL, 7.57 mmol) in THF (5 mL) was added benzylisothiocyanate (1.0 mL, 7.54 mmol) slowly to avoid excess heating. The solution was refluxed under N_2 for 3½ h. The solvent was stripped under vacuum, 10% H_2SO_4 (18 mL) was added and the solution refluxed (100 °C) overnight. The pH was adjusted to neutral and the product was extracted into dichloromethane. The dichloromethane solution was dried over magnesium sulphate and the solvent stripped. The resulting solid was washed with hexane (4 x 20 mL) and dried under vacuum. Yield 401 mg, 83%. ^{1}H NMR ($CDCl_3$, δ): 5.31 (s, 2H, C*H*$_2$), 6.65 (d, 1H, 4- or 5-C*H*), 6.79 (d, 1H, 4- or 5-C*H*), 7.35-7.45 (m, 5H, ar). ^{13}C NMR ($CDCl_3$, δ): 50.22 (*C*H_2), 114.47 (4- or 5-*C*H), 117.57 (4- or 5-*C*H), 128.03-135.56 (*C*H, ar), 160.63 (*C*S). FAB-MS: 190 [M^+]. *Anal.* Found: C, 63.2; H, 5.3; N, 14.4. Calc. for $C_{10}H_{10}N_2S$: C, 63.1; H, 5.3; N, 14.7%.

Sodium hydrotris(2-mercapto-1-benzylimidazolyl)borate, $NaTm^{Bn}$ (22)

An adaptation of the literature method[34] is described. A mixture of **21** (2.0 g, 10.51 mmol) and $NaBH_4$ (0.133 g, 3.52 mmol) in toluene (40 mL) was refluxed for 3 days. The volume of the solution was reduced and the product isolated by filtration. Yield 1.51 g, 71%. ^{1}H NMR ($CDCl_3$, δ): 5.21 (s, 6H, C*H*$_2$), 6.07 (d, 3H, 4- or 5-C*H*), 6.50 (d, 3H, 4- or 5-C*H*), 7.06-7.28 (m, 15H, ar). ^{13}C NMR ($CDCl_3$, δ): 50.48 (*C*H_2), 117.45

(4- or 5-*C*H), 119.20 (4- or 5-*C*H), 127.64 (*p*-*C*H), 128.01 (*o*-*C*H), 128.64 (*m*-*C*H), 136.44 (C_{quat}), 162.17 (*C*S). FAB-MS: 603 [M^+]. EI-MS: 580 [M^+– Na] IR (KBr, cm^{-1}): ν_{B-H} 2492. *Anal.* Found: C, 60.2; H, 5.2; N, 13.6. Calc. for $C_{30}H_{29}BN_6NaS_3$: C, 59.8; H, 4.9; N, 13.9%.

[ZnTm^{Et}Cl] (23)

To a stirred suspension of $ZnCl_2$ (34 mg, 0.249 mmol) in dichloromethane (10 mL) was added **20** (105 mg, 0.252 mmol) in one portion. After a few minutes the reactants had dissolved and a white precipitate had formed. The reaction was stirred for 2 h. The solution was filtered and layered with pentane. The crystals which formed were isolated by filtration and dried under vacuum. Crystals suitable for X-ray diffraction were obtained by slow diffusion of pentane into dichloromethane. Yield 75 mg, 61%. ^{1}H NMR ($CDCl_3$, δ): 1.28 (t, 9H, C*H*$_3$), 3.92-4.19 (m, 6H, C*H*$_2$), 6.80-6.83 (2 x d, 2 x 3H, 4- or 5-C*H*). ^{13}C NMR ($CDCl_3$, δ): 15.93 (*C*H$_3$), 43.16 (*C*H$_2$), 119.96 (4- or 5-*C*H), 122.26 (4- or 5-*C*H), 156.77 (*C*S). FAB-MS: 459 [M^+– Cl]. IR (KBr, cm^{-1}): ν_{B-H} 2422. *Anal.* Found: C, 36.5; H, 4.4; N, 16.3. Calc. for $C_{15}H_{22}BClN_6S_3Zn$: C, 36.5; H, 4.5; N, 17.0%.

[CdTm^{Et}Br] (24)

Complex **24** was prepared similarly to **23** by reacting $CdBr_2.4H_2O$ (83 mg, 0.241 mmol) and **20** (100 mg, 0.240 mmol) in dichloromethane (5 mL). The reaction was stirred at room temperature for 4 h. The solution was filtered through celite and the solvent stripped yielding a white solid. Yield 119 mg, 85%. ^{1}H NMR ($CDCl_3$, δ): 1.31 (t, 9H,

C*H*$_3$), 3.94-4.15 (m, 6H, C*H*$_2$), 6.82 (2 x d, br, 2 x 3H, 4- or 5-C*H*). ^{13}C NMR ($C_2D_2Cl_4$, δ): 15.24 (*C*H$_3$), 43.16 (*C*H$_2$), 119.02 (4- or 5-*C*H), 124.67 (4- or 5-*C*H), 154.90 (*C*S). FAB-MS: 585 [M$^+$], 506 [M$^+$– Br]. IR (KBr, cm^{-1}): ν_{B-H} 2406. *Anal.* Found: C, 31.2; H, 3.8; N, 12.6. Calc. for $C_{15}H_{22}BBrCdN_6S_3$: C, 30.8; H, 3.8; N, 14.6%.

[HgTm^{Et}Cl] (25)

Complex **25** was prepared similarly to complex **23** by reacting $HgCl_2$ (55 mg, 0.201 mmol) and **20** (84 mg, 0.202 mmol) in dichloromethane (10 mL). The reaction was stirred at room temperature for 2h. The solution was filtered and the solvent stripped yielding a pale yellow solid. Yield 124 mg, 98%. ^{1}H NMR ($CDCl_3$, δ): 1.27 (t, 9H, C*H*$_3$), 4.04 (m, br, 6H, C*H*$_2$), 6.72 (d, br, 3H, 4- or 5-C*H*), 6.90 (d, br, 3H, 4- or 5-C*H*). ^{13}C NMR ($CDCl_3$, δ): 14.77 (*C*H$_3$), 42.66 (*C*H$_2$), 118.19 (4- or 5-*C*H), 123.91 (4- or 5-*C*H), 155.30 (*C*S). FAB-MS: 629 [M$^+$], 594 [M$^+$– Cl]. IR (KBr, cm^{-1}): ν_{B-H} 2430. *Anal.* Found: C, 27.3; H, 3.1; N, 13.8. Calc. for $C_{15}H_{22}BClHgN_6S_3$: C, 28.6; H, 3.5; N, 13.4%.

[ZnTm^{Bn}Cl] (26)

Complex **26** was prepared similarly to **23** by reacting $ZnCl_2$ (102 mg, 0.748 mmol) and **22** (451 mg, 0.748 mmol) in dichloromethane (30 mL). The reaction was stirred at room temperature for 4 h, filtered through celite and the solvent stripped yielding a white solid. Yield 397 mg, 78%. ^{1}H NMR ($CDCl_3$, δ): 5.06-5.39 (q, 6H, C*H*$_2$), 6.69 (d, 3H, 4- or 5-C*H*), 6.81 (d, 3H, 4- or 5-C*H*), 7.19-7.32 (m, 15H, ar). ^{13}C NMR ($CDCl_3$, δ): 51.02 (*C*H$_2$), 118.95 (4- or 5-*C*H), 124.31 (4- or 5-*C*H), 128.28-128.90 (*C*H, ar), 135.19

(C_{quat}), 157.00 (*C*S). FAB-MS: 645 [M^+– Cl]. IR (KBr, cm^{-1}): ν_{B-H} 2435. *Anal.* Found: C, 53.6; H, 4.1; N, 12.4. Calc. for $C_{30}H_{28}BClN_6S_3Zn$: C, 53.0; H, 4.2; N, 12.4%.

[CdTm^{Bn}Br] (27)

Complex **27** was prepared similarly to complex **24** by reacting $CdBr_2.4H_2O$ (32 mg, 0.093 mmol) and **22** (56 mg, 0.093 mmol) in dichloromethane (5 mL). Yield 70 mg, 97%. ^{1}H NMR ($CDCl_3$, δ): 5.01-5.35 (q, 6H, C*H*$_2$), 6.71 (d, 3H, 4- or 5-C*H*), 6.81 (d, 3H, 4- or 5-C*H*), 7.19-7.33 (m, 15H, ar). ^{13}C NMR ($CDCl_3$, δ): 50.95 (*C*H$_2$), 119.07 (4- or 5-*C*H), 124.18 (4- or 5-*C*H), 128.29-128.92 (*C*H, ar), 135.18 (C_{quat}), 157.20 (*C*S). FAB-MS: 693 [M^+– Br]. IR (KBr, cm^{-1}): ν_{B-H} 2422. *Anal.* Found: C, 45.0; H, 3.5; N, 10.1. Calc. for $C_{30}H_{28}BBrCdN_6S_3$: C, 46.7; H, 3.7; N, 10.9%.

[HgTm^{Bn}Cl] (28)

Complex **28** was prepared similarly to complex **25** by reacting $HgCl_2$ (38 mg, 0.140 mmol) and **22** (84 mg, 0.139 mmol) in dichloromethane (5 mL). Yield 80 mg, 71%. ^{1}H NMR ($CDCl_3$, δ): 5.22 (q, br, 6H, C*H*$_2$), 6.52 (d, 3H, 4- or 5-C*H*), 6.77 (d, 3H, 4- or 5-C*H*), 7.06-7.28 (m, 15H, ar). ^{13}C NMR ($CDCl_3$, δ): 50.70 (*C*H$_2$), 117.78 (4- or 5-*C*H), 123.52 (4- or 5-*C*H), 127.83-128.68 (*C*, ar), 135.78 (C_{quat}), 157.69 (*C*S). FAB-MS: 780 [M^+– Cl]. IR (KBr, cm^{-1}): ν_{B-H} 2367. *Anal.* Found: C, 51.9; H, 4.1; N, 11.9. Calc. for $C_{30}H_{28}BClHgN_6S_3$: C, 44.2; H, 3.5; N, 10.3%.

[CuTm^{Et}PPh$_3$] (29)

To a stirred suspension of CuCl (12 mg, 0.121 mmol) and PPh_3 (63 g, 0.240 mmol) in methanol (5 mL) was added **20** (50 mg, 0.120 mmol) in one portion. The reaction was stirred for 2½ h. The white precipitate was isolated by filtration, washed with ether and dried under vacuum. Crystals suitable for X-ray diffraction were obtained by slow diffusion of diethyl ether into dichloromethane. Yield 60 mg, 70%. ^{1}H NMR ($CDCl_3$, δ): 1.27 (t, 9H, C*H*$_3$), 4.06-4.14 (m, br, 6H, C*H*$_2$), 6.74 (d, 3H, 4- or 5-C*H*), 6.87 (d, 3H, 4- or 5-C*H*). ^{13}C NMR ($CDCl_3$, δ): 15.71 (*C*H$_3$), 42.95 (*C*H$_2$), 117.32 (4- or 5-*C*H), 129.61 (4- or 5-*C*H), 162.10 (*C*S). FAB-MS: 719 [M$^+$], 457 [M$^+$– PPh_3]. IR (KBr, cm^{-1}): $\nu_{B\text{-}H}$ 2375. *Anal.* Found: C, 54.7; H, 5.1; N, 11.0. Calc. for $C_{33}H_{37}BCuN_6PS_3$: C, 55.1; H, 5.2; N, 11.7%.

[AgTm^{Et}PPh$_3$] (30)

To a stirred solution of $AgBF_4$ (50 mg, 0.257 mmol) and PPh_3 (139 g, 0.520 mmol) in THF (10 mL) was added **20** (107 mg, 0.257 mmol) in one portion. After a few minutes a white precipitate formed and the reaction was stirred at room temperature for 2h. The solvent was stripped and the product taken into dichloromethane, filtered and the solvent removed under vacuum. Yield 137 mg, 70%. ^{1}H NMR ($CDCl_3$, δ): 1.13 (t, 9H, C*H*$_3$), 3.65-3.71 (m, br, 6H, C*H*$_2$), 6.65 (d, 3H, 4- or 5-C*H*), 6.74 (d, 3H, 4- or 5-C*H*), 7.19-7.77 (m, 15H, ar). ^{13}C NMR ($CDCl_3$, δ): 14.32 (*C*H$_3$), 42.08 (*C*H$_2$), 116.74 (4- and 5-*C*H), 128.37-134.94 (*C*H, ar), 161.50 (*C*S). ^{31}P NMR ($CDCl_3$, δ): 30.82. FAB-MS: 764

$[M^+]$, 501 $[M^+ - PPh_3]$. IR (KBr, cm^{-1}): ν_{B-H} 2365. *Anal.* Found: C, 60.9; H, 4.9; N, 5.4. Calc. for $C_{33}H_{37}AgBN_6PS_3$: C, 51.9; H, 4.9; N, 11.0%.

[AuTm^{Et}PPh$_3$] (31)

To a stirred solution of [AuCl(PPh$_3$)] (100 mg, 0.202 mmol) in dichloromethane (10 mL) was added **20** (84 mg, 0.202 mmol) in one portion. The reaction was stirred at room temperature for 2 h. The solution was filtered through celite and the solvent stripped yielding a pale brown solid. Yield 162 mg, 94 %. ^{1}H NMR ($CDCl_3$, δ): 1.22 (t, 9H, C*H*$_3$), 3.97 (q, 6H, C*H*$_2$), 6.61 (d, 3H, 4- or 5-C*H*), 6.87 (d, 3H, 4- or 5-C*H*) 7.35-7.56 (m, 15H, ar). ^{13}C NMR (CD_3OD, δ): 14.50 (*C*H$_3$), 42.16 (*C*H$_2$), 115.01 (4- or 5-*C*H), 117.34 (4- or 5-*C*H), 128.28-134.29 (*C*H, ar). ^{31}P NMR ($CDCl_3$, δ) 36.19 FAB-MS: 853 $[M^+]$, 590 $[M^+ - PPh_3]$. IR (KBr, cm^{-1}): ν_{B-H} 2373. *Anal.* Found: C, 44.9; H, 4.3; N, 9.4. Calc. for $C_{33}H_{37}AuBN_6PS_3$: C, 46.5; H, 4.4; N, 9.9%.

[MnTm^{Et}(CO)$_3$] (32)

To a stirred suspension of [Mn(MeCN)$_3$(CO)$_3$]PF$_6$ (150 mg, 0.368 mmol) in ethanol (10 mL) was added **20** (153 mg, 0.367 mmol) in one portion. A yellow precipitate formed almost immediately and the reaction was stirred for 1h. The solid was isolated by filtration, washed with cold ethanol (2 x 5 mL) and dried under vacuum. Yield 156 mg, 80%. ^{1}H NMR ($C_2D_2Cl_4$, δ): 1.34 (t, 9H, C*H*$_3$), 4.01-4.31 (m, 6H, C*H*$_2$), 6.81 (d, 3H, 4- or 5-C*H*), 6.85 (d, 3H, 4- or 5-C*H*). ^{13}C NMR (CD_2Cl_4, δ): 17.86 (CH_3), 44.53 (*C*H$_2$), 120.31 (4- or 5-*C*H), 126.02 (4- or 5-*C*H), 160.05 (*C*S). FAB-MS: 532 $[M^+]$.

IR (KBr, cm^{-1}): ν_{B-H} 2437. IR ($CHCl_3$, cm^{-1}): ν_{C-O} 2007, 1908. *Anal.* Found: C, 41.2; H, 4.5; N, 14.7. Calc. for $C_{18}H_{22}BMnN_6O_3S_3$: C, 40.6; H, 4.2; N, 15.8%.

[RuTm^{Et}(*p*-cym)]Cl (33)

To a stirred and heating solution of $[Ru(p\text{-}cym)Cl_2]_2$ (37 mg, 0.060 mmol) in ethanol (5 mL) was added a solution of **20** (50 mg, 0.120 mmol) in ethanol (5 mL). The orange solution immediately turned reddish brown and the solution was refluxed for 1½ h. The solvent was removed under vacuum and the product dissolved in dichloromethane (20 mL), filtered and the solvent stripped yielding an orange powder. Crystals suitable for X-ray diffraction were obtained by slow diffusion of pentane into dichloromethane. Yield 65 mg, 81%. ^{1}H NMR ($CDCl_3$, δ): 1.15 (d, 6H, C*H*$_3$), 1.34 (t, 9H, C*H*$_3$), 2.17 (s, 3H, C*H*$_3$), 2.90 (m, 1H, C*H*), 4.05–4.20 (m, 6H, C*H*$_2$), 5.13–5.30 (m, 4H, ar), 6.81 (d, 3H, 4- or 5-C*H*), 7.02 (d, 3H, 4- or 5-C*H*). ^{13}C NMR ($CDCl_3$, δ): 15.35 (*C*H$_3$, imidazole), 18.31 (*C*H$_3$, me, *p*-cym), 22.17 (*C*H$_3$, pr, *p*-cym), 22.75 (*C*H$_3$, pr, *p*-cym), 30.12 (*C*H, pr, *p*-cym), 42.65 (*C*H$_2$, imidazole), 83.85-86.07 (*C*H, ar), 101.15 (C_{quat}, *p*-cym), 106.57 (C_{quat}, *p*-cym), 119.18 (4- or 5-*C*H), 124.58 (4- or 5-*C*H), 154.85 (*C*S). FAB-MS: 629 [M$^+$– Cl]. IR (KBr, cm^{-1}): ν_{B-H} 2428. *Anal.* Found: C, 44.0; H, 5.6; N, 12.3. Calc. for $C_{25}H_{36}BClN_6RuS_3.H_2O$: C, 45.2; H, 5.5; N, 12.7%

[RuTm^{Et}(*p*-cym)]PF$_6$ (34)

To a stirred suspension of [RuTm^{Et}(p-cym)]Cl (75 mg, 0.133 mmol) in THF (10 mL) was added NH_4PF_6 (22 mg, 0.135 mmol) in one portion. A white precipitate formed

almost immediately and the reaction was stirred at room temperature for 1 h. The mixture was filtered through celite and the solvent stripped yielding a purple solid. Yield 90 mg, 87%. ^{1}H NMR ($CDCl_3$, δ): 1.17 (d, 6H, C*H*$_3$), 1.25 (t, 9H, C*H*$_3$), 2.15 (s, 3H, C*H*$_3$), 2.90 (q, 1H, C*H*), 4.02-4.18 (m, 6H, C*H*$_2$), 5.11-5.30 (m, 4H, ar), 6.80 (d, 3H, 4- or 5-C*H*), 6.89 (d, 3H, 4- or 5-C*H*). ^{13}C NMR ($CDCl_3$, δ): 16.43 (*C*H$_3$), 19.39 (*C*H$_3$. me), 23.85 (*C*H$_3$, pr), 31.30 (*C*H), 43.82 (*C*H$_2$), 84.95-87.31 (*C*H, ar), 102.41 (C_{quat}, pr), 107.75 (C_{quat}, pr), 120.03 (4- or 5-*C*H), 125.66 (4- or 5-*C*H), 156.28 (*C*S). FAB-MS: 629 [M^+– PF_6]. IR (KBr, cm^{-1}): ν_{B-H} 2432

[RuTm^{Et}Cp] (35)

To a suspension of $[RuCl_2Cp]_2$ (25 mg, 0.053 mmol) in ethanol (20 mL) was added **20** (44 mg, 0.106 mmol) in one portion. The solution was stirred overnight. The solvent was removed under vacuum, dichloromethane (20 mL) added and the solution filtered. The solvent was stripped yielding a red crystalline solid. Yield 45 mg, 86%. ^{1}H NMR ($CDCl_3$, δ): 1.28 (t, 9H, C*H*$_3$), 4.05-4.31 (m, 6H, C*H*$_2$), 5.26 (s, 5H, C*H*), 6.93 (d, 3H, 4- or 5-C*H*), 7.07 (d, 3H, 4- or 5-C*H*). ^{13}C NMR ($CDCl_3$, δ): 16.31 (*C*H$_3$), 44.30 (*C*H$_2$), 88.27 (*C*H), 120.92 (4- or 5-*C*H), 126.04 (4- or 5-*C*H). FAB-MS: 560 [M^+]. IR (KBr, cm^{-1}): ν_{B-H} 2346.

[SnTm^{Et}Cl$_3$] (36)

To a stirred suspension of **20** (100 mg, 0.240 mmol) in dichloromethane (5 mL) was added $SnCl_4$ (0.57 mL of a 0.427M solution in dichloromethane). A yellow precipitate

formed immediately. The reaction was stirred for 2h. The solution was filtered yielding a yellow solid. Yield: 117 mg, 79%. ^{1}H NMR ($CDCl_3$, δ): 1.29 (t, 9H, C*H*$_3$), 2.48 (m, 6H, C*H*$_2$), 7.47 (d, 3H, 4- or 5-C*H*), 7.69 (d, 3H, 4- or 5-C*H*). ^{13}C NMR ($CDCl_3$, δ): 16.73 (*C*H$_3$), 43.85 (*C*H$_2$), 123.81 (4- or 5-*C*H), 127.93 (4- or 5-*C*H), 149.68 (*C*S). FAB-MS: 619 [M$^+$]. IR (KBr, cm^{-1}): $\nu_{B\text{-}H}$ 2370. *Anal.* Found: C, 28.1; H, 3.5; N, 12.5. Calc. for $C_{15}H_{22}BCl_3N_6S_3Sn$: C, 29.1; H, 3.6; N, 13.6%.

Attempted synthesis of [$MoCl_2O_2(THF)_2$]

$MoCl_2O_2$ (2.00 g, 10.058 mmol) was added in small portions to THF (60 mL) cooled to –20 °C. The reaction was stirred at low temperature for 30 min. The solution was filtered using a cannula and the solvent was stripped. The isolation of the product proved difficult as the initial white powder gradually turned blue. The complex was prepared in situ for subsequent reactions.

Reaction of $MoCl_2O_2$ with 20 in THF

$MoCl_2O_2$ (58 mg, 0.292 mmol) was added in small portions to THF (30 mL) cooled to –20 °C. The reaction was stirred at low temperature for 30 min. The solution was allowed to warm to room temperature and **20** (121 mg, 0.291 mmol) in one portion. The solution was stirred at room temperature for 2 h., filtered by cannula and the solution stripped yielding an orange powder. NMR and mass spectroscopy confirmed only the presence of unreacted ligand, **20**.

6.4 VARIABLE TEMPERATURE NMR AND *AB INITIO* CALCULATIONS

Variable Temperature ^{1}H NMR Experiments

NMR spectra were recorded on a Bruker 360AC spectrometer. ^{1}H chemical shifts are reported in ppm relative to $SiMe_4$ ($\delta = 0$) and were referenced internally with respect to the protio solvent impurity. Temperature measurement was by means of the thermometer integral to the NMR probe. The temperature of the sample was varied as necessary and controlled to the nearest degree. Multiplicities and peak types are abbreviated in the manner previously described in Section 6.1.

Ab initio Calculations

Ab initio MO geometry optimisations [MP2[138] (method) / LanL2DZ[139, 140] (basis set)] using the Gaussian 98 suite of quantum chemistry programs[141] were carried out on the ground and transition state structures C_3-symmetric complexes undergoing non-dissociative racemisation. Single-point energies, with electron correlation included at the MP2 level and using the same basis set, were computed for these optimised structures.

REFERENCES

1. Moberg, C. (1998) *Angewandte Chemie, International Edition* **37,** 248-268.

2. Garner, M., Reglinski, J., Cassidy, I., Spicer, M. D., and Kennedy, A. R. (1996) *Chemical Communications (Cambridge)*, 1975-1976.

3. Trofimenko, S. (1970) *Inorganic Syntheses* **12,** 99-109.

4. Trofimenko, S. (2004) *Polyhedron* **23,** 197-203.

5. Reglinski, J., Garner, M., Cassidy, I. D., Slavin, P. A., Spicer, M. D., and Armstrong, D. R. (1999) *Journal of the Chemical Society, Dalton Transactions: Inorganic Chemistry*, 2119-2126.

6. Garner, M., Armstrong, D. R., Reglinski, J., Smith, W. E., Wilson, R., and McKillop, J. H. (1994) *Bioorganic & Medicinal Chemistry Letters* **4,** 1357-60.

7. Ogretir, C., and Yarligan, S. (1996) *Journal of Molecular Structure (Theochem)* **366,** 227-231.

8. Ojo, J. F., Slavin, P. A., Reglinski, J., Garner, M., Spicer, M. D., Kennedy, A. R., and Teat, S. J. (2001) *Inorganica Chimica Acta* **313,** 15-20.

9. Bruce, M. I., and Ostazewski, A. P. P. (1972) *Journal of the Chemical Society, Chemical Communications*, 1124-5.

10. Bruce, M. I., and Ostazewski, A. P. P. (1973) *Journal of the Chemical Society, Dalton Transactions: Inorganic Chemistry (1972-1999)*, 2433-6.

11. Reglinski, J., Spicer, M. D., Garner, M., and Kennedy, A. R. (1999) *Journal of the American Chemical Society* **121,** 2317-2318.

12. Slavin, P. A., Reglinski, J., Spicer, M. D., and Kennedy, A. R. (2000) *Dalton*, 239-240.

13. Garner, M., Lehmann, M.-A., Reglinski, J., and Spicer, M. D. (2001) *Organometallics* **20,** 5233-5236.

14. Garner, M., Lewinski, K., Pattek-Janczyk, A., Reglinski, J., Sieklucka, B., Spicer, M. D., and Szaleniec, M. (2003) *Dalton Transactions*, 1181-1185.

15. Cassidy, I., Garner, M., Kennedy, A. R., Potts, G. B. S., Reglinski, J., Slavin, P. A., and Spicer, M. D. (2002) *European Journal of Inorganic Chemistry*, 1235-1239.

16. Dodds, C. A., Kennedy, A. R., Reglinski, J., and Spicer, M. D. (2004) *Inorganic Chemistry* **43,** 394-395.

17. Dodds, C. A., Jagoda, M., Reglinski, J., and Spicer, M. D. (2004) *Polyhedron* **23,** 445-450.

18. Reglinski, J., Spicer, M. D., Ojo, J. F., McAnally, G. D., Skorska, A., Smith, S. J., and Smith, W. E. (2003) *Langmuir* **19,** 6336-6338.

19. Santini, C., Lobbia, G. G., Pettinari, C., Pellei, M., Valle, G., and Calogero, S. (1998) *Inorganic Chemistry* **37,** 890-900.

20. Effendy, Lobbia, G. G., Pettinari, C., Santini, C., Skelton, B. W., and White, A. H. (2000) *Inorganica Chimica Acta* **308,** 65-72.

21. Santini, C., Pettinari, C., Gioia Lobbia, G., Spagna, R., Pellei, M., and Vallorani, F. (1999) *Inorganica Chimica Acta* **285,** 81-88.

22. Gioia Lobbia, G., Pettinari, C., Santini, C., Somers, N., Skelton, B. W., and White, A. H. (2001) *Inorganica Chimica Acta* **319,** 15-22.

23. Santini, C., Pellei, M., Gioia Lobbia, G., Pettinari, C., Drozdov, A., and Troyanov, S. (2001) *Inorganica Chimica Acta* **325,** 20-28.

24. Foreman, M. R. S. J., Hill, A. F., White, A. J. P., and Williams, D. J. (2003) *Organometallics* **22,** 3831-3840.

25. Foreman, M. R. S. J., Hill, A. F., Owen, G. R., White, A. J. P., and Williams, D. J. (2003) *Organometallics* **22,** 4446-4450.

26. Foreman, M. R. S. J., Hill, A. F., Tshabang, N., White, A. J. P., and Williams, D. J. (2003) *Organometallics* **22,** 5593-5596.

27. Hill, A. F., Owen, G. R., White, A. J. P., and Williams, D. J. (1999) *Angewandte Chemie, International Edition* **38,** 2759-2761.

28. Foreman, M. R. S. J., Hill, A. F., White, A. J. P., and Williams, D. J. (2004) *Organometallics* **23,** 913-916.

29. Garcia, R., Paulo, A., Domingos, A., and Santos, I. (2001) *Journal of Organometallic Chemistry* **632,** 41-48.

30. Bailey, P. J., Lorono-Gonzales, D. J., McCormack, C., Parsons, S., and Price, M. (2003) *Inorganica Chimica Acta* **354,** 61-67.

31. Kimblin, C., Bridgewater, B. M., Churchill, D. G., and Parkin, G. (1999) *Chemical Communications (Cambridge)*, 2301-2302.

32. Bridgewater, B. M., Fillebeen, T., Friesner, R. A., and Parkin, G. (2000) *Dalton*, 4494-4496.

33. Bridgewater, B. M., and Parkin, G. (2001) *Inorganic Chemistry Communications* **4,** 126-129.

34. Bakbak, S., Bhatia, V. K., Incarvito, C. D., Rheingold, A. L., and Rabinovich, D. (2001) *Polyhedron* **20,** 3343-3348.

35. Docrat, A., Morlok, M. M., Bridgewater, B. M., Churchill, D. G., and Parkin, G. (2004) *Polyhedron* **23,** 481-488.

36. Parkin, G. (2000) *Chemical Communications (Cambridge)*, 1971-1985.

37. Bridgewater, B. M., and Parkin, G. (2000) *Journal of the American Chemical Society* **122,** 7140-7141.

38. Bridgewater, B. M., and Parkin, G. (2000) *Inorganic Chemistry Communications* **3,** 534-536.

39. Kimblin, C., Bridgewater, B. M., Hascall, T., and Parkin, G. (2000) *Dalton*, 1267-1274.

40. Kimblin, C., Churchill, D. G., Bridgewater, B. M., Girard, J. N., Quarless, D. A., and Parkin, G. (2001) *Polyhedron* **20,** 1891-1896.

41. Tesmer, M., Shu, M., and Vahrenkamp, H. (2001) *Inorganic Chemistry* **40,** 4022-4029.

42. Seebacher, J., and Vahrenkamp, H. (2003) *Journal of Molecular Structure* **656,** 177-181.

43. Bakbak, S., Incarvito, C. D., Rheingold, A. L., and Rabinovich, D. (2002) *Inorganic Chemistry* **41,** 998-1001.

44. White, J. L., Tanski, J. M., and Rabinovich, D. (2002) *Journal of the Chemical Society, Dalton Transactions*, 2987-2991.

45. Mihalcik, D. J., White, J. L., Tanski, J. M., Zakharov, L. N., Yap, G. P. A., Incarvito, C. D., Rheingold, A. L., and Rabinovich, D. (2004) *Dalton Transactions*, 1626-1634.

46. Alvarez, H. M., Tanski, J. M., and Rabinovich, D. (2004) *Polyhedron* **23**, 395-403.

47. Garcia, R., Paulo, A., Domingos, A., and Santos, I. (2003) *Dalton Transactions*, 2757-2760.

48. Kimblin, C., Bridgewater, B. M., Hascall, T., and Parkin, G. (2000) *Dalton*, 891-897.

49. Garcia, R., Paulo, A., Domingos, A., Santos, I., Ortner, K., and Alberto, R. (2000) *Journal of the American Chemical Society* **122**, 11240-11241.

50. Maria, L., Domingos, A., and Santos, I. (2001) *Inorganic chemistry* **40**, 6863-4.

51. Garcia, R., Domingos, A., Paulo, A., Santos, I., and Alberto, R. (2002) *Inorganic Chemistry* **41**, 2422-2428.

52. Garcia, R., Xing, Y.-H., Paulo, A., Domingos, A., and Santos, I. (2002) *Journal of the Chemical Society, Dalton Transactions*, 4236-4241.

53. Alvarez, H. M., Krawiec, M., Donovan-Merkert, B. T., Fouzi, M., and Rabinovich, D. (2001) *Inorganic Chemistry* **40**, 5736-5737.

54. Alvarez, H. M., Tran, T. B., Richter, M. A., Alyounes, D. M., Rabinovich, D., Tanski, J. M., and Krawiec, M. (2003) *Inorganic Chemistry* **42**, 2149-2156.

55. Philson, L. A., Alyounes, D. M., Zakharov, L. N., Rheingold, A. L., and Rabinovich, D. (2003) *Polyhedron* **22**, 3461-3466.

56. Alvarez, H. M., Gillespie, P. A., Gause, C. D., Rheingold, A. L., Golen, J. A., and Rabinovich, D. (2004) *Polyhedron* **23**, 617-622.

57. Soares, L. F., Menezes, D. C., Silva, R. M., Doriguetto, A. C., Ellena, J., Mascarenhas, Y. P., and Castellano, E. E. (2004) *Polyhedron* **23**, 205-209.

58. Bailey, P. J., Lanfranchi, M., Marchio, L., and Parsons, S. (2001) *Inorganic Chemistry* **40,** 5030-5035.

59. Careri, M., Elviri, L., Lanfranchi, M., Marchio, L., Mora, C., and Pellinghelli, M. A. (2003) *Inorganic Chemistry* **42,** 2109-2114.

60. Lanfranchi, M., Marchio, L., Mora, C., and Pellinghelli, M. A. (2004) *Inorganica Chimica Acta* **357,** 367-375.

61. Gennari, M., Giannetto, M., Lanfranchi, M., Marchio, L., Pellinghelli, M. A., and Tegoni, M. (2004) *Polyhedron* **23,** 1829-1835.

62. Cammi, R., Lanfranchi, M., Marchio, L., Mora, C., Paiola, C., and Pellinghelli, M. A. (2003) *Inorganic Chemistry* **42,** 1769-1778.

63. Sargent, A. L., Titus, E. P., Riordan, C. G., Rheingold, A. L., and Ge, P. (1996) *Inorganic Chemistry* **35,** 7095-7101.

64. Ge, P., Haggerty, B. S., Rheingold, A. L., and Riordan, C. G. (1994) *Journal of the American Chemical Society* **116,** 8406-7.

65. Ohrenberg, C., Ge, P., Schebler, P., Riordan, C. G., Yap, G. P. A., and Rheingold, A. L. (1996) *Inorganic Chemistry* **35,** 749-54.

66. Ohrenberg, C., Saleem, M. M., Riordan, C. G., Yap, G. P. A., Verma, A. K., and Rheingold, A. L. (1996) *Chemical Communications (Cambridge)*, 1081-1082.

67. Ohrenberg, C., Riordan, C. G., Liable-Sands, L., and Rheingold, A. L. (1998) *Coordination Chemistry Reviews* **174,** 301-311.

68. Ohrenberg, C., Liable-Sands, L. M., Rheingold, A. L., and Riordan, C. G. (2001) *Inorganic Chemistry* **40,** 4276-4283.

69. Ge, P., Riordan, C. G., Yap, G. P. A., and Rheingold, A. L. (1996) *Inorganic Chemistry* **35,** 5408-5409.

70. Ge, P., Rheingold, A. L., and Riordan, C. G. (2002) *Inorganic Chemistry* **41,** 1383-1390.

71. Schebler, P. J., Riordan, C. G., Guzei, I. A., and Rheingold, A. L. (1998) *Inorganic Chemistry* **37,** 4754-4755.

72. Chiou, S.-J., Innocent, J., Riordan, C. G., Lam, K.-C., Liable-Sands, L., and Rheingold, A. L. (2000) *Inorganic Chemistry* **39,** 4347-4353.

73. Schebler, P. J., Mandimutsira, B. S., Riordan, C. G., Liable-Sands, L. M., Incarvito, C. D., and Rheingold, A. L. (2001) *Journal of the American Chemical Society* **123,** 331-332.

74. Craft, J. L., Mandimutsira, B. S., Fujita, K., Riordan, C. G., and Brunold, T. C. (2003) *Inorganic Chemistry* **42,** 859-867.

75. Krishnan, R., Voo, J. K., Riordan, C. G., Zahkarov, L., and Rheingold, A. L. (2003) *Journal of the American Chemical Society* **125,** 4422-4423.

76. Mandimutsira, B. S., Yamarik, J. L., Brunold, T. C., Gu, W., Cramer, S. P., and Riordan, C. G. (2001) *Journal of the American Chemical Society* **123,** 9194-9195.

77. Schenker, R., Mandimutsira, B. S., Riordan, C. G., and Brunold, T. C. (2002) *Journal of the American Chemical Society* **124,** 13842-13855.

78. Fujita, K., Rheingold, A. L., and Riordan, C. G. (2003) *Dalton Transactions,* 2004-2008.

79. Schebler, P. J., Riordan, C. G., Liable-Sands, L., and Rheingold, A. L. (1998) *Inorganica Chimica Acta* **270,** 543-549.

80. Peters, J. C., Feldman, J. D., and Tilley, T. D. (1999) *Journal of the American Chemical Society* **121,** 9871-9872.

81. Feldman, J. D., Peters, J. C., and Tilley, T. D. (2002) *Organometallics* **21,** 4065-4075.

82. Feldman, J. D., Peters, J. C., and Tilley, T. D. (2002) *Organometallics* **21,** 4050-4064.

83. Barney, A. A., Heyduk, A. F., and Nocera, D. G. (1999) *Chemical Communications (Cambridge, United Kingdom),* 2379-2380.

84. Shapiro, I. R., Jenkins, D. M., Thomas, J. C., Day, M. W., and Peters, J. C. (2001) *Chemical Communications (Cambridge, United Kingdom),* 2152-2153.

85. Jenkins, D. M., Betley, T. A., and Peters, J. C. (2002) *Journal of the American Chemical Society* **124,** 11238-11239.

86. Jenkins, D. M., Di Bilio, A. J., Allen, M. J., Betley, T. A., and Peters, J. C. (2002) *Journal of the American Chemical Society* **124,** 15336-15350.

87. Brown, S. D., Betley, T. A., and Peters, J. C. (2003) *Journal of the American Chemical Society* **125,** 322-323.

88. Thomas, J. C., and Peters, J. C. (2004) *Polyhedron* **23,** 489-497.

89. Betley, T. A., and Peters, J. C. (2003) *Inorganic Chemistry* **42,** 5074-5084.

90. Turculet, L., Feldman, J. D., and Tilley, T. D. (2003) *Organometallics* **22,** 4627-4629.

91. Jacobsen, E. N., Pfaltz, A., Yamamoto, H., and Editors (1999) Comprehensive Asymmetric Catalysis, Springer, Berlin.

92. Klaeui, W. (1979) *Zeitschrift fuer Naturforschung, Teil B: Anorganische Chemie, Organische Chemie* **34B,** 1403-7.

93. Klaeui, W. (1990) *Angewandte Chemie, International Edition in English* **29,** 627-637.

94. Lam, T. C. H., Mak, W.-L., Wong, W.-L., Kwong, H.-L., Sung, H. H. Y., Lo, S. M. F., Williams, I. D., and Leung, W.-H. (2004) *Organometallics* **23,** 1247-1252.

95. Nugent, W. A. (1992) *Journal of the American Chemical Society* **114,** 2768-9.

96. Nugent, W. A. (1998) *Journal of the American Chemical Society* **120,** 7139-7140.

97. Nugent, W. A., and Harlow, R. L. (1994) *Journal of the American Chemical Society* **116,** 6142-8.

98. Di Furia, F., Licini, G., Modena, G., Motterle, R., and Nugent, W. A. (1996) *Journal of Organic Chemistry* **61,** 5175-5177.

99. Herrmann, W. A. (2002) *Angewandte Chemie, International Edition* **41,** 1290-1309.

100. Kuhn, N., Bohnen, H., Kreutzberg, J., Blaeser, D., and Boese, R. (1993) *Journal of the Chemical Society, Chemical Communications* **14,** 1136-7.

101. Frankel, R., Kernbach, U., Bakola-Christianopoulou, M., Plaia, U., Suter, M., Ponikwar, W., Noth, H., Moinet, C., and Fehlhammer, W. P. (2001) *Journal of Organometallic Chemistry* **617-618,** 530-545.

102. Kuhn, N., Bohnen, H., Blaeser, D., and Boese, R. (1994) *Chemische Berichte* **127,** 1405-7.

103. Schumann, H., Glanz, M., Winterfeld, J., Hemling, H., Kuhn, N., Bohnen, H., Blaeser, D., and Boese, R. (1995) *Journal of Organometallic Chemistry* **493,** C14-18.

104. Bohnen, H., Henkel, G., and Kreutzberg, J. (1996) *Zeitschrift fuer Naturforschung, B: Chemical Sciences* **51,** 1267-1278.

105. Zaidi, S. A. A., Khan, T. A., Shaheer, S. A., and Zaidi, S. R. A. (1988) *Acta Chimica Hungarica* **125,** 229-37.

106. Jones, R. G., Kornfeld, E. C., McLaughlin, K. C., and Anderson, R. C. (1949) *Journal of the American Chemical Society* **71,** 4000-2.

107. Forrest, T. P., Dauphinee, G. A., and Chen, F. M. F. (1974) *Canadian Journal of Chemistry* **52,** 2725-9.

108. Wong, O., Tsuzuki, N., Richardson, M., Rytting, H., Konishi, R., and Higuchi, T. (1987) *Heterocycles* **26,** 3153-8.

109. Huheey, J. E. (1983) Inorganic Chemistry, Harper International SI Edition.

110. Clayden, J., Greeves, N., Warren, S., and Wothers, P. (2001) Organic Chemistry, Oxford University Press.

111. Beaumont, D., Waigh, R. D., Sunbhanich, M., and Nott, M. W. (1983) *Journal of Medicinal Chemistry* **26,** 507-15.

112. Quick, M. H., and Angelici, R. J. (1979) *Inorganic Syntheses* **19,** 160-1, 163.

113. Reimann, R. H., and Singleton, E. (1974) *Journal of the Chemical Society, Dalton Transactions: Inorganic Chemistry (1972-1999)*, 808-13.

114. Jensen, S. B., Rodger, S. J., and Spicer, M. D. (1998) *Journal of Organometallic Chemistry* **556,** 151-158.

115. Trost, B. M., and Older, C. M. (2002) *Organometallics* **21,** 2544-2546.

116. Bennett, M. A., and Smith, A. K. (1974) *Journal of the Chemical Society, Dalton Transactions: Inorganic Chemistry (1972-1999)*, 233-41.

117. Connolly, J., Genge, A. R. J., Levason, W., Orchard, S. D., Pope, S. J. A., and Reid, G. (1999) *Journal of the Chemical Society, Dalton Transactions: Inorganic Chemistry*, 2343-2352.

118. Patel, B., and Reid, G. (2000) *Dalton*, 1303-1307.

119. Elias, H., Schmidt, G., Kueppers, H. J., Saher, M., Wieghardt, K., Nuber, B., and Weiss, J. (1989) *Inorganic Chemistry* **28,** 3021-4.

120. Bailey, P. J., Grant, K. J., and Parsons, S. (1998) *Organometallics* **17,** 551-555.

121. Cadierno, V., Diez, J., Garcia-Garrido, S. E., Garcia-Granda, S., and Gimeno, J. (2002) *Journal of the Chemical Society, Dalton Transactions*, 1465-1472.

122. Bhambri, S., and Tocher, D. A. (1996) *Polyhedron* **15,** 2763-2770.

123. Campion, B. K., Heyn, R. H., and Tilley, T. D. (1988) *Journal of the Chemical Society, Chemical Communications*, 278-80.

124. Arliguie, T., Border, C., Chaudret, B., Devillers, J., and Poilblanc, R. (1989) *Organometallics* **8,** 1308-14.

125. Gemel, C., Mereiter, K., Schmid, R., and Kirchner, K. (1997) *Organometallics* **16,** 5601-5603.

126. Gemel, C., Sapunov, V. N., Mereiter, K., Ferencic, M., Schmid, R., and Kirchner, K. (1999) *Inorganica Chimica Acta* **286,** 114-120.

127. Yamaguchi, Y., and Nagashima, H. (2000) *Organometallics* **19,** 725-727.

128. Jimenez Tenorio, M., Mereiter, K., Puerta, M. C., and Valerga, P. (2000) *Journal of the American Chemical Society* **122,** 11230-11231.

129. Braunstein, P., Lehner, H., and Matt, D. (1990) *Inorganic Syntheses* **27,** 218-21.

130. Suzuki, E., and Okada, M. (1979) *Chemical & Pharmaceutical Bulletin* **27,** 541-4.

131. Kister, J., Assef, G., Mille, G., and Metzger, J. (1979) *Canadian Journal of Chemistry* **57,** 813-21.

132. Cotton, F. A., and Wilkinson, G. (1980) Advanced Inorganic Chemistry: A Comprehensive Text. 4th Ed.

133. Shriver, D. F., and Atkins, P. W. (1999) Inorganic Chemistry 3rd Ed, Oxford University Press.

134. Harwood, L. M., Claridge, T. D. w., and Editors (1996) Introduction to Organic Spectroscopy.

135. Hore, P. J. (1995) Nuclear Magnetic Resonance.

136. Denk, M. K. (2004).

137. Shannon, R. D. (1976) *Acta Crystallographica* **A32,** 751-767.

138. Møller , C., and S., P. M. (1934) *Physical Review* **46,** 618.

139. Hay, P. J., and Wadt, W. R. (1985) *Journal of Chemical Physics* **82,** 270.

140. Wadt, W. R., and Hay, P. J. (1985) *Journal of Chemical Physics* **82,** 284.

141. Frisch, M. J., Trucks, G. W., Schlegel, H. B., Scuseria, G. E., Robb, M. A., Cheeseman, J. R., Zakrzewski, V. G., Montgomery, J. A., Stratmann, R. E., Burant, J. C., Dapprich, S., Millam, J. M., Daniels, A. D., Kudin, K. N., Strain, M. C., Farkas, O., Tomasi, J., Barone, V., Cossi, M., Cammi, R., Mennucci, B., Pomelli, C., Adamo, C., Clifford, S., Ochterski, J., Petersson, G. A., Ayala, P. Y., Cui, Q., Morokuma, K., Malick, D. K., Rabuck, A. D., Raghavachari, K., Foresman, J. B., Cioslowski, J., Ortiz, J. V., Stefanov, B. B., Liu, G., Liashenko, A., Piskorz, P., Komaromi, I., Gomperts, R., Martin, R. L., Fox, D. J., Keith, T., Al-Laham, M. A., Peng, C. Y., Nanayakkara, A., Gonzalez, C., Challacombe, M., Gill, P. M. W., Johnson, B. G., Chen, W., Wong, M. W., Andres, J. L., Head-Gordon, M., Replogle, E. S., and Pople, J. A. (1998), Pittsburgh PA.

142. Zaidi, S. A. A., Khan, T. A., Zaidi, S. R. A., and Siddiqi, Z. A. (1985) *Polyhedron* **4,** 1163-6.

APPENDICES

APPENDIX 1 NUMERICAL ASSIGNMENT OF COMPOUNDS

1

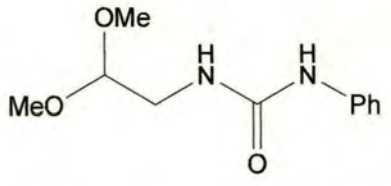

N-(2,2-dimethoxyethyl)-N-phenylurea

2

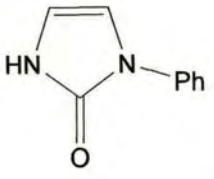

1-Phenyl-4-imidazolin-2-one

3

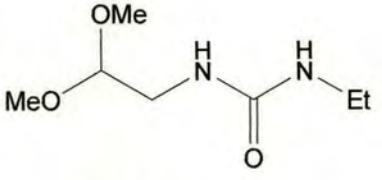

N'-Ethyl-N-(2,2-dimethoxyethyl)urea

4

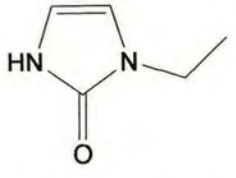

1-Ethyl-4-imidazolin-2-one

5

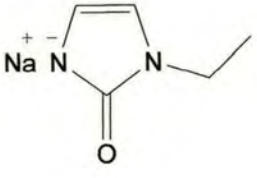

Sodium 1-Ethyl-4-imidazolin-2-one

6

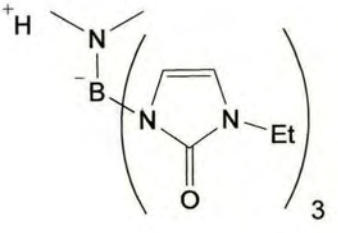

Tris(1-ethyl-4-imidazolin-2-one)(dimethylamine)borate

7

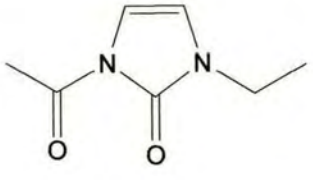

1-Ethyl-4-acetyl-4-imidazolin-2-one

8

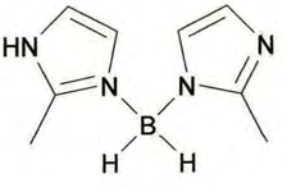

Hydrogen dihydrobis(2-methylimidazolyl)borate

9

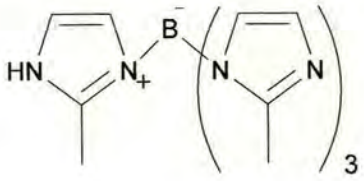

Hydrogen tetrakis(2-methylimidazolyl)borate

10

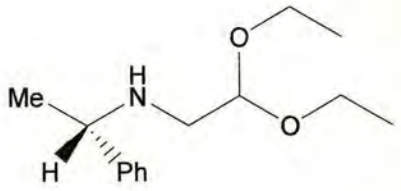

(L)-(-)-α-Methylbenzylaminoacetaldehyde diethyl acetal

11

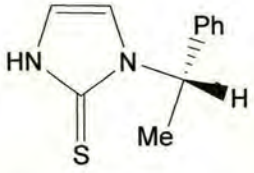

2-Mercapto-1-((L)-(-)-α-methylbenzyl)imidazole

12

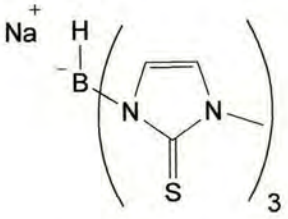

Sodium hydrotris(methimazolyl)borate

13

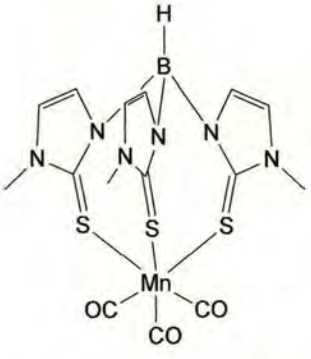

Tris(methimazolyl)hydroborato-manganese(I)tricarbonyl

14

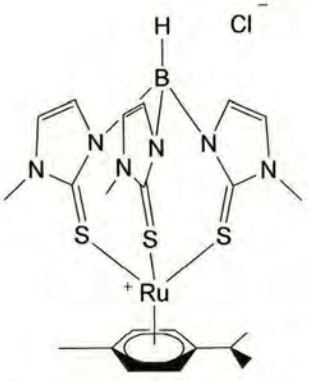

Tris(methimazolyl)hydroborato-ruthenium(II)*para*-cymene chloride

15

[RuTmCp]

Tris(methimazolyl)hydroborato-ruthenium(II)cyclopentadiene

16

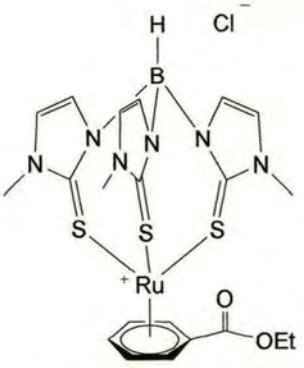

Tris(methimazolyl)hydroborato-ruthenium(II)ethylbenzoate

17

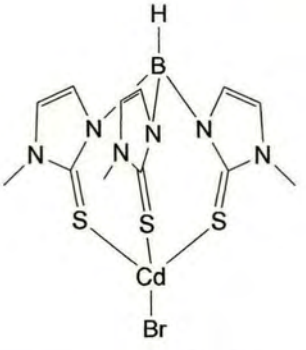

Tris(methimazolyl)hydroborato-cadmium(II)bromide

18

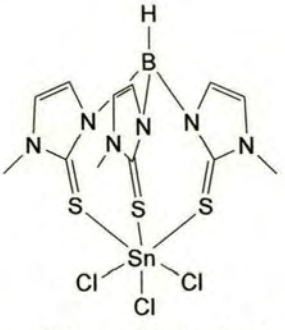

Tris(methimazolyl)hydroborato-tin(IV)trichloride

19

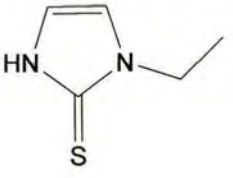

2-mercapto-1-ethylimidazole

20

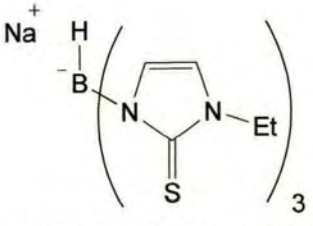

Sodium hydrotris(2-mercapto-1-ethylimidazolyl)borate

21

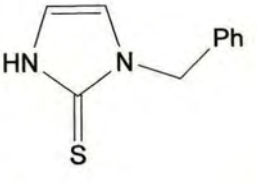

2-mercapto-1-benzylimidazole

22

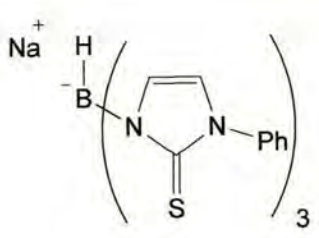

Sodium hydrotris(2-mercapto-1-benzylimidazolyl)borate

23

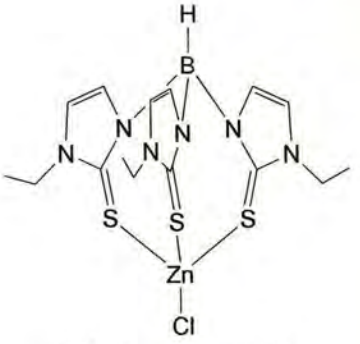

Tris(2-mercapto-1-ethylimidazolyl)hydroborato-zinc(II)chloride

24

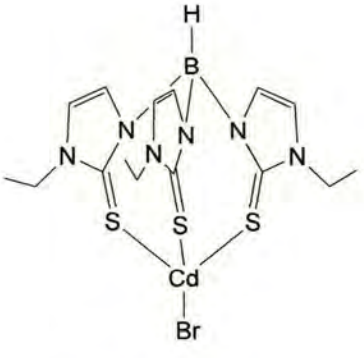

Tris(2-mercapto-1-ethylimidazolyl)hydroborato-cadmium(II)bromide

25

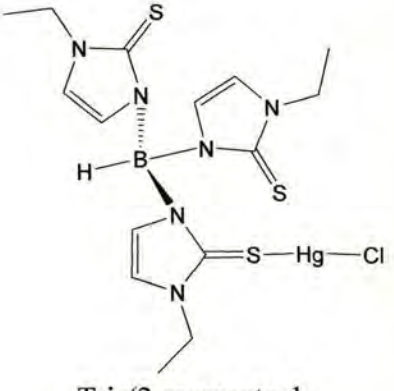

Tris(2-mercapto-1-ethylimidazolyl)hydroborato-mercury(II)chloride

26

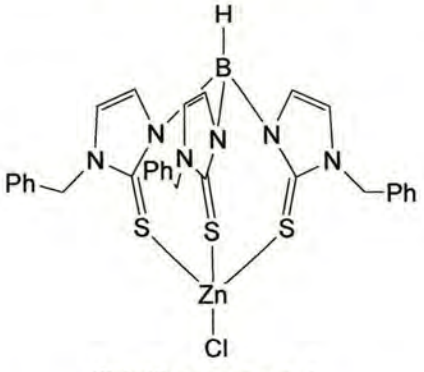

Tris(2-mercapto-1-benzylimidazolyl)hydroborato-zinc(II)chloride

27

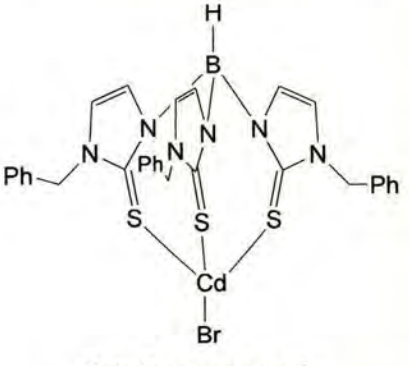

Tris(2-mercapto-1-benzylimidazolyl)hydroborato-cadmium(II)bromide

28

$[HgTm^{Bn}Cl]$

Tris(2-mercapto-1-benzylimidazolyl)hydroborato-mercury(II)chloride

29

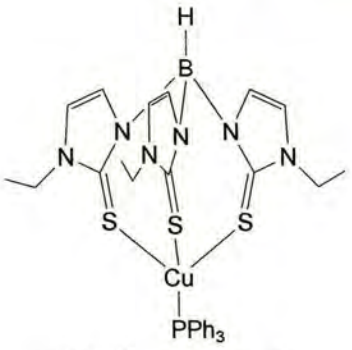

Tris(2-mercapto-1-ethylimidazolyl)hydroborato-copper(I)triphenylphosphine

30

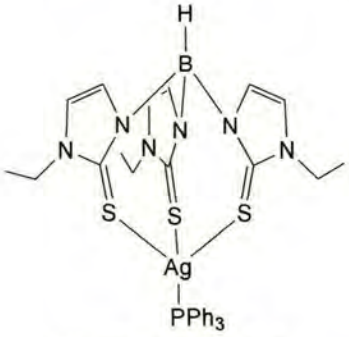

Tris(2-mercapto-1-ethylimidazolyl)hydroborato-silver(I)triphenylphosphine

31

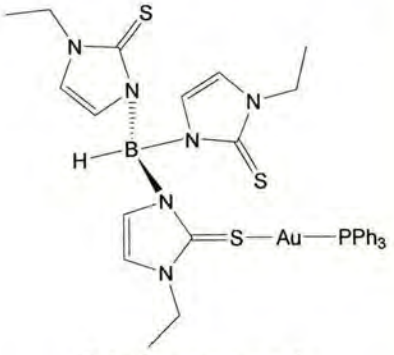

Tris(2-mercapto-1-ethylimidazolyl)hydroborato-gold(I)triphenylphosphine

32

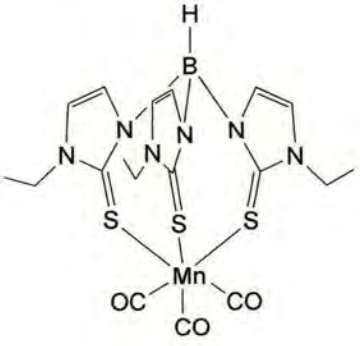

Tris(2-mercapto-1-ethylimidazolyl)hydroborato-manganese(I)tricarbonyl

33/34

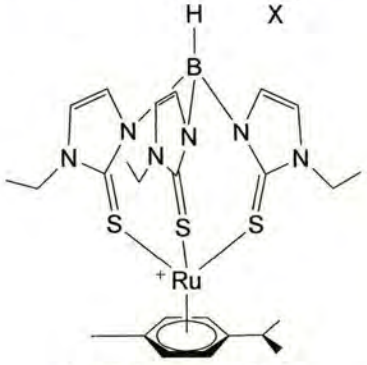

Tris(2-mercapto-1-ethylimidazolyl)hydroborato-ruthenium(II)*para*-cymene
X = Cl (**33**), PF_6 (**34**)

35

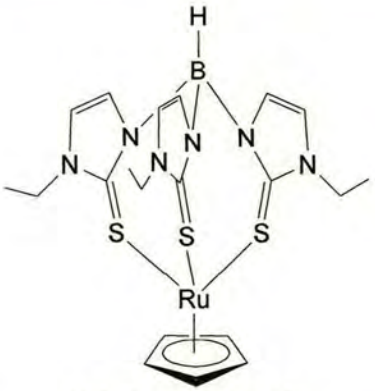

Tris(2-mercapto-1-ethylimidazolyl)hydroborato-ruthenium(II)cyclopentadiene

36

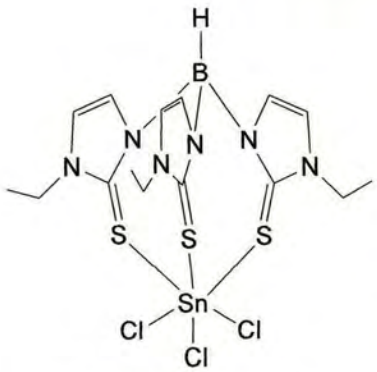

Tris(2-mercapto-1-ethylimidazolyl)hydroborato-tin(IV)trichloride

APPENDIX 2

APPARATUS FOR THE MEASUREMENT OF GAS EVOLUTION

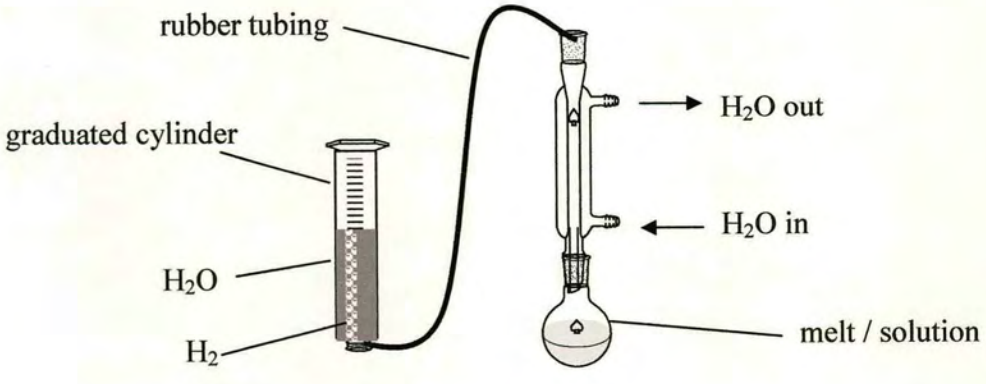

Figure A-1 Apparatus for measurement of hydrogen evolution

APPENDIX 3[24]

TORSION PARAMETERS

Anthony F. Hill has introduced a set of parameters to describe the deformation which occurs in complexes of the Tm ligand. For clarity only this system is used throughout this work and will be briefly described below.

As described in Section 1.1, tripodal ligands of the type $[E(L_2D)_3]$ (and hence the Tm ligand) form complexes of C_3-symmetry. Upon coordination of the ligand, three eight-membered rings are formed and due to the inherent strain the ligand twists giving rise to a propeller-like or helical geometry [Scheme 1-1(b)]. To describe the chirality and the degree of torsion in such complexes a system of nomenclature is needed.

Hill suggested that θ denotes the N-B-M-S torsional angle for each methimazolyl buttress (Fig. A-2).

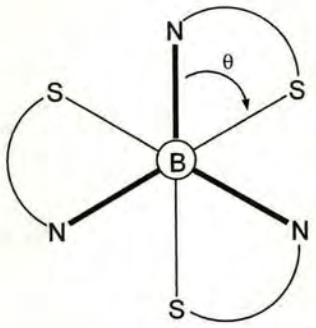

λ ($\theta < 0$)

δ ($\theta > 0$)

Figure A-2

He noted that this parameter implicitly contains the chirality of the molecule as $\theta<0$ implies the $\lambda\lambda\lambda$ stereochemistry of the three buttresses, and $\theta>0$ indicates the $\delta\delta\delta$ absolute configuration. Since it is not possible to have mixtures of λ and δ configuration in one complex, the sign of θ denotes the absolute configuration.

A second parameter was introduced to describe the degree of displacement of the metal from the methimazole plane, a feature also induced by the twisting of the structure. Thus, the angle that the normal to the plane of the methimazole ring makes with the B-M vector was defined as ω (Fig. A-3).

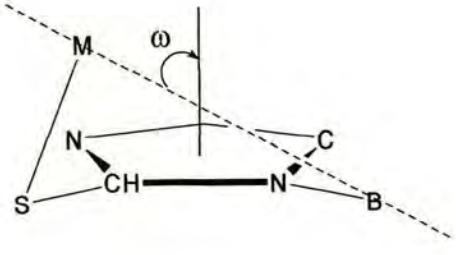

Figure A-3

As we did not have the means to measure ω, we have defined ω' as the C-N-B-M torsional angle and this parameter is employed in our discussion in Section 5.4.

APPENDIX 4

SOLVENT DRYING

Solvent	*Drying Agent*
Acetonitrile	Calcium hydride
Benzene	Sodium/benzophenone
Chloroform	Calcium hydride
Dichloromethane	Calcium hydride
Diethyl Ether	Sodium/benzophenone
Diglyme	Sodium/benzophenone
Dimethylacetamide	Barium oxide/molecular sieves
Dimethylformamide	Magnesium sulphate/molecular sieves
Ethanol	Calcium hydride
Hexane	Sodium/benzophenone
Methanol	Calcium hydride
Pentane	Calcium hydride
Tetrahydrofuran	Sodium/benzophenone
Toluene	Sodium
Xylene	Calcium hydride

APPENDIX 5

CRYSTAL TABLES

Table A-1. Selected bond lengths and angles for hydrogen dihydrobis(2-methylimidazolyl)borate (8)

Bond Lengths (Å)	
B(1)-N(11)	1.549(3)
B(1)-N(12)	1.578(3)
B(1)-H(1)	1.120
B(1)-H(2)	1.120
C(21)-N(31)	1.324(2)
C(22)-N(32)	1.333(2)
N(11)-C(21)	1.349(2)
N(12)-C(22)	1.332(2)
C(21)-C(61)	1.487(3)
C(22)-C(62)	1.481(3)
N(31)-C(41)	1.374(3)
N(32)-C(42)	1.380(2)
N(11)-C(51)	1.383(2)
N(12)-C(52)	1.375(2)
C(41)-C(51)	1.342(3)
C(42)-C(52)	1.350(3)
Bond Angles (°)	
N(11)-B(1)-N(12)	107.97(16)
H(1)-B(1)-N(11)	110.10
H(1)-B(1)-N(12)	110.11
H(2)-B(1)-N(11)	110.09
H(2)-B(1)-N(12)	110.11
C(21)-N(11)-B(1)	129.55(17)
C(22)-N(12)-B(1)	124.65(16)
C(51)-N(11)-B(1)	124.97(17)
C(52)-N(12)-B(1)	128.01(15)

Table A-2. Selected bond lengths and angles for [MnTm(CO)$_3$] (13)

Bond Lengths (Å)	
Mn(1)-S(1AA)	2.4015(5)
Mn(1)-S(1AB)	2.4015(5)
Mn(1)-C(5A)	1.8020(18)
Mn(1)-C(5AA)	1.8020(18)
Mn(1)-C(5AB)	1.8020(18)
N(1A)-B(1A)	1.5533(17)
N(1AA)-B(1A)	1.5533(17)
N(1AB)-B(1A)	1.5533(17)
N(1A)-C(1A)	1.348(2)
N(1AA)-C(1AA)	1.348(2)
N(1AB)-C(1AB)	1.348(2)
S(1A)-C(1A)	1.7163(17)
S(1AA)-C(1AA)	1.7163(17)
S(1AB)-C(1AB)	1.7163(17)
Bond Angles (°)	
S(1A)-Mn(1)-S(1AA)	94.329(18)
S(1A)-Mn(1)-S(1AB)	94.329(18)
S(1AA)-Mn(1)-S(1AB)	94.329(18)
C(5A)-Mn(1)-C(5A)	91.86(8)
C(5AA)-Mn(1)-C(5AA)	91.86(8)
C(5AB)-Mn(1)-C(5AB)	91.86(8)
C(5A)-Mn(1)-S(1AA)	85.81(6)
C(5A)-Mn1-S(1AB)	85.81(6)
C(1A)-S(1A)-Mn(1)	111.54(6)
C(1AA)-S(1AA)-Mn(1)	111.54(6)
C(1AB)-S(1AB)-Mn(1)	111.54(6)
N(1A)-B(1A)-N(1AA)	113.22(11)
N(1A)-B(1A)-N(1AB)	113.22(11)
N(1AA)-B(1A)-N(1AB)	113.22(11)
N(1A)-C(1A)-S(1A)	129.18(13)
N(1AA)-C(1AA)-S(1AA)	129.18(13)
N(1AB)-C(1AB)-S(1AB)	129.18(13)
C(1A)-N(1A)-B(1A)	132.67(17)
C(1AA)-N(1AA)-B(1AA)	132.67(17)
C(1AB)-N(1AB)-B(1AB)	132.67(17)

Table A-3. Selected bond lengths and angles for [RuTm(*p*-cym)]Cl (14)

Bond Lengths (Å)	
Ru(1)-S(1)	2.4206(8)
Ru(1)-S(2)	2.4254(7)
Ru(1)-S(3)	2.4106(8)
B(1)-H(1)	1.09(3)
Ru(1)-C(45)	2.171(3)
Ru(1)-C(41)	2.191(3)
Ru(1)-C(44)	2.198(3)
Ru(1)-C(42)	2.213(3)
Ru(1)-C(46)	2.223(3)
Ru(1)-C(43)	2.239(3)
N(11)-B(1)	1.547(4)
N(21)-B(1)	1.544(4)
N(31)-B(1)	1.547(4)
N(11)-C(12)	1.341(4)
N(21)-C(22)	1.347(3)
N(31)-C(32)	1.355(3)
S(1)-C(12)	1.729(3)
S(2)-C(22)	1.730(3)
S(3)-C(32)	1.727(3)
Bond Angles (°)	
S(1)-Ru(1)-S(2)	93.12(3)
S(3)-Ru(1)-S(1)	90.76(3)
S(3)-Ru(1)-S(2)	88.97(3)
C(12)-S(1)-Ru(1)	108.41(9)
C(22)-S(2)-Ru(1)	108.92(9)
C(32)-S(3)-Ru(1)	110.68(10)
N(11)-B(1)-H(1)	106.3(15)
N(21)-B(1)-H(1)	107.2(15)
N(31)-B(1)-H(1)	107.2(16)
N(21)-B(1)-N(31)	112.2(2)
N(21)-B(1)-N(11)	113.7(2)
N(31)-B(1)-N(11)	109.9(2)
N(11)-C(12)-S(1)	128.0(2)
N(21)-C(22)-S(2)	129.1(2)
N(31)-C(32)-S(3)	128.8(2)
C(12)-N(11)-B(1)	130.7(2)
C(22)-N(21)-B(1)	132.0(2)
C(32)-N(31)-B(1)	132.0(2)

Table A-4. Selected bond lengths and angles for [Ru{κ^3-HB(mt)$_3$}Cp] (15b)

Bond Lengths (Å)	
Ru(1)-S(2)	2.400(5)
Ru(1)-S(3)	2.415(5)
Ru(1)-S(4)	2.401(5)
B(1)-H(1)	1.316
Ru(1)-C(11)	2.218(3)
Ru(1)-C(12)	2.264(3)
Ru(1)-C(13)	2.188(3)
Ru(1)-C(14)	2.174(3)
Ru(1)-C(15)	2.186(2)
B(1)-N(26)	1.5845(19)
B(1)-N(36)	1.557(2)
B(1)-N(46)	1.5961(16)
C(21)-N(26)	1.3860(14)
C(31)-N(36)	1.3220(13)
C(41)-N(46)	1.3709(16)
S(2)-C(21)	1.721(4)
S(3)-C(31)	1.713(5)
S(4)-C(41)	1.723(4)
Bond Angles (°)	
S(2)-Ru(1)-S(3)	93.8(2)
S(2)-Ru(1)-S(4)	93.44(16)
S(3)-Ru(1)-S(4)	94.04(19)
Ru(1)-S(2)-C(21)	104.45(18)
Ru(1)-S(3)-C(31)	106.3(2)
Ru(1)-S(4)-C(41)	104.75(19)
H(1)-B(1)-N(26)	112.896
H(1)-B(1)-N(36)	110.468
H(1)-B(1)-N(46)	104.264
N(26)-B(1)-N(36)	111.02(10)
N(26)-B(1)-N(46)	109.73(4)
N(36)-B(1)-N(46)	108.15(6)
S(2)-C(21)-N(26)	129.28(13)
S(3)-C(31)-N(36)	129.79(14)
S(4)-C(41)-N(46)	130.02(13)
B(1)-N(26)-C(21)	130.96(7)
B(1)-N(36)-C(31)	132.64(5)
B(1)-N(46)-C(41)	130.74(9)

Table A-5. Selected bond lengths and angles for [CdTmBr] (17)

Bond Lengths (Å)	
Cd(1)-S(2)	2.5362(15)
Cd(1)-S(3)	2.5464(15)
Cd(1)-S(4)	2.6193(17)
Cd(1)-Br(2)	2.5647(9)
B(1)-H(1)	1.07(5)
N(22)-B(1)	1.546(8)
N(32)-B(1)	1.548(8)
N(42)-B(1)	1.566(8)
N(22)-C(21)	1.363(7)
N(32)-C(31)	1.358(7)
N(42)-C(41)	1.340(7)
S(2)-C(21)	1.725(6)
S(3)-C(31)	1.723(5)
S(4)-C(41)	1.715(6)
Bond Angles (°)	
S(2)-Cd(1)-S(3)	102.64(5)
S(2)-Cd(1)-S(4)	100.44(5)
S(3)-Cd(1)-S(4)	100.29(5)
S(2)-Cd(1)-Br(2)	124.89(4)
S(3)-Cd(1)-Br(2)	121.63(4)
S(4)-Cd(1)-Br(2)	101.90(4)
C(21)-S(2)-Cd(1)	97.01(19)
C(31)-S(3)-Cd(1)	100.14(18)
C(41)-S(4)-Cd(1)	98.19(19)
N(22)-B(1)-H(1)	104(3)
N(32)-B(1)-H(1)	108(3)
N(42)-B(1)-H(1)	107(3)
N(22)-B(1)-N(32)	113.0(4)
N(22)-B(1)-N(42)	112.5(4)
N(32)-B(1)-N(42)	112.0(5)
N(22)-C(21)-S(2)	129.3(4)
N(32)-C(31)-S(3)	129.1(4)
N(42)-C(41)-S(4)	129.6(4)
C(21)-N(22)-B(1)	133.5(5)
C(31)-N(32)-B(1)	132.2(5)
C(41)-N(42)-B(1)	133.2(5)

Table A-6. Selected bond lengths and angles for [ZnTm^{Et}Cl] (23)

Bond Lengths (Å)	
Zn(1)-S(1)	2.3560(7)
Zn(1)-S(2)	2.3660(7)
Zn(1)-S(3)	2.3633(7)
Zn(1)-Cl(1)	2.2464(7)
B(1)-H(1)	1.15(2)
B(1)-N(11)	1.549(3)
B(1)-N(21)	1.545(3)
B(1)-N(31)	1.549(3)
N(11)-C(12)	1.349(3)
N(21)-C(22)	1.351(3)
N(31)-C(32)	1.348(3)
S(1)-C(12)	1.720(2)
S(2)-C(22)	1.724(2)
S(3)-C(32)	1.722(2)
Bond Angles (°)	
S(1)-Zn(1)-S(3)	107.67(3)
S(1)-Zn(1)-S(2)	102.64(2)
S(3)-Zn(1)-S(2)	105.57(2)
Cl(1)-Zn(1)-S(1)	108.24(3)
Cl(1)-Zn(1)-S(2)	118.52(3)
Cl(1)-Zn(1)-S(3)	113.27(3)
C(12)-S(1)-Zn(1)	96.25(7)
C(22)-S(2)-Zn(1)	97.76(7)
C(32)-S(3)-Zn(1)	97.60(8)
N(11)-B(1)-H(1)	106.8(13)
N(21)-B(1)-H(1)	106.6(12)
N(31)-B(1)-H(1)	106.5(13)
N(21)-B(1)-N(31)	112.07(18)
N(21)-B(1)-N(11)	111.59(18)
N(31)-B(1)-N(11)	112.74(18)
N(11)-C(12)-S(1)	129.20(16)
N(21)-C(22)-S(2)	128.58(17)
N(31)-C(32)-S(3)	129.35(17)
C(12)-N(11)-B(1)	132.54(18)
C(22)-N(21)-B(1)	132.52(18)
C(32)-N(31)-B(1)	133.06(19)

Table A-7. Selected bond lengths and angles for [CdTm^{Et}Br] (24)

Bond Lengths (Å)	
Cd(1)-S(2)	2.5568(5)
Cd(1)-S(3)	2.5370(5)
Cd(1)-S(4)	2.5339(5)
Cd(1)-Br(1)	2.5517(2)
B(1)-H(1)	1.06(2)
B(1)-N(25)	1.557(3)
B(1)-N(35)	1.548(3)
B(1)-N(45)	1.546(3)
C(21)-N(25)	1.349(2)
C(31)-N(35)	1.355(2)
C(41)-N(45)	1.361(2)
S(2)-C(21)	1.7200(19)
S(3)-C(31)	1.722(2)
S(4)-C(41)	1.7239(19)
Bond Angles (°)	
S(4)-Cd(1)-S(3)	101.478(17)
S(4)-Cd(1)-S(2)	103.801(16)
S(3)-Cd(1)-S(2)	101.642(17)
S(4)-Cd(1)-Br(1)	114.304(13)
S(3)-Cd(1)-Br(1)	120.399(14)
S(2)-Cd(1)-Br(1)	113.094(13)
C(21)-S(2)-Cd(1)	94.55(6)
C(31)-S(3)-Cd(1)	96.74(6)
C(41)-S(4)-Cd(1)	98.30(6)
N(25)-B(1)-H(1)	106.3(12)
N(35)-B(1)-H(1)	105.2(12)
N(45)-B(1)-H(1)	106.9(12)
N(45)-B(1)-N(35)	113.04(15)
N(45)-B(1)-N(25)	111.62(16)
N(35)-B(1)-N(25)	113.08(15)
N(25)-C(21)-S(2)	129.03(14)
N(35)-C(31)-S(3)	129.54(15)
N(45)-C(41)-S(4)	129.41(14)
C(21)-N(25)-B(1)	133.29(16)
C(31)-N(35)-B(1)	132.85(16)
C(41)-N(45)-B(1)	132.46(16)

Table A-8. Selected bond lengths and angles for [CdTm^{Bz}Br] (27)

Bond Lengths (Å)	
Cd(1)-S(4)	2.5116(18)
Cd(1)-S(3)	2.5406(17)
Cd(1)-S(2)	2.5656(19)
Cd(1)-Br(1)	2.5352(9)
B(1)-H(1)	1.067
B(1)-N(22)	1.571(9)
B(1)-N(32)	1.567(9)
B(1)-N(42)	1.535(9)
N(22) -C(21)	1.347(8)
N(32)-C(31)	1.340(8)
N(42) -C(41)	1.361(8)
S(2)-C(21)	1.721(7)
S(3)-C(31)	1.719(7)
S(4)-C(41)	1.726(7)
Bond Angles (°)	
S(4)-Cd(1)-S(3)	104.27(6)
S(4)-Cd(1)-S(2)	103.01(6)
S(3)-Cd(1)-S(2)	101.93(6)
S(4)-Cd(1)-Br(1)	122.03(5)
S(3)-Cd(1)-Br(1)	108.91(5)
S(2)-Cd(1)-Br(1)	114.50(5)
C(21)-S(2)-Cd(1)	96.9(2)
C(31)-S(3)-Cd(1)	95.3(2)
C(41)-S(4)-Cd(1)	99.1(2)
H(1)-B(1)-N(22)	104.681
H(1)-B(1)-N(42)	112.807
H(1)-B(1)-N(32)	103.456
N(42)-B(1)-N(32)	114.0(6)
N(42)-B(1)-N(22)	110.2(6)
N(32)-B(1)-N(22)	110.8(6)
N(22)-C(21)-S(2)	128.7(5)
N(32)-C(31)-S(3)	129.1(5)
N(42)-C(41)-S(4)	130.0(5)
C(21)-N(22)-B(1)	134.2(6)
C(31)-N(32)-B(1)	134.0(6)
C(41)-N(42)-B(1)	133.1(6)

Table A-9. Selected bond lengths and angles for [CuTm^{Et}PPh$_3$] (29)

Bond Lengths (Å)	
Cu(1)-S(2)	2.3868(8)
Cu(1)-S(2)#1	2.3868(9)
Cu(1)-S(2)#2	2.3868(8)
Cu(1)-P(1)	2.2306(16)
B(1)-H(1)	1.174
B(1)-N(22)	1.541(3)
B(1)-N(22)#1	1.541(3)
B(1)-N(22)#2	1.541(3)
C(21)-N(22)	1.349(5)
S(2)-C(21)	1.719(4)
Bond Angles (°)	
S(2)-Cu(1)-S(2)#1	102.47(3)
S(2)-Cu(1)-S(2)#2	102.47(3)
S(2)#1-Cu(1)-S(2)#2	102.47(3)
P(1)- Cu(1)-S(2)	115.80(2)
P(1)-Cu(1)-S(2)#1	115.80(2)
P(1)-Cu(1)-S(2)#2	115.80(2)
C(21)-S(2)-Cu(1)	97.52(12)
H(1)-B(1)-N(22)	106.658
H(1)-B(1)-N(22)#1	106.658
H(1)-B(1)-N(22)#2	106.658
N(22)-B(1)-N(22)#1	112.1(2)
N(22)-B(1)-N(22)#2	112.1(2)
N(22)#1-B(1)-N(22)#2	112.1(2)
N(22)-C(21)-S(2)	128.1(3)
C(21)-N(22)-B(1)	132.4(3)

Table A-10. Selected bond lengths and angles for [RuTm^{Et}(*p*-cym)] (33)

Bond Lengths (Å)	
Ru(1)-S(1)	2.4206(8)
Ru(1)-S(2)	2.4254(7)
Ru(1)-S(3)	2.4106(8)
B(1)-H(1)	1.09(3)
Ru(1)-C(45)	2.171(3)
Ru(1)-C(41)	2.191(3)
Ru(1)-C(44)	2.198(3)
Ru(1)-C(42)	2.213(3)
Ru(1)-C(46)	2.223(3)
Ru(1)-C(43)	2.239(3)
N(11)-B(1)	1.547(4)
N(21)-B(1)	1.544(4)
N(31)-B(1)	1.547(4)
N(11)-C(12)	1.341(4)
N(21)-C(22)	1.347(3)
N(31)-C(32)	1.355(3)
S(1)-C(12)	1.729(3)
S(2)-C(22)	1.730(3)
S(3)-C(32)	1.727(3)
Bond Angles (°)	
S(1)-Ru(1)-S(2)	93.12(3)
S(3)-Ru(1)-S(1)	90.76(3)
S(3)-Ru(1)-S(2)	88.97(3)
C(12)-S(1)-Ru(1)	108.41(9)
C(22)-S(2)-Ru(1)	108.92(9)
C(32)-S(3)-Ru(1)	110.68(10)
N(11)-B(1)-H(1)	106.3(15)
N(21)-B(1)-H(1)	107.2(15)
N(31)-B(1)-H(1)	107.2(16)
N(21)-B(1)-N(31)	112.2(2)
N(21)-B(1)-N(11)	113.7(2)
N(31)-B(1)-N(11)	109.9(2)
N(11)-C(12)-S(1)	128.0(2)
N(21)-C(22)-S(2)	129.1(2)
N(31)-C(32)-S(3)	128.8(2)
C(12)-N(11)-B(1)	130.7(2)
C(22)-N(21)-B(1)	132.0(2)
C(32)-N(31)-B(1)	132.0(2)